Using human iPSC-derived neural progenitor cells to increase integrin expression in the CNS

Lindsey H Forbes, BSc

University of
St Andrews

This thesis is submitted in partial fulfilment for the degree of PhD
at the
University of St Andrews

19 October 2017

Declaration

1. Candidate's declarations:

I, Lindsey Forbes, hereby certify that this thesis, which is approximately 60,500 words in length, has been written by me, and that it is the record of work carried out by me, or principally by myself in collaboration with others as acknowledged, and that it has not been submitted in any previous application for a higher degree.

I was admitted as a research student in March, 2014 and as a candidate for the degree of PhD in March, 2014; the higher study for which this is a record was carried out in the University of St Andrews between 2014 and 2017.

Date: Signature of candidate:

2. Supervisor's declaration:

I hereby certify that the candidate has fulfilled the conditions of the Resolution and Regulations appropriate for the degree of PhD in the University of St Andrews and that the candidate is qualified to submit this thesis in application for that degree.

Date: Signature of supervisor:

3. Permission for publication:

In submitting this thesis to the University of St Andrews I understand that I am giving permission for it to be made available for use in accordance with the regulations of the University Library for the time being in force, subject to any copyright vested in the work not being affected thereby. I also understand that the title and the abstract will be published, and that a copy of the work may be made and supplied to any bona fide library or research worker, that my thesis will be electronically accessible for personal or research use unless exempt by award of an embargo as requested below, and that the library has the right to migrate my thesis into new electronic forms as required to

ensure continued access to the thesis. I have obtained any third-party copyright permissions that may be required in order to allow such access and migration, or have requested the appropriate embargo below.

The following is an agreed request by candidate and supervisor regarding the publication of this thesis:

PRINTED COPY

~~a) No embargo on print copy~~

b) Embargo on all or part of print copy for a period of 2 years on the following ground(s):
    - ~~Publication would be commercially damaging to the researcher, or to the supervisor, or the University~~
    - Publication would preclude future publication
    - ~~Publication would be in breach of laws or ethics~~

~~c) Permanent or longer term embargo on all or part of print copy for a period of … years (the request will be referred to the Pro-Provost and permission will be granted only in exceptional circumstances).~~

Supporting statement for printed embargo request if greater than 2 years:

ELECTRONIC COPY

~~a) No embargo on electronic copy~~

b) Embargo on all or part of electronic copy for a period of 2 years on the following ground(s):
    - ~~Publication would be commercially damaging to the researcher, or to the supervisor, or the University~~
    - Publication would preclude future publication
    - ~~Publication would be in breach of law or ethics~~

~~c) Permanent or longer term embargo on all or part of electronic copy for a period of … years (the request will be referred to the Pro-Provost and permission will be granted only in exceptional circumstances).~~

Supporting statement for electronic embargo request if greater than 2 years:

ABSTRACT AND TITLE EMBARGOES

If you have selected an embargo option indicate below if you wish to allow the thesis abstract and/or title to be published. If you do not complete the section below the title and abstract will remain embargoed along with the text of the thesis.

a) I agree to the title and abstract being published YES
b) I require an embargo on abstract NO
c) I require an embargo on title NO

Date: Signature of candidate:

Signature of supervisor:

Sections from Chapter 1 of this thesis have been submitted as an invited review for Neural Plasticity in October 2017:
Quraishe S*, Forbes LH* and Andrews MR. The extracellular environment of the CNS: Influence on Plasticity, Sprouting and Regeneration after spinal cord injury. *Invited review to Neural Plasticity, submitted Oct 2017* (*These authors contributed equally).

Contents

Table of Figures

List of Tables

Acknowledgements

I would first like to acknowledge my supervisors, Melissa Andrews and Simon Powis, as well as the School of Medicine for giving me the opportunity to take on my PhD for which I am very grateful.

I also gratefully acknowledge the University of St Andrews and particularly the 600th Anniversary Scholarship fund which enabled me to carry out my PhD and to The RS Macdonald Charitable Trust for contributions to funding for which I am very thankful.

I would also like to thank past and present lab members in 248 and 249, Gavin, Ben, Laura, Madhurima, Wardiya, Zoe, Andrew, Patrick, Sophie, Bob, Sanya, John, Kate, Swatti, Raisa, Sarah, Michael and Ian for all the great times in and out of the lab, the well baked cakes and competitive lab Olympics over the years. You have all made my experience in St Andrews a very happy memorable one!

Most of all I would like to thank my family, friends and Scott. During the many challenges I have encountered throughout this PhD experience, they have always been there to offer their endless support and remind me there is life outside the lab! I could not have completed this without them and I cannot thank them enough.

Abstract

Repair of the adult mammalian spinal cord is prohibited by several extrinsic and intrinsic factors. As the CNS matures, growth-promoting proteins such as integrins are developmentally downregulated resulting in a reduced capacity for axonal outgrowth. Integrins are heterodimeric receptors involved in cell-cell and cell-matrix interactions. Specifically, within mature corticospinal tract (CST) axons, integrins are not transported into the axonal compartment. One integrin heterodimer, α9β1, is of particular interest for its ability to promote neurite outgrowth when bound to a component of the injury-induced milieu, tenascin-C. This project aimed to increase integrin expression within the CNS using induced pluripotent stem cell-derived human neural progenitor cells (iPSC-hNPCs).

Using immunocytochemistry and western blotting, endogenous integrin expression within iPSC-hNPCs was determined. In addition, overexpression of α9 integrin was achieved using transfection and lentiviral transduction. The capacity of wild type (WT) and α9-hNPCs to extend neurites on tenascin-C was assessed using neurite outgrowth assays. Results revealed increasing α9 integrin expression in hNPCs significantly promoted neurite outgrowth when cultured on tenascin-C. Interestingly, increasing the concentration of human tenascin-C, resulted in increasingly longer neurites from WT hNPCs suggesting hNPCs could actively upregulate integrin expression. Subsequently, WT and α9-hNPCs were transplanted into layer V of the neonatal rat sensorimotor cortex, which projects to the CST. WT and α9-hNPCs survived up to 8 weeks post-transplantation and produced projections along white matter tracts, including areas of the CST. Additionally, hNPCs retained α9-eYFP protein expression *in vivo* over time and was localised within axonal projections.

These results highlight the capabilities of iPSC-hNPCs to promote integrin expression within the rodent CNS presenting one potential avenue to target neuronal replacement following spinal injury. Future research should focus on assessing the regenerative capacity of WT and α9-hNPCs within an injury model concentrating on the ability of these cells to adapt within an injured environment.

Abbreviations

A-P	Anterior-posterior
AIS	Axon initial segment
ANOVA	Analysis of variance
BBB	Basso, Beattie, Bresnahan
BCA	Bicinchoninic acid
BDA	Biotinylated dextran amine
BDNF	Brain-derived neurotrophic factor
BLI	Bioluminescence imaging
BMP	Bone morphogenetic protein
cAMP	Cyclic adenosine monophosphate
CCNs	Cerebral cortical neurons
Cdks	Cyclin-dependent kinases
ChABC	Chondroitinase ABC
CNS	Central nervous system
CNTF	Ciliary neurotrophic factor
Crtl1	Cartilage link protein 1
CSPGs	Chondoitin sulphate proteoglycans
CST	Corticospinal tract
Ctip2	Chicken ovalbumin upstream promoter transcription factor (COUP-TF) interacting protein 2
D-V	Dorsal-ventral
DAPI	4',6'-diamidino-2-phenylindole
DCX	Doublecortin
ddH_2O	Double-distilled water

dH_2O	Distilled water
DIV	Days *in vitro*
DMEM	Dulbecco's Modified Eagle Medium
DMEM/F12	Dulbecco's Modified Eagle Medium/Nutrient Mixture F-12
DNA	Deoxyribonucleic acid
DRG	Dorsal root ganglia
E22	Embryonic day 22
ECL	Enhanced chemiluminescence
ECM	Extracellular matrix
EDTA	Ethylenediaminetetraacetic acid
EGF-L	Epidermal growth factor-like
eGFP	Enhanced green fluorescent protein
ESCs	Embryonic stem cells
EtOH	Ethanol
eYFP	Enhanced yellow fluorescent protein
FAK	Focal adhesion kinase
FBS	Fetal bovine serum
FERM	4.1, ezrin, radixin, moesin
FG	Fibrinogen globe
fGFP	Farnesylated green fluorescent protein
FNIII	Fibronectin type III
GAG	Glycosaminoglycan
GAP-43	Growth-associated protein-43
GDNF	Glial cell-derived neurotrophic factor
GFAP	Glial fibrillary acid protein

GRPs	Glial-restricted progenitors
GSK3- β	Glycogen synthase kinase 3-β
GTPase	Guanosine triphosphatase
HEK293T	Human embryonic kidney 293 cells expressing SV40 T antigen
hNCAM	Human neural cell adhesion molecule
hNPCs	Human neural progenitor cells
HRP	Horseradish peroxidase
HuNu	Human nuclear antigen
hyCCNs	Human young cerebral cortical neurons
Iba-1	Ionised calcium-binding adaptor molecule-1
ICC	Immunocytochemistry
IHC	Immunohistochemistry
iPSCs	Induced pluripotent stem cells
JAK/STAT	Janus tyrosine kinases/signal transducers and activators of transcription
kDa	Kilodalton
KO	Knockout
LB	Luria bertani
LSFM	Light sheet fluorescent microscopy
LTR	Long terminal repeat
LV	Lentivirus
M-L	Medial-lateral
MAG	Myelin-associated glycoprotein
MAPK	Mitogen-activated protein kinase
MBP	Myelin basic protein

MSCs	Mesenchymal stem/stromal cells
mTOR	Mechanistic target of rapamycin
NG2	Neuron/glial antigen 2
NGF	Nerve growth factor
NgR1	Nogo receptor 1
NOD/SCID	Non-obese diabetic/severe combined immunodeficiency
NPC	Neural progenitor cell
NRPs	Neural restricted progenitors
NSCs	Neural stem cells
NSPCs	Neural stem and progenitor cells
OECs	Olfactory ensheathing cells
OMgp	Oligodendrocyte-myelin glycoprotein
OPCs	Oligodendrocyte precursor cells
P0-2	Postnatal day 0-2
PBS	Phosphate buffered saline
PBS-T	Phosphate buffered saline containing tween-20
PC12	Pheochromocytoma-12
PDL	Poly-D-Lysine
PEI	Polyethylenimine
PFA	Paraformaldehyde
PI	Protease inhibitor
PI3-K	Phosphoinositide 3-kinase
PIP2	Phosphatidylinositol 4,5-bisphosphate
PIP3	Phosphoinositide 3,4,5-triphosphate
PirB	Paired immunoglobulin-like receptor B

PKCγ	Protein kinase C gamma
PLO	Poly-L-ornithine
PNNs	Perineural nets
PNS	Peripheral nervous system
PS	Penicillin and streptomycin
PTB	Phosphotyrosine binding site
PTEN	Phosphatase and tensin homolog
PTPσ	Protein tyrosine phosphatase sigma
RGD	Arginine-Glycine-Asparagine
RIPA	Radioimmunoprecipitation assay
ROCK	Rho-associated protein kinase
RPE	Retinal pigmented epithelial cells
RT	Room temperature
SC	Schwann cell
SCI	Spinal cord injury
SEM	Standard error of the mean
SOCS3	Suppressor of cytokine signalling 3
TA	Tenascin assembly
Tbr1	T-box brain 1
TBS	Tris-buffered saline
TBS-T	Tris-buffered saline containing tween-20
TC-grade	Tissue culture-grade
TLRs	Toll-like receptors
TN-C	Tenascin-C
TN-R	Tenascin-R

TNF-α	Tumour necrosis factor alpha
Trk/TrkB	Tropomyosin receptor kinase/B
Tuj	βIII-tubulin
VGlut1	Vesicular glutamate transporter 1
WFA	Wisteria floribunda agglutinin
WT	Wild type

Chapter 1: Introduction

1.1 CNS injury

1.1.1 General background and statistics on SCI

Repair of the central nervous system (CNS) after injury is one of the biggest challenges facing neuroscientists today. Currently, 1,000 people each year suffer a spinal cord injury (SCI) in the UK and Ireland (Spinal Research UK, 2016) and this number increases to between 250,000 and 500,000 worldwide (Bickenbach, 2013). Traumatic SCI is estimated to have a global incidence rate of 23 cases per million (Lee *et al.,* 2014). The most common causes of traumatic SCI are preventable and include road traffic accidents, falls, violence and contact sports (National SCI Statistical Center, 2017) which often leave individuals with various types of sensory, motor and/or autonomic deficits. Non-traumatic SCI often results from pathophysiological causes including cancer, infectious diseases or genetic conditions including spina bifida (Bickenbach, 2013). Traumatic SCI is more common in males than females and occurs most commonly in young adulthood (15-29 years) and older age (over 60) (Bickenbach, 2013). Treatment is limited for SCI, and mainly revolves around preventing further damage however rehabilitation interventions are currently the main line of treatment.

The spine consists of 33 vertebrae within five distinct regions, cervical, thoracic, lumbar, sacral and coccygeal. Within the spinal column lies the spinal cord, a bundle of myelinated and unmyelinated axonal nerve fibres that transmit information between the brain and the rest of the body. There are 31 pairs of spinal nerves that branch out from the spinal cord, one on each side of the body, into the spaces between the vertebrae termed intervertebral foramina each making their way to the periphery thereby connecting the CNS and the peripheral nervous system (PNS). These branches consist of a number of ventral roots, comprising motor fibres, and dorsal roots, comprising sensory fibres. Each set of spinal nerves corresponds to a particular area of the body, termed dermatomes (Figure 1.1). The spinal cord, contained within the vertebrae of the spinal column, is encased in three meningeal layers known as the pia mater, the arachnoid mater and the dura mater.

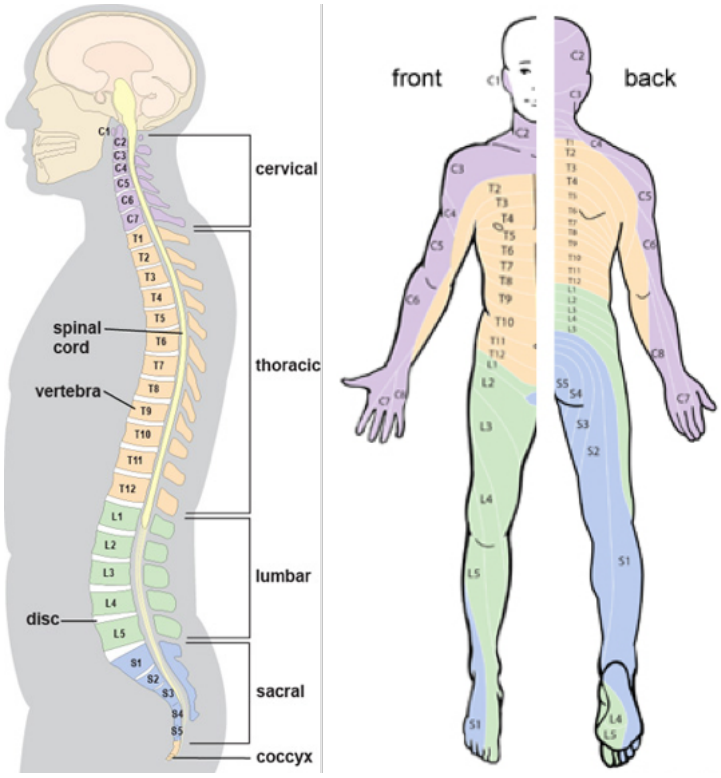

Figure 1.1 The human spinal cord and corresponding dermatomes. The spinal column consists of five different regions, cervical, thoracic, lumbar, sacral and coccygeal, and comprises the spinal cord, a long bundle of nerve fibres emanating from the brain stem. From the spinal cord 31 pairs of spinal nerves branch out between the vertebrae, one set at each level. Each set of spinal nerves control the sensory and motor function for one particular part of the body termed dermatomes. For example, C1, C2 and C3 spinal nerves control sensory and motor function of the head and neck. Injury to this region is considered the most severe as it can result in loss of motor and or/sensory function below this leaving an individual tetraplegic. Figure modified from Mayfield Brain and Spine, 2016.

An injury to the spinal cord can leave individuals with various losses in sensory, motor and/or autonomic function depending on the level of the injury. SCI can be classified as complete or incomplete, and can affect either side of the body or both. In general, any damage to one particular level of the spine often affects the areas of the body at and/or below that level. The severity of symptoms is greater the more rostral the location of the injury. For example, a complete injury between C1-C4 will leave an individual paralysed from the neck down and hinder autonomic activity, including breathing ability and heart rate. In these situations, individuals require assistance with ventilation and often 24-hour care. An injury within the lower cervical region (C5 and below) would still likely leave an individual tetraplegic, without complete use of their

arms and legs, but is likely to leave breathing and heart rate intact. An injury occurring lower in the spine, such as the lower thoracic and lumbar regions, would likely leave an individual paraplegic without control of their bladder, bowel or sexual function, however they would still have use of their upper body including their arms.

1.1.2 Pathophysiology after CNS injury

One of the reasons the spinal cord is so difficult to repair after injury is due to the complex and distinctive pathophysiology that occurs following impact. The underlying biology of SCI consists of a primary and a secondary phase. The primary phase is the initial injury suffered upon impact. This can include pressure on the spine, severed axons and nerves as well as internal bleeding. Depending on the type of injury, the blood-brain barrier may become permeable resulting in leukocyte infiltration (Reviewed in Trivedi *et al.,* 2006; Trahanas *et al.,* 2015) as well as disruption of the ionic homeostasis creating changes in calcium and potassium concentrations at the injury site (Young and Koreh, 1986; Chesler *et al.,* 1994). Furthermore, disruption of blood supply to the injury site can result in inadequate oxygen and nutrient supply. At this stage, emergency treatment is required to prevent further damage, which includes stabilisation of the spine often followed by surgical decompression in order to reduce the inflammatory response and stop any bleeding. Over the subsequent weeks and months, the injury enters the secondary phase resulting in progressive neurodegeneration. This phase is associated with a second set of symptoms including inflammation, axonal demyelination, apoptosis, glutamate excitotoxicity and reactive astrogliosis leading to formation of a glial scar. Much of spinal cord and axonal injury research focuses on treatment and prevention of these secondary mechanisms.

1.1.3 Extrinsic mechanisms inhibiting CNS regeneration

1.1.3.1 The glial scar and associated inhibitory proteins

Unlike the PNS, the adult mammalian CNS has a reduced ability to regenerate. The differences in capacity for regeneration between the two nervous systems was demonstrated by Aguayo and colleagues who showed peripheral nerve grafts into the injured rat spinal cord create a permissive environment allowing axons of the CNS to regenerate (Richardson *et al.,* 1980; David and Aguayo, 1981; Munz *et al.,* 1985).

Following a SCI, the lack of regeneration from the CNS is, in part, a result of these secondary mechanisms and the formation of a characteristic glial scar at the injury site. This is a fluid-filled cavity surrounded by reactive astrocytes and fibroblasts which acts not only as a barrier to prevent further damage, but also inhibits axonal regeneration (Figure 1.2) (Reviewed in Silver and Miller, 2004). Alongside scar formation, there is axonal demyelination and Wallerian degeneration, and as a result, axonal retraction (George and Griffin, 1994), apoptosis, potential disruption of the blood-brain barrier as well as an upregulation of a number of inhibitory proteins including chondroitin sulphate proteoglycans (CSPGs), myelin-associated proteins and chemorepellent proteins (Reviewed in Silver and Miller, 2004). Furthermore, the immune system reacts after injury resulting in microglial, macrophage and astrocyte activation. Activation of microglia after SCI has been shown to contribute to sustained chronic pain often suffered by individuals following injury (Hains and Waxman, 2006; Reviewed in Milligan and Watkins, 2009). Together this biological cascade of events creates an inhibitory environment, reducing axonal plasticity and preventing repair.

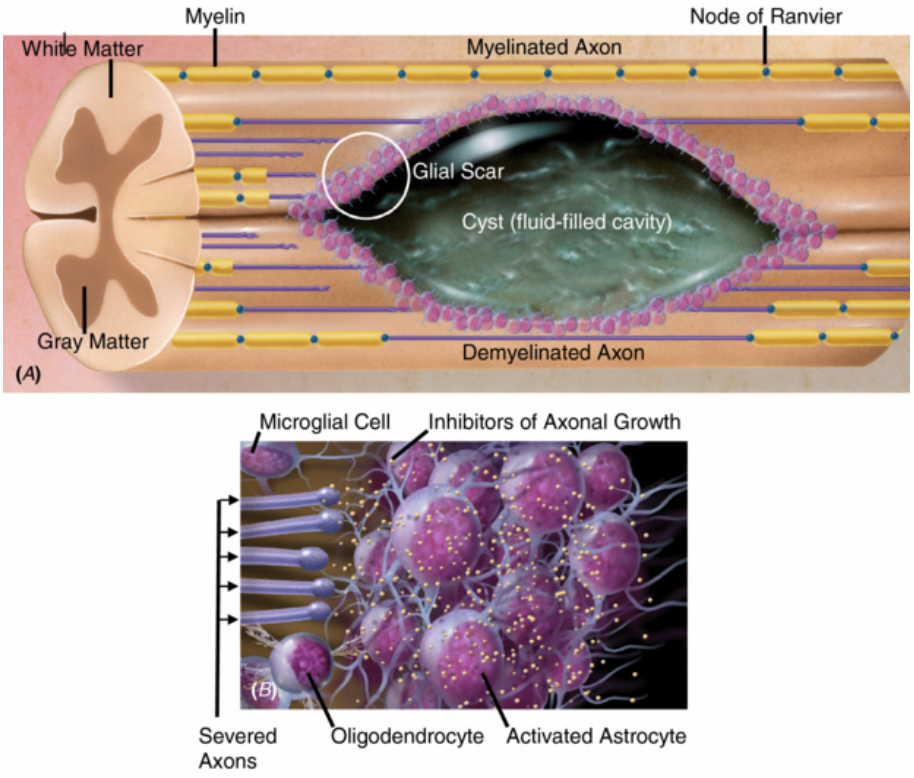

Figure 1.2 Glial scar formation after axonal injury. Following CNS injury, a fluid-filled cystic cavity, termed a glial scar, forms around the lesion site (**A**). This scar consists of reactive astrocytes and fibroblasts that act to protect the spread of further damage, but also impedes repair of injured axons.

Alongside the scar there can be severed axons, demyelination and Wallerian degeneration, apoptosis, glutamate excitotoxicity and activation of the immune response including activated microglia (**B**). Furthermore, a number of inhibitory proteins that prevent axonal repair are secreted, including CSPGs, such as aggrecan, and myelin-associated proteins, such as Nogo. Figure modified from Macaya and Spector, 2012.

CSPGs are the main family of inhibitory proteins associated with axonal injury. This includes the subgroup lecticans (comprising aggrecan, brevican, versican and neurocan), small leucine-rich proteoglycans (including biglycan and decorin), phosphacan/receptor-type-protein-tyrosine phosphatase β and other proteoglycans, including neuron-glial antigen 2 (NG2) and neuroglycan-C (Reviewed in Galtrey and Fawcett, 2007). The CSPGs are secreted into the extracellular matrix (ECM), mainly by reactive astrocytes and neurons (Asher *et al.,* 2000; Carulli *et al.,* 2006), but research suggests they are also secreted by macrophages and oligodendrocytes (Uhlin-Hansen *et al.,* 1993; Asher *et al.,* 2002; Jones *et al.,* 2003) increasing their abundance at the injury site. The main feature contributing to the inhibitory nature of CSPGs are their structure as they have a number of glycosaminoglycan (GAG) side chains. Each CSPG varies in the number of side chains they have, for example research suggests aggrecan contains over 100 GAG side chains and others contain less than 10 (Reviewed in Galtrey and Fawcett, 2007). The number of chains and the sulphation status of CSPGs can determine the functional effect of the CSPGs (Lin *et al.,* 2008; Wang *et al.,* 2008; Yi *et al.,* 2012). At the site of injury astrocytes become reactive and secrete CSPGs into the ECM creating an increased presence of CSPGs at the injury site contributing to an inhibitory milieu.

CSPGs bind to the transmembrane-associated protein tyrosine phosphate sigma (PTPσ) receptors located on neurons (Shen *et al.,* 2009). When CSPGs bind to PTPσ they initiate activation of the guanosine triphosphatase (GTPase) Rho signalling pathway resulting in inhibition of axonal growth (Monnier *et al.,* 2003; Shen *et al.,* 2009). Animal models of SCI lacking PTPσ show increased regeneration of the corticospinal tract (CST) (Fry *et al.,* 2010). The enzyme chondroitinase ABC (ChABC) acts to digest the GAG sugar chains of CSPGs preventing CSPGs from interacting with their receptors and has been shown to be effective in promoting axonal plasticity and regeneration in many models of SCI (Bradbury *et al.,* 2002; Carulli *et*

al., 2010). Interestingly after thoracic contusion injury in adult rats and treatment with ChABC, the microglial phenotype changed from M1 to the more regenerative M2 phenotype and resulted in improved sensorimotor function (Bartus *et al.,* 2014). Because ChABC is an enzyme it has its limitations, primarily degradation over time (Lin *et al.,* 2008). As a result, repeated dosing is required to maintain adequate enzymatic activity in order to promote repair. Long-term expression of ChABC has been obtained in rat models of SCI using lentivirus (LV) or adeno-associated virus (Alves *et al.,* 2014), promoting regeneration of CST axons (Zhao *et al.,* 2011). However, constitutive expression of ChABC over a long period of time may result in unwanted plasticity within the CNS.

1.1.3.2 Perineuronal nets

Within the CNS, CSPGs can associate with structures termed perineuronal nets (PNNs) which surround the soma and dendrites of mature neurons. PNNs are comprised of ECM proteins including hyaluronan; linking proteins, including cartilage link protein 1 (Crtl1) and brain-specific link protein 2 (Bral2); CSPGs; and tenascin-R (TN-R) (Galtrey *et al.,* 2008). This structure forms a highly stable and robust net-like structure (Deepa *et al.,* 2006), stabilising mature neurons and reducing dendritic spine plasticity (de Vivo *et al.,* 2013). Within the PNN structure, there are a number of CSPGs, including brevican, neurocan, aggrecan, phosphacan and versican, which bind to the hyaluronan back bone of the PNN (Deepa *et al.,* 2006). When specific components of cortical neuron PNNs are missing, for example the link protein Crtl1, PNN formation is reduced and neuronal plasticity is enhanced following damage to the visual or somatosensory pathways (Carulli *et al.,* 2010). CSPGs are located within the PNN structure and digestion of these structures using ChABC can promote neuronal plasticity, but it has also been suggested that PNNs contain only 2% of all CSPGs within the brain (Reviewed in Fawcett, 2015). Moreover, some CSPGs have been shown to have an important role during development of the CST, surrounding CST axons aiding axonal guidance and likely preventing unwanted migration and deviation of developing axons (Hsu *et al.,* 2005).

1.1.3.3 Demyelination and inhibitory myelin-associated proteins

After axonal insult, significant demyelination occurs (Gledhill *et al.,* 1973; Griffiths and McCulloch, 1983; Olby and Blakemore, 1996) resulting in increased myelin debris

at the injury site. After demyelination, a number of myelin-associated proteins, including Nogo-A (Chen *et al.,* 2000; Reviewed in Schweigreiter and Bandtlow, 2006), oligodendrocyte myelin glycoprotein (OMgp) (Mikol *et al.,* 1990; Wang *et al.,* 2002) and myelin-associated glycoprotein (MAG) (McKerracher *et al.,* 1994; Mukhopadhyay *et al.,* 1994) remain at the injury site contributing to the inhibitory environment. Research shows the presence of this debris can persist for years after the event (Buss *et al.,* 2005) further adding to the inhibition of axonal repair. All three proteins, Nogo-A, OMgp and MAG, bind to the same receptors, Nogo receptor 1 (NgR1), a glycosylphosphatidylinositol-anchored receptor (Fournier *et al.,* 2001; Domeniconi *et al.,* 2002; Wang *et al.,* 2002), and paired immunoglobulin-like receptor B (PirB) (Atwal *et al.,* 2008), which suggests they share common signalling pathways presenting focal targets to aid repair.

From mice knockout (KO) studies of all three proteins (OMgp, Nogo-A and MAG), research has shown that Nogo-A exerts the greatest inhibitory effect on axonal repair (Cafferty *et al.,* 2010). The myelin-associated protein, Nogo-A, binds to NgR1 on neurons via a specific 66 amino acid sequence on the C-terminus of Nogo-A (Fournier *et al.,* 2001), and acts to destabilise synapses (Aloy *et al.,* 2007) and promote growth cone collapse via Rho A signalling (Joset *et al.,* 2010). Nogo-A is a splice variant of which the others include Nogo-B and Nogo-C. Nogo activity can be inhibited by blocking its interaction with NgR1, using antibodies against Nogo-A (Caroni and Schwab, 1988; Brösamle *et al.,* 2000; Liebscher *et al.,* 2005), or by targeting downstream signalling proteins, such as cyclic adenosine monophosphate (cAMP). Literature suggests Nogo signalling reduces phosphorylated cAMP levels which has further been linked to reduced axonal trafficking (Qiu *et al.,* 2002). Interestingly, increasing cAMP levels by exposing dorsal root ganglia (DRGs) to dibutryl-(db) cAMP allows cells to overcome the inhibitory effects of Nogo resulting in increased neurite outgrowth (Joset *et al.,* 2010). Application of anti-Nogo-A monoclonal antibodies, bind to specific Nogo-A inhibitory domains blocking its function and resulting in axonal regeneration (Liebscher *et al.,* 2005). However, the beneficial effects of Nogo-A antibodies are time dependent with research showing delayed treatment (2 weeks after injury) cannot promote robust regeneration of CST motor fibres after incomplete thoracic SCI in rats (Gonzenbach *et al.,* 2012). However,

combining both anti-Nogo-A with ChABC treatment along with rehabilitation was able to promote significant regeneration after partial cervical SCI in adult rats, more so than either treatment alone (Zhao *et al.,* 2013). Additionally, research into treatments for SCI has focused on the reduction of myelin debris at the lesion site by increasing phagocytic activity of macrophages. This has resulted in beneficial effects for axonal regrowth when myelin-derived proteins are cleared using lipopolysaccharide in the mouse spinal cord (Vallières *et al.,* 2006).

Not all myelin-derived proteins are inhibitory following axonal injury however as research suggests some oligodendrocyte populations may attempt to remyelinate injured and sprouting axons (McTigue *et al.,* 2001). Furthermore, Schwann cells (SCs) infiltrating from the PNS have been shown to remyelinate injured CNS axons (Black *et al.,* 1986; Guest *et al.,* 2005). Similarly MAG, has previously been shown to promote neurite outgrowth in developing DRG neurons (Mukhopadhyay *et al.,* 1994) suggesting myelin-derived proteins may also have an age-specific function in axonal elongation.

1.1.3.4 TN-C and semaphorins

Alongside the increased levels of CSPGs, there are a number of developmental proteins that are upregulated after axonal injury in the mature CNS, including tenascin-C (TN-C), semaphorins, ephrins and netrins (Zhang *et al.,* 1997; De Winter *et al.,* 2002; Willson *et al.,* 2003; Petit *et al.,* 2007). In the developing CNS, these proteins act to promote axonal extension, guidance and growth cone formation but in the injured mature CNS, they become inhibitory to regrowth. In addition to a glial scar formation at the lesion site, reactive astrocytes secrete further inhibitory proteins into the extracellular milieu including the glycoprotein TN-C (Zhang *et al.,* 1997). TN-C, the most abundant ECM glycoprotein within the CNS, is highly expressed during development, aiding axonal growth. However, as the mammalian CNS matures, TN-C is downregulated. Conversely, TN-R levels are increased as the mammalian CNS matures, due to the increased formation of PNNs, acting to stabilise mature neurons (Carulli *et al.,* 2007). Generally, TN-C exerts an inhibitory effect on mature axons. However, when bound to a specific heterodimeric integrin receptor, α9β1, which is downregulated in the mature CNS, TN-C can promote neurite outgrowth (Andrews *et al.,* 2009; Cheah *et al.,* 2016) (see section 1.2.4.1 for further discussion on TN-C).

Semaphorins are a class of membrane-associated proteins involved in axonal growth, guidance and formation of new synaptic connections during embryonic development (Reviewed in Jongbloets and Pasterkamp, 2014), however they are also expressed within the adult CNS including within the glial scar post-injury (Pasterkamp *et al.,* 1999; Reviewed in Pasterkamp and Verhaagen, 2001; De Winter *et al.,* 2002). Interestingly particular semaphorin subtypes, such as sema4D, are upregulated after CNS injury and can prevent axonal growth *in vitro* suggesting it may contribute to the myelin-associated inhibitory environment at the lesion site *in vivo* (Moreau-Fauvarque *et al.,* 2003). A further subtype that is upregulated after injury is sema3A (DeWinter *et al.,* 2002), which has been implicated in preventing regeneration after SCI (Kaneko *et al.,* 2006; Wanigasekara and Keast, 2006), with expression remaining 4 weeks after the initial injury (Kaneko *et al.,* 2006). Selective inhibition of sema3A using SM-216289 can promote axonal regeneration, enhance SC migration to the lesion site, inhibit apoptosis and significantly improve functional recovery of the hindlimb following transection of the spinal cord in adult rats (Kaneko *et al.,* 2006).

1.1.3.5 The inflammatory and immune response after SCI

Following injury to the CNS, an immune response is initiated recruiting microglia, macrophages and activated astrocytes to the site of impact. Both microglia and astrocytes are known support cells within the CNS aiding homeostatic neuronal function (Elkabes *et al.,* 1996; Reviewed in Walz, 2000; Christopherson *et al.,* 2005; Magistretti, 2011; Suzuki *et al.,* 2011). However, after injury these cells can secrete a number of inhibitory proteins, including chemokines and cytokines (Yang *et al.,* 2004). In addition, *in vitro* research has shown nitric oxide and peroxynitrite are released by microglia in response to pathological conditions, both of which contribute to a neurotoxic and harmful environment (Kaushal *et al.,* 2007). Furthermore, if the blood-brain barrier is compromised after injury, the release of these inhibitory proteins results in recruitment of leukocytes, such as neutrophils and monocyte-derived macrophages, to the injury site further exacerbating the area. This range of inhibitory pro-inflammatory proteins are produced in response to ligands binding to toll-like receptors (TLRs) and P2 purinoceptors expressed on the surface of glial and neuronal cells (Reviewed in Burnstock and Knight, 2004; Olson and Miller, 2004). TLR ligands include ECM proteins, such as the proteoglycan biglycan (Schaefer *et al.,* 2005),

hyaluronan-derived oligosaccharides (Termeer *et al.,* 2002), and heat shock proteins (Reviewed in Asea, 2008) secreted from damaged and apoptotic cells (Willis *et al.,* 2005; Lehnardt *et al.,* 2007). Ligands for P2 purinoceptors are the nucleotide-associated proteins, purines and pyrimidines, and signalling via this receptor can result in microglia activation, microglial migration towards the injury site (Haynes *et al.,* 2006; Ohsawa *et al.,* 2007) and phagocytosis (Koizumi *et al.,* 2007). In response to this, inhibition of P2 signalling has been shown to promote repair and functional recovery following acute thoracic SCI in adult rats (Wang *et al.,* 2004).

Research into TLR signalling has shown that it is directly linked to the inflammatory response associated with both PNS (Boivin *et al.,* 2007) and CNS injury (Babcock *et al.,* 2006; Kigerl *et al.,* 2007). However, the mechanisms underlying TLR signalling are not fully understood as research has also shown it may actually be beneficial after CNS and PNS injury. For example, activation of macrophages and TLR downstream signalling can promote regeneration and may be essential for recovery of function after PNS nerve injury (Perrin *et al.,* 2005; Boivin *et al.,* 2007). Similarly, agonists of TLR can promote clearance of myelin debris by stimulating macrophages and microglia activity (Vallières *et al.,* 2006), axonal sprouting (Chen *et al.,* 2008b) and axonal regeneration (Yin *et al.,* 2003). Moreover, injecting TLR agonists such as zymosan into SCI sites has resulted in improved DRG regeneration, however the regeneration is not sustained as there is a simultaneous increase in neurotoxicity (Gensel *et al.,* 2009). Research has further suggested the immune response may also have a beneficial role in CNS injury, acting to prevent further damage (Faulkner *et al.,* 2004; Myer *et al.,* 2006). For example, Myer and colleagues demonstrated neurodegeneration worsened after moderate cortical stab injury in mice where astrocytes had been conditionally ablated (Myer *et al.,* 2006). Similarly, conditional deletion of reactive astrocytes at the injury site resulted in reduced infiltration of macrophages and increased neural degeneration after two different types of lumbar SCI, a longitudinal stab injury and a crush injury, in transgenic mouse models (Faulkner *et al.,* 2004). Furthermore, these animals were unable to repair the leaky blood-brain barrier after injury and showed reduced motor recovery compared to control animals (Faulkner *et al.,* 2004), highlighting the beneficial role activated astrocytes have at the injury site.

Other studies have shown macrophages can adopt two different morphologies, M1 and M2, in response to cytokines within the lesioned environment (Stout *et al.,* 2005). Out of these two phenotypes, the M2 phenotype is thought to be anti-inflammatory and able to promote long-distance axon outgrowth *in vitro* (Kigerl *et al.,* 2009).

Currently, acute SCI patients can be administered glucocorticoids, such as methylprednisolone or naloxone, to reduce the inflammatory response which have shown to improve functional recovery (Bracken *et al.,* 1992), however this treatment can be accompanied by a wide range of risks including respiratory infections and pneumonia (Reviewed in Hurlbert, 2014) and more recent research has questioned the efficacy of methylprednisolone (Evaniew *et al.,* 2015). It is clear that the underlying pathways associated with TLR signalling and macrophage activation require further investigation before anti-inflammatory treatments can be considered safe and effective for promoting neuroregeneration. However, it is also clear that many inflammatory proteins have a dual role, on one hand adding to or adversely affecting the inhibitory injured environment and on the other, promoting regeneration and preventing further damage. This therefore suggests suppressing or dampening the immune system may not be entirely beneficial.

1.1.4 Intrinsic factors inhibiting CNS repair

Alongside the inhibitory extracellular environment created after injury, mature mammalian neurons have reduced capabilities for regeneration (Muramatsu *et al.,* 2009; Reviewed in Eva *et al.,* 2012). This means that any successful treatment for SCI would need to address both the extrinsic and intrinsic obstacles. During development, the CNS is more prone to regenerate due to the plastic nature of the immature nervous system. Therefore, research on regeneration of the mature CNS has focused on reinstating the intrinsic signalling pathways, associated with the developing CNS in order to promote plasticity and regeneration after injury. Some target proteins of interest include, phosphatase and tensin homolog (PTEN), mammalian target of rapamycin (mTOR), suppressor of cytokine signalling 3 (SOCS3), Rho/ Rho-associated kinase (ROCK) and cAMP (Reviewed in Chew *et al.,* 2012). Alongside the changes in these proteins, growth-promoting receptors within the mature CNS,

including tropomyosin-related kinase (Trk) and integrin receptors, are downregulated illustrating further gaps in signalling pathways that are viable targets for repair.

1.1.4.1 The PTEN/mTOR pathway

The tumour suppressor protein, PTEN, converts phosphoinositide 3,4,5-triphosphate (PIP3) to phosphatidylinositol 4,5-bisphosphate (PIP2), within the phosphoinositide 3-kinase (PI3-K) pathway. Downstream of PIP3 is Akt (protein kinase B), which can promote cell survival and axon growth via downstream effectors, including inhibition of glycogen synthase kinase 3-β (GSK3-β) and activation of mTOR activity. For example, activation of mTOR can promote cell growth via increased expression of growth-associated protein-43 (GAP-43). Therefore, the reduction of PTEN activity will result in increased PIP3 activity, increased mTOR expression and thus cell growth making the PTEN/mTOR pathway a target for CNS regeneration (Park *et al.,* 2008; Ning *et al.,* 2010; Mao *et al.,* 2013; Ohtake *et al.,* 2014). Furthermore, research has shown conditional deletion of PTEN in the nervous system can promote regeneration of the optic nerve (Park *et al.,* 2008) and the CST in mice following injury (Liu *et al.,* 2010; Du *et al.,* 2015).

1.1.4.2 The JAK/STAT pathway

A further target for enhancing intrinsic axonal repair is deletion of SOCS3. This is responsible for inhibiting the janus tyrosine kinases/signal transducers and activators of transcription (JAK/STAT) pathway (Reviewed in Krebs and Hilton, 2001). Specifically, STAT3 phosphorylation via this pathway can result in neurite outgrowth and regeneration (Schwaiger *et al.,* 2000; Miao *et al.,* 2006; Bareyre *et al.,* 2011) and inhibition of this pathway via SOCS3, which is upregulated after CNS injury, prevents neurite outgrowth (Miao *et al.,* 2006; Park *et al.,* 2014). Increasing STAT3 activity has been shown to promote regeneration within the CNS and PNS (Bareyre *et al.,* 2011; Lang *et al.,* 2013; Mehta *et al.,* 2016). For example, following unilateral pyramidotomy in mice, sustained STAT3 activity using adeno-associated virus resulted in remodelling of CST axons and functional recovery of the forelimb after injury (Lang *et al.,* 2013). Similarly, deletion of SOCS3, thereby removing the negative regulation on the JAK/STAT pathway, promoted axonal outgrowth and regeneration within the optic nerve after a crush injury in adult mice (Smith *et al.,* 2009). SOCS3 deletion can also stimulate dendritic growth within white matter tracts

of the spinal cord and prevent demyelination after complete thoracic SCI in adult rats (Park *et al.,* 2015). In addition, dual deletion of SOCS3 and PTEN has resulted in greater regeneration of the optic nerve (Sun *et al.,* 2011) and sprouting of the CST (Jin *et al.,* 2015) than deletion of either alone suggesting targeting both intrinsic pathways may result in enhanced regeneration.

STAT3 activation has also been implicated in the proliferation of astrocytes and glial scar formation after SCI (Herrmann *et al.,* 2008; Wanner *et al.,* 2013). Although the glial scar is thought to be inhibitory to repair and many experimental treatments target the removal of glial scar components, research has also shown it has a protective role. For example, ablation of the glial scar via STAT3 KO does not promote spontaneous regrowth after severe crush of the mouse thoracic spinal cord (Anderson *et al.,* 2016). Rather, it can promote spread of inflammation and axonal degeneration (Wanner *et al.,* 2013). Together this research suggests modulation of the JAK/STAT pathway may have a number downstream effectors targeting multiple aspects of SCI pathophysiology.

1.1.4.3 Rho GTPases

The family of Rho GTPases are involved in modulation of the cell cytoskeleton and axongenesis, three of which are of particular interest in regeneration, namely RhoA, Rac1 and Cdc42. This is because each can promote actin and microtubule reorganisation stimulating axonal growth, guidance and migration by a number of effector proteins and pathways including PI3-K and mitogen-activated protein kinase (MAPK). Both Rac1 and Cdc42 are involved in lamellipodial and filopodial extension during growth cone formation (Brown *et al.,* 2000; Sayyad *et al.,* 2016). Following a lesion of the adult rat thoracic CST, delivery of constitutively active Rac1 and Cdc42 within a hydrogel bridge alongside brain-derived neurotrophic factor (BDNF), promoted axonal regeneration of CST axons through the lesion site (Jain *et al.,* 2011). Specifically, this combination of treatments resulted in reduction of CSPGs and reactive astrocytes at the lesion site and promoted regrowth of injured CST axons within the glial scar. Furthermore, Rac1 has been implicated in axonal guidance with Rac1 KO mice displaying defects in corticothalamic and thalamocortical pathways (Chen *et al.,* 2007).

Largely, Rho GTPases promote growth cone formation via reorganisation of the actin cytoskeleton however other GTPases including Rho and the ROCK pathway have the opposite effect and act to promote growth cone collapse (Dergham *et al.,* 2002; Monnier *et al.,* 2003; Joset *et al.,* 2010). Research has shown Nogo-A signalling via NgR can promote growth cone collapse via RhoA signalling (Niederöst *et al.,* 2002; Joset *et al.,* 2010). Inhibiting Rho signalling *in vitro* with either C3 transferase, a Rho inhibitor, or Y27632, a ROCK inhibitor, can promote growth of rat primary cortical neurons cultured on inhibitory substrates including CSPGs and myelin (Dergham *et al.,* 2002). Similarly, inhibiting the Rho signalling pathway can promote regeneration after CNS injury (Lehmann *et al.,* 1999; Dergham *et al.,* 2002; Fehlings *et al.,* 2011). For example, following thoracic CST lesioning, injection of Rho signalling inhibitors, either C3 transferase or Y27632, at the lesion site promoted regrowth of CST fibres beyond the injury site. It also significantly improved motor function demonstrated in the open field locomotor test after just 24 hours of treatment thought to be due to treatment-induced localised axonal sprouting (Dergham *et al.,* 2002). Interestingly, this study identified inhibition of Rho using C3 transferase provided a better regenerative outcome than inhibition of ROCK using Y27632, suggesting Rho may initiate a downstream cascade, independent of ROCK, acting to prevent regeneration (Dergham *et al.,* 2002).

1.1.4.4 Integrins

One further group of proteins that are of particular interest in axonal regeneration are integrins. Integrins are a family of transmembrane receptors involved in mediating cell-cell and cell-matrix adhesions. Within the nervous system they are involved in neurodevelopment, promoting neurite outgrowth and axonal elongation, but their expression is downregulated as the CNS matures. Research has shown overexpression of integrin subunits can promote neurite outgrowth in the presence of their ligand *in vitro* (Condic, 2001; Andrews *et al.,* 2009). Furthermore, reintroducing integrin subunits into the CNS can stimulate axonal regeneration after injury (see section 1.2 for further discussion on integrins).

1.1.4.5 Trk receptors

Alongside integrins, expression of another group of transmembrane receptors, Trk receptors, do not have a high enough expression to promote regeneration within the

adult mammalian CNS (Lu *et al.,* 2001; Kwon *et al.,* 2004). There are three subclasses of Trk receptors (TrkA, TrkB and TrkC) which bind a number of neurotrophic proteins, such as BDNF and nerve growth factor (NGF) resulting in modulation of cell survival and neurite outgrowth (Reviewed in Huang and Reichardt, 2003). Similar to integrins, there is a lack of Trk receptors in the adult CNS, specifically the receptor for BDNF, TrkB, located within the projections from adult CST axons (Lu *et al.,* 2001). Indeed modulation of BDNF and TrkB has shown to be promising targets for promoting regeneration (Cheng *et al.,* 2002; Song *et al.,* 2008; Hollis *et al.,* 2009). For example, increasing TrkB expression using lentivirus in rat corticospinal motor neurons *in vivo*, resulted in increased axonal outgrowth following a subcortical lesion in rats (Hollis *et al.,* 2009). Furthermore, these TrkB-expressing cells located within the motor cortex were able to project towards a BDNF-secreting graft located in the C3 region of the spinal cord (Hollis *et al.,* 2009). This suggested the trafficking mechanisms for TrkB were still active within axons of the CST and holds promise for future modulation of intrinsic signalling mechanisms for CNS repair.

1.1.4.6 Ephs and ephrins

Other intrinsic signalling proteins of note are the transmembrane receptor tyrosine kinases, ephs, and their ligands, ephrins, which form complexes with one another and work to modulate the cell cytoskeleton, thereby altering neurite outgrowth, migration and cell proliferation (Reviewed in Goldshmit *et al.,* 2006). However, after SCI injury in the adult rat, a number of the EphA family of receptors are upregulated (Willson *et al.,* 2002; Goldshmit *et al.,* 2004; Fabes *et al.,* 2006) and work to promote growth cone collapse (Willson *et al.,* 2002). Using a blocking peptide, the activity of these receptors, such as EphA4 which is known to be upregulated within the CST after injury (Fabes *et al.,* 2006), can be inhibited. This has proved to be a promising target for promoting CNS regeneration in rodents, resulting in increased sprouting of injured axons into the lesion site as well as improved functional recovery (Fabes *et al.,* 2007; Goldshmit *et al.,* 2011).

1.1.5 Treatment and current research for SCI

After SCI, some axons attempt to regenerate via axonal sprouting and dendritic remodelling however environmental and intrinsic challenges still remain suggesting

further intervention is required to achieve robust functional recovery. Currently there are no pharmacological or surgical treatments that will repair spinal cord axons and fully restore function. The aim of pharmacological treatments is therefore to reduce inflammation and pain with patients often receiving physiotherapy and rehabilitation. As mentioned earlier, patients can be prescribed methylprednisolone in an attempt to reduce inflammation, however it can result in some serious side effects and its clinical efficacy is not widely accepted (Bracken *et al.,* 1998; Evaniew *et al.,* 2015). Other types of pharmacological treatments currently prescribed include non-steroidal anti-inflammatories, such as ibuprofen, calcium channel blockers, such as nimodipine, and opioid antagonists, such as naloxone. In the UK, prescription of high dose methylprednisolone, nimodipine and naloxone to SCI patients is not recommended for neuroprotection due to side effects associated with them (National Institute for Clinical Excellence, 2016). Pharmacological treatments are therefore limited but most often patients will receive extensive physiotherapy and rehabilitation. In recent years new clinical trial data has emerged from patients receiving epidural stimulation. This involves a small electrode being surgically placed onto the dura mater of the spinal cord. While this is not yet a mainline treatment as testing involved only a few patients, encouraging results were observed, such as stimulating muscles in the lower limbs to allow individuals who previously could not stand to stand unassisted (Reviewed in Edgerton and Harkema, 2011; Rejc *et al.,* 2015).

Current research for treatment of SCI in animal models is largely focused around three aspects: digestion of the glial scar and removal of inhibitory signalling, including removal of Nogo-A and other myelin-associated proteins; reinstating growth-promoting signalling; and cell transplantation. For example, the inhibitory environment created at the lesion site harbours a number of proteins preventing axonal repair, including CSPGs, myelin-derived inhibitory proteins and semaphorins. Arguably some of the most promising studies have focused on targeting these proteins using various routes, such as removal or inhibition of these proteins. Specifically, studies have included use of monoclonal antibodies against Nogo-A (Caroni and Schwab, 1988; Brösamle *et al.,* 2000; Liebscher *et al.,* 2005), using ChABC enzyme to digest the glycosaminoglycan sugar chains of CSPGs (Bradbury *et al.,* 2002; García-Alías *et al.,* 2009) or increasing the phagocytic activity of macrophages to enhance

clearance of inhibitory proteins at the lesion site (Vallières *et al.,* 2006). Implemented individually, these treatments do not always result in extensive regrowth or restoration of function (Vallières *et al.,* 2006). Therefore a combination of treatments may result in a greater level of repair and functional recovery (Zhao *et al.,* 2013), suggesting that to enable robust repair multiple aspects of SCI pathophysiology should be targeted.

Experimental approaches towards enhancing repair post-SCI have offered great advancements in this field. Yet, arguably, the technique with the most universal application is cell replacement. Replacing lost and injured cells may promote remyelination or provide new neuronal networks for axonal guidance. Cell therapy has focused on transplantation of various cell types including, but not limited to, oligodendrocytes, SCs, astrocytes and neural stem cells (NSCs). However, considering the nature of the inhibitory environment created after injury, it is not surprising that transplanted cells can react differently in an injured spinal cord environment compared to uninjured controls (Sontag *et al.,* 2014). Research has shown that the lesioned environment can have a major impact on grafted NSCs, altering cell proliferation, survival, differentiation and engraftment into the host tissue (Sontag *et al.,* 2014). However, when stem cell grafts are used in conjunction with ChABC for treatment of SCI in rodent models, greater survival and integration of grafted cells is observed (Karimi-Abdolrezaee *et al.,* 2010). This strengthens the case for combination therapies for SCI, targeting multiple aspects for repair. Furthermore, grafted cells can be modified prior to transplantation to express a variety of different factors including fluorescent tags or specific growth-promoting proteins, the latter of which equips the cells with the necessary tools to adapt to and thrive within the injured environment. Nevertheless, cell transplantation also has its limitations, namely in terms of triggering an immune response. However with this in mind, recent research from a clinical trial in stroke patients revealed the neuroprotective effects of a stem cell transplant outlasted the survival of the cells (Steinberg *et al.,* 2016) likely due to secretion of neurotrophic factors. This study is promising for the field of neuroregeneration and suggests long-term cell survival and immunosuppression after cell transplant may not be necessary to induce CNS repair.

It has been suggested that only 10-15% of fibres need to regenerate to restore function (Reviewed in Dietz and Curt, 2006), therefore providing hope that axonal repair is

possible using stem cell transplants if given the correct guidance, support and environment. Cell therapy could promote regeneration by creating a bridge or a bypass for new regenerating neurons to navigate the injury site and restore connections. Whether this is required in combination with pharmacological agents to modify the inhibitory lesion site or modification of cells prior to transplant is yet to be fully determined. It is clear that both extrinsic and intrinsic mechanisms are preventing regeneration after SCI and therefore future research and treatments must tackle both of these aspects if robust functional regeneration is to be achieved.

1.2 Integrins

1.2.1 Integrin function and structure

Integrins are heterodimeric transmembrane receptors expressed by all cells within the body except red blood cells. They govern a wide range of cell-cell and cell-matrix interactions, including cell motility, migration, adhesion, proliferation and survival (Letourneau and Shattuck, 1989; Miyamoto *et al.,* 1995; Reviewed in Jones and Walker, 1999; Gardiner *et al.,* 2005). They are involved in a number of physiological processes including nervous system development, aiding cell growth and neural plasticity (Reviewed in Reichardt and Tomaselli, 1991; Reviewed in Clegg *et al.,* 2003; Huang *et al.,* 2006; Reviewed in Denda and Reichardt, 2007), immune system functioning (Reviewed in Zhang and Wang, 2012), regeneration of the PNS (Werner *et al.,* 2000; Gardiner *et al.,* 2005), as well as the progression of cancer (Reviewed in Lu *et al.,* 2008). However, one function of integrins that is of particular interest for CNS regeneration is their ability to promote neurite outgrowth and plasticity within the developing brain (Reviewed in Gupton and Gertler, 2010; Harper *et al.,* 2010) as well as after injury (Tan *et al.,* 2012; Cheah *et al.,* 2016).

Integrins are comprised of an α and a β subunit with currently 24 recognised heterodimers, consisting of 18 α and eight β subunits (Hynes, 2002). Integrin subunits are glycoproteins and bind to each other via non-covalent bonds. The combination of different integrin subunits, and particularly the α subunit, confers the ECM binding specificity, with many integrins binding more than one ligand. The heterodimers can be categorised into four subdomains including collagen receptors, laminin receptors, leukocyte-specific receptors and arginine-glycine-asparagine (RGD) receptors (Figure 1.3).

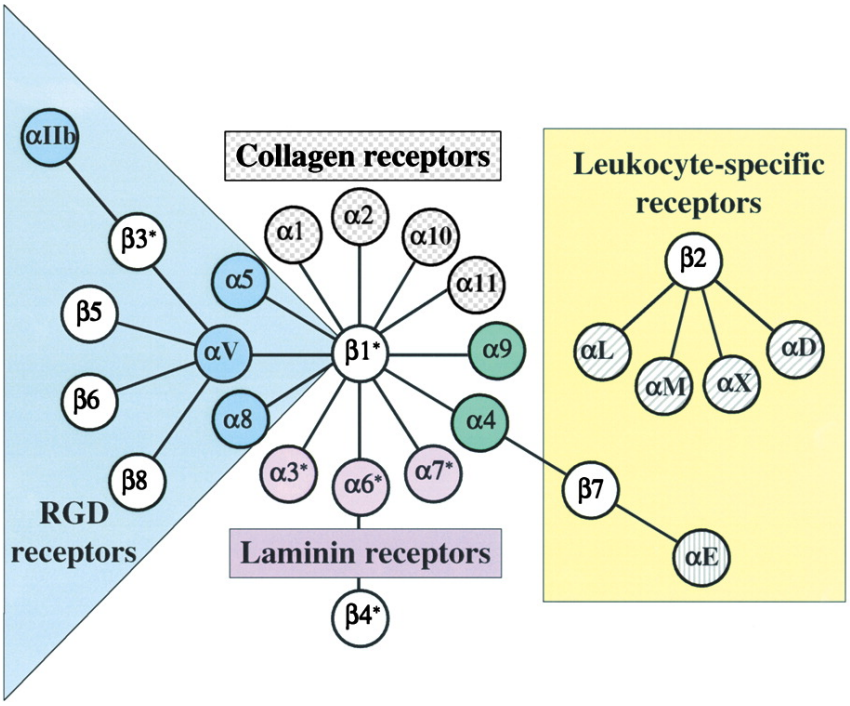

Figure 1.3 Integrin subunits and their binding partners. Integrins consist of an α and a β subunit of which there are currently 24 recognised heterodimers in mammals. The integrin heterodimer confers the binding specificity to the ECM ligand, with some subunits able to bind more than one partner, however they can be categorised in four distinct subgroups. These include collagen receptors, laminin receptors, RGD receptors and leukocyte-specific receptors. Figure modified from Hynes, 2002.

Structurally, integrin receptors have a large extracellular domain that allows the receptors to interact and bind different components of the ECM including proteoglycans, glycoproteins and growth factors (Reviewed in Kim *et al.,* 2011), which in turn activate intracellular signalling cascades resulting in cell adhesion and motility (Reviewed in Zhao and Guan, 2011; Reviewed in Danen, 2013; Reviewed in Moreno-Layseca and Streuli, 2014). The ectodomain of integrin receptors essentially act as gateways by which the cells communicate with and respond to the external environment. The cytoplasmic domain, in comparison, is much smaller and interacts with components of the cell cytoskeleton via adaptor proteins, including actin, vinculin, paxillin, kindlin and talin (Reviewed in DeMali *et al.,* 2003; Rose *et al.,* 2003; Humphries *et al.,* 2007; Reviewed in Calderwood *et al.,* 2013). Integrins bind their ligands with a relatively low affinity, however in response to this, there are usually high levels of integrin expression at the cell surface. This characteristic allows

integrins to act as guardians of cell movement interacting with a number of ECM molecules aiding in cell migration through the ECM (Figure 1.4).

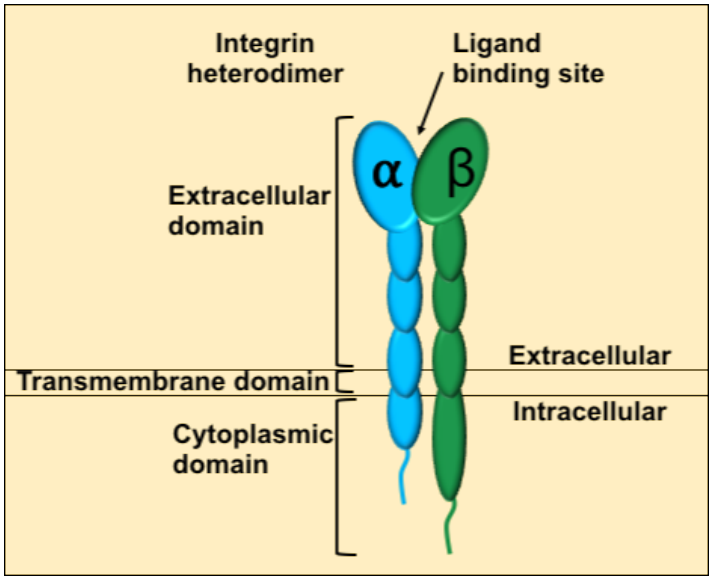

Figure 1.4 Structure of an integrin heterodimer. The integrin heterodimer consists of an α subunit (blue) binding non-covalently to a β subunit (green). Each consists of a large extracellular domain, a transmembrane domain that spans the lipid bilayer and a small cytoplasmic domain. The ligand binding site is located within the globular head of the α subunit. This site, termed the metal ion-dependent adhesion site, is controlled by the concentration of calcium and magnesium ions. The intracellular domain of the β subunit binds to integrin activators as well as adaptor proteins linking the integrin receptor with the cell's cytoskeleton components, such as actin.

1.2.2 Integrin activation and signalling

As discussed above, integrin heterodimers can bind a wide variety of ECM ligands, however to do so they must first be activated. Integrin receptors can have two basic states of activation and following analysis of its crystal structure (Xiong *et al.,* 2003), more is now known about this two-state model. Integrins are bi-directional signallers via 'inside-out' and 'outside-in' signalling. Due to the basal inactivation state of integrins in the bent conformation, they require activation before they can bind proteins in the extracellular domain. When integrins are in their inactive form they take on a bent appearance, bending the head of the extracellular compartment towards the cell surface (Figure 1.5, A). Binding of activator proteins, such as talin and kindlin

(Moser *et al.,* 2009; Tan *et al.,* 2012; Cheah *et al.,* 2016), to the cytoplasmic domain of the β subunit instructs both integrin subunits to straighten out exposing the extracellular ligand binding site (Takagi *et al.,* 2002). This conformational change is termed 'inside-out' signalling (Figure 1.5, B) and results in high-affinity ligand binding (Takagi *et al.,* 2002). Once this conformational change has occurred, an ECM ligand can bind to the recognition site located on the α subunit resulting in intracellular signalling, termed 'outside-in' signalling (Figure 1.5, C) (Takagi *et al.,* 2002).

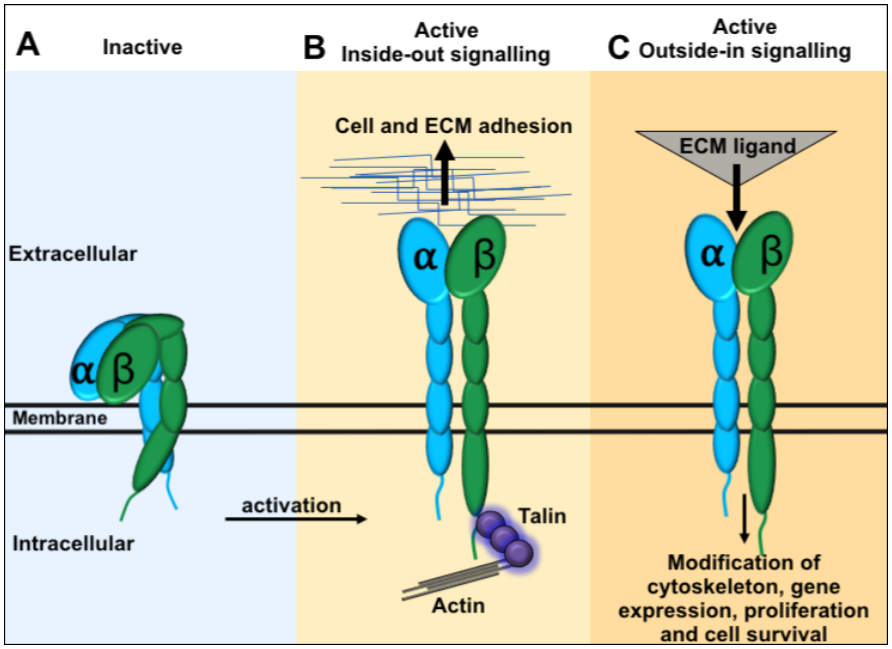

Figure 1.5 Inside-out and outside-in signalling via integrin receptors. Integrins must be activated to induce modification of the cell's cytoskeleton. They exist on the cell surface in an inactive state with the head of each subunit bent down towards the cell membrane (**A**). Integrin activators, such as talin and kindlin, bind to the cytoplasmic domain of the β subunit to induce a conformational change in the integrin receptors, allowing both subunits to straighten out and exposing the ligand binding site located on the globular head of the α subunit (**B**). This is a process termed inside-out signalling. This conformation change allows the integrin receptor to bind an ECM ligand promoting intracellular signalling pathways that result in modification of the cell's cytoskeleton, gene expression, cell proliferation and survival (**C**). This is termed outside-in signalling.

Ligand binding to the α subunit is governed by Ca^{2+} and Mg^{2+} ions present in the extracellular globular domain of the α subunit, known as the metal ion-dependent adhesion site (Lee *et al.,* 1995). These different divalent cations will confer different

specificities as well as affinities and can be used to modify integrin activation status in culture to keep the receptor in a high-affinity ligand binding state (Reviewed in Zhang and Chen, 2012).

Integrin activation can also be modified using integrin activators, such as kindlin or talin. Talin is a cytoskeletal protein usually found within the cytoplasm of mammalian cells and consists of a 4.1, ezrin, radixin, moesin (FERM) domain and a rod domain (Figure 1.6, A). In newly forming cell-cell adhesions, the F3 subdomain of the FERM domain within the N-terminal region of talin binds to the cytoplasmic region of β integrin subunits, to 'switch-on' the integrin into the active state (Calderwood *et al.,* 1999, 2002; Di Paolo *et al.,* 2002; Wegener *et al.,* 2007). Within this F3 subdomain there is a phosphotyrosine binding (PTB) site that binds to specific tyrosine residues within the cytoplasmic domain of β subunits (Wegener *et al.,* 2007). The talin c-terminal tail can bind to the actin cytoskeleton which therefore allows talin to act as a linking protein between β integrin cytoplasmic domains and the actin cytoskeleton, mediating cell motility (Zhang *et al.,* 2008).

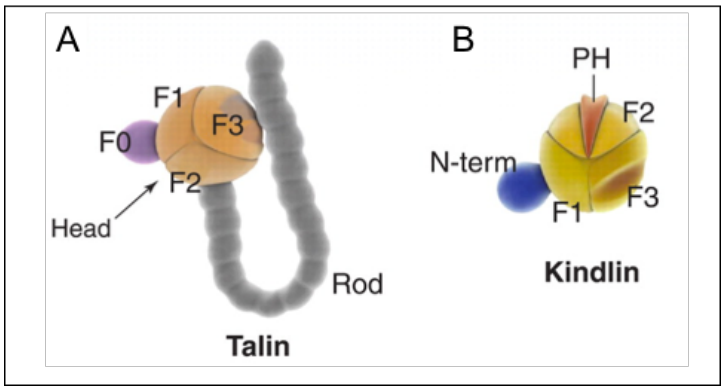

Figure 1.6 Structure of integrin activators talin and kindlin. Talin and kindlin are two integrin activators able to bind the cytoplasmic domain of the β subunit to stimulate a conformational change in the receptor and allow exposure of the ECM ligand site (inside-out signalling). Talin consists of a FERM domain, which binds to the β subunit, and a rod domain, which binds to actin, thereby linking integrin activity to the cell cytoskeleton (**A**). Kindlin also contains a FERM domain with a pleckstrin homology domain within the F2 subdomain, and also binds to the β subunit to promote inside-out signalling (**B**). Following activation via kindlin and talin, a conformational change in the integrin receptor results in a high affinity for ligand binding. Figure adapted from Moser *et al.,* 2009.

Like talin, kindlin contains a FERM domain that binds the integrin β subunit to promote integrin activation (Figure 1.6, B) (Rogalski *et al.,* 2000) which modulates the actin cytoskeleton indirectly by interacting with linking kinases including integrin-linked kinase (Fukuda *et al.,* 2014). There are three kindlin isoforms, -1, -2 and -3, however it is the effect of kindlin-1 on integrin activation to promote axonal regeneration which has most appeal. For example, overexpression of kindlin-1 in sensory neurons can enhance axonal growth in the presence of inhibitory CSPG proteins *in vitro*, but overexpression of kindlin-2 cannot (Tan *et al.,* 2012). Further to this, activation of exogenously expressed integrins alongside kindlin-1 can promote sensory axon recovery through integrin-mediated signalling after dorsal root crush in adult rats (Cheah *et al.,* 2016). Unfortunately, kindlin-1 is not expressed within the mammalian CNS (Ussar *et al.,* 2006; Tan *et al.,* 2012) and therefore presents a further obstacle for repair of the CNS after injury.

As integrins are involved in cell adhesion and cell-cell interactions they are recruited to nascent adhesion sites. This is a process called integrin clustering, which has recently been discovered to be mediated by talin and focal adhesion kinase (FAK), a scaffolding protein, which together form a protein complex (Reviewed in Calderwood, 2004; Wegener *et al.,* 2007; Zhang *et al.,* 2008; Reviewed in Myers *et al.,* 2011). This complex interacts with integrins and as more integrins cluster at the membrane, more cytoskeletal components, such as actin, are recruited to the membrane resulting in dynamic changes to the cytoskeleton. In this way, cells are able to respond to the ECM by extending integrin-containing filopodia allowing movement of the cell. FAK can form other protein complexes within nascent adhesions including Src tyrosine kinase (Schaller *et al.,* 1994) and paxillin, a focal adhesion-associated signalling protein, to promote and regulate cytoskeleton assembly and cell protrusion (Choi *et al.,* 2011).

As a result of integrin activation and outside-in signalling, a number of intracellular pathways can be activated including PI3-K, Src kinase and MAP kinase resulting in modulation of the cytoskeleton and cell adhesion and growth (Reviewd in Jones and Walker, 1999; Reviewed in Moreno-Layseca and Streuli, 2014). Furthermore, integrins can also promote cell proliferation through activation of cyclin-dependent kinases (Cdks), specifically Cdk4/6 and Cdk2, which are involved in advancement of the cell cycle beyond G1 (Reviewed in Schwartz and Assoian, 2001). Further

downstream effectors include Rho GTPases which have been implicated in cell migration and adhesion (Reviewed in Schwartz and Shattil, 2000) as well as axonal outgrowth and regeneration. Specifically, inhibition of Rho GTPases results in increased axon outgrowth (Lehmann *et al.,* 1999; Dergham *et al.,* 2002; Winton *et al.,* 2002; Hiraga *et al.,* 2006). For example, Rho inhibition in cultured rat pheochromocytoma-12 (PC12) cells (Lehmann *et al.,* 1999) and in cultured primary cortical neurons (Dergham *et al.,* 2002) promoted neurite extension when cultured on an inhibitory myelin substrate. Similarly *in vivo*, inhibition of Rho prompted regrowth of axons within the injured optic nerve in adult rats (Lehmann *et al.,* 1999) and in CST axons after thoracic spinal cord lesion in mice (Dergham *et al.,* 2002).

In order for cells to respond to the ECM, integrins embedded within the cell membrane must be internalised and trafficked to newly forming sites of adhesion (Roberts *et al.,* 2001; Woods *et al.,* 2004). These receptors are recycled via endocytosis controlling the expression of integrins at the cell membrane (Reviewed in Bridgewater *et al.,* 2012; Reviewed in Paul *et al.,* 2015), yet the causative and underlying processes that govern integrin recycling are not fully understood. For this reason, the endocytic pathway is of great interest as changes in the recycling and trafficking of integrins will directly alter cell growth and motility. Research has shown integrins can be internalised by both clathrin-dependent and clathrin-independent mechanisms (Reviewed in Paul *et al.,* 2015), and active and inactive integrins are recycled through short- and fast-loop pathways respectively (Arjonen *et al.,* 2012). Specifically, integrin recycling and trafficking is mediated via small GTPases, including Rab and Arf (Dunphy *et al.,* 2006; Eva *et al.,* 2012; Mendoza *et al.,* 2013; Chen *et al.,* 2014). Integrins expressed on the cell membrane are internalised into early endosomes where they either follow a short-loop recycling pathway, mediated by Rab4, which involves direct transport of the integrin back to the cell membrane, or a long-loop recycling pathway, mediated by Rab11 and Arf6, which involves transport of the integrin to the perinuclear recycling compartment before transport back to the cell membrane (Reviewed in Caswell and Norman, 2006). In this way, integrins can mediate a rapid response to the ECM resulting in cell motility and migration.

1.2.3 Integrins and CNS regeneration

As discussed earlier, integrin expression within the mammalian CNS is high during embryogenesis and development, resulting in proliferation, synaptogenesis, axonal elongation, axonal guidance and neuroplasticity. However, as the CNS matures, a number of integrin subunits are downregulated resulting in reduced ability for axonal growth (Condic, 2001). This change in integrin expression is thought to be an important contributing intrinsic factor in the prevention of CNS regeneration after axonal injury and there is now a large body of research highlighting the use of integrins in promoting CNS regeneration (Werner *et al.,* 2000; Ekström *et al.,* 2003; Gardiner *et al.,* 2005; Andrews *et al.,* 2009; Tonge *et al.,* 2012; Cheah *et al.,* 2016). After injury in the PNS, integrin subunits are upregulated in both sensory (Ekstrom *et al.,* 2003; Gardiner *et al.,* 2005) and motor (Werner *et al.,* 2000) neurons. Yet the same compensatory mechanism of integrin expression is not mimicked in the mature CNS after injury.

Increasing integrin expression after injury presents a number of benefits, as not only are integrins linked to increased cell survival (Reviewed in Vachon, 2011), their increased expression has been linked to increased growth cone formation and regeneration within the PNS (Reviewed in Previtali *et al.,* 2001). Furthermore, integrins have the ability to interact with the inhibitory components of the lesion site, specifically CSPGs and TN-C. For example, in the presence of CSPGs, immature neonatal, but not mature adult, CNS axons have the ability to extend neurites (Condic, 2001; Blackmore and Letourneau, 2006). This greater regenerative ability is thought to be due to the high expression of integrins within immature CNS neurons. In fact, embryonic neurons have the ability to upregulate integrin expression in the presence of inhibitory stimuli, including the CSPG, aggrecan, whereas mature neurons do not (Condic *et al.,* 1999). However, if integrin heterodimers, such as α1β1 and α5β1, are overexpressed using exogenous gene transfer, neurite outgrowth from adult DRG neurons successfully occurs in the presence of CSPGs, producing outgrowth similar to that of embryonic neurons (Condic, 2001).

During development, neurons have high levels of cAMP that are reduced upon maturation (Cai *et al.,* 2001). Furthermore, there is a large body of research showing

integrin activation and intracellular cAMP levels can greatly alter growth cone motility and neurite extension. For example, when embryonic chick DRGs are cultured on low levels of laminin, basal integrin activation suppresses cAMP activity, which in turn facilitates Rho-GTPase-mediated growth cone motility. If integrins are activated (using Mn^{2+}) or intracellular cAMP levels are increased (with Sp-cAMP, a cAMP analog) Rho-GTPase-mediated growth cone motility is also increased. However, if both are increased at the same time, integrin subunits are internalised which results in subsequent growth cone collapse (Lemons and Condic, 2006). Furthermore, this interaction is dependent upon the cell substrate as this outcome was only observed when cells were cultured on low concentrations, but not high concentrations of laminin or fibronectin (Lemons and Condic, 2006). In line with this and as discussed in section 1.1.3.3, after injury a number of inhibitory proteins are upregulated after injury, such as Nogo-A, resulting in growth cone collapse (Joset *et al.,* 2010) however reintroduction of cAMP has shown to have significant potential for stimulating neurite outgrowth in dorsal column axon (Qiu *et al.,* 2002) and DRGs (Joset *et al.,* 2010).

To add to this complex issue, after axonal injury, there are a number of upregulated inhibitory proteins that can interfere with and inhibit integrin signalling preventing neurite outgrowth, including CSPGs (Tan *et al.,* 2011) and myelin-associated proteins (Hu and Strittmatter, 2008). For example, Nogo-A signalling, and specifically the N-terminal domain, amino-Nogo, can prevent integrin-mediated neurite outgrowth within COS-7 cells when cultured on fibronectin substrate *in vitro* (Hu and Strittmatter, 2008). However, this inhibition from amino-Nogo appears to be selective for specific integrin heterodimers including α4β1, α5β1, and αvβ3. Increasing activation of integrin subunits, such as β1, using Mn^{2+}, selective activating antibodies or integrin activators such as kindlin-1, can overcome Nogo- or CSPG-mediated inhibitory signalling (Hu and Strittmatter, 2008; Tan *et al.,* 2011; Cheah *et al.,* 2016). This suggests that if integrin expression were increased after CNS injury, they would also need be activated to allow them to overcome the inhibitory environment.

Furthermore, recent research has suggested the trafficking of integrin subunits, such as the α6, α9 and β1 subunits, within the adult CNS can be both age and region dependent with integrin transport restricted in adult CST and rubrospinal tract axons (Andrews *et al.,* 2016). This is in contrast to the free movement of integrins in

embryonic CST axons and adult sensory and DRG axons (Andrews *et al.,* 2016). As discussed earlier, trafficking of integrins is mediated by small GTPases. Specifically *in vitro* studies have shown that within the axons of the mature CNS, integrins are transported back to the cell soma via the GTPase Arf6 (Franssen *et al.,* 2015), yet modulation of Rab11/Arf6 coupling, specifically Arf6 inactivation, can reinstate integrin trafficking in the anterograde direction in primary cortical neurons *in vitro* (Franssen *et al.,* 2015). Furthermore, the axon initial segment (AIS) acts as a barrier of integrin transport within mature CNS axons, yet disruption of ankyrin-G within the AIS, restores integrin anterograde trafficking (Franssen *et al.,* 2015). The reason for this exclusion of integrins in mature CNS axons is not fully understood, however it is widely accepted to be an evolutionary trait. As the mammalian CNS matures, it no longer requires widespread expression of growth-promoting proteins and therefore they are downregulated and trafficked out of axons back to the cell soma. It seems that even though increasing integrin expression can promote neurite outgrowth, there are both regional and age-dependent differences in the trafficking of integrins into the axonal compartment presenting a further complication for repair of the CNS.

1.2.4 TN-C signalling through the α9β1 integrin heterodimer

A number of downregulated integrin subunits have been researched for their ability to induce neurite outgrowth and axonal regeneration including α1 (Condic, 2001); α4 (Vogelezang *et al.,* 2001), α5 (Condic, 2001; Tonge *et al.,* 2012) and α9 (Andrews *et al.,* 2009). Of particular interest is the capacity of integrins to interact with components of the lesioned environment and specifically the ability of the α9β1 heterodimer to promote neurite outgrowth when bound to the glycoprotein TN-C (Andrews *et al.,* 2009).

1.2.4.1 TN-C

As discussed earlier, TN-C is one of the main ECM constituents of the CNS highly expressed during embryonic and neonatal development (Götz *et al.,* 1997; Schweitzer *et al.,* 2005). It is secreted by astrocytes and radial glial cells and is one of the growth-promoting proteins associated with growth cone formation within the developing cerebral cortex (Götz *et al.,* 1997), with fibronectin (Sheppard *et al.,* 1991) and proteoglycans (Bignami *et al.,* 1992) also being implicated in this process.

Additionally, it is also highly upregulated after CNS injury as it is secreted mainly by reactive astrocytes into the lesion site and surrounding area (Zhang *et al.,* 1997; Tang *et al.,* 2003; Andrews *et al.,* 2009).

Four tenascin isoforms have been identified including, TN-C, TN-R, TN-X and TN-W, which differ in the number of epidermal growth factor-like (EGF-L) repeats and fibronectin type III (FNIII) domains they contain (Figure 1.7). The first isoform characterised was TN-C, which has nine different splice variants identified in humans (A1, A2, A3, A4, B, AD1, AD2, C and D) (Reviewed in Joester and Faissner, 2001). The TN-C protein is comprised of six protein monomers linked by disulphide bridges, forming a hexameric protein structure (Figure 1.7, A). Each monomer comprises a tenascin assembly (TA) domain/cysteine-rich heptad repeats, EGF-L repeats, FNIII domains and a fibrinogen (FG) globe located on the C-terminus (Figure 1.7, B).

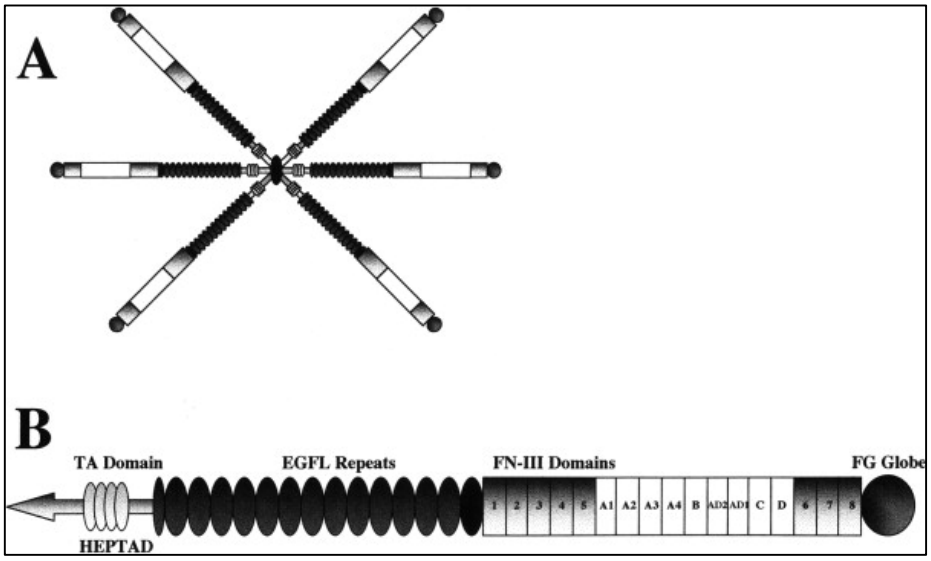

Figure 1.7 Structure of TN-C. TN-C structure forms a hexabrachion, consisting of six protein monomers joined by disulphide bridges (**A**). Each monomer contains a TA domain/cysteine-rich heptad repeats, EGF-L repeats, FNIII domains and a FG globe located on the C-terminal (**B**). The FNIII domains can give rise to nine different splice variants; A1, A2, A3, A4, B, AD1, AD2, C and D. Figure modified from Jones and Jones, 2000.

TN-C, located on chromosome nine in humans, is expressed within most tissues, including the brain, during embryonic and neonatal development (Bartsch *et al.,* 1992b; Götz *et al.,* 1997; Schweitzer *et al.,* 2005); however, within the brain

expression rapidly decreases with age (Bartsch *et al.,* 1992a). During post-natal development in the somatosensory cortex, TN expression in deep layers five and six is reduced before upper layers with all TN expression diminished after postnatal day 15 (Mitrovic *et al.,* 1994). However, some regions of the adult brain are reported to maintain a basal expression of TN-C including the olfactory bulb, retina, and areas of the cerebellum (Bartsch *et al.,* 1992a, 1992b; Miragall and Dermietzel, 1992; Bartsch *et al.,* 1994).

From KO mouse studies, research has shown TN-C is important for development and structure of the somatosensory and motor cortices (Irintchev *et al.,* 2005). For example, cell densities within TN-C KO mice differed and although they displayed less GABAergic parvalbumin interneurons, overall KO mice had a larger proportion of neurons and astrocytes than controls. Furthermore, they also displayed aberrant dendritic morphology from pyramidal neurons in the motor and somatosensory cortices compared to control mice. Likewise, TN-C KO mice showed increased firing within the somatosensory cortex, likely due to the reduced inhibitory input from parvalbumin interneurons (Irintchev *et al.,* 2005). With help from KO studies, the role of TN-C in neuronal plasticity has become clearer over the past decade, highlighting the contribution of TN-C in regulation of L-type voltage-gated channels to modify synaptic plasticity (Evers *et al.,* 2002) and hippocampal learning and plasticity (Strekalova *et al.,* 2002). Many of these contributions could potentially be explained by TN-C binding to integrins and subsequent ion channel activity via intracellular signalling (Gall *et al.,* 2003).

Research has shown TN-C can bind to two specific integrin receptors, α7β1 (Mercado *et al.,* 2004) and α9β1 (Yokosaki *et al.,* 1994) to promote neurite outgrowth. Specifically, α9β1 binds to the third FNIII repeat on TN-C (Yokosaki *et al.,* 1994) via a specific three amino acid motif arginine-alanine-alanine (RAA) (Yokosaki *et al.,* 1998). This is unique as integrins commonly bind to a ligand recognition site containing the amino acid sequence, RGD (Reviewed in Hynes, 1987). TN-C can also induce neurite outgrowth by binding to other receptors including contactin, belonging to the immunoglobulin family (Rigato *et al.,* 2002; Michele and Faissner, 2009). However, because α9 integrin when bound to β1 can interact with the inhibitory components of the lesioned CNS environment, specifically TN-C, to promote neurite

outgrowth, its expression and regulation is a promising area of research for axonal regeneration.

1.2.4.2 The α9β1 integrin heterodimer

The α9 subunit binds non-covalently with the β1 integrin subunit, forming the α9β1 heterodimer (Palmer *et al.,* 1993). The heterodimer is expressed in many mammalian cells including endothelial cells, muscle cells, and neutrophils (Palmer *et al.,* 1993; Tarui *et al.,* 2001; Vlahakis *et al.,* 2005; Staniszewska *et al.,* 2007). This expansive tissue expression profile may explain why this heterodimer can bind a diverse range of ligands including NGF, vascular adhesion molecule 1, osteopontin, thrombospondin, vascular endothelial growth factor, and TN-C (Smith *et al.,* 1996; Yokosaki *et al.,* 1998; Taooka *et al.,* 1999; Vlahakis *et al.,* 2005; Staniszewska *et al.,* 2007, 2008). It has also been implicated in a number of diseases including angiogenesis (Vlahakis *et al.,* 2007), respiratory failure (Huang *et al.,* 2000) and granulopoiesis (Chen *et al.,* 2006).

In contrast to β1, which has many binding partners, the α9 subunit only binds to the β1 subunit (Figure 1.3). The α9 integrin subunit is highly expressed during embryonic and neonatal development (Cohen *et al.,* 1986; Lefcort *et al.,* 1992; Condic, 2001) and is developmentally downregulated in the adult CNS. The α9 subunit is comprised of 1,006 amino acids, which is split into an extracellular domain (947 amino acids), transmembrane domain (26 amino acids) and an intracellular domain (33 amino acids) (Palmer *et al.,* 1993). Even though the α9 integrin intracellular domain is short in comparison to the extracellular domain, it is reportedly required for activation and associates with a number of intracellular signalling proteins including Src tyrosine kinase, inducible nitric oxide synthase (Gupta and Vlahakis, 2009), FAK, the adaptor protein p130Cas and Rho GTPases, including Rac1 (Gupta and Vlahakis, 2009).

Upon TN-C binding to α9β1 integrin, it can promote cell migration, but this is dependent upon the adaptor protein, paxillin, binding to the α9 cytoplasmic domain (Young *et al.,* 2001). Paxillin is a focal adhesion-associated signalling protein which links the integrin subunit with the cell cytoskeleton and other focal adhesion proteins including FAK and vinculin which further promotes binding of talin and actin to promote cell motility (discussed in section 1.2.2).

In summary, within the adult CNS the expression of α9β1 integrin subunit is developmentally downregulated. This integrin receptor however can modulate cell cytoskeleton activity to produce neurite outgrowth when bound to TN-C which is upregulated after injury. Increasing expression of α9β1 *in vitro* and indeed in DRG neurons *in vivo* can promote regeneration and neurite outgrowth. However, in an SCI environment where TN-C is upregulated, the α9β1 integrin subunit is not transported down axons of the adult CST (Andrews *et al.,* 2016). This is thought to be due to reduced anterograde trafficking from small GTPases (Franssen *et al.,* 2015; Andrews *et al.,* 2016). Furthermore, inhibitory proteins at the lesion site inactivate integrins, yet research has shown that activation of integrins can overcome this. For the α9β1 integrin to promote regeneration of the CST, it must firstly be expressed at or transported to the lesioned environment to interact with the upregulated TN-C and promote regrowth through the glial scar, whether that be by modulation of intrinsic signalling pathways, such as inactivation of Arf6 (Franssen *et al.,* 2015) or use of cell transplantation, such as neural progenitor cells (NPCs). Yet as the literature has demonstrated, this is only the first step, and it is likely further modification will be required, such as integrin activation or ECM inhibition, to enable α9β1 integrin expression to remain present and activated at the lesion site to stimulate recovery.

1.3 Cell transplantation

1.3.1 General background on cell transplantation after CNS injury

Currents treatments for SCI are limited, however current research has offered up many potential therapies in the field of cell transplantation. Cell replacement is now widely accepted as a promising tool to help promote repair within the injured CNS. By replacing cells that have been lost or damaged due to an injury, there is hope cell transplants can aid axonal repair, regrowth, guidance, axonal sprouting, plasticity as well as stimulate remyelination. Following research, a number of cell types have been identified as potential candidates for cell replacement, each targeting a different aspect of SCI pathophysiology. These include oligodendrocyte precursor cells (OPCs), SCs, olfactory ensheathing cells (OECs), astrocytes, mesenchymal stem/stromal cells (MSCs), and neural stem and progenitor cells (NSPCs) (Reviewed in Tetzlaff *et al.,* 2011).

Primarily, research has focused on physiological and functional outcomes following *in vivo* cell transplantation for SCI. These include cell survival, functional integration, migration, growth-promoting properties, and evidence of restoration in sensory, motor or autonomic function. The question remains as to how transplanted cells promote regeneration. The answer to this lies in the number of downstream effects occurring after cell transplantation including neurotrophin secretion, modulation of the immune response, axonal sprouting, enhancement of axonal guidance and restoration of myelination. Early clinical trial data has shown promising results for cell transplantation, including OECs and SCs, in SCI (Féron *et al.,* 2005; Mackay-Sim *et al.,* 2008; Saberi *et al.,* 2011; Tabakow *et al.,* 2013). Furthermore, tissue grafts have also been trialled in rat SCI models for CNS repair for example grafts of human embryonic spinal cord into immunodeficient rats with acute or chronic SCI (Wictorin and Björklund, 1992; Akesson *et al.,* 2001) and although grafts can extend both caudally and rostrally from the lesion site, no significant functional improvements were demonstrated in these studies.

Cell transplants can be autologous, allogenic or xenogeneic. Autologous transplantation takes cells from one individual to be transplanted into the same individual, i.e. the host and donor are the same, negating the need for immunosuppression and hopefully reducing the likelihood of immune-mediated rejection. An allogenic transplant is where the recipient receives donor cells from the same species but the donor is not genetically identical to the host. This is the most common type of transplant in humans and requires immunosuppression. A xenograft is transplantation of cells from one species to a different species, for example transplant of human cells into a rat model, where immunosuppression is required to prevent graft rejection.

1.3.2 The immune response following cell transplantation after CNS injury

Following xenogeneic transplant, a host immune response is elicited against the donor cells. This largely consists of an upregulation of activated microglia and astrocytes, proliferation of activated T-cells and potential for infiltrating lymphocytes. Alongside this a vast number of chemokines and cytokines are secreted from these cells which further add to the inflammatory cascade (Reviewed in Hoornaert *et al.,* 2017). This results in reduced graft survival and therefore immunosuppressant drugs are often used to prolong transplant survival. Alternatively, research studies may use neonatal transplant models to avoid immune-mediated rejection of transplants (Ideguchi *et al.,* 2010; Mattis *et al.,* 2014).

Research has shown transplantation of some cell types can actually modulate the host immune response and promote a pro-regenerative environment. For example, grafted mouse NPCs into the mouse spinal cord after either subacute or early chronic thoracic injury promoted a pro-regenerative environment by reducing the activation of pro-inflammatory M1 macrophages and increasing the expression of regenerative genes including *Nos2* (Cusimano *et al.,* 2012). Even though only 10% of grafted cells survived 6 weeks post-transplant, the NPCs remained undifferentiated and clustered around the injury site, but were able to promote remyelination and functional recovery after subacute, but not chronic thoracic injury. Furthermore, this study identified a therapeutic window of opportunity for repair after less severe subacute injury as cells

were transplanted either 7 or 21 days post subacute injury with functional recovery only observed following the former. These results suggest that firstly, the type of cell used in transplantation studies may be a large factor in repair after SCI where certain cell types, such as NPCs, producing dual effects, such as stimulating remyelination as well as altering the immune response. Secondly, cell transplantation alone may not be able to promote functional recovery in more chronic injuries which likely requires further pharmacological intervention.

One alternative to transplanting cells is to transplant the conditioned medium, which can contain secreted neurotrophins (Cantinieaux *et al.,* 2013). Conditioned medium from bone marrow-derived MSCs promoted functional recovery of motor skills just 4 days after thoracic contusion injury in the adult rat reducing the likelihood of cell rejection. Furthermore, these functional improvements are comparable to bone marrow-derived MSC grafts after spinal contusion (Karaoz *et al.,* 2012) providing support for the beneficial effects of secreted neurotrophic factors in regeneration. Although this method of treatment resulted in no changes in gliosis or axonal regeneration when compared to controls, it did reduce neuronal apoptosis, increased angiogenesis and reduced the size of the lesion site, thereby promoting a pro-regenerative environment. Similarly, conditioned media containing exosomes, such as those from primary rat SC-derived exosomes, can promote neurite outgrowth in rat mechanically-injured DRG explant cultures *in vitro* and stimulate regeneration of the rat sciatic nerve after a crush injury *in vivo* (Lopez-Verrilli *et al.,* 2013). These mechanisms provide potential cell-free alternatives for bypassing the immune response to enable repair after injury.

1.3.3 Types of cells used in transplant for research of SCI

1.3.3.1 Transplant of oligodendrocytes and SCs after SCI

One of the main issues preventing regeneration after injury is the distinctive and drastic demyelination and Wallerian degeneration of severed or injured axons (Totoiu and Keirstead, 2005). Promoting remyelination by transplanting cell types, such as oligodendrocytes and SCs, is one of the main goals of cell replacement therapy for SCI. Oligodendrocytes are the main myelinating cell of the CNS and transplants of OPCs can promote remyelination after CNS and spinal injury (Bambakidis and Miller,

2004; Cao *et al.,* 2010; Chen *et al.,* 2015; Sun *et al.,* 2013). For example, following contusion of the thoracic spinal cord in adult rats, transplant of adult OPCs expressing ciliary neurotrophic factor (CNTF), which supports the survival and generation of oligodendrocytes (Barres *et al.,* 1993, 1996), differentiated into oligodendrocytes *in vivo* and promoted remyelination which resulted in recovery of hindlimb function when assessed using the Basso, Beattie, Bresnahan (BBB) locomotor scale after injury (Cao *et al.,* 2010). Similarly, mouse embryonic stem cell (ESC)-derived OPC grafts promoted remyelination and functional recovery following radiation-induced SCI in adult rats (Sun *et al.,* 2013) and hypoxic-induced brain injury in neonatal rats (Chen *et al.,* 2015), thus exhibiting pro-regenerative effects across a wide range of CNS injuries.

Unlike, the CNS, the PNS has an intrinsic capacity to regenerate after injury, in part owing to the presence of SCs (Reviewed in Jessen and Mirsky, 2016), the myelinating cells of the PNS. The ability for SCs to promote remyelination of the CNS was discovered in the early 1980s (Duncan *et al.,* 1981) and since then SC transplantation has been of great interest in the field of SCI repair. Research shows SC grafts can prompt axonal remyelination, improve conductance and enhance repair in the CNS after injury (Honmou *et al.,* 1996; Xu *et al.,* 1997; Kohama *et al.,* 2001; Takami *et al.,* 2002; Pearse *et al.,* 2004; Sparling *et al.,* 2015). Furthermore, SC grafts alone can promote functional repair of hindlimb movements, assessed using the BBB locomotor scale (Takami *et al.,* 2002). Literature suggests SCs may have better functional outcomes when used as a co-treatment, for example with cAMP or matrices (Pearse *et al.,* 2004; Hurtado *et al.,* 2006; Pearse *et al*., 2007). Transplant of SCs alone show that, although regeneration can occur, it is restricted and does not go much further than the lesion site (Montgomery *et al.,* 1996; Shields *et al.,* 2000) as transplanted SCs do not migrate out of the glial scar (Andrews and Stelzner, 2007). In contrast, after SCI endogenous SCs migrate long distances to invade the lesion site to aid axonal repair and remyelination (Guest *et al.,* 2005; Reviewed by Zhang *et al.,* 2013). This process of migration can also be enhanced using transplant of other cell types, including exogenous SCs and OECs (Ramer *et al.,* 2004; Zhang *et al.,* 2013). This body of research formed the basis for the start of clinical trials using SC grafts for SCI treatment (Saberi *et al.,* 2011).

1.3.3.2 Transplant of OECs after SCI

OECs are located within the olfactory bulb and olfactory mucosa working to aid guidance and elongation of olfactory axons going from the PNS to the CNS (Graziadei and Graziadei, 1979; Doucette, 1991). Similar to SCs, OECs have the ability to promote regeneration of PNS axons and therefore their ability to promote regeneration of the CNS has also been investigated (Ramón-Cueto and Nieto-Sampedro, 1994; Li *et al.,* 1997; Ramón-Cueto *et al.,* 1998; Reviewed in Mackay-Sim and St John, 2011). Regenerative characteristics of OECs include secretion of neurotrophins, including NGF and BDNF (Woodhall *et al.,* 2001; Lipson *et al.,* 2003), expression of adhesion proteins, including neural cell adhesion molecule (NCAM) (Miragall *et al.,* 1988) and secretion of laminin, known for its axonal guidance and outgrowth properties (Ramón-Cueto and Nieto-Sampedro, 1992). Research has shown OEC grafts are able to promote physiological axonal regeneration after crush of the dorsolateral funiculus within the adult rat cervical spinal cord shown by increased sprouting into the lesion site and reduction of reactive astrocytes around the lesion (Ramer *et al.,* 2004). This result may have been enhanced by the ability of OECs to stimulate endogenous SC infiltration to the injury site (Ramer *et al.,* 2004; Zhang *et al.,* 2013), further adding to the pro-regenerative environment.

Research has suggested functional recovery after OEC grafts in SCI models can be limited. For example, following transplant of OECs into an adult rat thoracic contusion SCI model, no hindlimb functional recovery was observed following assessment using the BBB locomotor scale (Takami *et al.,* 2002). In contrast, OEC grafts in combination with rehabilitation involving treadmill step training were able to promote hindlimb functional regeneration after complete thoracic transection in adult rats (Kubasak *et al.,* 2008). Recent encouraging research in humans has demonstrated OEC transplants can induce functional movements in a previously paraplegic individual following transplant into the injured thoracic spinal cord (Tabakow *et al.,* 2014). The autologous OEC graft also contained olfactory nerve fibroblasts and was combined with a peripheral nerve graft alongside rigorous physical rehabilitation. As a result, the patient's sensory, motor and autonomic function improved, progressing from Grade A to Grade C on the American Spinal Injury Association (ASIA) impairment scale with the patient showing an increase in muscle mass within the left thigh, return of reflex

activity within the Achilles tendon and an increase in bladder sensation (Tabakow *et al.,* 2014).

1.3.3.3 Transplant of astrocytes after SCI

Astrocytes are known to have a crucial support role within the CNS, including metabolic support (Reviewed in Magistretti, 2011; Suzuki *et al.,* 2011), promotion of synaptogenesis (Ullian *et al.,* 2001, 2004; Christopherson *et al.,* 2005) and secretion of neurotrophic factors (Bozoyan *et al.,* 2012). However due to the understanding that reactive astrocytes are associated with inhibition of SCI regeneration, it is only in recent years that the regenerative potential of glial support cells, such as astrocytes, has been discovered with research now showing astrocyte grafts can promote repair of injured axons after SCI (Davies *et al.,* 2006; Filous *et al.,* 2010; Fan *et al.,* 2012; Haas and Fischer, 2013).

It has been suggested that immature glial-derived astrocytes hold a better regenerative capacity compared to glial precursors (Davies *et al.,* 2006) or mature astrocytes (Filous *et al.,* 2010). This may be due to the ability of immature astrocytes to overcome a CSPG-rich barrier *in vitro* (Filous *et al.,* 2010). In addition, the methods used for differentiation of astrocytes from precursor cells, such as bone morphogenetic protein (BMP) and CNTF, can affect their regenerative ability, with transplant of BMP-differentiated astrocytes resulting in better functional recovery after SCI (Davies *et al.,* 2008, 2011). Specifically, rats that received a graft of BMP-differentiated immature astrocytes improved faster when subjected to a grid-walk test compared to those that received a CNTF-differentiated astrocyte graft or a glial progenitor cell graft, promoting a discernible difference in behavioural recovery following unilateral transection of the dorsolateral funiculus (Davies *et al.,* 2011). In contrast, subsequent research has shown transplant of human glial-restricted progenitors (hGRPs) from frozen stocks were compared to transplants of hGRP-derived astrocytes into cervical dorsal column lesion of adult rats (Haas and Fischer, 2013). Results show both have equal ability to promote axonal regeneration indicating hGRPs may not require *in vitro* differentiation before transplant. Furthermore, because these cells were from frozen stocks, this reduced the *in vitro* culture time for these cells before transplant and increases their potential for clinical application, however the full extent of their regenerative capacity has yet to be examined.

Astrocytes express a lower level of inhibitory CSPGs and a higher level of glial cell-derived neurotrophic factor (GDNF) than other astrocyte subsets and other populations of glial precursor cells. This suggests astrocytes have an endogenous pro-regenerative capacity to survive in an inhibitory environment highlighting their potential for transplantation to promote repair after SCI (Davies *et al.,* 2011). However, what is now also becoming clear is that grafted cells do not need to survive to promote a regenerative effect on the CNS. Davies and colleagues have also shown that the neuroprotective effects of transplanted astrocytes into the injured CNS outlast survival of the grafts (Davies *et al.,* 2011) questioning the survival requirement of grafted cells.

1.3.3.4 Transplant of MSCs after SCI

Mesenchymal stem/stromal cells (MSCs), isolated from a number of sources, such as human bone marrow and adipose tissue, can be expanded in culture and differentiated into a variety of cell types including neuronal and glial cells (Sanchez-Ramos *et al.,* 2000; Woodbury *et al.,* 2000; Kim *et al.,* 2006; Radtke *et al.,* 2009; Bae *et al.,* 2011; Ma *et al.,* 2011). MSCs have been researched for their use in regeneration for a number of different CNS conditions including multiple sclerosis (Yamout *et al.,* 2010), Parkinson's disease (Venkataramana *et al.,* 2010) and SCI (Neuhuber *et al.,* 2005; Cízková *et al.,* 2006; Jung *et al.,* 2009; Pal *et al.,* 2009; Osaka *et al.,* 2010; Xiong *et al.,* 2017).

How MSCs promote regeneration is not completely understood, however, research has shown MSC transplants can reduce the inflammatory response following ischaemic injury in mice (Ohtaki *et al.,* 2008) and at the injury site following contusion SCI in rats (Abrams *et al.,* 2009). Furthermore, intravenous injection of MSCs can reduce lesion size and increase expression of neurotrophins, such as BDNF, within the lesion site following thoracic contusion SCI in rats (Osaka *et al.,* 2010), which is known to promote CST recovery after SCI (Jakeman *et al.,* 1998; Sasaki *et al.,* 2009). In fact whilst in culture, human MSCs can secrete a number of other neurotrophins alongside BDNF including NGF, vascular endothelial growth factor and hepatocyte growth factor, potentially encouraging the creation of a permissive environment for axonal repair (Chen *et al.,* 2002). In addition, MSCs can promote angiogenesis after ischaemic injury (Toyama *et al.,* 2009), axonal sprouting in a rat stroke model (Shen *et al.,* 2006) and dorsal hemisection in a rat SCI model (Sasaki *et al.,* 2009).

Within the past decade clinical trial data has emerged for MSC use after SCI in human patients (Callera and do Nascimento, 2006; Yoon *et al.,* 2007; Saito *et al.,* 2008) and even though functional improvements were observed in patients with an acute SCI, no improvements were observed in those with a chronic SCI (Yoon *et al.,* 2007). One reason MSCs attract interest is because they can be used for autologous transplantation and therefore it is of great interest to explore their mechanisms and uses for regeneration after SCI as well as other neurologic conditions and diseases.

1.3.3.5 Transplant of NSPCs after SCI

NSPCs have the ability to self-renew and continuously proliferate until they differentiate into neuronal or glial cells. These attributes highlight the potential for their ability to promote regeneration after CNS injury where a number of different cell types are lost or injured. NSPCs can be either embryonic, active during embryogenesis and neurodevelopment, or adult, active in the certain areas of the mature CNS. The adult mammalian brain has a small proportion of NSPCs, located within the subventricular zones and the hippocampus (Reviewed in Ma *et al.,* 2009). In rodents, NSPCs have also been identified within the spinal cord (Johansson *et al.,* 1999; Horner *et al.,* 2000).

A large body of research has now shown transplantation of NSPCs promotes regeneration and functional recovery after SCI (Ogawa *et al.,* 2002; Cummings *et al.,* 2005; Karimi-Abdolrezaee *et al.,* 2006; Bonner *et al.,* 2011; Lu *et al.,* 2012b; Kadoya *et al.,* 2016). For example, following complete transection of the thoracic (T3) spinal cord in rats, grafted embryonic rat NSCs promoted recovery when embedded in a fibrin matrix alongside growth factors (Lu *et al.,* 2012b). Specifically, the grafted NSCs were able to project long-distances both caudal, reaching L1, and rostral to the lesion site, reaching C4, within the spinal cord. These projecting fibres were observed within host white matter tissue and were myelinated by rat host oligodendrocytes, likely leading to the enhanced electrophysiological recovery observed and improvements in hindlimb function assessed using the BBB open field locomotion test (Lu *et al.,* 2012b). Myelination of grafted mouse NSCs was also observed following transplant into a rat subacute SCI model, however this myelination was due to approximately 50% of mouse grafted cells differentiated into myelinating oligodendrocytes *in vivo* post-transplantation (Karimi-Abdolrezaee *et al.,* 2006), however this did result in functional

recovery when animals were assessed using grid-walking and footprint analysis. In contrast, myelination of transplanted rat NPCs has been supported by recent research showing 24% of axons extending from transplanted rat NPCs can become myelinated by host rat oligodendrocytes in rat models of cervical SCI (Hunt *et al.,* 2017). Interestingly, this myelination was dependent on the axon diameter, and in particular axons with a larger diameter were preferentially myelinated over smaller diameter axons (Hunt *et al.,* 2017). Together this research indicates host rat oligodendrocytes may be able to promote myelination of projections extending from rat, but not mouse NSPCs. If transplanted NPC-derived neurons within the injured spinal cord are to promote functional recovery, the ability of host oligodendrocytes to myelinate grafted axons will be important for long-term sustainable recovery.

The underlying mechanisms of NPC-induced regeneration, like many cell grafts, are largely unknown, however NPCs are able to promote neurotrophin release at the site of SCI (Hawryluk *et al.,* 2012), reduce lesion cavity size (Hong *et al.,* 2014), promote remyelination (Karimi-Abdolrezaee *et al.,* 2006) and modify the immune response (Cusimano *et al.,* 2012). However, the means by which NSPCs promote regeneration likely depends upon the differentiation status of the cells both before and after transplant. The differentiation status of NSPC transplants and the associated regenerative outcome has also come under debate with research suggesting NSCs must be differentiated into a neuronal lineage before transplantation to promote repair. NSCs transplanted into a contused thoracic (T8) rat spinal cord were restricted to a glial phenotype, while NSCs transplanted into an uninjured control favoured differentiation into a neuronal phenotype suggesting the inhibitory environment prevented the NSCs differentiation into a neuronal phenotype (Cao *et al.,* 2002). Indeed, research has shown transplanting a mixed population of neuronal-restricted progenitors (NRPs) and glial-restricted progenitors (GRPs) into a dorsal column lesion of the rat spinal cord, promoted formation of relay connections between grafted and host cells across the lesion site (Bonner *et al.,* 2011). Furthermore, this combination of cells was previously shown to overcome a CSPG-rich inhibitory environment to promote axon growth in hippocampal cultures (See *et al.,* 2010). However, in addition to their benefits, use of NSCs pose some challenging questions including their ability to form colonies elsewhere in the brain via migration and induce aberrant signalling

(Steward *et al.,* 2014). This research adds to the growing debate highlighting that if cell replacement and specifically replacement of neuronal connections is an aim of NSPC transplants after SCI, differentiating cells into a neuronal lineage before transplantation is of high importance.

1.3.4 Use of stem cells for CNS repair: ESCs vs iPSCs

First characterised almost 20 years ago (Thomson *et al.,* 1998), human embryonic stem cells (hESCs) start life within the inner mass of mammalian blastocysts (Figure 1.8). Blastocyst formation is an early stage of embryo development which has raised ethical concerns surrounding the use of hESCs in research. Because stem cells can differentiate into all three germ layers (Evans and Kaufman, 1981) and therefore any cell type, their therapeutic potential for modelling disease and replacing damaged cells is endless. However, because of the limitation of this cell source as well as the ethical issues surrounding ESC use, researchers sought alternative mechanisms and sources. A breakthrough came in 2006 which radically changed the field of stem cell research. This Nobel Prize winning work was carried out by John B. Gurdon and Shinya Yamanaka, who discovered that somatic cells could be dedifferentiated to a pluripotent state with expression of just four transcription factors, Oct3/4, Sox2, Klf-4 and C-Myc (Takahashi and Yamanaka, 2006; Takahashi *et al.,* 2007). Cells within this pluripotent state were then able to differentiate into any somatic cell and were therefore termed induced pluripotent stem cells (iPSCs). As with ESCs, iPSCs have self-renewal and proliferative properties, resulting in an endless supply of stem cells, which can be produced by dedifferentiating any somatic cell type, such as fibroblasts. The discovery of this groundbreaking technique has resulted in widespread use of iPSCs *in vitro,* analysing gene and protein expression, and also *in vivo*, examining their capabilities and functions in modelling and treatment of human diseases, with the eventual hope of personalised medicine. As a result, stem cell transplantation has become a viable possibility in the treatment of a wide range of CNS conditions and diseases, including Parkinson's disease, cancers, multiple sclerosis, Alzheimer's disease, stroke and SCI.

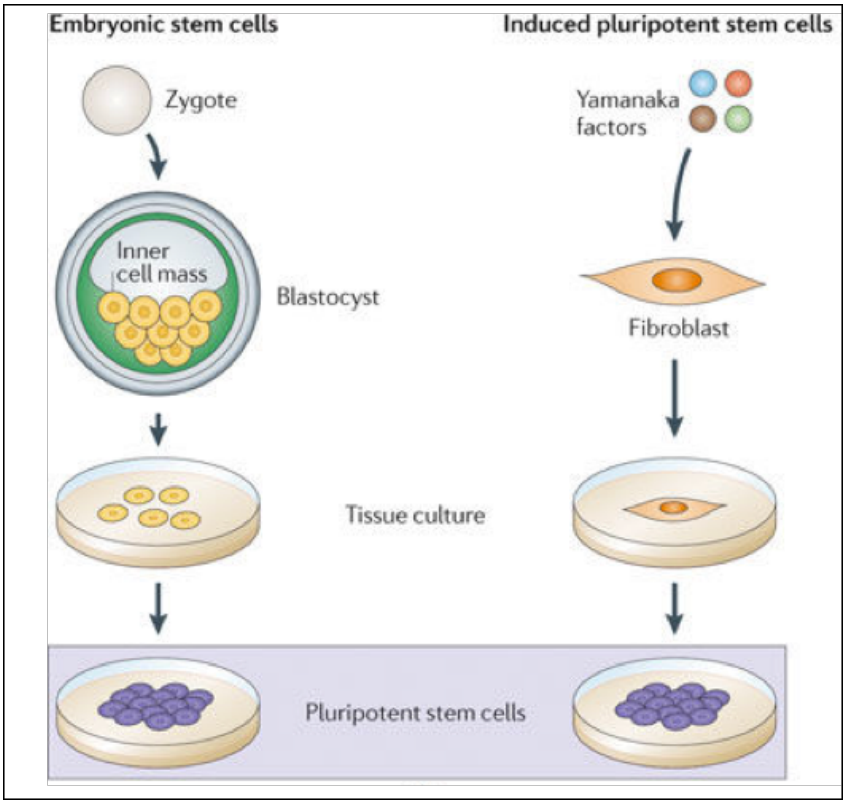

Figure 1.8. Differences in culture of ESCs and iPSCs. ESCs originate within the fertilised egg (a zygote), which develops into a ball of cells termed a blastocyst. The inner cell mass of the blastocyst contains pluripotent ESCs, which can be harvested for *in vitro* and *in vivo* experimentation. In contrast, iPSCs can be derived from any cell type, such as a fibroblast, which can be virally modified to express four transcription factors, (also termed Yamanka factors) including Oct3/4, Sox2, Klf4 and c-Myc. Once expressed, the fibroblast dedifferentiates into a pluripotent state comparable to the pluripotent state of ESCs. At this stage both ESCs and iPSCs can differentiate into any of the three germ layers, mesoderm, ectoderm or endoderm, and therefore any cell type within the body. Figure modified from Zhu *et al.*, 2011.

There is however concern that use of iPSC-derived cells are not equivalent to ESC-derived cells and cannot replace ESCs. While there are a number of aspects in which both ESCs and iPSCs are similar, including self-renewal, proliferative potential and morphology, there are also some distinct differences associated with genome integrity, gene expression and proliferative regulation (Baker *et al.,* 2007; Chin *et al.,* 2009; Mayshar *et al.,* 2010). As a result, questions remain about the therapeutic potential of iPSCs.

Specifically, the genomic integrity of iPSCs has come into question with research highlighting loss of genomic stability following both dedifferentiation and

differentiation (i.e. reprogramming) (Mayshar *et al.,* 2010). When stem cells are maintained in culture, they are exposed to a different environment than an *in vivo* environment and are kept in an unnatural proliferative state. Research has shown that over time this progressive selective pressure on iPSCs can introduce chromosomal abnormalities resulting in the cell adopting a continuous growth rate (Mayshar *et al.,* 2010). Karyotypic abnormalities have however been identified in both ESCs (Draper *et al.,* 2004; Baker *et al.,* 2007) and iPSCs (Kim *et al.,* 2009; Mayshar *et al.,* 2010) as a result of *in vitro* culture adaptation. Genomic aberrations have been identified in chromosome 1, chromosome 9 (Kim *et al.,* 2009) and chromosome 12 (Mayshar *et al.,* 2010) in iPSCs. Chromosome 9 has been linked with germ cell tumours (Reuter, 2005; Looijenga *et al.,* 2006), and abnormalities in chromosome 12, particularly trisomy, can result in upregulation of cell cycle-associated genes, as well as increased expression of pluripotency genes, such as *NANOG* and growth differentiation factor 3 (*GDF3*) (Mayshar *et al.,* 2010). Within ESCs, karyotypic abnormalities have also been identified in chromosome 12 (Draper *et al.,* 2004; Baker *et al.,* 2007), as well as chromosome 17 (Baker *et al.,* 2007; Mayshar *et al.,* 2010), which has been linked with cancers including neuroblastomas (Łastowska *et al.,* 2002) and breast cancer (Tirkkonen *et al.,* 1998). The abnormalities discussed could be due to a number of aspects of stem cell culture. Differences in oxygen concentration between *in vitro* and *in vivo* environments, which can result in abnormal shortening of telomeres (von Zglinicki *et al.,* 2000), or the enzymatic passaging of cells in bulk using trypsin, which can induce stress and result in chromosomal abnormalities in early cell passages (Mitalipova *et al.,* 2005). Together these results suggest both ESCs and iPSCs can contain aberrant karyotypes some of which may confer increased growth rate and tumorigenicity, all of which are important factors when considering stem cell transplantation.

Research has also shown that early-passage iPSCs have a different gene expression profile to ESCs, with iPSCs expressing more genes involved in differentiation compared to ESCs (Chin *et al.,* 2009). Furthermore, this distinct gene expression pattern was conserved between mouse and human iPSCs derived from a number of different cells types. Yet, with increased passage of iPSCs in culture, the gene expression profile becomes more similar to ESCs (Chin *et al.,* 2009). These karyotypic

changes result in either, potential changes in chromosomes involved in tumour formation, or increased cell cycle protein expression, resulting in uncontrollable proliferation, another major concern when using stem cells *in vivo*.

1.3.5 ESC and iPSC and cell derivatives in CNS transplantation

When considering stem cell-based therapies in humans, it is likely that stem cells or stem cell-derived cells will be either pre-differentiated, to reduce the presence of undifferentiated cells and minimise the risks associated with uncontrollable proliferation, or preconditioned *in vitro* prior to transplant to enhance the cells ability to survive *in vivo* (Reviewed in Khatiwala and Cai, 2016). The type of pre-conditioning is likely to vary depending on the cell type and the injury/disease for which the treatment is targeting, but could include prior differentiation into a specific cell lineage, such as neuronal or glial cell, or exposure to certain culture conditions, such as hypoxia to promote cell survival (Stacpoole *et al.,* 2011).

Nonetheless research has demonstrated successful transplantation of undifferentiated stem cells which differentiated after transplant *in vivo* with minimal karyotypic changes identified (Bjorklund *et al.,* 2002; Park *et al.,* 2005). Within the field of CNS injury, embryonic-derived cells have shown promise with the ability to differentiate into cortical neurons *in vitro* (Gaspard *et al.,* 2008) which functionally integrate into the host mouse brain after transplant (Espuny-Camacho *et al.,* 2013). Furthermore, research has demonstrated transplanted ESCs can differentiate *in vivo*, for example into dopaminergic neurons, when transplanted into the striatum of rodent models of Parkinson's disease (Bjorklund *et al.,* 2002; Park *et al.,* 2005). However, direct transplantation of undifferentiated stem cells is associated with risks, including tumour formation, and therefore for clinical application differentiation of stem cells prior to transplant will most likely be required. Indeed, ESCs have been successfully differentiated prior to transplantation into a number of cell types including OPCs and NPCs prior to transplant. For example, ESC-derived OPCs promoted remyelination and repair after SCI (Keirstead *et al.,* 2005; Sharp *et al.,* 2010) and ESC-derived NPCs injected into the deep layers of the mouse cerebral cortex were able to further differentiate *in vivo* into pyramidal neurons (Ideguchi *et al.,* 2010). Research has also shown that following transplantation of pre-differentiated neurons derived from ESCs

into the rat neonatal brain, donor axons are able to follow host white matter tracts (Denham *et al.,* 2012).

Similarly, research has demonstrated iPSC-derived cells are beneficial in animal models of CNS and spinal injury (Nori *et al.,* 2011; Tornero *et al.,* 2013; Lu *et al.,* 2014). Not only are iPSC-derived cortical neurons capable of forming functional synapses *in vitro* (Shi *et al.,* 2012a, 2012b), transplants of human iPSC-derived NPCs, which have been induced *in vitro* to develop into cortical neurons, can integrate within the injured cortex, promote recovery and restore function following stroke-induced injury in the rat somatosensory cortex (Tornero *et al.,* 2013). Tornero and colleagues also transplanted un-fated hiPSC-NPCs as a control into the same injury model. Following transplant analysis of both un-fated and fated hiPSC-NPCs at the graft site, results showed the number of un-fated cells was almost double that of cortically-fated cells at the graft site. This was due to a higher proportion of proliferative cells indicated by positive Ki67 expression within the un-fated cell graft. These results suggest that although no tumour formation was observed within this study, un-fated cells have a higher risk of tumour formation due to the increased proliferation rate and implies over time tumour formation may occur. Despite this reduction in the number of cortically fated cells, functional recovery of the forelimb was comparable between the two groups and while no functional differences were observed in regeneration, the fated cells were able to extend higher density projections within the host brain (Tornero *et al.,* 2013). Collectively these results suggest cortically-fated hiPSC-derived NPCs may be better suited to clinical applications than un-fated equivalents.

One of the main advantages iPSCs have over ESCs is their potential for autologous transplantation, thereby evading the host immune response, allowing for further graft integration. Other than skin fibroblasts, there are a number of different cell types being investigated for generation into iPSCs including keratinocytes, melanocytes, cord blood cells and adipose tissue-derived stem cells (Reviewed in Khazaei *et al.,* 2014). This type of personalised medicine is however both time-consuming and costly as cells would need to be tailor made to match the patient, so alternative easier methods for producing patient-specific cell types need to be found. One potential avenue may be the creation of iPSC banks which contain stem cells from donors screened for specific human leukocyte antigens which match a large percentage of the population

(Reviewed in Cyranoski, 2012; Baghbaderani *et al.,* 2015; Reviewed in Solomon *et al.,* 2015; Holmqvist *et al.,* 2016).

1.3.6 Transplantation of stem cell-derived NSPCs for repair of CST axons

One of the key pathways within the spinal cord which governs communication of both sensory and motor information between the brain and the rest of the body is the CST. This projects from the cerebral cortex through the brain and down the spinal cord (Figure 1.9). Research has shown CST axons have a reduced capacity to regenerate (discussed in section 1.1.4) compared to the reticulospinal, raphespinal and propriospinal tracts (Xu *et al.,* 1995; Vavrek *et al.,* 2007; Lu *et al.,* 2012a; Lee *et al.,* 2013). After injury there can be spontaneous sprouting and recovery of CST axons (Weidner *et al.,* 2001; Bareyre *et al.,* 2004), however functional recovery is limited.

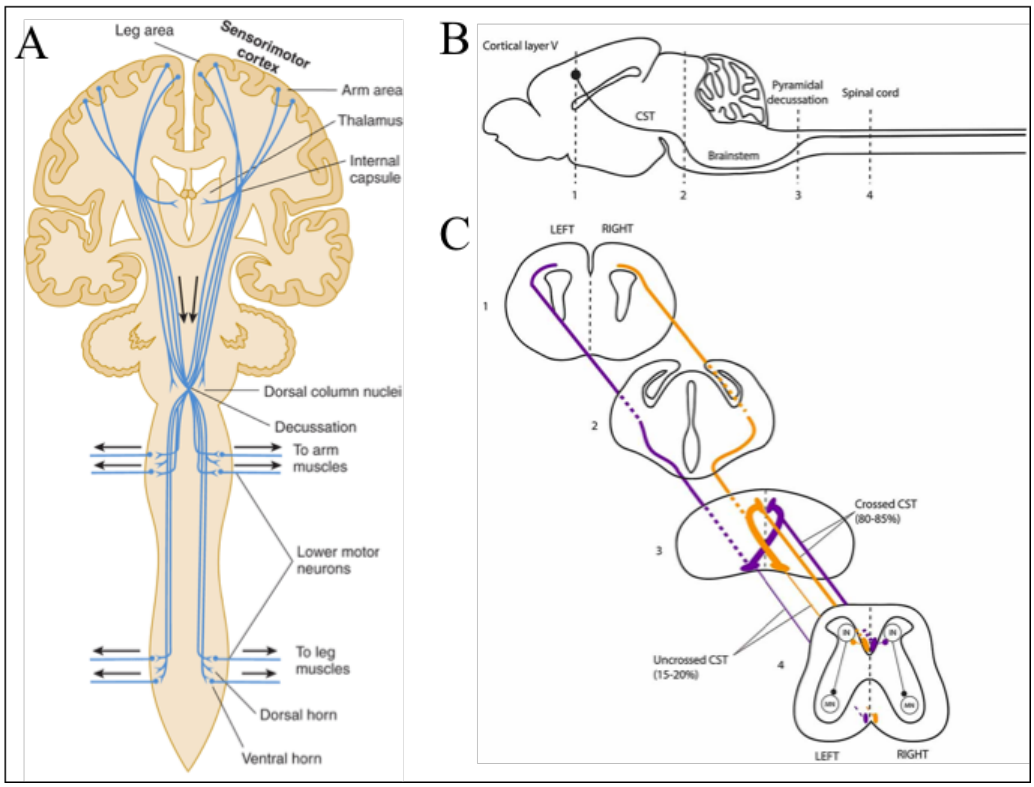

Figure 1.9 Neuroanatomical location of the corticospinal pathway in humans and rats. Within humans (**A**) and rats (**B, C**) the CST, one of the main sensorimotor pathways in the brain, follows a similar pathway. The descending CST originates within layer V of the sensorimotor cortex where axons, mainly from pyramidal neurons, project towards and bundle within the corona radiata projecting into

the internal capsule. They then extend down towards the cerebral peduncles within the midbrain. From there the fibres extend into the brain stem into the ventral pons and pyramids within the medulla before crossing at the pyramidal decussation located at the caudal medulla, where the axons then enter the spinal cord. Around 80-85% of fibres cross over at the pyramidal decussation where fibres originating in one hemisphere cross over to control the opposite side of the body. These fibres go on to form the lateral CST which synapse with cells within the ipsilateral anterior horn. The remaining 10-15% of uncrossed fibres carry on to form the anterior CST which projects down the spinal cord and cross over to the contralateral spinal cord once they reach the spinal level they are innervating. The point at which they cross is termed the anterior white commissure located within the anterior spinal cord and they synapse within the anterior horn. Figure A modified from Waxman, 2010, figures B and C modified from Welniarz *et al.,* 2015.

Transplantation of stem cell-derived NSPCs has tremendous potential to promote repair following CST injury by replacing damaged cells, re-connecting neuronal circuitry, modulating the immune response or secreting growth-promoting proteins in both rodent and non-human primate SCI models (Ideguchi *et al.,* 2010; Nori *et al.,* 2011; Cusimano *et al.,* 2012; Kobayashi *et al.,* 2012; Lu *et al.,* 2012b, 2014; Kadoya *et al.,* 2016; Lu *et al.,* 2017). For example, 9 days following moderate cervical spinal cord contusion in adult immunosuppressed marmosets, human iPSC-derived NSCs were transplanted into the lesion site (Kobayashi *et al.,* 2012). Results showed grafted cells survived up to 12 weeks *in vivo* (longest time point analysed), promoted angiogenesis, axonal regeneration and neurotrophin release, whilst also preventing axonal demyelination. However, in contrast to recent research in rats (Hong *et al.,* 2014) the lesion size was not reduced. Together these outcomes resulted in significant motor recovery of both upper and lower limbs following assessment in the open field, bar grip and cage climbing tests (Kobayashi *et al.,* 2012). This work also highlighted the lack of tumour formation within these un-fated iPSC-derived NSCs reinforcing their potential for clinical application.

Furthermore, significant CST regeneration has been observed following transplantation of multipotent rat NPCs (derived from embryonic spinal cord) into the rat spinal cord 2 weeks after complete thoracic (T3) transection (Kadoya *et al.,* 2016). Specifically, regenerating fibres were observed within the NPC graft and beyond the lesion site, with host axons forming synaptic connections with grafted cells (Kadoya *et al.,* 2016). In contrast and contradictory to previous research, grafts of SCs or MSCs

secreting neurotrophic factors were unable to induce regrowth of CST axons within the same injury model which suggests the regenerative effects were specific to NPCs (Kadoya *et al.,* 2016). Results from this study also showed NPC grafts reduced the presence of reactive astrocytes at the graft-host interface, adding a further potential mechanism by which NPCs can promote regeneration. Interestingly, this work demonstrated that for NPCs to exert a regenerative effect, they need to be in contact with injured CST axons, signifying potential ligand-receptor interactions (Kadoya *et al.,* 2016).

Moreover, Kadoya and colleagues suggested that the tissue origin of transplanted NPCs impacts the ability of endogenous CST axons to regenerate (Kadoya *et al.,* 2016). For example, NPCs derived from embryonic spinal cord were able to promote regrowth of endogenous CST fibres into the lesion site compared to NPCs derived from embryonic telencephalon which resulted in no CST axons penetrating the graft site. Similarly, when human iPSC-derived NPCs were injected into the same injury model, results showed extensive CST regrowth into the lesion site, but only if the hNPCs were caudalised (Kadoya *et al.,* 2016). Therefore, endogenous CST axons are capable of regeneration, however it appears the origin and location of the graft can significantly impact the regenerative outcome. This finding is of particular interest, especially when considering use of iPSC-derived cells which can originate from a number of different somatic cell types. For the most part the cells used by Kadoya and colleagues in this instance were derived from embryonic tissue; however, they did repeat the experiment with human iPSC-derived NPCs, which were able to promote significant CST regeneration and strengthened the potential of iPSC-based regeneration (Kadoya *et al.,* 2016).

Previous work from Lu and colleagues (Lu *et al.,* 2012b) has shown that rat iPSC-NSCs as well as human NSCs within a fibrin matrix containing growth factors can overcome the inhibitory environment created after injury and therefore this treatment does not need to be combined with further treatments targeting the inhibitory ECM. Perhaps these cells have the ability to combat this inhibitory milieu. Indeed, research has shown NSPC grafts are able to reduce the inflammatory response after thoracic contusion in mice and reduce the activation of M1 macrophages (Cusimano *et al.,* 2012). However, the full extent of iPSC-derived NPC on regeneration has not yet been

uncovered, but the differentiation of NPCs into different cell types, including neuronal and glial phenotype, will likely decipher the regenerative impact and outcome.

Nevertheless, stem cell-derived cells can be pre-differentiated or set onto a particular differentiation pathway prior to transplantation. In these situations, where cells have been forcefully guided towards a specific neuronal phenotype, the gene expression within these cells must be carefully considered to prevent unwanted projections to off-target neuroanatomical regions. For example, for grafted cells to project subcortically and selectively within the CST, analysis of the expression profile, including expression of chicken ovalbumin upstream promoter transcription factor interacting protein 2 (Ctip2) (Arlotta *et al.,* 2005; Chen *et al.,* 2008a) and neuropilin-1 (Sano *et al.,* 2017) is required. Before cells can be considered for transplant the expression profile of cells needs to be fully examined and expression of genes, outside of those expressed within the target area, may need to be masked or knocked down. Similarly, the method of differentiation of ESC-derived NPCs in culture prior to transplant can have a noticeable effect on the gene expression (Ideguchi *et al.,* 2010). ESC-derived NPCs were targeted to differentiate into a cortical neuron phenotype by either co-culturing them with mouse MS5 stromal cells *in vitro* or treatment with retinoic acid prior to transplantation into the neonatal cerebral cortex of mice. In culture, the NPCs grown on a MS5 feeder layer expressed a higher proportion of deep-layer cortical neuron markers, including Ctip2, compared to the cells that received the retinoic acid treatment. Furthermore, following transplant NPCs grown on MS5 feeder cells were able to project large fibre bundles within the descending CST compared to sparse fibres from retinoic acid-treated NPCs (Ideguchi *et al.,* 2010). These results indicate the type of mechanism of neuronal differentiation can greatly affect the gene expression of cells, and although these cell types both differentiated into cortical neurons, the distinct profile expression of layer V is required in order for projections to extend large fibre bundles within the CST. Importantly this study demonstrated ESC-derived NPCs transplanted into the motor cortex of neonatal mice were able to project within the CST, as far as the cervical spinal cord (the furthest location analysed) only 2-3 weeks after transplantation (Ideguchi *et al.,* 2010) indicating that these cells are capable of extending long-distance projections.

1.3.7 Combination of treatments likely to give best chance of functional recovery

Although individually each type of cell transplant discussed above has promising regenerative potential and some are even able to evade or even modify the external environment, such as the inflammatory response, it is likely long-term robust functional regeneration will be achieved using a combination of treatments. Transplanting cells after CNS injury to either replace damaged cells or promote remyelination, alongside treatments which can modulate the inhibitory milieu, will likely address multiple obstacles associated with prevention of SCI repair. Regeneration of axons in general is impeded by the glial scar and inhibitory environment and therefore the best outcome may come from cell transplants used in co-treatments alongside modulatory agents of the ECM (Fouad *et al.,* 2005; Filous *et al.,* 2010; Kanno *et al.,* 2015). For example, combining a cell graft containing myelinating SCs and OECs in conjunction with ChABC treatment resulted in better regeneration following complete SCI in adult rats compared to cell grafts alone or controls (Fouad *et al.,* 2005). This approach attempted to address multiple aspects of SCI pathophysiology and resulted in remyelination and regrowth of damaged fibres through and caudal to the graft site and significant functional improvements in the forelimb and hindlimb following assessment using the BBB scale (Fouad *et al.,* 2005). Similarly, when immature astrocytes were transplanted alongside ChABC into the lesion site, regeneration of sensory axons was observed within and caudal to the lesion site within host white matter tracts. However, beyond this, regeneration was restricted (Filous *et al.,* 2010) suggesting further intervention to promote intrinsic growth promoting properties may be required.

Indeed, increasing intrinsic growth-promoting properties, such as increasing TrkB (Fang *et al.,* 2017) or integrin expression (Cheah *et al.,* 2016), increasing BDNF secretion (Butenschön *et al.,* 2016), increasing cAMP signalling (Pearse *et al.,* 2004) or reducing PTEN activity (Lewandowski and Steward, 2014; Danilov and Steward, 2015), within injured axons have shown promise in promoting regeneration *in vivo*. However, increasing the growth-promoting properties of some CNS axons, such as those within the CST, is hindered by the reduced trafficking of growth-promoting

proteins within these axons (Lu *et al.,* 2001; Andrews *et al.,* 2016). Promising results have come from research into the trafficking mechanisms which prevent integrin transport within the CST (Franssen *et al.,* 2015), however this adds yet more complexity to combating the already complex SCI pathophysiology. Considering the vast number of inhibitory processes working to prevent axonal regeneration after SCI, it is likely a combination of treatments targeting multiple aspects, including the intrinsic inability of axons to repair, cell replacement, extrinsic inhibitory glial scar, inhibitory myelin-associated proteins and inflammation, will likely be required to change a patient's symptomatic outcome after SCI.

1.4 Project aims and objectives

As integrins are downregulated within the CNS, here we aimed to increase integrin expression, specifically the α9 subunit, within the CST. As literature shows integrins are not trafficked within the mature CST (Andrews *et al.,* 2016), therefore here we used iPSC-derived hNPCs as a vehicle to promote this expression within neonatal rats with the main aim of characterising the cells *in vivo* and assessing the integrin expression over time. In order to achieve this goal the project was divided into three major aims as detailed below.

1. **Characterisation of integrin expression and function in iPSC-derived hNPCs *in vitro***

This aspect of the project examined the endogenous expression level of integrin subunits within iPSC-derived hNPCs. In particular, the expression levels of both α9 and β1 was assessed; the two growth-promoting integrin subunits of interest. The hNPCs used within this project were derived from iPSCs and were treated so that when cultured, they differentiate into cortical neurons (Axol Bioscience). Additionally, using lentiviral methods, the aim was to overexpress the α9 integrin subunit within cells and assess its expression. Finally, the functionality of the overexpressed protein was determined and assessed for its ability to induce neurite outgrowth *in vitro* in the presence of TN-C.

2. **Transplant and survival of wild type (WT) iPSC-derived hNPCs *in vivo***

The first *in vivo* component of the project investigated whether WT iPSC-derived hNPCs were able to survive and integrate following transplantation into the sensorimotor cortex of rodent hosts. This involved examining graft integration and survival at a number of different time points following the initial transplant. The area into which these cells were grafted was layer V of the sensorimotor cortex of neonatal rats, where the CST originates. This is one of the main pathways involved in motor control and skeletal muscle coordination. This aspect of the project aimed to examine the grafted cells *in vivo* to determine if they were able to project from the injection site within the CST to the spinal cord. Using IHC, we also characterised the cortical neuron

and progenitor marker expression of transplants and analysed the grafts for evidence of maturation over time

3. Transplant and survival analysis of α9-expressing iPSC-derived hNPCs *in vivo*

The survival and integration of grafted α9-expressing iPSC-derived hNPCs *in vivo* was investigated and the localisation of the integrin within these transplanted cells was determined. Using similar techniques as in the second aim above, integrin-expressing hNPCs were transplanted into the neonatal sensorimotor cortex. Cells were analysed at several different time points post-transplantation from 2 weeks up to 8 weeks. The results obtained from α9-eYFP hNPC transplants in regard to survival and growth were compared to the results from WT hNPC transplants.

Chapter 2: General materials and methods

2.1 Preparation of solutions

2.1.1 Preparation of PBS

A 0.1 M (1X) phosphate buffered saline (PBS) solution was made using 1.0 M (10X) stock consisting of 160 g NaCl, 4 g KCl, 28.8 g $Na_2HPO_4.2H_2O$, 4.8 g KH_2PO_4 and 1.6 L distilled water (dH_2O), topped up with dH_2O to a final volume of 2 L. To obtain a 0.1 M (1X) solution, 50 mL of 1.0 M stock was diluted with 450 mL dH_2O. The 1X PBS solution was autoclaved for sterility before use and stored at room temperature (RT).

2.1.2 PBS-Tween 20

PBS-Tween was prepared by adding 100 µL of Tween-20 detergent (Sigma) to 500 mL of 1X PBS solution (section 2.1.1) to obtain a 0.02% stock used for ICC (section 2.6.1) and IHC (section 2.8.1).

2.1.3 Preparation of TBS

A 10X tris-buffered saline (TBS) solution was prepared by adding 87.7 g NaCl and 100 mL of 1 M Tris-HCl (pH 7.5) to 1 L of dH_2O. The 1 M Tris-HCl was made by dissolving 121.1 g of Tris base (Sigma) in 800 mL of dH_2O and adjusted to pH 7.5 using concentrated HCl (Sigma). A 1X TBS solution was made by diluting 100 mL of 10X TBS stock in 900 mL distilled H_2O.

2.1.4 TBS-Tween 20

TBS-Tween was prepared by adding 1 mL of Tween-20 detergent (Sigma) to 1 L of 1X TBS solution (section 2.1.3) to obtain a 0.1% stock used for western blotting (WB) (section 2.6.4).

2.1.5 Preparation of LB broth

Luria Bertani (LB) broth was prepared by dissolving 10 g LB powder (Sigma, L3022) in 500 mL dH_2O and autoclaving before use. Once cooled to RT, antibiotic, either kanamycin or ampicillin (section 2.2.2), was added as required.

2.1.6 Preparation of LB agar plates

Agar was prepared by dissolving Lennox LB powder containing agar (Sigma) in 1 L dH_2O (as per manufacturer's instructions) which was then autoclaved and left to cool to RT. The set agar was heated to allow the agar to melt and cooled slightly before adding antibiotic, either kanamycin or ampicillin (section 2.2.2). The agar was poured into 10 cm plates and left to set at RT before sealing with parafilm and storing at 4°C prior to use.

2.2 Preparation and purification of plasmid DNA

2.2.1 DNA transformation and culture inoculation

Approximately 100 ng of the plasmid deoxyribonucleic acid (DNA) was added to a 1.5 mL tube along with 50 µL of competent DH5α cells before being incubated on ice for 30 minutes. Following this, the 1.5 mL tube was placed at 42°C (in a heat block) for 45 seconds to heat shock the cells before returning the tube to ice. After heat shocking, 250 µL of pre-warmed to 37°C bacterial SOC medium (Invitrogen, 15544-034) was added to the tube and placed in a 37°C shaking incubator for 1 hour at 220 rpm. Following the incubation, between 50-100 µL of the bacterial solution was spread onto agar plates containing the necessary antibiotic (Table 2.1 and section 2.2.2). Bacterial solution was allowed to air dry on plates for 15-30 minutes before incubating plates upside down at 37°C overnight. The following day an individual colony was picked using a sterile pipette tip and used to inoculate an 8 mL LB broth culture containing the corresponding antibiotic. The culture was placed at 37°C for 12-16 hours in a shaking incubator at 220 rpm.

If glycerol stocks were already available for certain DNA plasmids, a bacterial transformation was not required. In these instances, an 8 mL culture was inoculated using a sterile pipette tip which had been used to scrape the glycerol stock before being transferred into a 50 mL tube containing 8 mL LB broth and the relevant antibiotic (see Table 2.1 and section 2.2.2). The culture was incubated overnight for 12-16 hours in a shaking incubator set at 220 rpm at 37°C. At this stage, a glycerol stock was made

from the culture by transferring 500 µL of the bacterial media into a 1.5 mL tube along with 250 µL of a 50% glycerol (Fisher Scientific) in dH_2O stock. The bacterial glycerol stock was stored at -80°C and used for future inoculations. Following this step, the plasmid DNA was purified from the remainder of the bacterial culture using a miniprep kit (section 2.2.3).

In situations where a larger amount of DNA was required, for example multiple viral transductions, a larger culture was prepared. Initially, an 8 mL starter culture was inoculated either using an individual colony or a glycerol stock and incubated for approximately 8 hours at 37°C at 220 rpm. After 8 hours, approximately 1-2 mL of the original 8 mL culture was transferred to a larger culture of 200-300 mL LB broth with the appropriate antibiotic and incubated overnight (12-16 hours) at 37°C at 220 rpm. DNA was then purified out from the culture using a Macherey-Nagel Maxiprep kit as per manufacturer's instructions (section 2.2.4).

Table 2.1 Different plasmid DNA used and corresponding antibiotic resistance

Plasmid	Antibiotic resistance
α9-eYFP	Kanamycin
eGFP	Kanamycin
LV-α9-eYFP	Ampicillin
LV-fGFP	Ampicillin
pMDLg/pRRE	Ampicillin
pRSV-REV	Ampicillin
pMD2.G	Ampicillin
pSD11	Ampicillin
pSD16 (psPAX2)	Ampicillin

2.2.2 Ampicillin and kanamycin stocks

A 100 mg/mL stock of ampicillin was prepared by dissolving 1 g of ampicillin sodium salt (Fisher, BP1760-5) in 10 mL dH_2O. The solution was filtered through a 0.22 µm filter and syringe before storing at -20°C in aliquots. A working concentration of 100 µg/mL was obtained by diluting the stock solution 1:1,000 in LB broth or LB agar.

A 50 mg/mL stock of kanamycin was prepared by dissolving 0.5 g of kanamycin sulphate (Gibco^{TM}, 11815-024) in 10 mL of dH_2O. The solution was filtered through a 0.22 µm filter and syringe before storing at -20°C in aliquots. A working

concentration of 50 μg/mL was obtained by diluting the stock solution 1:1,000 in LB broth or LB agar.

2.2.3 DNA plasmid purification using a miniprep kit

Plasmid DNA purification from an 8 mL overnight culture was carried out using a Qiagen® Spin Miniprep Kit as per manufacturer's instructions. Briefly, the bacterial culture was centrifuged at 3,500 rpm for 8 minutes at 4°C to pellet the cells. The bacterial supernatant was discarded and the pellet was resuspended in 250 μL of Buffer P1 and transferred to a microcentrifuge tube. Following this, 250 μL of Buffer P2, a lysis buffer, was added to the microcentrifuge tube and mixed by inverting the tube five times. After this, 350 μL of Buffer P3 was added to neutralise the lysate and the contents of the tube were mixed by inverting the tube a further five times before centrifuging the tube for 10 minutes at 13,000 rpm at RT in a benchtop centrifuge. The supernatant, which now contained the contents of the lysed cells including the DNA, was collected and transferred to a QIAprep spin column for purifying out the DNA. This spin column was subsequently centrifuged for 60 seconds at 13,000 rpm. The flow through in the collection tube was discarded and 750 μL of Buffer PE was added to the spin column which was again centrifuged for 60 seconds. The flow through was again discarded and the spin column inside the collection tube was centrifuged for 60 seconds once more to remove any buffer remaining in the column and filter. The spin column was removed from the collection tube and transferred to an autoclaved 1.5 mL tube for the final steps of eluting and collecting the purified DNA. To elute the DNA, 50 μL of double-distilled water (ddH_2O) was added to the filter and left to stand for 5 minutes before centrifuging for 60 seconds. The concentration of DNA was measured using a NanoDrop 2000 spectrophotometer and DNA was stored at -20°C.

2.2.4 DNA plasmid purification using a maxiprep kit

Larger amounts of DNA were purified from the larger bacterial cultures using the Macherey-Nagel NucleoBond® Xtra Maxi Plasmid DNA Purification Kit as per manufacturer's instructions for high-copy plasmids. Briefly, the culture was transferred to a centrifuge bottle (Beckman) and bacterial cells were pelleted by centrifugation at 6,000 rcf for 20 minutes at 4°C. The supernatant was discarded and

the cell pellet was resuspended in 12 mL Resuspension Buffer RES containing ribonuclease A. To lyse the cells, 12 mL of Lysis Buffer LYS was added to the suspension and the bottle was inverted five times and incubated at RT for 5 minutes. During this incubation, the NucleoBond® Xtra column and filter were equilibrated by slowly pipetting 25 mL Equilibration Buffer EQU onto the filter sides to saturate the entire filter. After the 5-minute incubation, the suspension was neutralised using 12 mL Neutralisation Buffer NEU, which was added to the bottle before gently inverting five times to mix. The suspension was then added to the filter and allowed to flow through. The column was then washed with 15 mL of Equilibration Buffer EQU and allowed to flow through before removing and discarding the filter from the column. The column was subsequently washed with 25 mL Wash Buffer, which was allowed to flow through the column before transferring the column to a 50 mL collection tube. The DNA was eluted using 15 mL of Elution Buffer ELU which was added to the column and collected in the collection tube. Once the column emptied, it was removed and discarded and 10.5 mL of isopropanol was added to the collection tube and vortexed to precipitate the DNA from suspension. This was centrifuged for 30 minutes at 15,000 rcf at 4°C to pellet the DNA. The supernatant was discarded and 4 mL of 70% ethanol (EtOH) was added and the tube was centrifuged at 15,000 rcf for 5 minutes at RT. The EtOH wash was discarded leaving behind the pellet in the bottle which was allowed to air dry for 15-30 minutes before dissolving the pellet in ddH_2O by manually pipetting and transferring to a 1.5 mL tube. The concentration of DNA was measured using a NanoDrop 2000 spectrophotometer and DNA was stored at -20°C.

2.3 Preparation of cell culture reagents, flasks, plates and coverslips

2.3.1 Preparation of PDL

A 10 mg/mL stock of poly-D-lysine (PDL) was prepared by resuspending 100 mg PDL hydrobromide powder (Sigma, P1149) in 10 mL tissue culture (TC)-grade dH_2O. The PDL stock solution was aliquoted into 500 µL and kept at -20°C for long-term storage. PDL was used at a working concentration of 20 µg/mL by adding 15 µL of PDL stock to 7.5 mL TC-grade dH_2O.

2.3.2 Preparation of PDL-coated flasks and coverslips

In preparation for tissue culture, 5 mL PDL solution (20 µg/mL) was incubated in a T-75 flask for 1 hour at 37°C. Following incubation, the PDL was removed and the dishes were washed three times with sterile PBS before seeding cells at desired density. The same protocol applied for PDL-coated 13 mm glass coverslips (VWR). Glass coverslips were sterilised in 70% EtOH before being placed into a Nunc™ 24-well plate (Thermo Scientific™) and allowed to air dry. In each well, 500 µl of PDL solution was added and the plate was incubated for 1 hour at 37°C, after which the PDL was removed and coverslips washed three times with sterile PBS. Following use, PDL working solution was stored at 4°C and was re-used up to a maximum of 10 times.

2.3.3 Preparation of PLO

A 10 mg/mL stock of poly-L-ornithine (PLO) was prepared by diluting 100 mg PLO (Sigma, P3655) in 10 mL TC-grade dH_2O and stored in aliquots at -20°C. PLO was used at a working concentration of 20 µg/mL by diluting 20 µL of stock in 10 mL TC-grade dH_2O.

2.3.4 Preparation of NGF

NGF was prepared by dissolving 1 mg NGF powder (Sigma, N2513) in 10 mL TC-grade dH_2O to give a concentration of 100 µg/mL. Aliquots of 50 µL were kept at -80°C for long-term storage.

2.3.5 Preparation of PEI

A 1 mg/mL stock of polyethylenimine (PEI) solution was prepared by dissolving 100 mg PEI (Polysciences, 239662) in 100 mL TC-grade dH_2O by heating to approximately 80°C. The pH of the solution was measured and brought to pH 7.2 using HCl and filter sterilised using a 0.22 µm filter and syringe. The solution was stored in aliquots at -20°C for long-term storage or 4°C for short-term use.

2.3.6 Preparation of hexadimethrine bromide/polybrene

A 2 mg/mL stock solution was prepared by adding 0.002 g Hexadimethrine bromide (Sigma, H9268) to 1 mL TC-grade dH_2O. The solution was filter sterilised using a 0.22 μm filter and syringe and stored at -20°C in aliquots.

2.4 Culture of cell lines

2.4.1 Thawing of tissue culture cell lines

All cell lines, retinol pigmented epithelial (RPE) cells, rat pheochromocytoma-12 (PC12) cells and human embryonic kidney (HEK) 293T cells, were thawed using the same protocol. A vial of cells was taken from liquid nitrogen and placed on dry ice before thawing in a 37°C water bath. The contents of the vial were then transferred to a 15 mL tube along with 9 mL of the appropriate warmed media before being pelleted by centrifugation at 1,000 rpm for 3 minutes. The media was aspirated from the tube leaving the cell pellet which was resuspended in 10 mL of media before being transferred to a Nunc™ T-75 culture flask (Thermo Scientific™). Flasks were placed in a 37°C incubator with 5% CO_2.

2.4.2 Culture of RPE cells

RPE cells were cultured in Nunc™ T-75 flasks (Thermo Scientific™) at 37°C with 5% CO_2 and grown in complete Dulbecco's Modified Eagle Medium/Nutrient Mixture F-12 (DMEM/F12, Gibco™) containing 10% fetal bovine serum (FBS, Seralabs) and 1% penicillin and streptomycin (PS, 5000 U/mL Pen; 5000 μg/mL Strep, Gibco™). Media was prepared under sterile conditions and filtered using a 0.22 μm filter. Cells were split when approximately 70-80% confluent using 0.05% trypsin-ethylenediaminetetraacetic acid (EDTA) (Gibco™) (section 2.4.6). In preparation for collecting lysates for WB, RPE cells were plated onto uncoated Nunc™ 6-well tissue culture plates (Thermo Scientific™) at a density of 2 x10^5 cells per well. For analysing cells using immunocytochemistry (ICC), RPE cells were grown on uncoated glass 13 mm diameter coverslips (VWR, 631-0149) in Nunc™ 24-well tissue culture plates (Thermo Scientific™) at a density of 4 x10^4 cells per well. In preparation for collection

of WB lysates, RPE cells were plated onto uncoated Nunc™ 6-well plates (Thermo Scientific™).

2.4.3 Culture of HEK293T cells

HEK293T cells, which express the SV40 T antigen, were cultured in Nunc™ T-75 flasks (Thermo Scientific™) in a 37°C incubator with 5% CO_2. Cells were cultured in complete Dulbecco's Modified Eagle Medium (DMEM, Gibco™) containing 10% FBS (Seralabs) and 1% PS. Media was prepared under sterile conditions and filtered using a 0.22 µm filter. When around 70-80% confluent, cells were split using 0.05% trypsin-EDTA (section 2.4.6). In preparation for transfection of viral plasmids HEK293T cells were plated onto 10 cm tissue culture plates at 4 x10^6 the day before transfection (sections 2.4.9 and 2.4.10).

2.4.4 Culture of rat proliferating PC12 cells

Proliferating rat PC12 cells were maintained on a substrate of 20 µg/mL PDL diluted in TC-grade dH_2O (section 2.3.2). Proliferating PC12s were cultured in proliferation media containing 10% horse serum (Sigma, H1270), 5% FBS (Seralabs) and 1% PS (Gibco™) in DMEM (Gibco™). Cells were split at 70-80% confluency using 0.05% trypsin-EDTA (section 2.4.6). Media was prepared under sterile conditions and filtered using a 0.22 µm filter. In preparation for collection of cell lysates, proliferating PC12 cells were seeded onto 20 µg/mL PDL-coated 6-well dishes. For analysing cells using ICC, PC12 cells were plated on 13 mm PDL-coated glass coverslips.

2.4.5 Differentiation of rat PC12 cells

For differentiating, PC12 cells were plated onto double-coated dishes of 20 µg/mL PDL and 10 µg/mL laminin (Sigma, L2020). The laminin was diluted in PBS and incubated with the PDL-coated dishes overnight at 37°C. The laminin was subsequently removed and plates were washed three times with PBS. Differentiating PC12s were cultured in differentiation media containing DMEM (Gibco™), 1% FBS (Seralabs), 1% insulin, human transferrin and selenous acid (ITS^+) supplement (BD Life Sciences, 354352), 1% PS (Gibco™) and 100 ng/mL NGF (Sigma). For analysing

cells using ICC, PC12 cells were plated on 13 mm PDL-laminin-coated glass coverslips.

2.4.6 Passaging tissue culture cell lines

PC12 cells were passaged using 0.05% trypsin-EDTA (Gibco™) diluted in PBS. Culture media was removed from cells and adherent cells were washed gently with 5 mL PBS. Following the wash, trypsin-EDTA (Gibco™) diluted in PBS was added to the flask and incubated at 37°C for 3-5 minutes to detach cells. Once cells had detached from the flask they were pipetted into a single cell suspension and transferred to a 15 mL tube along with 6 mL of the appropriate media, (proliferation media for PC12s and complete DMEM/F12 for RPE and compete DMEM for HEK293T cells). The cells were pelleted by centrifugation at 1,000 rpm for 3 minutes at RT. The supernatant was aspirated from the tube leaving the cell pellet. Cells were counted using a haemocytometer, split and seeded at the desired density.

2.4.7 Live cell imaging

To assess cell survival during culture cells were imaged using a Leica DM IL LED fluorescence inverted microscope and an Axiovert 40 CFL inverted microscope equipped with an Axiocam ICm1 camera (Zeiss).

2.4.8 Transient transfections of PC12 cells and hNPCs

PC12 cells were transfected with either a plasmid containing the human α9 integrin sequence tagged with enhanced yellow fluorescent protein (α9-eYFP) or a plasmid containing enhanced green fluorescent protein (eGFP), using GeneJammer (Agilent), PEI (Sigma) or JetPrime (Polyplus). For each reagent, proliferating PC12 cells were approximately 70-80% confluent at the time of transfections. Transfections carried out in a 6-well plate if cells were to be used for lysates and in 24-well plate with coverslips if cells were to be used for ICC. All of the transfection details can be found in Table 2.2 with all volumes and concentrations given per well. The buffer used for GeneJammer and PEI was serum-free optiMEM and for JetPrime it was the JetPrime dilution buffer.

Table 2.2 Summary of transfection reagents and protocols

Transfection reagent	Well size	Volume of transfection reagent (µL)	Amount of DNA per well (ng)	Final volume of transfection mix (µL)
GeneJammer	6 -well	6.0	2,000	100
	24-well	1.2	400	20
PEI	6-well	15.0	3,750	150
	24-well	3.0	750	30
JetPrime	6-well	4.0	2,000	200

2.4.9 Production of third generation LV

HEK293T cells were grown in complete DMEM (10% FBS and 1% PS in DMEM) on 10 cm plates. For preparation of viral supernatant HEK293T cells were plated out at a density of 4 x10^6 the night before use. The following day, HEK293T cells were given fresh complete DMEM 2 hours before transfection. Cells were transfected using a 4:2:1:1 ratio of the four lentiviral (LV) plasmids (Table 2.3), using 1 mg/mL PEI. The cells were transfected with the four LV plasmids, including the two LV packaging plasmids pMDLg/pRRE (Addgene, 12251) and pRSV/REV (Addgene, 12253), the envelope expressing plasmid pMD2.G (Addgene,12259) and the LV transfer plasmid either LV-α9-eYFP or LV-farnesylated green fluorescent protein (fGFP).

The required volume of DNA from each of the four plasmids was added to 500 µL pre-warmed optiMEM along with 65 µg PEI. The transfection was briefly mixed by pipetting before vortexing for 10 seconds. The mix was incubated for 15-30 minutes at RT before adding dropwise to the 10 cm plate of HEK293T cells. The plate was gently tilted back and forth to ensure even coverage of the transfection mix before incubating for 24 hours at 37°C in a class two incubator. All viral work from this point was carried out in a class two tissue culture hood and incubator. After 24 hours, media was replaced with 5 mL fresh complete DMEM and incubated for a further 24 hours at 37°C. After this incubation (48 hours after the initial transfection) viral media was collected and filter sterilised using a 0.45 µm filter and stored at 4°C. Another 5 mL of fresh media was added to each plate before incubating for a final 24 hours at 37°C. Media was collected and filter sterilised as above. Viral supernatant was stored at 4°C for short-term use or aliquoted into 1 mL microcentrifuge tubes and stored at -80°C for long-term storage.

Table 2.3 Viral plasmids used in third generation LV

3rd generation LV plasmids	Plasmid name	Ratio	Amount required/10 cm plate
Transfer vector	LV- α9-eYFP	4	10 µg
	LV-fGFP		
Packaging plasmid #1	pMDLg/pRRE	2	5 µg
Packaging plasmid #2	pRSV-REV	1	2.5 µg
Envelope plasmid	pMD2.G	1	2.5 µg

2.4.10 Production of second generation LV

Similar to third generation LV production, HEK293T cells were plated out at a density of 4 x10^6 the night before use. The following day cells were transduced with the three second generation LV plasmids (Table 2.4) using TransIT® LT-1 transfection reagent (Mirus). Briefly, TransIT® LT-1 reagent was diluted in 1.5 mL pre-warmed optiMEM (Gibco™) and incubated for 20 minutes at RT. Different volumes of TransIT® LT-1 were used for different sizes of transfer plasmids and used at a ratio of 200 base pairs: 1 µL of TransIT® LT-1. After the 20-minute incubation, the required volume of DNA from each of the three plasmids was added to the transfection mix and incubated at RT for 30 minutes before adding dropwise to the 10 cm plate of HEK293T cells. Plates were tilted gently before incubating for 24 hours at 37°C. After 24 hours, the media was replaced on the HEK293T cells with 4 mL fresh complete DMEM. After a further 24-hour incubation, the viral supernatant was collected and filter sterilised through a 0.45 µm filter and stored at 4°C. This was replaced with another 4 mL of complete DMEM for a further 24-hour incubation. After this time the viral supernatant was collected, filtered and stored at 4°C for short-term use or aliquoted into 1 mL microcentrifuge tubes and stored at -80°C for long-term storage.

Table 2.4 Plasmids used in production of second generation LV

2nd Generation viral plasmids	Plasmid name	Amount required/10cm plate
Transfer vector	LV- α9-eYFP	10 µg
	LV-fGFP	6.5 µg
Packaging plasmid	psPAX2 (pSD16)	5 µg
Envelope plasmid	pMD2.G-VSV.G	2.1 µg

2.4.11 Transduction of PC12 cells with second or third generation LV

In preparation for viral transduction, proliferating PC12 cells were plated onto a 6-well plate the night before at a density of 2 x10^5. PC12 cells were transduced with 1 mL/well of viral supernatant, either second or third generation, containing 2 μg/mL polybrene. Viral media was incubated with cells for 4 hours at 37°C before washing cells once with fresh media and replacing with fresh complete DMEM. Cells were incubated at 37°C and monitored daily for cell death. Media was replaced with fresh complete DMEM when required. Cells were kept in culture until for 4-9 days until taken for cell lysates (section 2.6.4), split onto coverslips or used for neurite outgrowth assays (section 2.6.2).

2.4.12 Transduction of hNPCs with second generation LV

hNPCs were transduced with second generation LV supernatant 72 hours after thawing. As with the PC12 cells, hNPCs were transduced with 1 mL/well of viral supernatant containing 2 μg/mL polybrene. Viral media was incubated with cells for 4 hours at 37°C before removing the spent media, washing cells once with fresh media and replacing with Axol Neural Maintenance Medium. Cells were incubated at 37°C and were monitored for cell death. Media was changed as required, usually every 24-48 hours. Cells were kept in culture for a further 4-5 days until they were either collected for transplantation (section 2.5.6 and 2.7.1), taken for cell lysates (section 2.6.4), split onto coverslips for ICC (section 2.5.4) or used for neurite outgrowth assays (section 2.6.2).

2.4.13 Cryopreservation of tissue culture cell lines

Proliferating PC12, RPE and HEK293T cells were frozen and stored in liquid nitrogen when around 70-80% confluency. Media was removed from cells and washed with sterile PBS, before adding 3-4 mL 0.05% trypsin-EDTA (Gibco^{TM}) diluted in PBS to the flask. The flask was incubated at 37°C for 3-5 minutes to allow cells to dissociate. Once cells had detached from the flask they were pipetted into a single cell suspension and transferred to a 15 mL tube along with 6 mL of the appropriate media, (proliferation media for PC12s, compete DMEM/F12 for RPEs and complete DMEM

for HEK293T cells). The cells were pelleted by centrifugation at 1,000 rpm for 3 minutes at RT. The supernatant was aspirated from the tube leaving the cell pellet. Cells were frozen down in a freezing media containing 90% FBS (Seralabs) and 10% dimethyl sulfoxide (DMSO, Fisher Scientific, BP231-100). The freezing media was prepared under sterile conditions and filtered using a 0.22 μm filter (Millipore, SLGP033RS) and 10 mL syringe before use. The cell pellet was resuspended in the desired amount of freezing media and subsequently aliquoted into 1 mL cryovials (Thermo Scientific™, 363401) for freezing. The cryovials were transferred to a polystyrene box and placed at -80°C for 3-6 days before transferring to liquid nitrogen for long-term storage.

2.5 Culture of iPSC-derived hNPCs

2.5.1 Preparation of media and components

hNPCs were cultured in Axol Neural Maintenance media (Axol Bioscience) supplemented with Neural Maintenance Supplement (Axol Bioscience). The supplement was aliquoted into 750 μL aliquots and stored at -80°C. Media was aliquoted into 50 mL aliquots and stored at 4°C. One vial of supplement was thawed when required to add to one 50 mL tube of media.

2.5.2 Preparation of tissue culture plates

Human iPSC-derived NPCs (Axol Bioscience) were maintained on 6-well tissue culture dishes coated with 20 μg/mL PLO and 10 μg/mL laminin (Sigma, L2020). Plates were incubated with PLO diluted in TC-grade dH_2O for 2 hours at 37°C. Following incubation, the PLO was removed and plates were washed three times with TC-grade dH_2O before being incubated with 10 μg/mL laminin diluted in TC-grade dH_2O overnight at 37°C. The following day the laminin was removed and plates were washed three times with TC-grade dH_2O before plating the cells.

2.5.3 Thawing and maintenance of iPSC-derived hNPCs

Frozen cell stocks were slowly thawed in a 37°C water bath and added to a 15 mL tube with 9 mL Neural Maintenance Medium (Axol Bioscience). Cells were pelleted by centrifugation at 1,000 rpm for 3 minutes at RT. The supernatant was discarded and the cell pellet was carefully resuspended in Neural Maintenance Medium (Axol Bioscience) supplemented with media supplement (Axol Bioscience) and 1 µL/mL Axol Sure Boost (1,000X, Axol Bioscience). Cells were counted using a haemocytometer and plated at a density of 50,000 cells/cm^2 with 1.5 mL media onto PLO-laminin coated 6–well plates. The cells were incubated for 2 hours at 37°C, after which the medium was replaced with fresh Neural Maintenance Medium supplemented media supplement and 1 µL/mL Axol Sure Growth (1,000X, Axol Bioscience). The medium was replaced every 2 days with Neural Maintenance Medium and media supplement until the cells were removed from the dish after 8-9 days in culture for transplantation (section 2.7.1), lysate collection (section 2.6.4) or for viral transduction (section 2.4.12).

2.5.4 Passaging of iPSC-derived hNPCs

hNPCs were passaged using StemPro Accutase (Gibco^{TM}). Spent media was aspirated from plates and cells were gently washed once with sterile 1X PBS before adding 1 mL of Accutase to each well of a 6-well plate and incubating at 37°C for 3-5 minutes to allow cell dissociation. Cells were then collected and transferred to a 15 mL tube with 9 mL of Axol Neural Maintenance media. The cells were pelleted by centrifugation at 1,000 rpm for 3 minutes at RT. Supernatant was removed and cells were resuspended in 1 mL of media for counting using a haemocytometer. For viral transduction or ICC analysis cells were plated at a density of 50,000 cells/cm^2 onto PLO and laminin double coated plates or acid-washed coverslips.

2.5.5 Preparation of acid-washed glass coverslips

Glass coverslips were washed in hot dH_2O with glassware detergent in a beaker, and sonicated for 30 minutes in a water bath. The coverslips were then rinsed four times with ddH_2O and sonicated once more in ddH_2O for 15 minutes. Coverslips were then

submerged in 1 M HCl, and heated to 50-60°C for 4-6 hours in a designated fume hood. The beaker was shaken every 30 minutes to ensure an even acid wash and to stop the coverslips from sticking together. Following the incubation time, coverslips were allowed to cool to RT before being washed three times with ddH_2O to remove any residual HCl and sonicating once more in ddH_2O for 30 minutes. Following this, the coverslips were washed twice more in 70% EtOH and sonicated for 15 minutes in EtOH after each wash. The coverslips were then autoclaved for sterility. Before use, coverslips were washed in 70% EtOH and allowed to air dry before coating with PLO and laminin for plating cells.

2.5.6 Preparation of iPSC-derived hNPCs for transplant

For transplantation, cells were collected as described in section 2.5.4 and resuspended at 100,000 cells/µL in Axol Neural Maintenance media and supplement with 1 µL/mL Sure Boost (Axol Bioscience) in a 1.5 mL tube.

2.6 Cell culture analysis

2.6.1 Analysis of cells *in vitro* using ICC

To visualise expression of specific proteins, cells were analysed using ICC. Media was removed from wells and cells were washed with 1X PBS before fixing with 4% paraformaldehyde (PFA) for 10 minutes at RT. Cells were subsequently washed three times with 1X PBS. To block non-specific staining and permeabilise cells, coverslips were incubated with 10% goat serum (Sigma) or 10% donkey serum (Sigma) and 0.4% Triton-X100 (Sigma) in PBS on parafilm for 20-60 minutes at RT. Following the blocking step, cells were incubated with primary antibodies (see Table 2.5) diluted in the same blocking solution at 4°C overnight. The following day, the primary antibody was removed and cells were rinsed three times with 1X PBS containing 0.02% tween-20 before incubation with AlexaFluor secondary antibodies in 1X PBS (see Table 2.6) for 2 hours at RT. Cells were then washed a further three times with PBS before staining the nuclei with 4',6'-diamidino-2-phenylindole (DAPI) (Thermo Scientific™, 62248, 1:10,000) in PBS for 10 minutes at RT. Cells

were washed a further three times with 1X PBS before being mounted onto slides with FluorSave (Calbiochem). Slides were imaged using a Leica D5500 epifluorescent microscope equipped with a DFC550 digital camera (Leica).

Table 2.5 List of all primary antibodies used in ICC and IHC

Antibody	Species	Dilution		Supplier	Cat No.
		ICC	IHC		
BDNF	Polyclonal, rabbit	1:200	1:200	Abcam	AB72439
Ctip2	Monoclonal, rat	1:500	1:500	Abcam	AB18465
Ctip2	Polyclonal, rabbit	1:500	1:500	Abcam	Ab70453
DAPI	----	1:10,000	1:10,000	Thermo Scientific™	62248
DCX	Polyclonal, rabbit	1:500	1:500	Abcam	AB18723
GFAP	Polyclonal, rabbit	1:750	1:500	DAKO	ZO33429-2
GFP	Polyclonal, rabbit	1:1,000	1:1,000	Invitrogen	A11122
HuNu	Monoclonal, mouse	----	1:500	Millipore	MAB1281
Iba-1	Polyclonal, rabbit	1:500	1:500	Wako	019-19741
Ki67	Monoclonal, mouse	1:100	1:100	Novus Biologicals	NBP2-22112
MBP	Monoclonal, rabbit	1:50	1:50	Cell signalling	D8X4Q
hNCAM	Monoclonal, mouse	----	1:200	Santa Cruz, Insight	sc-106
Oct4	Polyclonal, rabbit	1:500	----	Abcam	Ab18976
Tbr1	Polyclonal, rabbit	1:200	1:400	Abcam	AB31940
TN-C	Monoclonal, rabbit	1:250	1:250	Abcam	ab108930
TrkB	Polyclonal, rabbit	1:1,000	1:1,000	Santa Cruz Biotechnology	SC-12
VGlut 1	Polyclonal, Guinea Pig	1:500	----	Synaptic Systems	135 304
WFA	----	----	1:200	Sigma	L1516
α9-integrin	Polyclonal, rabbit	1:1,000	----	Pierce (Thermo Scientific™)	PA5-27771
βIII-tubulin	Monoclonal, mouse	1:1,000	1:1,000	Sigma	T8660
βIII-tubulin	Polyclonal, rabbit	1:1,000	1:1,000	Covance	MRB-435P
β1-integrin	Monoclonal, mouse	1:500	----	BD Transductions	610467

Table 2.6 List of all secondary antibodies used for ICC and IHC

Antibody	Dilution		Supplier	Cat. No.
	ICC	IHC		
Goat anti-mouse AlexaFluor 488	1:1,000	1:750	Invitrogen	A21121
Goat anti-mouse AlexaFluor 568	1:1,000	1:750	Invitrogen	A11004
Goat anti-rabbit AlexaFluor 488	1:1,000	1:750	Invitrogen	A11008
Goat anti-rabbit AlexaFluor 568	1:1,000	1:750	Invitrogen	A11011
Goat anti-rat AlexaFluor 488	1:1,000	1:750	Invitrogen	A11006
Donkey anti-guinea pig AlexaFluor488	1:1,000	----	Jackson Immunoresearch	706-545-148
Donkey anti-mouse AlexaFluor 568	1:1000	----	Invitrogen	A21202
Streptavidin 488	----	1:250	Invitrogen	S32354
Streptavidin 568	----	1:250	Invitrogen	S11226

2.6.2 Neurite outgrowth assay

Neurite outgrowth assays were performed on Permanox© 8-well chamberslides (Thermo Scientific™). Differentiating PC12s were grown on a substrate of 20 µg/mL PDL (section 2.3.2) and 10 µg/mL chicken TN-C (Millipore) and the hNPCs were grown on 20 µg/mL PLO and 10 µg/mL chicken TN-C or varying concentrations of human TN-C (Millipore): 1 µg/mL, 5 µg/mL, 10 µg/mL, 15 µg/mL, 20 µg/mL, 25 µg/mL or 30 µg/mL. The dishes for hNPCs were prepared as in section 2.5.2. Cells were plated onto coated chamberslides at a density $5x10^4$/well. The cells were incubated for 72 hours at 37°C, following PBS wash and fixation with 4% PFA for 10 minutes at RT. The PFA was then removed and cells were washed three times with sterile PBS and stored at 4°C in preparation for staining.

2.6.3 Neurite outgrowth statistical analysis

Neurite outgrowth was analysed at 72 hours post-plating of cells onto TN-C. For ICC analysis, cells were first incubated in blocking buffer (0.1 M PBS containing 10% goat serum (Sigma) and 0.4% Triton-X100 (Sigma)) before being stained with GFP (1:1,000) and βIII-tubulin (1:1,000) (Table 2.5) diluted in the same blocking solution overnight at 4°C. After incubation, the cells were washed three times with PBS-T before incubation with the secondary antibodies AlexaFluor goat-anti rabbit 488 and AlexaFluor goat-anti mouse 568, 1:1,000 (Table 2.6) for 2 hours at RT. The cells were subsequently washed twice more with PBS-T before using DAPI at 1:10,000 diluted in PBS for 10 minutes at RT. Following two more washes with PBS-T, a coverslip was placed onto the slide using FluorSave (Calbiochem) and imaged using a Leica DM5500 fluorescent microscope. Analysis was performed using NeuronJ, an ImageJ add on (Meijering *et al.,* 2004), and statistical analysis was performed using Microsoft Excel and Prism 5 GraphPad software. For each condition a total of 30 axons were measured in microns using NeuronJ. One replicate consists of one vial of cells using one chamberslide (with two wells/condition) and a total of 30 cells were counted per condition for each replicate. Comparisons between the data sets were analysed using one-way analysis of variance (ANOVA) (non-parametric) and Tukey *post hoc* to determine statistical significance.

2.6.4 Western blot protocol

2.6.4.1 Protein preparation

Cell lysates were collected on ice from confluent hNPCs, PC12 or RPE cultures using 1X radioimmunoprecipitation assay (RIPA) buffer (from a 5X stock containing 250mM Tris, 750mM NaCl, 5% NP-40 and 2.5% sodium deoxycholate) supplemented with 25X complete protease inhibitor (PI, Roche, 11873580001) at a volume of 100 µL per well of a 6-well plate. Briefly, media was removed and cells were gently washed with 1X PBS. PBS was removed before adding the RIPA and PI solution followed by an incubation at RT for 1 minute. Cells were removed from the dish using a cell scraper, collected into a 1.5 mL microcentrifuge tube and incubated on ice for 15 minutes. Following incubation, the cells were centrifuged at 13,000 rcf at 4°C for 15 minutes. The supernatant was transferred to a fresh microcentrifuge tube and sample protein concentration was determined using a bicinchoninic acid (BCA) assay (section 2.6.4.2). Cell lysates were stored at -80°C.

2.6.4.2 Determining protein concentration using a BCA assay

Protein concentration was determined using a BCA assay kit (Thermo Scientific^{TM}) and the protocol was followed as per manufacturer's instructions. Briefly, protein samples were diluted 1:10 with RIPA buffer and 10 µL of each were plated into a 96-well plate. Each sample was run in triplicate. Samples were run against a serial dilution (eight samples) of bovine serum albumin diluted in RIPA buffer ranging from 0 mg/mL up to 2 mg/mL, with 10 µL per well. Each standard was run in triplicate. The kit reagents of solution A and solution B were mixed in a ration of 1:50 with 200 µL of this solution was added to each well. The plate was incubated at 37°C for 30-45 minutes before reading absorbance at 570 nM wavelength on a plate reader. A standard curve was produced using the absorbance readout from the protein standards and the concentration of protein samples were determined from this information.

2.6.4.3 Sample preparation and running of WB

Cell lysates (20 µg of protein per well for cell lines and 40 µg for hNPC samples) were separated by electrophoresis on a 4-12% bis-tris pre-cast gel (Invitrogen). Diluted samples with NuPAGE^{TM} loading dye (Thermo Fisher) were heated to 90°C for 10 minutes before loading and were run alongside a PageRuler Plus Prestained protein

ladder (Thermo Fisher, 26619). The gel was run at 200 V, 120 mA and 25 W for 40 minutes with 1X NuPAGE™ 3-(N-morpholino)propanesulfonic acid (MOPS) sodium dodecyl sulfate (SDS) running buffer (Thermo Scientific™, NP0001) diluted in dH_2O, before being transferred to a nitrocellulose membrane (GELifesciences) and at 25V, 125mA and 17W for 90 minutes with 1X NuPAGE™ transfer buffer (Thermo Scientific™, NP0006). Following transfer, the membrane was processed for immunolabelling.

2.6.4.4 WB membrane staining

The nitrocellulose membrane was incubated for 1 hour in 5% milk powder (Marvel) in 0.1% TBS-T at RT on a shaker to block non-specific binding. Primary antibodies were then diluted in 5% milk powder in 0.1% TBS-T at desired concentration (Table 2.7). A β-actin antibody (Sigma) was used to assess equal loading of protein per well. The blot was incubated with the primary antibody overnight at 4°C on a shaker. Following this, the primary antibody was removed and stored at -20°C. Primary antibodies were reused up to a maximum of three times before using fresh. Following this, the blot was washed three times each for 10 minutes with 0.1% TBS-T on a shaker followed by incubation with secondary antibody for 45 minutes at RT. The secondary antibodies (Table 2.7) were used at a dilution of 1:15,000 and diluted in 3% milk powder (Marvel) in 0.1% TBS-T. Following this, the blot was washed three times for 10 minutes each with 0.1% TBS-T before analysis.

Table 2.7 List of primary and secondary antibodies used in analysis of WB

Primary antibodies				
Antibody	**Species**	**Dilution**	**Supplier**	**Cat. No.**
GFP	Polyclonal, rabbit	1:1,000	Invitrogen	A11122
α9-integrin	Polyclonal, rabbit	1:1,000	Pierce (Thermo Scientific™)	PA5-27771
β-actin	Monoclonal, mouse	1:10,000	Sigma	A5441
β1-integrin	Monoclonal, mouse	1:1,000	BD Transductions	610467
Secondary antibodies				
HRP-Mouse	Goat anti-mouse	1:15,000	Invitrogen	A16072
HRP-Rabbit	Goat anti-rabbit	1:15,000	Invitrogen	A16096

2.6.4.5 WB analysis

WBs were analysed using chemiluminescence. Enhanced chemiluminescence (ECL) detection reagents (GE Healthcare) were mixed and used immediately in a 1:1 ratio as per manufacturer's instructions. The imaging reagents were continuously pipetted over

the membrane for 4-5 minutes before imaging using the LAS-3000 Lite imaging system (Fuji).

2.7 Transplant of iPSC derived-hNPCs and tissue fixation

2.7.1 Neonatal cerebral cortex transplants of WT and α9-expressing hNPCs

All procedures were carried out under the Project Licence number 60/4472 and Personal Licence number IC71C2B2B, conformed to the UK Animals (Scientific Procedures) Act (1986) and were approved by the Animal Welfare Ethics Committee of the University of St Andrews.

The transplant procedure for both WT hNPCs and α9-eYFP-expressing hNPCs followed the same protocol. Cells were removed from the dish after 8-9 days in culture (section 2.5.6). Newborn Sprague Dawley rat pups were injected between postnatal day 0-2 (P0-2), using hypothermic anaesthesia. For the anaesthesia, each pup was anaesthetised on ice for 3-5 minutes until they had stopped moving, after which they were transferred to a platform, also containing ice to maintain anaesthesia during surgery. Animals were injected either unilaterally or bilaterally in two specific sites with 100,000 cells per site (1 μL/injection site) for the predicted neonatal sensorimotor cortex (Altman and Bayer, 1995) (Table 2.8). Following analysis of initial tissue batches, coordinates for subsequent batches were adjusted to improve accuracy of injection (detailed in Table 2.8). Animals were placed beneath a stereotaxic frame and injected using a Hamilton syringe with an attached custom made 30-gauge stainless steel needle (ESSLAB UK). Cells were injected manually over the course of 1 minute. Following the transplant animals were transferred to a pre-warmed cage to recover. Once the entire litter had undergone surgery and woken up, they were returned to the cage with the mother. Pups were monitored closely for 48-72 hours post-surgery to assess any sign of rejection from the mother.

Table 2.8 Stereotaxic coordinates and overview of each batch of transplants

Batch No.	Cell type received	Unilateral L/R or Bilateral	No. of pups	Injection site #1 (mm)			Injection site #2 (mm)		
				A-P	M-L	D-V	A-P	M-L	D-V
1*	WT hNPCs	Unilateral, Left	15	-1.0	1.0	-0.7	-0.5	1.0	-0.7
2	WT hNPCs	Unilateral, Left	11	-1.0	1.0	-0.7	-0.5	1.0	-0.7
3	WT hNPCs	Bilateral	13	-1.0	1.0	-0.5	-1.0	-1.0	-0.5
4	WT hNPCs	Bilateral	11	-1.0	1.0	-0.5	-1.0	-1.0	-0.5
5**	WT hNPCs	Bilateral	11	-1.0	1.0	-0.5	-1.0	-1.0	-0.5
6	WT hNPCs	Bilateral	14	-1.0	1.0	-0.45	-1.0	-1.0	-0.45
7	α9-hNPCs	Unilateral, Right	14	0.0	1.5	-0.5	1.0	1.5	-0.5
8	α9-hNPCs	Bilateral	4	0.0	1.5	-0.5	0.0	-1.5	-0.5
9	α9-hNPCs	Unilateral, Right	15	0.0	1.5	-0.5	1.0	1.5	-0.5
10	α9-hNPCs	Bilateral	15	0.0	1.5	-0.5	0.0	-1.5	-0.5
11	α9-hNPCs + BDA	Unilateral, Right	11	0.0	1.5	-0.4	1.0	1.5	-0.4
12	WT hNPCs +BDA	Unilateral, Right	14	0.0	1.5	-0.4	1.0	1.5	-0.4

* Surgery carried out by Dr Melissa Andrews
** Batch 5 pups were rejected by mother following transplant and cannibalised
A-P: Anterior-posterior; M-L: Medial-lateral; D-V: Dorsal-ventral

2.7.2 Neural tracing experiments

2.7.2.1 Preparation of BDA solution

A 100 mg/mL stock solution was prepared by dissolving 10 mg biotinylated dextran amine (BDA) powder (10,000 molecular weight, Invitrogen D1956) in 100 µL Axol Neural Maintenance media. Solution was prepared fresh for use.

2.7.2.2 BDA tracing *in vivo*

Two litters were grafted with hNPCs that included 5% BDA (one WT hNPCs batch 12 and one α9-eYFP-expressing hNPCs batch 11). When resuspending cells for transplant, instead of using 100% Axol Neural Maintenance media containing Sure Boost, 50% of the re-suspension solution consisted of the 100 mg/mL BDA stock solution, giving a final BDA concentration of 50 mg/mL. The 50% media contained 2000X Sure Boost to compensate.

2.7.3 Solutions for perfusion

2.7.3.1 Preparation of 0.2 M sodium phosphate buffer

Two stock solutions were produced consisting of 27.8 g sodium phosphate monobasic stock ($NaH_2PO_4*H_2O$, Sigma) in 1 L dH_2O and consisting of 28.4 g sodium phosphate

dibasic stock (Na_2HPO_4, Sigma) in 1 L dH_2O. A 0.2 M sodium phosphate buffer was prepared by adding 81% sodium phosphate monobasic stock and 19% sodium phosphate dibasic stock. Both the monobasic and dibasic stock solutions were kept at RT.

2.7.3.2 Preparation of 0.9% saline solution

Equal parts dH_2O and 0.2 M sodium phosphate buffer were combined before adding 0.9% NaCl. The pH of the solution was measured and adjusted to pH 7.4 using HCl and NaOH, and then filtered using 11 µm Whatman® filter paper (Sigma) and a porcelain Büchner funnel. The solution was stored at RT before use and was prepared no earlier than 48 hours before perfusion.

2.7.3.3 Preparation of 4% PFA solution

An 8% PFA solution was prepared by dissolving PFA powder (Fisher) in dH_2O at 60-65°C using a stir plate and a magnetic stir bar. The solution was cooled to RT and 2-4 mL of 10 M NaOH was added to increase the pH to fully dissolve the PFA. Equal parts 8% PFA solution and 0.2 M sodium phosphate buffer were mixed to give a final 4% PFA (in 0.1 M buffer) solution. The pH of the solution was measured and adjusted to pH 7.4 using HCl and NaOH, and then filtered using 11 µm Whatman® filter paper (Sigma) and a porcelain Büchner funnel. The solution was stored at 4°C before use and was prepared no earlier than 48 hours before perfusion.

2.7.4 Tissue perfusion and sectioning

Sprague Dawley rats were administered an overdose of sodium pentobarbital and perfused transcardially using saline solution followed by 4% PFA at one of five different time points following transplantation (Table 2.9). The brain and spinal cord from each animal were removed and post-fixed in 4% PFA solution for 48 hours at 4°C before being transferred to a 30% sucrose solution in 1X PBS for 48-72 hours for cryoprotection. Cryoprotection was verified when the brain had sunk to the bottom of the storage tube when held in a vertical position. Using a sliding microtome (Leica) and dry ice, brain tissue was cryo-sectioned in the coronal or sagittal plane at 40 µm thickness and stored in 0.05% sodium azide (Sigma) in 1X PBS in a Nunc™ 48-well plate (Thermo Scientific™) at 4°C until processed for staining.

Table 2.9 Number of pups perfused at each time point post-transplantation

Type of graft received	Tissue collection time points post-transplant					
	2 weeks	4 weeks	6 weeks	7 weeks	8 weeks	Total
No. of pups with WT hNPC grafts	17	16	17	15	13	78
No. of pups with α9-hNPC grafts	13	12	12	11	11	59
Total	30	28	29	26	24	137

2.8 IHC analysis of hNPC transplants

2.8.1 IHC of free-floating tissue

Brain tissue was analysed using fluorescent immunohistochemistry (IHC). Tissue sections were first washed in 1X PBS in a Nunc™ 24-well plate (Thermo Scientific™) for 5 minutes before non-specific staining was blocked by incubation in blocking buffer containing 10% goat serum (Sigma) and 0.4% Triton-X in 1X PBS for 2 hours at RT. The tissue was then incubated with primary antibody diluted in blocking solution overnight at 4°C. The primary antibodies used are detailed in Table 2.5. Specifically, to assess graft survival and hNPC projections, human-specific markers including human nuclear antigen (HuNu) and human neural cell adhesion molecule (hNCAM) were used. To assess exogenous α9 integrin expression in α9-eYFP-expressing hNPCs, an anti-GFP antibody (Invitrogen) was used. Following primary antibody incubation, tissue sections were washed three times for 10 minutes each with 0.02% Tween-20 in PBS. For certain antibodies (specifically TN-C), pre-treatment with 0.03% hydrogen peroxidase diluted in PBS for 30 minutes at RT before primary antibody incubation was required. Sections were rinsed once with 1X PBS before continuing with blocking and primary antibody incubation. Tissue was subsequently incubated at RT for 2 hours with fluorescently-tagged secondary antibodies of the corresponding species. All secondary antibodies were used at 1:750 diluted in 1X PBS and are detailed in Table 2.6. Tissue was washed after the secondary antibody incubation using 0.02% Tween-20 in PBS before staining nuclei using DAPI (Thermo Scientific™, 62248) at 1:10,000 diluted in PBS for 10 minutes at RT. For staining of PNNs tissue sections were incubated with biotinylated Wisteria floribunda agglutinin (WFA) diluted in PBS (Table 2.5) for 2 hours at RT before incubation with streptavidin

488 or 568 diluted 1:250 in PBS for 1 hour at RT. Tissue was subsequently stained for DAPI. To analyse BDA expression tissue was incubated with streptavidin 488 or 568 (Table 2.6) diluted 1:250 in PBS for 2 hours at RT before staining with DAPI. Sections were washed a further three times with PBS before mounting onto 0.25% gelatine-coated slides (section.2.8.2). Mounted tissue was covered and allowed to air dry for approximately 1 hour at RT before mounting coverslips (VWR) using FluorSave (Calbiochem). Coverslips were dried at RT for a minimum of 1-2 hours before imaging. Slides were stored at 4°C and covered to protect from the light. Slides were imaged using a Leica D5500 epifluorescent microscope equipped with a DFC550 digital camera (Leica). Initially, every one in six to eight tissue sections of the sensorimotor cortex was analysed for presence of an hNPC bolus and hNCAM-positive projections. Subsequent tissue sections were analysed either rostral or caudal to this depending on where positive HuNu or hNCAM staining was observed. This continued until no further positive staining was detected. In this way the projections were mapped, taking images and creating brain maps by hand for each animal. Images were analysed and scale bars were added using ImageJ software.

2.8.2 Preparation of gelatin-coated slides

Gelatin was prepared fresh for each use by dissolving, 0.5 g gelatin from porcine skin (Sigma) in 500 mL dH_2O at 56°C over a period of 5-10 minutes. The solution was then removed from the heat to cool to RT before adding 0.25 g chromium potassium sulphate. Slides were dipped in and out of the gelatin solution for 1 minute, making sure there were no air bubbles between or on the slides, before being left to air dry at RT for 48 hours.

Chapter 3: *In vitro* expression and functional analysis of integrin and cell-specific protein expression in iPSC-derived hNPCs

3.1 Introduction and aims

Both neurite and axonal growth are highly dependent upon cellular interactions with the surrounding ECM. Neurons communicate and respond to environmental stimuli via growth-promoting transmembrane receptors, such as integrins. These interactions result in reorganisation of the cytoskeleton to modulate axon growth, guidance and elongation. Each integrin heterodimer can bind to different extracellular ligands. The α9β1 heterodimer binds the glycoprotein TN-C, the main ECM component of the mammalian CNS, which is also upregulated following CNS injury. However, as the mammalian CNS matures there is a reduced expression of integrins in neurons, including α9. This is likely to be due to the reduced requirement for developmental proteins within the mature CNS. In both cell culture and after SCI, it has been shown that α9 integrin binding to TN-C promotes neurite outgrowth and extension, as has been demonstrated by overexpression of the α9 integrin subunit in rat PC12 cells and DRGs (Andrews *et al.,* 2009). Increasing integrin expression within the CNS has previously been investigated with regard to axonal regeneration and protein localisation; however, this research showed exogenously expressed α9 integrin is not transported down the axons of the mature CST (Andrews *et al.,* 2016). Therefore, here we suggest hNPCs could be used as a vehicle to increase exogenous expression of integrins within the CNS.

The aim of this chapter was to characterise hNPCs *in vitro* before transplantation into neonatal rat sensorimotor cortex. Our interests mainly focused on analysing endogenous expression of both the α9 and β1 integrin subunits, as well as developing and optimising a protocol for overexpressing the α9 subunit within hNPCs using initially transient transfection and followed by LV for constitutive expression. We utilised LV to overexpress α9 integrin in both rat PC12 cells to confirm the results of others (Andrews *et al.,* 2009), followed by overexpression in hNPCs. In both cases we investigated neurite outgrowth when grown on TN-C with protocol optimisation initially in PC12 cells before moving to the hNPCs. Overexpression was confirmed using ICC and WB, and outgrowth was analysed using neurite outgrowth assays. To gain further insight into their general protein expression profile, additional ICC was carried out on hNPCs to analyse expression of deep-layer cortical neuron markers,

further growth-promoting proteins, as well as examine the presence of other cell types within the cultures.

3.2 Methods

3.2.1 Transient transfection

Proliferating PC12 cells were transfected with α9-eYFP and eGFP plasmids, using GeneJammer (Agilent), PEI (Sigma) or JetPrime (Polyplus) (see section 2.4.8 and Table 2.2 for full protocol). PC12 cells were seeded onto PDL-coated 6-well plates or PDL-coated glass coverslips in 24-well plates (section 2.4.2) the day before transfection. WT PC12 cells were used as a transfection control, which received proliferation media and either no transfection reagent (n=3) or with transfection reagent only (n=1). Transfections were carried out in either a 6-well plate (cell lysates for WB) or a 24-well plate (with coverslips used for ICC analysis). Each transfection using GeneJammer and PEI was replicated (n=3) for each condition and JetPrime transfections for WB were repeated only once (n=1) since the GeneJammer outperformed the JetPrime from the start.

3.2.2 Preparation of second and third generation LV

See sections 2.4.9 and 2.4.10.

3.2.3 Viral transduction of PC12 cells and hNPCs

See sections 2.4.11 and 2.4.12.

3.2.4 Western blot protocol

The full western blot protocol is described in section 2.6.4. Briefly, cell lysates were collected and protein concentration was determined using a BCA assay kit (Thermo Scientific^{TM}). For PC12 lysates, 20 μg of protein was loaded per well and 40 μg of protein per well for hNPC lysates. Cell lysates were separated via electrophoresis using a 4-12% bis-tris pre-cast gel (Invitrogen) and followed by transfer to a nitrocellulose membrane (Gelifesciences). The membrane was subsequently blocked for 1 hour at RT using TBS-T containing 5% milk powder (Marvel). It was then incubated with primary antibody overnight at 4°C with one or more of the following: α9 integrin, GFP, β1 integrin and β-actin (see Table 2.7 for full antibody details). Following

overnight incubation, the blot was washed three times with TBS-T and then incubated with secondary antibody, either horseradish peroxidase (HRP) goat anti-mouse or HRP goat anti-rabbit (Table 2.7), for 45 minutes at RT; which was used at a dilution of 1:15,000 in TBS-T containing 3% milk powder. Membranes were analysed using chemiluminescence. ECL imaging reagents were pipetted over the membrane for 4-5 minutes before imaging using an LAS-3000 Lite imaging system (Fuji).

3.2.5 ICC analysis of PC12 cells and hNPCs *in vitro*

For full ICC protocol, see section 2.6.1. Briefly, PC12 cells and hNPCs grown on coverslips were washed with PBS, fixed with 4% PFA for 10 minutes at RT and subsequently washed three times with PBS. The coverslips were then blocked for 20 minutes using 10% goat or donkey serum and 0.4% Triton-X100 in 1X PBS and then incubated with primary antibody (see Table 3.1, full details in Table 2.5) at 4°C overnight. The coverslips were subsequently washed three times with PBS before being incubated with secondary antibody of the corresponding species (see Table 2.6) for 2 hours at RT. Coverslips were then washed a further three times with PBS before staining the nuclei with DAPI (1:10,000) in PBS for 10 minutes at RT. Coverslips were washed a further three times with PBS before being mounted onto slides.

3.2.6 Neurite outgrowth analysis

Neurite outgrowth assays are described in section 2.6.2 and 2.6.3. Differentiating PC12s were grown on a substrate of both 20 µg/mL PDL and 10 µg/mL chicken TN-C (Millipore) and the hNPCs were grown on 20 µg/mL PLO and 10 µg/mL chicken TN-C or varying concentrations of human TN-C (Millipore): 1 µg/mL, 5 µg/mL, 10 µg/mL, 15 µg/mL, 20 µg/mL, 25 µg/mL or 30 µg/mL. Cells were plated onto coated chamberslides at a density of $5x10^4$/well. The cells were incubated for 72 hours at 37°C, followed by a PBS wash and fixation with 4% PFA for 10 minutes at RT. The PFA was then removed and cells were gently washed three times with PBS and stored at 4°C. Chamberslides were stained following the protocol for ICC (section 2.6.1) with the primary antibodies GFP (1:1,000) and β-III tubulin (1:1,000) (Table 3.1) and secondary antibodies, goat anti-rabbit AlexaFluor 488, goat anti-mouse AlexaFluor 568, donkey anti-guinea pig AlexaFluor 488 and donkey anti-mouse

AlexFluor 568 at 1:1,000 (Table 2.6) incubated for 2 hours at RT. Following imaging, analysis was performed using NeuronJ, Microsoft Excel and Prism 5 GraphPad software. For each condition a total of 30 axons were measured in microns using NeuronJ. Each assay was replicated a minimum of three times (see Tables 3.2 and 3.3), except for the hNPCs grown on 15 µg/mL, 20 µg/mL, 25 µg/mL or 30 µg/mL of human TN-C which were replicated once (n=1) due to time constraints. The results from each replicate are detailed in Table 3.2 for PC12s and Table 3.3 for hNPCs (full details of hNPC outgrowth assays in Appendix A). One replicate consists of one vial of cells using one chamberslide (with two wells/condition) and a total of 30 cells were counted per condition for each replicate. Comparisons between the data sets were analysed using one-way ANOVA (non-parametric) and Tukey *post hoc* to determine statistical significance.

Table 3.1 Primary antibodies and dilutions used for ICC analysis

Antibody	Species	ICC dilution
BDNF	Rabbit	1:200
Ctip2	Rabbit	1:500
DCX	Rabbit	1:500
GFAP	Rabbit	1:750
GFP	Rabbit	1:1,000
Ki67	Mouse	1:100
MBP	Rabbit	1:50
Oct4	Rabbit	1:500
Tbr1	Rabbit	1:200
TN-C	Rabbit	1:250
TrkB	Rabbit	1:1,000
VGlut1	Guinea Pig	1:500
α9 integrin	Rabbit	1:500
β1 integrin	Mouse	1:500
βIII-tubulin	Mouse	1:1,000
βIII-tubulin	Rabbit	1:1,000

3.3 Results

3.3.1 Analysis of α9- and GFP-transfected PC12 cells by ICC and WB

Overexpression of α9-eYFP and GFP was first achieved using transient transfection using two different reagents, GeneJammer and PEI, and results were analysed using ICC and WB. After staining cells for anti-GFP (Invitrogen), the ICC results indicate positive GFP staining in both the α9-eYFP (Figure 3.1, A and D) and GFP (Figure 3.1, B and E) transfected PC12s for both GeneJammer and PEI transfection reagents. The WT PC12 cells showed no positive staining for GFP (Figure 3.1, C and F). For WB, PC12 cells were also transfected using GeneJammer and PEI, however no bands were detected following staining for GFP and β-actin (data not shown). PC12 cells were subsequently transfected with α9-eYFP using JetPrime (Polyplus). From these transfection experiments, the overexpression of α9-eYFP was confirmed by WB (Figure 3.1, G) using the cell lysates from α9-eYFP PC12s (lane 2) and WT PC12 cells (lane 1). These lysates were run alongside lysates collected from WT RPE cells (Lane 3), as a positive α9 integrin control. Following the transfer and blocking step, the blot was stained using anti-α9-integrin antibody and an anti-β-actin antibody. Chemiluminescence detection identified a band in lane 2 at approximately 150 kilodalton (kDa) indicating α9-eYFP expression in PC12 cells and a band between 100-130 kDa in lane 3 indicating endogenous α9 expression in RPE cells. No bands were observed for WT PC12 cells (lane 1), apart from one at approximately 42 kDa indicating β-actin which was observed in all lanes.

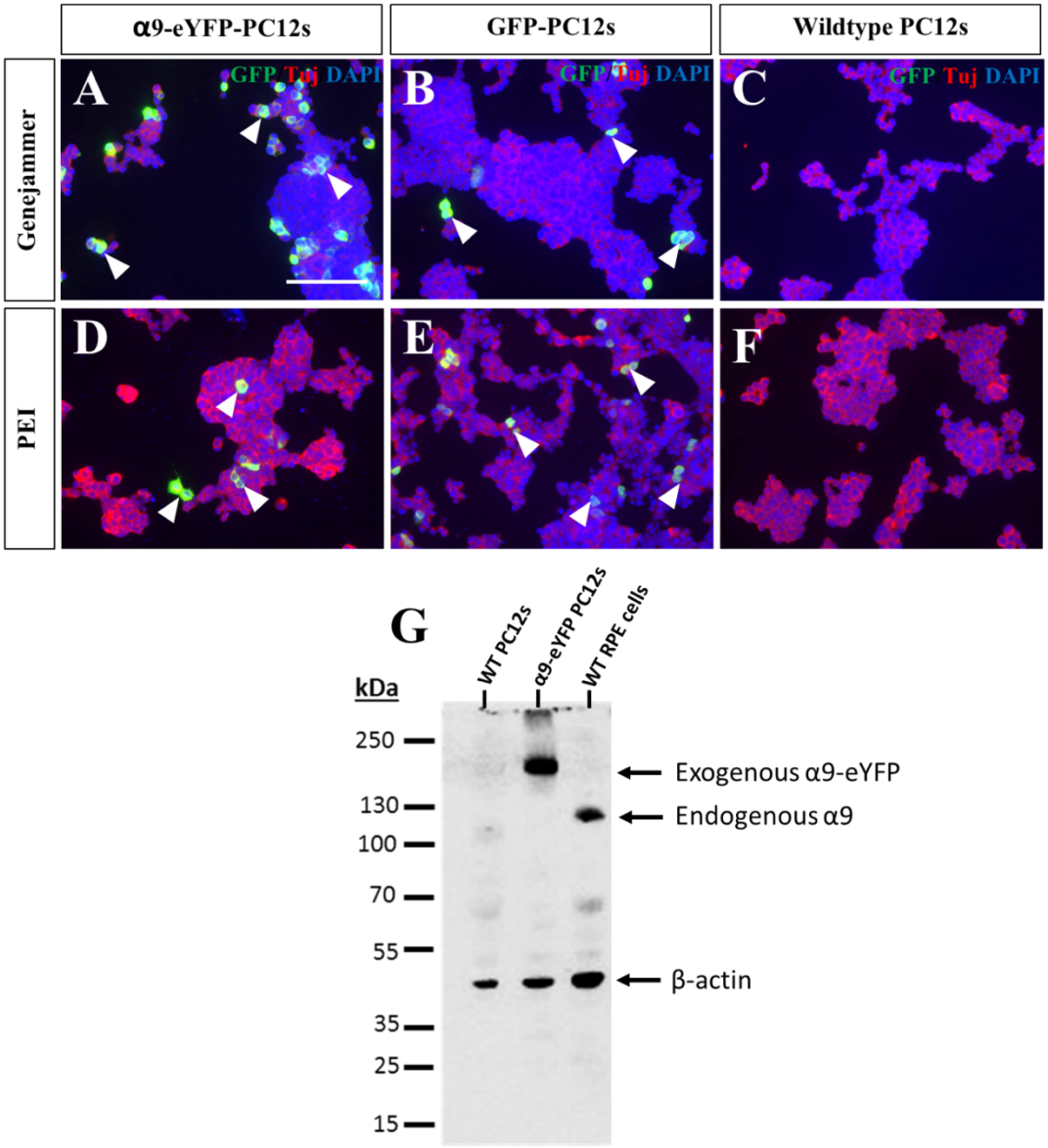

Figure 3.1 Overexpression results following transient transfection of rat PC12 cells with α9-eYFP protein. Proliferating rat PC12 cells were transfected with either a α9-eYFP or a GFP plasmid using either GeneJammer (**A-C**), polyethylenimine (PEI, **D-F**) or JetPrime (**G**). Cells were fixed 72 hours post-transfection using 4% PFA and were stained using antibodies against GFP (Invitrogen) or βIII-tubulin (Sigma) along with a DAPI stain (Thermo Scientific™). Both GeneJammer and PEI reagents resulted in transfection of the α9-eYFP plasmid detected by ICC and indicated by the white arrows highlighting the α9-eYFP positive cells (**A** and **D**). Transfection of GFP was also achieved using both GeneJammer and PEI reagents, indicated by the white arrows highlighting the GFP positive cells (**B** and **E**). No positive GFP staining was detected in WT cells (**C** and **F**) following PEI and GeneJammer transfections. Cells were also transfected using JetPrime reagent which was detected and confirmed using WB at approximately 150 kDa (**G**, lane 2). The endogenous level of α9 integrin was detected in WT RPE cells with a band between 100 and 130 kDa (**G**, lane 3). Lysates from WT PC12s were run in lane 1 and no observed bands were observed apart from β-actin at approximately 42 kDa which was

observed in each lane. Transfections and ICC were repeated three times, n = 3, WB repeated once, n =1. Scale bar in A-F = 100 µm.

3.3.2 Overexpression of α9 integrin and GFP plasmids in PC12 cells using LV

Stable expression of α9-eYFP and GFP in PC12 cells was trialled using third generation LV methods. Different concentrations of polybrene (hexadimethrine bromide) reagent were used to optimise and enhance transduction efficiencies. Following transduction, approximately 30-50% of cells detached from the dish, likely due to the cytotoxic effects of the polybrene. Results from WB show GFP expression was achieved using 0 µg/mL, 2 µg/ml and 4 µg/mL polybrene, but no α9-eYFP expression was observed under the same concentrations of polybrene (Figure 3.2, A). Equal β-actin bands were observed in all lanes at approximately 42 kDa and indicated equal protein loading per well. The blot in Figure 3.2 was the result from cells being incubated with viral supernatant for 4 hours. The experiment was also repeated with an overnight incubation of viral supernatant with the cells, however this did not alter the results (data not shown). Results from ICC confirmed this, as no positive GFP-expression was observed in PC12 cells transduced with third generation LV-α9-eYFP viral supernatant and 2 µg/mL polybrene, following staining using an anti-GFP antibody (Figure 3.2, B and C).

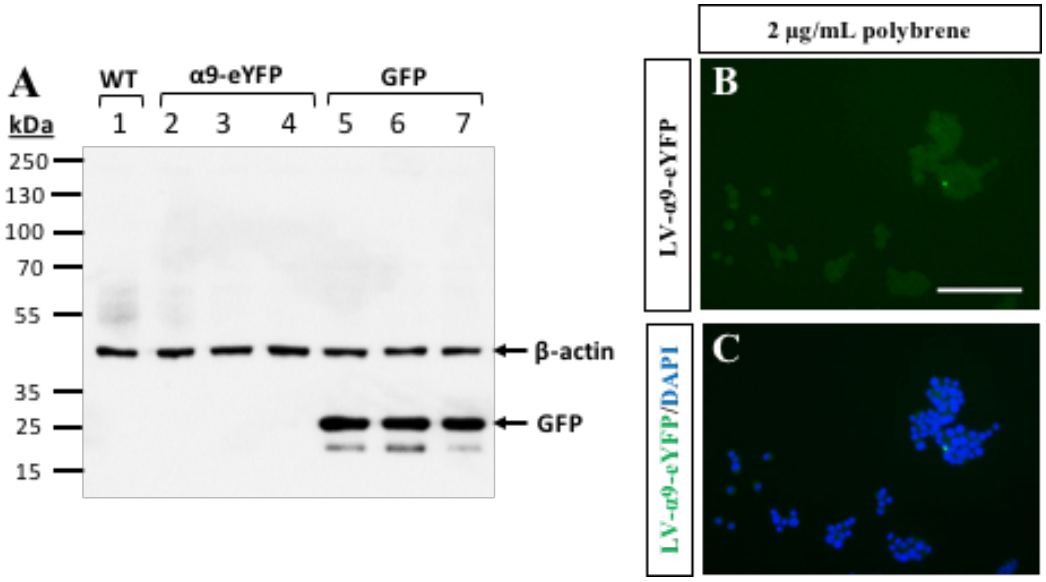

Figure 3.2 WB and ICC results following transduction of PC12 cells using third generation LV. Results show GFP expression was achieved using third generation LV methods with either 0, 2 or 4 µg/mL of polybrene however no expression was observed for α9-eYFP. No expression of α9-eYFP or GFP was observed in WT PC12s (**A**, lane 1). Blot stained with anti-GFP (Invitrogen) and anti-β-actin (Sigma). WB lanes = 1: WT PC12, 2: LV-α9-eYFP PC12 (0 µg/mL PB); 3: LV-α9-eYFP PC12 (2 µg/mL PB), 4: LV-α9-eYFP PC12 (4 µg/mL PB), 5: LV-fGFP PC12 (0 µg/mL PB), 6: LV-fGFP PC12 (2 µg/mL PB), 7: LV-fGFP PC12 (4 µg/mL PB). ICC results shown no positive staining for GFP in PC12 cells that received LV-α9-eYFP third generation supernatant containing 2 µg/mL PB (**B** and **C**). Scale bar in B and C =100 µm.

A second generation LV production and transduction protocol was trialled next and successful expression of LV-α9-eYFP was achieved (Figure 3.3). PC12 cells were transduced with two different LV-α9-eYFP plasmids (denoted '1.1.1' and '2.2.1') using second generation LV, and different volumes of viral supernatant, 1 mL, 2 mL or 3 mL with 2 µg/mL polybrene. Following WB analysis, a double band was observed at the expected 150 kDa in the lanes from cells which received the LV-1.1.1 -α9-eYFP plasmid (Figure 3.3, A lanes 1-3). Within these same lanes, bands at approximately 27 and 37 kDa were also observed. No bands were detected at either of these molecular weights in the PC12 cells which received the LV-2.2.1-α9-eYFP plasmid (Figure 3.3, A lanes 4-6) or in the WT PC12 cells (Figure 3.4, A lane 7). Equal β-actin bands were observed in all lanes at approximately 42 kDa and confirmed equal protein loading per well. Results from ICC confirmed the α9-eYFP expression in cells that received 1 mL of LV-1.1.1-α9-eYFP viral supernatant and 2 µg/mL polybrene (Figure 3.3, B-E, ICC

results for other conditions not shown). Together these optimisation experiments resulted in the subsequent use of second generation LV supernatant using 1 mL LV (LV-1.1.1-α9-eYFP or LV-fGFP) in the presence of 2 µg/mL polybrene (Figure 3.4).

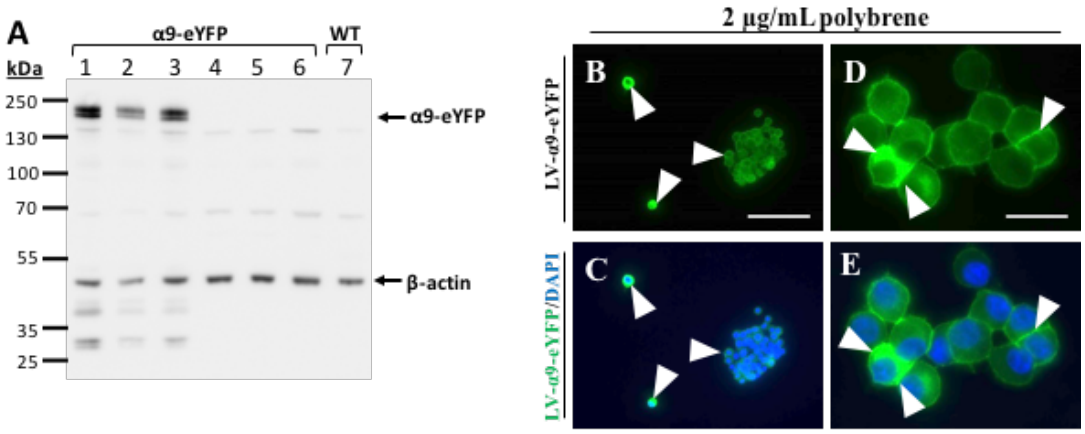

Figure 3.3 Second generation LV results in expression of LV-α9-eYFP in the PC12 cell line. Two different LV-α9-eYFP plasmid preparations were tested using second generation LV production (1-1-1 and 2-2-1) as well as different volumes of viral supernatant (1 mL, 2 mL or 3 mL) with 2µg/ml polybrene. The plasmid 1-1-1 LV-α9-eYFP produced the expected bands at approximately 150 kDa (**A**, lanes 1-3) and no obvious difference in protein expression was observed using either 1 mL (lane1), 2 mL (lane 2) or 3 mL (lane 3) of viral supernatant. Furthermore, small faint bands were observed in these same lanes at around 27 kDa, which may be YFP degradation product. On the other hand, transduction of 2-2-1 LV-α9-eYFP did not result in any overexpression of the α9-eYFP protein following WB (**A**, lanes 4-6). No bands for α9-eYFP were detected in WT PC12 cells (**A**, lane 7). The WB membrane was stained for GFP and β-actin (Table 2.7). WB lanes = 1: LV α9-eYFP PC12 1-1-1 (1 mL supernatant); 2: LV α9-eYFP PC12 1-1-1 (2 mL supernatant); 3: LV α9-eYFP PC12 1-1-1 (3 mL supernatant); 4: LV α9-eYFP PC12. 2-2-1 (1 mL supernatant); 5: LV α9-eYFP PC12. 2-2-1 (2 mL supernatant); 6: LV α9-eYFP PC12. 2-2-1 (3 mL supernatant); 6: WT PC12 cells. Overexpression of α9-eYFP using 1 mL of viral LV-1.1.1 α9-eYFP supernatant and 2 µg/mL supernatant in PC12s was confirmed using ICC (**B-E**). Using a GFP antibody, α9-eYFP could be detected along the PC12 cell surface (white arrows in **B-E**). Scale bar in B-C= 100 µm and D-E = 20 µm.

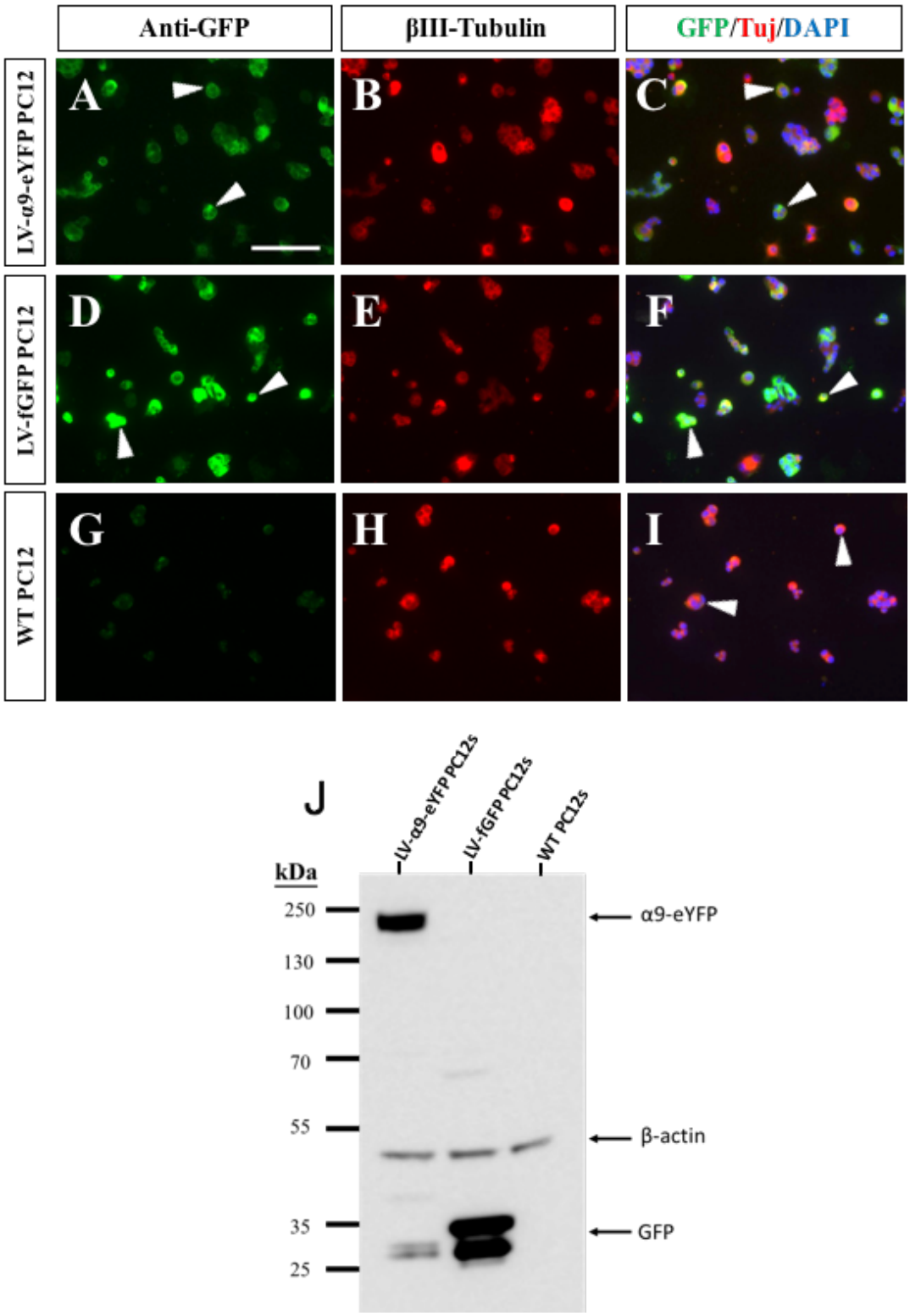

Figure 3.4 Confirmation of second generation LV transduction of α9-eYFP and fGFP in proliferating PC12 cells using ICC and WB. Proliferating PC12 cells grown on PDL were transduced with second generation LV supernatant for either LV-α9-eYFP or LV-fGFP with 2µg/ml polybrene. Successful transduction and expression of the LV-α9-eYFP plasmid was achieved indicated by positive GFP staining (**A**) which co-labelled with βIII-tubulin (**B**) and DAPI (**C**). Positive staining shown for

GFP, following transduction with LV-fGFP supernatant (**D**) shown co-labelled with βIII-tubulin and DAPI (**E, F**). WT (untransfected) PC12 cells did not show positive staining when probed for GFP (**G**). Scale bar A-I = 100 µm. Following WB analysis (**J**), the overexpression of LV-α9-eYFP was detected in lane 1 at the approximately 150 kDa. Furthermore, the over expression of GFP control was detected in lane 2 at roughly 30 kDa. β-actin control staining indicated by the band at 42 kDa in each lane specified equal protein loading per lane.

3.3.3 Functional analysis of α9-expressing PC12 cells on TN-C

To assess if the overexpressed LV-α9-eYFP within the PC12s was functional, virally-transduced cells were grown on 10 µg/mL chicken TN-C (Andrews *et al.,* 2009) and neurites were measured using a neurite outgrowth assay. Measurements were taken from PC12 cells stained for βIII-tubulin. Fluorescent images were converted to black and white to allow for measurement analysis and neurite tracing using NeuronJ (Figure 3.5, A-C). Examples of neurites measured are indicated by the black arrows in images Figure 3.5, A-C. Measurements from three replicate outgrowth assays, totalling 90 measurements for each condition (α9-eYFP, GFP and WT) are shown in Table 3.2. Overexpressing LV-α9-eYFP in PC12s resulted in an average neurite outgrowth of 135.36 µm (n=3) which was significantly longer, $P<0.001$, compared to neurite outgrowth from GFP-transduced PC12 cells (70.99 µm) and WT PC12 cells (75.21 µm) (Figure 3.5, D). There was no significant difference in neurite outgrowth between the GFP-transduced and WT PC12 cells (Figure 3.5, D). From these results we can conclude that the overexpressed α9 integrin from the LV transduction of LV-α9-eYFP leads to expression of functional α9 protein.

Table 3.2 Neurite outgrowth measurements taken from virally-transduced PC12 cells grown on chicken TN-C

Repeat	Average outgrowth in µm on 10 µg/mL chicken TN-C		
	α9–PC12	**GFP–PC12**	**WT PC12**
1	129.55	73.81	84.98
2	128.63	69.69	63.40
3	147.90	69.48	77.26
Average	**135.36**	**70.99**	**75.21**
St Dev.	10.87	2.44	10.94
SEM	6.27	1.41	6.31

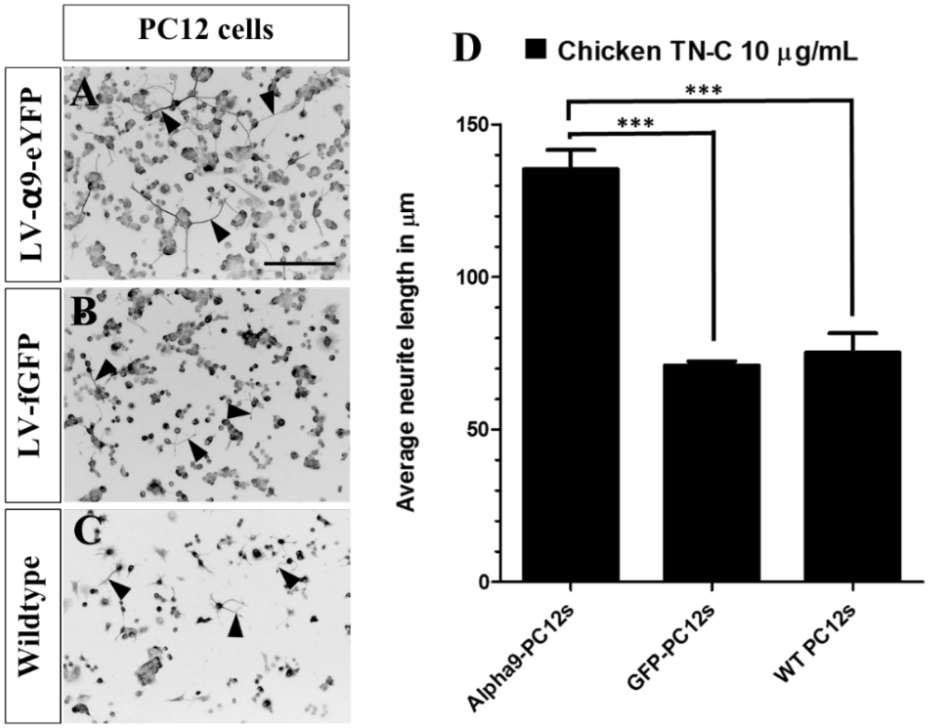

Figure 3.5 Overexpressing of α9 integrin subunit increases neurite outgrowth in PC12 cells when grown on chicken TN-C. PC12 cells transduced with α9-eYFP LV supernatant were able to put out neurites that averaged 135.36 μm in length, which was significantly longer than PC12 cells that expressed GFP, 70.99 μm, and WT PC12 cells, 75.21 μm. Scale bar in A-C = 200 μm. Neurite outgrowth analysed by one-way ANOVA and expressed as mean ± standard error of the mean (SEM), n=3, *** $P < 0.001$.

3.3.4 Endogenous expression and LV overexpression of integrin within hNPCs

Endogenous expression of both α9 and β1 integrin subunits within hNPCs was analysed using ICC and WB. Results showed hNPCs endogenously express β1 integrin (Figure 3.6) and α9 integrin (Figure 3.7, A, B, P and Q) subunits. ICC results showed that α9 was expressed within the cell body of the cultured hNPCs (Figure 3.7, A and B), whereas the β1 integrin appeared to be localised within the neurites and the cell body (Figure 3.6, A and B). Expression of endogenous α9 integrin in human young cerebral cortical neurons (hyCCNs, Axol Bioscience) further differentiated from the progenitor cells (hNPCs) were also examined. ICC results indicated these cells retained the α9 integrin expression into the early stages of neuronal development with

α9 present within neurites (Figure 3.7, C-D, white arrows). Research has previously shown some cells including PC12 cells can express and secrete TN-C into the ECM (Andrews *et al.,* 2009). Our results indicated hNPCs expressed TN-C within the cell (Figure 3.7, E-F). To assess whether these cells would eventually secrete TN-C, further long-term monitoring of *in vitro* hNPCs would be needed.

To confirm the ICC results, WB was carried out on WT hNPC lysates. Both integrin subunits were detected by WB but only after the protein concentration was increased from 20 μg/well to 40 μg/well. Firstly, expression of β1 integrin was observed, however the blots had to be exposed at a higher setting to visualise a band of the expected weight, 145 kDa (Figure 3.6, C and D, lanes 1 and 3). Endogenous β1 expression was also observed in RPE cells at the same molecular weight (Figure 3.6, C and D, lane 2).

The LV protocol developed for overexpression of LV-α9-eYFP and LV-fGFP in PC12 cells was repeated in hNPCs. As noted with PC12 cells, approximately 40% of cells detached in the days following transduction until cells were collected for analysis by ICC or WB, prompting the use of a lower concentration of polybrene without compromising transduction efficiency. Cells were fixed using 4% PFA before staining for GFP with an anti-GFP antibody. Cells were immunopositive for GFP staining in both LV-α9-eYFP hNPCs (Figure 3.7, G-I) and LV-fGFP hNPCs (Figure 3.7, J-L), shown in cells co-labelled with βIII-tubulin. Furthermore, GFP and α9-eYFP expression was observed within both the cell body and extending the length of the neurites (Figure 3.7, G-L, white arrows). The WT hNPCs were negative for GFP expression (Figure 3.7, M-O) as expected. Lysates of LV-α9-eYFP hNPCs, LV-fGFP hNPCs and WT hNPCs were collected for WB analysis, which subsequently confirmed the ICC results. Nitrocellulose membranes were immunostained for GFP alongside β-actin antibodies (Figure 3.7, P and Q). Staining the membrane for GFP detected a band at around 150 kDa in lane 2 containing LV-α9-eYFP hNPC lysates (Figure 3.7, P) indicating α9-eYFP expression, and GFP was detected at around 27 kDa in lane 3 containing LV-fGFP hNPC lysates (Figure 3.7, P). No protein bands at 27 kDa were seen in lane 1 containing WT hNPC lysates. A single β-actin band was seen in each lane at the expected 42 kDa to confirm equal protein loading in each well.

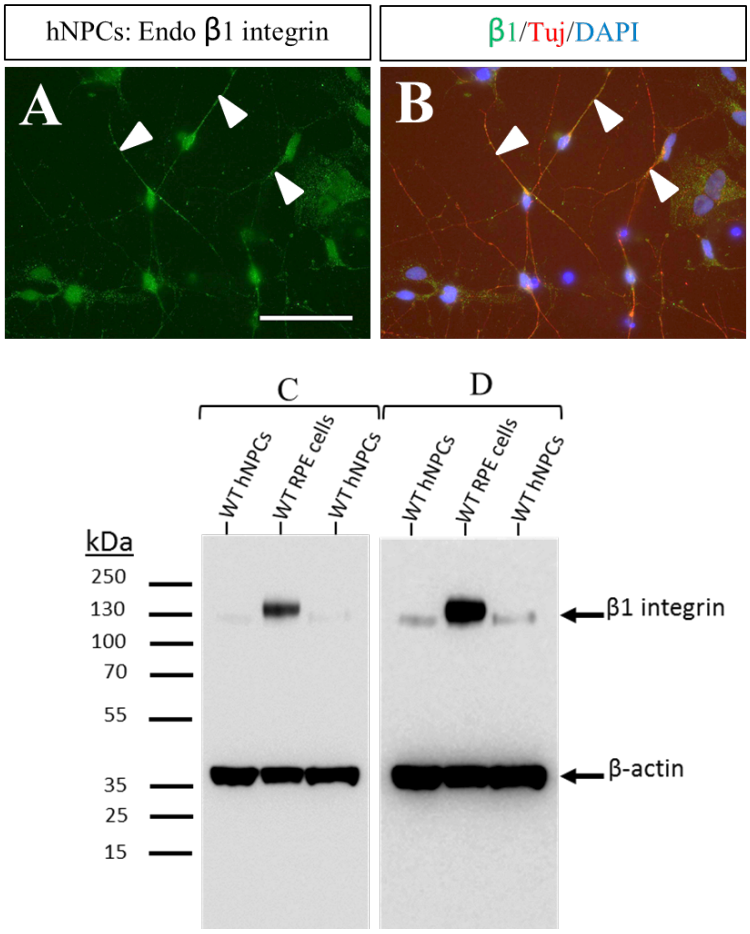

Figure 3.6 Endogenous expression of the β1 integrin subunit in hNPCs. Following ICC analysis hNPCs show expression of endogenous β1 integrin expression within the cell body and neurites (**A**, white arrows) which co-labelled with βIII-tubulin and the nuclear stain DAPI (**B**). Endogenous expression of the β1 integrin subunit was further confirmed using WB. When WT hNPC lysates were stained for β1 integrin subunit, bands were detected at around 130 kDa in lanes 1 and 3, containing WT hNPCs. Lane 2 contained WT RPE cells, which endogenously express β1 integrin to a much higher degree. The blot shown in C is at a low exposure setting and the β1 integrin bands in WT hNPCs are barely detectable (**C**). However, when the membrane is exposed to a higher setting (**D**), the endogenous β1 integrin expression within the WT hNPCs is evident and β-actin bands can be seen in each lane, at around 42 kDa indicating equal protein loading per well. Scale bar in A-B = 50 µm

A separate blot was stained for α9 integrin to enable detection of endogenous protein levels in WT hNPCs alongside RPE cell lysates as a positive α9 integrin control (Figure 3.7, Q). A faint band at 114 kDa was observed in lanes 1 (WT hNPCs) and 2 (LV-α9-eYFP hNPCs) (Figure 3.7, Q) indicating a low level of endogenous α9 integrin. Overexpression of α9-eYFP was indicated by a 150 kDa band in lane 2 (LV-

α9-eYFP hNPCs) indicating an overexpression of the α9 protein (Figure 3.7, Q). Together these results confirm our previous ICC results that hNPCs do express a low level of α9 integrin, however this expression can be increased using LV transduction.

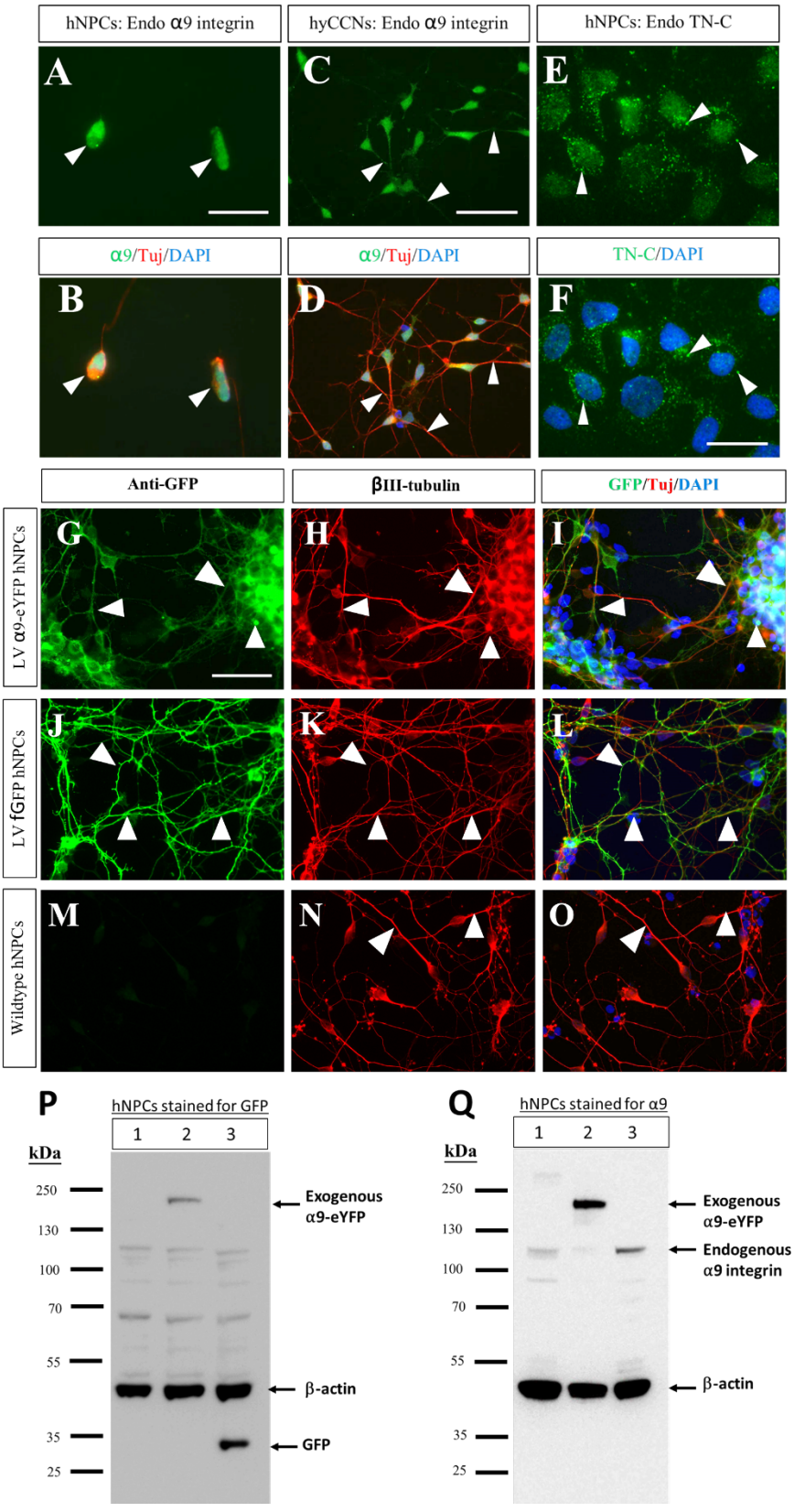

Figure 3.7 Endogenous expression of α9 and LV overexpression of α9-eYFP and GFP in hNPCs. Following ICC endogenous α9 integrin expression was observed within the cell bodies of the hNPCs (**A-B**, white arrows). Within hyCCNs, integrin expression was retained and detected within the neurites

(**C** and **D**, white arrows). ICC results indicate the hNPCs also express TN-C (**E** and **F**, white arrows). Overexpression of both the LV-α9-eYFP and LV-fGFP plasmids in hNPCs was confirmed by ICC (**G-O**) and WB (**P** and **Q**). Using an anti-GFP antibody, the LV-α9-eYFP was detected in hNPCs following LV transduction (**G**) and co-labelled with βIII-tubulin and the nuclear marker DAPI (**H** and **I**). Overexpression of GFP was also detected using the same antibody (**J**) which also co-localised within βIII-tubulin-stained projections (**K**, white arrows) and with DAPI (**L**). No positive GFP expression was detected in WT hNPCs (**M**), but both the βIII-tubulin (**N**) and DAPI (**O**) were positive. Furthermore, overexpression of LV-α9-eYFP was detected using WB and staining for GFP antibody (**P**) and α9 integrin antibody (**Q**). In lane 2, blot P and Q, containing lysates from LV-α9-eYFP hNPCs, an approximate 150 kDa band was detected indicating overexpression of the α9-eYFP protein, detected by both a GFP antibody (**P**) and an α9 integrin antibody (**Q**). Overexpression of GFP was detected in lane 3 (**P**) containing LV-fGFP hNPCs, at around 27 kDa and no bands except for β-actin was observed in lane 1 (**P**) which contained WT hNPCs. β-actin bands were visible in each lane, at around 42 kDa confirming equal protein loading per well. When staining for α9 integrin (**Q**), endogenous α9 expression was detected in WT hNPCs in lane 1 at around 114 kDa. This was the same molecular weight as in lane 3 (**Q**), containing WT RPE cells, which endogenously express the α9 integrin subunit. WB lanes in P = 1: WT hNPCs, 2: LV-α9-eYFP hNPCs, 3: LV-fGFP hNPCs. WB lanes in K = 1: WT hNPCs, 2: LV-α9-eYFP hNPCs, 3: WT RPE cells. Scale bars in A, B, E and F = 20 μm, C and D, G-O = 50 μm.

3.3.5 Expression of α9 integrin promotes neurite outgrowth in hNPCs when grown on TN-C

To examine whether the overexpressed α9-eYFP protein was functional when expressed within hNPCs, neurite outgrowth was measured following the same protocol previously used for the PC12 cells. Following transduction using LV, α9-eYFP hNPCs, fGFP hNPCs and WT hNPCs were plated onto chamberslides coated with either chicken (10 μg/mL) (Figure 3.8) or human (1 μg/mL, 5 μg/mL, 10 μg/mL, 15 μg/mL, 20 μg/mL, 25 μg/mL or 30 μg/mL) TN-C. Cells were grown on TN-C for 72 hours before fixing with 4% PFA and subsequent ICC analysis. Neurite measurements were taken from βIII-tubulin-stained cells (Figure 3.8). Examples of neurites measured for each condition are highlighted by the white arrows in Figure 3.9. The averages from each replicate were pooled and combined (Table 3.3) and the final average was taken and plotted with SEM (Figure 3.10). The raw data from each replicate is detailed in Appendix A.

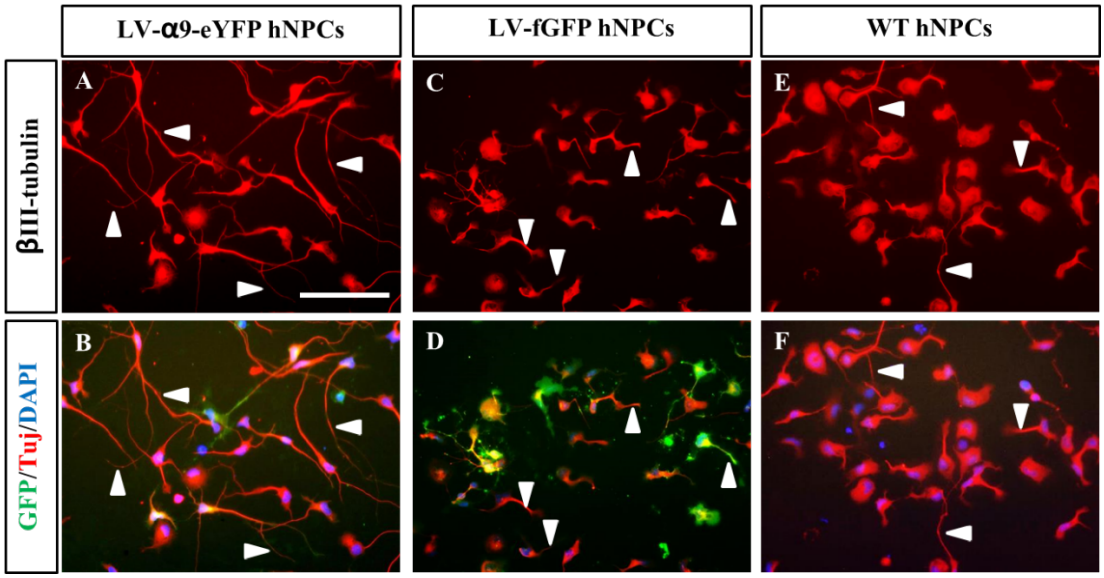

Figure 3.8 Overexpression of α9 in hNPCs promoted neurite outgrowth when grown on chicken TN-C. When grown on 10 µg/mL chicken TN-C, WT hNPCs extended small neurites (**E** and **F**, white arrows), likely as a result of an endogenous integrin expression within these cells. Overexpression of α9 integrin in hNPCs using LV promoted a marked increase in neurite outgrowth (**A** and **B**, white arrows) on the TN-C substrate. Overexpression of GFP alone had no significant result on neurite outgrowth (**C** and **D**, white arrows). Scale bar A-F= 100 µm.

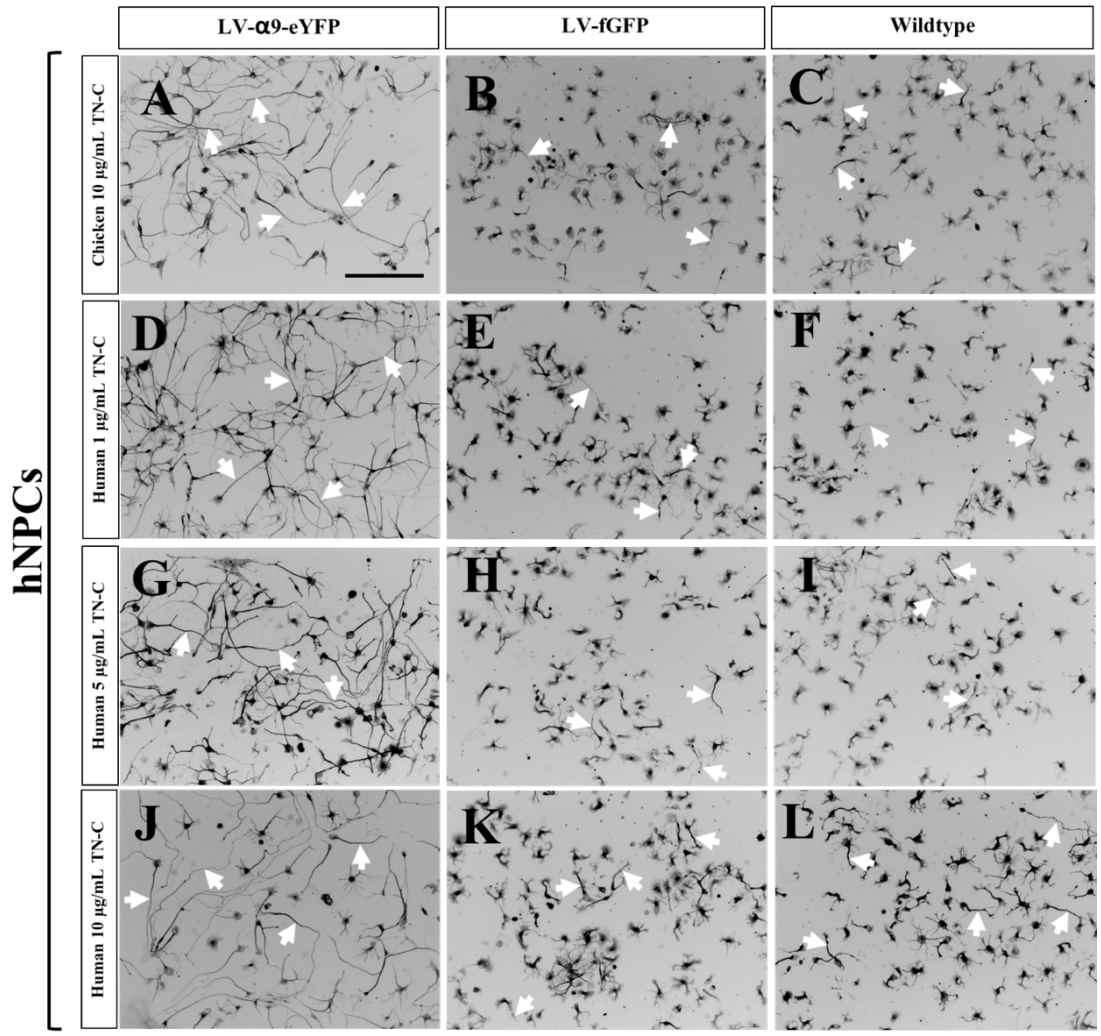

Figure 3.9 Representative images from neurite outgrowth analysis of hNPCs grown on different species and concentrations of TN-C. Following LV transduction, LV-α9-hNPCs, LV-fGFP-hNPCs and WT hNPCs were grown on either 1 µg/mL human, 5 µg/ mL human, 10 µg/mL human or 10 µg/mL chicken TN-C. After 72 hours, cells were fixed and stained for βIII-tubulin (Tuj). Fluorescent images were converted to black and white in Image J, as these were better detected by the Neuron J software. White arrows in each image indicate example neurites that were measured. Scale bar in A-L = 200 µm.

Table 3.3 Combined measurements taken from hNPC neurite outgrowth assays on different species and concentrations of TN-C

Repeat	Time in Culture	Passage fixed	Average outgrowth in µm		
			α9 –hNPC	**GFP-hNPC**	**WT hNPCs**
10 µg/mL Chicken TN-C					
1	10 days	P=2	279.39	47.63	49.31
2	10 days	P=2	225.95	43.65	39.72
3	10 days	P=2	160.21	55.71	38.85
4	27 days	P=2	160.24	56.19	64.53
5	27 days	P=3	149.78	63.15	66.03
6	10 days	P=2	212.60	65.10	55.36
		Average	**198.03**	**55.24**	**52.30**
		St Dev	50.59	8.41	11.79
		SEM	20.65	3.43	4.82
1 µg/mL Human TN-C					
1	10 days	P=2	234.75	49.44	52.30
2	10 days	P=2	250.31	46.72	40.85
3	27 days	P=2	130.79	75.05	75.87
4	27 days	P=3	120.97	95.83	95.53
5	10 days	P=2	192.83	50.35	54.03
		Average	**185.93**	**63.48**	**63.72**
		St Dev	58.81	21.39	21.83
		SEM	26.30	9.57	9.76
5 µg/mL Human TN-C					
1	10 days	P=2	203.29	59.21	72.99
2	10 days	P=2	256.84	53.01	53.76
3	27 days	P=2	126.05	90.29	74.76
4	27 days	P=3	124.45	89.56	83.65
5	10 days	P=2	193.80	132.98	124.79
		Average	**180.89**	**85.01**	**81.99**
		St Dev	56.19	31.78	26.29
		SEM	25.13	14.21	11.76
10 µg/mL Human TN-C					
1	10 days	P=2	185.20	90.10	78.56
2	10 days	P=2	283.48	81.48	75.78
3	27 days	P=2	139.20	105.20	104.10
4	27 days	P=3	158.90	124.10	129.10
5	11 days	P=2	184.42	165.80	124.61
6	10 days	P=2	192.51	152.82	154.70
		Average	**190.62**	**119.92**	**111.14**
		St Dev	49.69	34.02	30.86
		SEM	20.29	13.89	12.60
15 µg/mL Human TN-C					
1	10 days	P=2	177.35	162.76	144.19
		St Dev	76.57	59.28	31.00
		SEM	13.98	10.82	5.66
20 µg/mL Human TN-C					
1	10 days	P=2	187.95	183.12	176.68
		St Dev	129.13	60.47	44.58
		SEM	23.58	11.04	8.14
25 µg/mL Human TN-C					
1	10 days	P=2	191.50	155.65	240.89
		St Dev	84.84	74.43	68.96
		SEM	15.49	13.59	12.59
30 µg/mL Human TN-C					
1	10 days	P=2	190.30	229.38	183.6
		St Dev	95.91	58.41	56.87
		SEM	17.51	10.66	10.38

A significant difference in LV-α9-eYFP hNPCs outgrowth was observed for each condition (chicken 10 μg/mL, human 1 μg/mL, human 5 μg/mL and human 10 μg/mL) compared to both LV-fGFP hNPCs and WT hNPCs (Figure 3.10, A-D). Furthermore, when hNPCs were cultured on human TN-C, a significant increase in neurite outgrowth was observed with increasing concentrations of human TN-C (Figure 3.10, A-D and I), specifically in the GFP hNPCs, between those grown on 10 μg/mL chicken TN-C and the 10 μg/mL human TN-C ($P<0.01$) and also between those grown on 10 μg/mL human TN-C and 1 μg/mL human TN-C ($P<0.01$). Additionally, a significant difference was observed between the WT hNPCs grown on 10 μg/mL human TN-C and 10 μg/mL chicken TN-C ($P<0.01$) and those grown on 1 μg/mL human TN-C and 10 μg/mL human TN-C ($P<0.05$). No significant difference was observed between the four different LV-α9-eYFP hNPCs grown on any of the TN-C substrates.

To assess this further, initial experiments were carried out using higher concentration of human TN-C (15, 20, 25 or 30 μg/mL). Results for 15 μg/mL and 20 μg/mL of human TN-C showed an increase in neurite outgrowth from the GFP-hNPCs and WT hNPCs, whilst outgrowth from LV-α9-hNPCs remained consistently high at around 200 μm (Table 3.3 and Figure 3.10). These results were in line with the trend observed in 1-10 μg/mL, which demonstrated an increased concentration of human TN-C resulted in increased neurite length from both GFP and WT hNPCs. At higher concentrations of 25 μg/mL or 30 μg/mL human TN-C, expression from each of the three cell types (WT, α9-eYFP and GFP) did not follow the expected trend, however each of these latter experiments (15, 20, 25 and 30 μg/mL) was carried out only once and will need to be repeated to assess reliability (Table 3.3 and Figure 3.10).

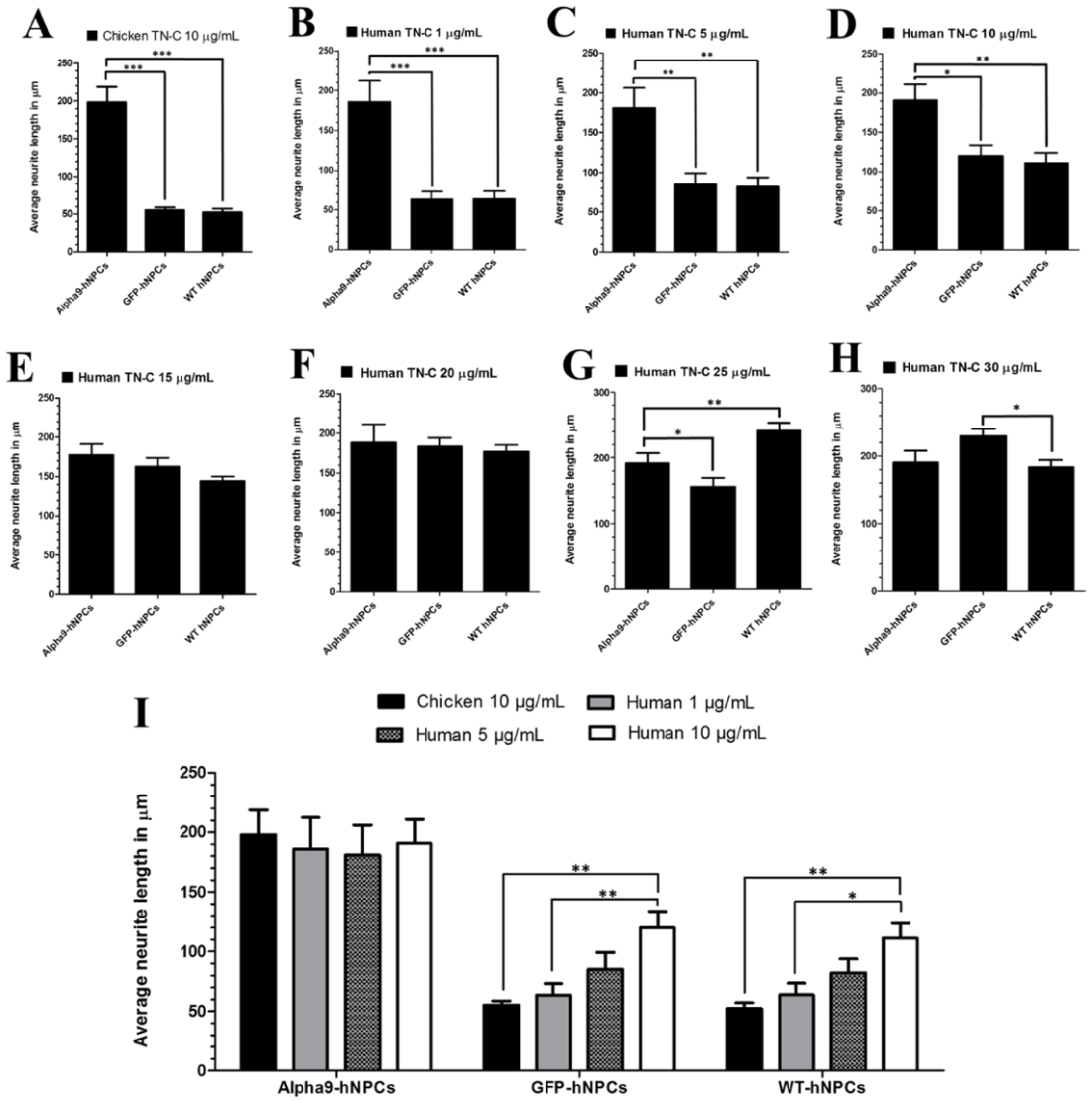

Figure 3.10 Increasing α9 integrin expression in hNPCs promotes neurite outgrowth when grown on different concentrations of chicken and human TN-C. Overexpressing α9-eYFP in hNPCs promoted significant neurite outgrowth when grown on 10 µg/mL chicken TN-C and on 1 µg/mL, 5 µg/mL or 10 µg/mL of human TN-C compared to GFP-hNPCs and WT control hNPCs. (**A-D** and **I**). Furthermore, as the concentration of human TN-C increased from 1 µg/mL to 10 µg/mL the neurite outgrowth from both the GFP- and WT hNPCs increased (**I**). No significant difference was observed between the four different LV-α9-eYFP hNPCs grown on any of the TN-C substrates (**I**). When the concentration of human TN-C was increased further (15 µg/mL, 20 µg/mL, 25 µg/mL or 30 µg/mL), neurite outgrowth from the GFP-hNPCs and WT hNPCs also increased, however further repeats will be required to confirm this (**E-H**). Results were analysed by one-way ANOVA and expressed as mean ± SEM (chicken 10 µg/mL n=6; human 1 µg/mL n=5; human 5 µg/mL n = 5; human 10 µg/mL n = 6;

human 15 µg/mL n = 1; human 20 µg/mL n =1; human 25 µg/mL n = 1 and human 30 µg/mL n = 1); *P<0.05, ** P<0.01, ***P<0.001.

3.3.6 Further hNPC characterisation for cell-specific protein markers

To gain further insight into the protein expression profile of hNPCs, ICC was performed for a number of cell-specific protein markers. These included analysing the cells for other phenotypes, examining deep-layer cortical neuron markers, assessing expression of other growth-promoting proteins, analysing potential neuronal phenotypes as well as assessing progenitor and prolific markers.

Human NPCs (Axol Bioscience) were pre-programmed to become cerebral cortical neurons (CCNs) and therefore hNPC cultures would be expected to largely consist of a neuronal phenotype. Nevertheless, we analysed the cultures for other potential cell types that neural progenitors may differentiate into, including astrocytes and oligodendrocytes. Following staining for glial fibrillary acidic protein (GFAP), myelin basic protein (MBP) and βIII-tubulin, the hNPC cultures contained a small proportion of GFAP-positive cells indicative of astrocytes (Figure 3.11, B); however, there was no presence of MBP, a protein expressed by myelinating oligodendrocytes (Figure 3.11, C). The cells that were stained for MBP were kept in culture for 21 days to allow for the potential development of myelin, however, MBP staining was not present within the culture at this time point. The majority of cells within the culture were βIII-tubulin-positive indicating a high proportion of the hNPCs had a neuronal phenotype as expected (Figure 3.11, A).

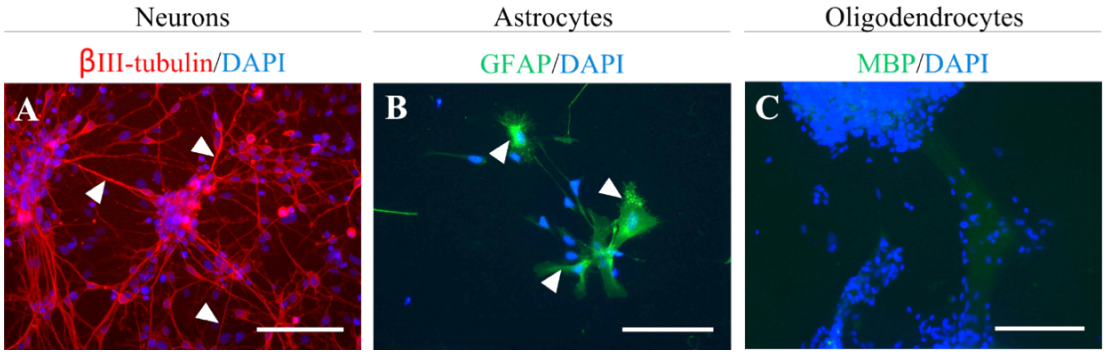

Figure 3.11 WT hNPC cultures contained neuronal and astrocytic cells, but no MBP-positive oligodendrocytes. The hNPCs were pre-programmed to become CCNs, which was confirmed by ICC results as the majority of the culture expressed the neuronal marker βIII-tubulin (**A**). A small proportion of the culture was also positive for GFAP indicative of astrocytes (**B**), however no positive staining was observed in 21-day old cultures probed for myelin basic protein (MBP), a marker for oligodendrocytes (**C**). Scale bar in A-C = 100 µm.

As the hNPCs were intended for transplantation into the deep layers of the rat sensorimotor cortex, the hNPCs were analysed for expression of deep-layer cortical neuron markers Ctip2 and T-box brain 1 (Tbr1) before being transplantated. Both of these neuronal markers are associated with the projection of neurons to subcortical targets. We found a high proportion, approximately 80%, of hNPCs expressed Tbr1 (Figure 3.12, A-C) and Ctip2 (Figure 3.12, D-F), colocalising with the cell nucleus.

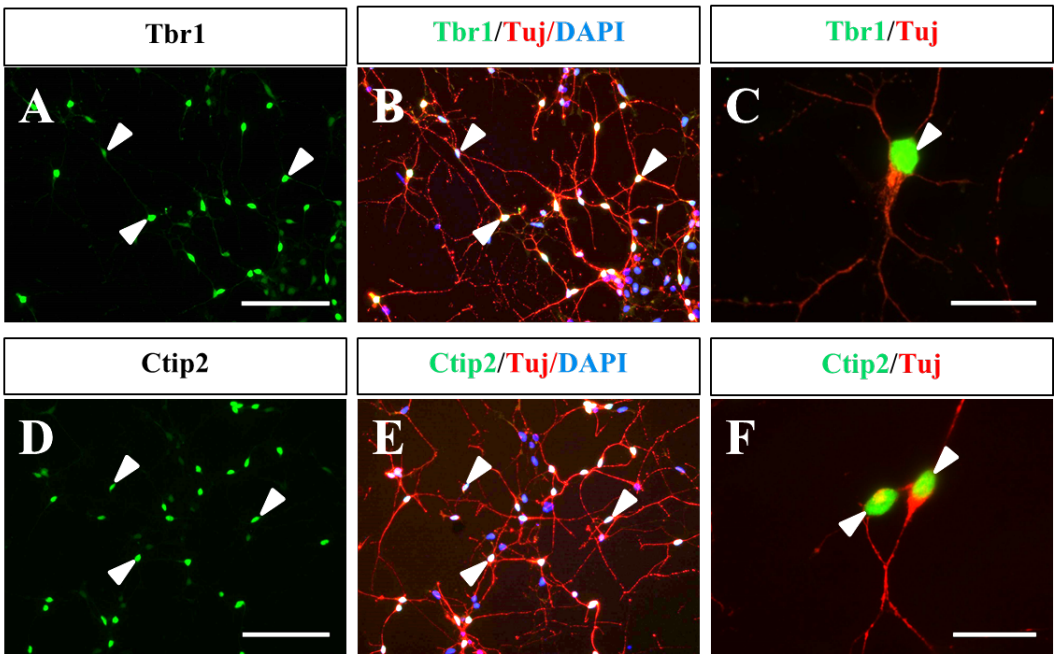

Figure 3.12 hNPCs expressed deep-layer cortical neuron markers *in vitro*. The WT hNPCs were analysed for their expression of deep-layer cortical neuron markers, as this was the area that we targeted for transplantation. Two such markers include Tbr1 (**A-C**) and Ctip2 (**D-E**). ICC results show both were expressed within the nucleus of the hNPCs, which co-labelled with the nuclear stain DAPI (white arrows in **B** and **E**, respectively). Scale bars in A, B, D and E= 100 µm; C and F= 20 µm.

For further characterisation into the developmental state of the cells, the hNPCs were analysed for their expression of the progenitor marker doublecortin (DCX). DCX is a protein expressed in immature neuronal cells and was anticipated to be highly expressed within these developing cells. Our ICC analysis confirmed that DCX was expressed and co-labelled with the βIII-tubulin-expressing cells (Figure 3.13, A-B).

Alongside integrin expression, hNPCs were also found to express TrkB, a growth-promoting receptor, involved in axonal elongation, as well as its ligand, BDNF, known for its growth-promoting properties (Reviewed in Binder and Scharfman, 2004). Both proteins were observed with punctate expression within the cell body and neurites (Figure 3.13, E, F and C, D, respectively). Moreover, as a high proportion of cortical projection neurons are excitatory glutamatergic neurons, presence of this phenotype using a vesicular glutamate transporter 1 (VGlut1) antibody was assessed. Human NPCs were found to express high levels of VGlut1 (Figure 3.13, G-H) and suggested the hNPCs had an excitatory phenotype.

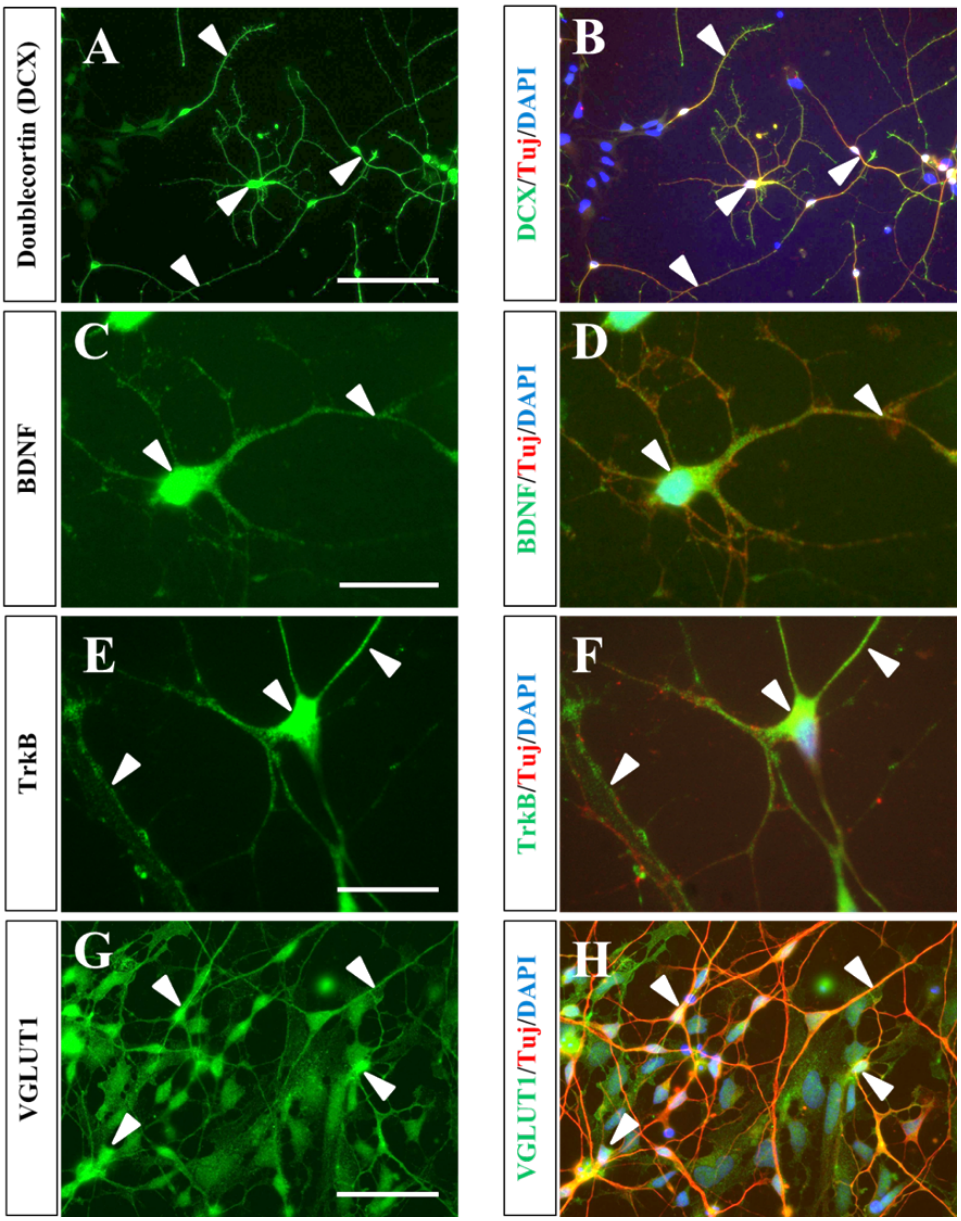

Figure 3.13 Further characterisation of hNPCs *in vitro*. Following ICC analysis, results show hNPCs expressed the progenitor marker DCX (**A-B**), the neurotrophin BDNF (**C-D**) and its receptor TrkB (**E-F**) as well as the glutamate transporter VGlut1 (**G-H**). Scale bars A-B = 100 µm; C-F =20 µm and G-H = 50 µm.

Furthermore, as these hNPCs have been pre-programmed to differentiate into CCNs, we would expect there to be very few cells maintaining the expression of stem cell markers, such as Oct4. Following ICC, hNPCs were immunopositive staining for Oct4 (Figure 3.14, A-B). Oct4 is associated with undifferentiated cells, which does not align with our previous results. Research has suggested Oct4 expression is finely balanced

and overexpression of Oct4, can stimulate differentiation (Niwa *et al.,* 2000), a characteristic which may explain the high expression level seen within the hNPCs. Conversely, hNPCs were also positive for the proliferation marker Ki67 (Figure 3.14, C-E), which is highly expressed in stem cells but also cancerous cells and its expression can be of concern when using stem cell-derived cells *in vivo*.

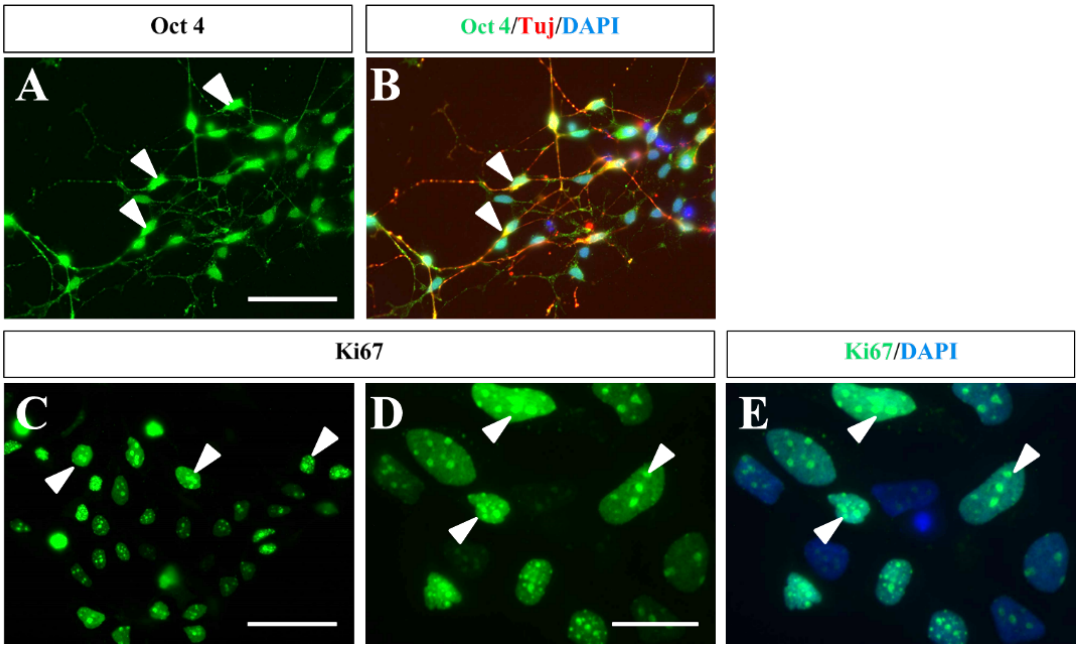

Figure 3.14 hNPCs express stem cell and proliferation markers. hNPCs were positive for the transcription factor Oct4 (**A**, white arrows), a recognised stem cell marker, using an anti-Oct4 antibody. Within the hNPCs positive Oct4 expression was observed co-localising with the nuclear stain, DAPI (**B**, white arrows). Furthermore, the hNPCs were positive for Ki67 (**C** and **D**), a nuclear protein involved in cell proliferation and within the hNPCs this co-localised with DAPI (**E**, white arrows). Scale bars A-B = 100 µm; C= 50 µm and D-E =20 µm.

The hNPCs were transplanted at around 8-9 days in culture. Prior to transplant, WT hNPCs cells were able to extend neurites *in vitro* (Figure 3.15, A white arrows) and neural rosette formation was observed (data not shown). Interestingly, after cells were maintained in culture for 21 days, mature fibre bundles were observed extending from boluses of WT hNPCs (Figure 3.15, C white arrows). These bundles appeared larger in size, suggesting the axon diameter may have grown in size or the axons were bundling together.

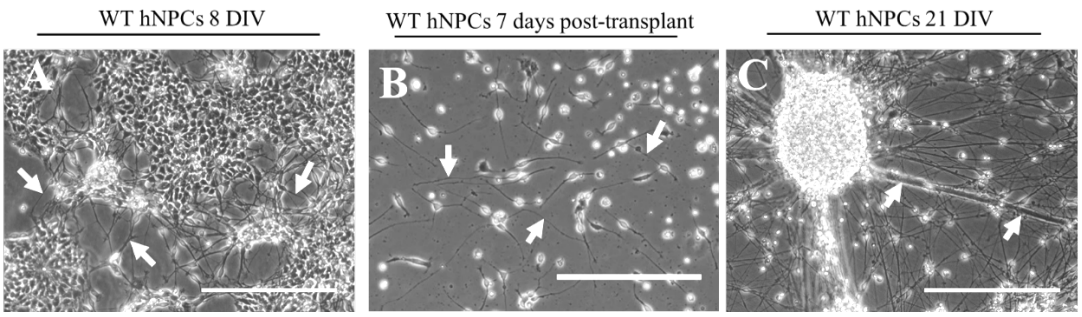

Figure 3.15 WT hNPCs before and after transplantation. The hNPCs were transplanted after 8-9 days *in vitro* (DIV). At this point cells were able to extend neurites (**A,** white arrows). Following transplantation, remaining cells were placed back into culture. WT hNPCs were able to extend neurites after being at RT for an extended period of time during the transplantation procedure (**B**, white arrows). When hNPCs were kept in culture for 21 days they displayed large fibre bundles projecting from hNPC boluses which suggested projections were bundling together or the axon diameter had grown (**C**, white arrows). Scale bar A-C= 250 µm.

Finally, the hNPCs were analysed after transplantation to assess their viability and ability to extend neuronal projections following the transplantation protocol. Following the transplant procedure, the remaining WT hNPCs and α9-eYFP hNPCs were returned to cell culture to analyse the cell population used for transplants (Figure 3.15, B and Figure 3.16, A). Cells extended axonal projections indicating both their viability as well as their ability to extend projections at the time of transplant, and up to a week following transplant, the longest time point analysed. Furthermore, the exogenous α9-eYFP expression was analysed 7 days post-transplant, indicating cells expressed α9-eYFP protein at the time of grafting (Figure 3.16, B-F). The α9-eYFP protein was detected within the neurites from these cells and also clustering within potentially newly forming growth cones (Figure 3.16, D-F).

The hNPCs were also stained for presence of Rab11, a small GTPase involved in integrin trafficking/recycling (Eva *et al.,* 2010; Franssen *et al.,* 2015), microglia using an anti-ionised calcium binding adapter molecule-1 (Iba-1) antibody and synapse formation using an anti-postsynaptic density protein-95 (PSD-95) antibody, all of which were negative (data not shown).

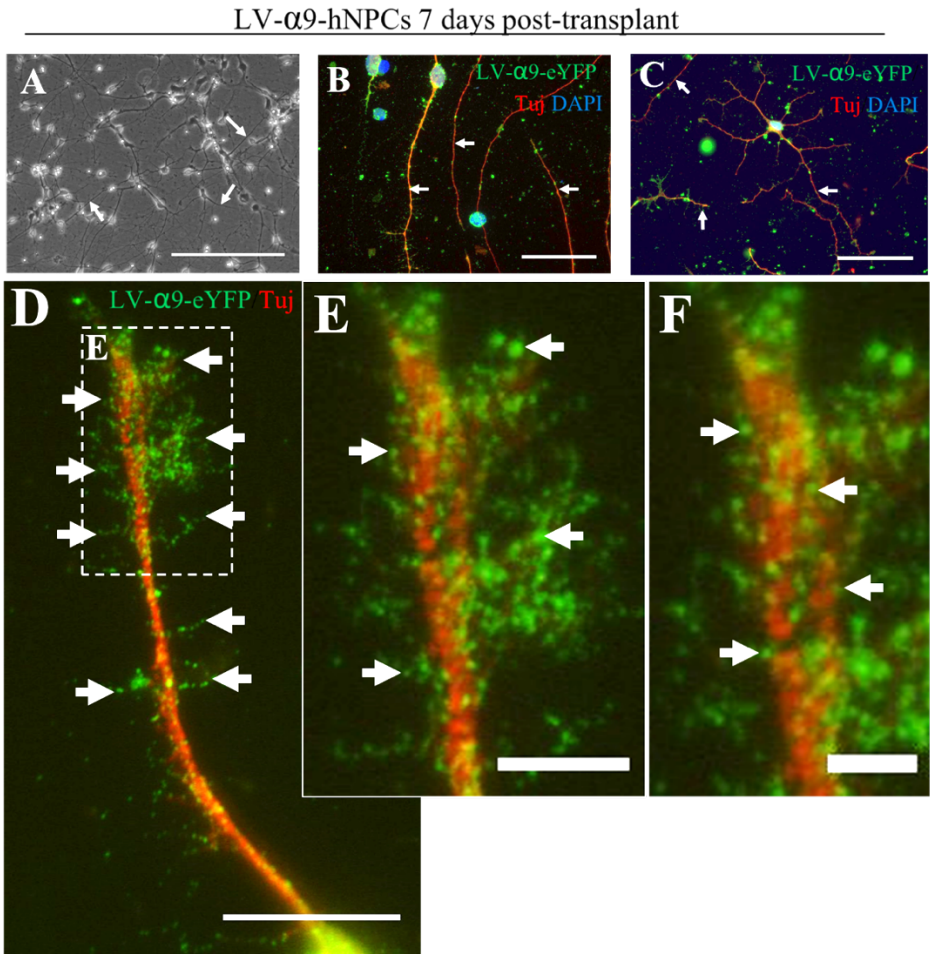

Figure 3.16 α9-hNPCs in culture including under the conditions of transplantation. Following collection for transplantation, remaining hNPCs were returned to culture and were able to extend neurites 7 days post-transplant (**A**, white arrows) (longest time-point analysed) indicating cell viability at the time of transplant. Furthermore, following ICC analysis excess LV-α9-eYFP hNPCs maintained expression of α9-eYFP (**B-F**). The α9-eYFP protein was detected within the neurites from these cells and also clustering within potentially newly forming growth cones (**D-F**). Scale bar in A= 250 µm; B and C = 50 µm; D = 15 µm; E = 5 µm; F = 2.5 µm.

3.4 Discussion

Integrins are involved in cell-cell and cell-matrix interactions. As the mammalian CNS matures, developmental proteins, such as integrins, involved in neuronal outgrowth and elongation are downregulated. As a result, the adult CNS is unable to repair or regenerate. The α9 integrin subunit forms a heterodimer with the β1 subunit and when expressed it can bind TN-C, the main ECM component of the CNS, highly expressed during development and also upregulated after a CNS injury (Zhang *et al.,* 1997; Tang *et al.,* 2003; Andrews *et al.,* 2009). Furthermore, the environment created after CNS injury is characterised by a number of inhibitory molecules namely CSPGs and myelin-derived inhibitory proteins, such as Nogo-A, preventing regeneration. In an attempt to promote regeneration within the injured CNS, α9 integrin has been researched for its ability to promote repair after injury. Indeed, increasing α9 integrin expression *in vivo* using adeno-associated virus in DRG promotes axonal regeneration following a dorsal column crush injury (Andrews *et al.,* 2009). However, recent research has demonstrated that exogenously expressed α9 integrin subunit is not trafficked into the axonal compartment within certain neuronal subtypes, including adult CST axons (Andrews *et al.,* 2016). It is unclear why the integrin is inhibited from localising within those axons but it may be due to Rab11-Arf6 coupling promoting retrograde integrin transport and hence restricting expression of integrins to the somato-dendritic domain (Franssen *et al.,* 2015). However, Andrews and colleagues (2016) also discovered integrin transport is present within developing CST axons. Together this research suggests a requirement for an alternative method to overexpress the α9 integrin subunit in order to promote repair and long-distance axonal regeneration within the adult CNS. One such alternative described in this work is using developmental hNPCs to act as a vehicle to reintroduce integrin into the mature CNS.

In this chapter we have presented extensive *in vitro* characterisation of iPSC-derived hNPCs including demonstration of the endogenous levels of both the α9 and β1 integrin subunits and the overexpression of the α9 subunit using both transient transfection and stable viral transduction. Additionally, we assessed the *in vitro* capacity of these cells to promote neurite outgrowth on TN-C. Furthermore, we

showed an increase in α9 integrin expression in hNPCs can have a significant effect on promoting neurite outgrowth when cells are cultured on TN-C.

To confirm previously published work, a number of proof-of-principle experiments were performed using the α9-eYFP plasmid in the rat neuronal PC12 cell line. Firstly, transient transfection was used to overexpress the α9-eYFP protein to confirm overexpression within PC12s. Owing to the lack of commercially available antibodies for α9 integrin *in vivo*, the α9 plasmid had been tagged with eYFP. This allowed exogenous expression of α9 integrin to be easily detected using an anti-GFP antibody *in vitro* as well as *in vivo*. Alongside these transfections a GFP-only plasmid was used as a transfection control along with untransfected WT cells. The use of a GFP-only plasmid allowed us to ascertain that any functional effect coming from the α9-eYFP protein was due to the presence of the α9-integrin and not the transfection procedure. The results here indicate expression of either the α9-eYFP or GFP plasmid in PC12 cells was achieved using either GeneJammer or PEI transfection reagents with similar efficiencies, and no GFP expression was observed within the WT PC12 cells, confirmed by ICC (Figure 3.1). For WB, expression was also assessed following GeneJammer and PEI transfections, however no bands were detected on the blots after probing for GFP and β-actin. This was considered to be a problem that occurred during the collection of cell lysates. The transfections and WB were repeated (n=3), and fresh cell lysis buffer was used for each replicate, however no bands were observed. One further transfection reagent, JetPrime, was used to transfect PC12 cells with the α9-eYFP plasmid. Following WB detection, an α9-eYFP band was observed at approximately 150 kDa. This was slightly higher than endogenous (untagged) α9, at around 114 kDa. The reason for this is due to the exogenous protein being tagged to eYFP which adds roughly another 26 kDa, causing the molecular weight of the protein to be increased (Figure 3.1).

With transplantation experiments in mind, stable expression of the α9-eYFP protein was assessed using third generation LV. The LV system is a commonly used gene transfer approach allowing expression of proteins of interest in both dividing and non-dividing cells compared to retrovirus which only allows expression of the transfer plasmid in dividing cells. As the hNPC culture had the potential to contain both dividing and non-dividing cells, the LV system was the more appropriate choice

compared with the retroviral system. Furthermore, LV is thought to be more stable when used *in vivo* compared to retrovirus (Naldini *et al.,* 1996). A third generation LV system is considered safer compared to the other two systems (first generation and second generation) (Dull *et al.,* 1998) as it requires transfection of four different plasmids; two packaging plasmids, one envelope plasmid and one transfer plasmid. In this system six out of the nine virulent human immunodeficiency virus genes have been removed leaving *gag, pol* and *rev*, which are split over two packaging constructs, one carrying *gag* and *pol* and the other carrying *rev* (Dull *et al.,* 1998). This system also requires the transfer plasmid to contain a customised 5' long terminal repeat (LTR) containing constitutive promoters. Use of third generation LV did not result in successful overexpression of the α9-eYFP protein, but did result in overexpression of GFP. The transductions were repeated with freshly prepared virus and consistently produced no expression of the α9-eYFP protein. After closer inspection of the LV-α9-eYFP transfer plasmid, it was discovered this construct was designed to be used within a second generation system only as it did not contain the chimeric 5' LTR. It therefore required the presence of the *tat* gene to promote expression. This gene is contained within the packaging plasmid of a second generation system. Following this discovery, the LV system was changed from third generation to second generation.

A second generation LV system uses only one packaging and one envelope plasmid alongside the transfer plasmid and is considered less safe than the third generation system. Within this system *gag, pol* and *rev* genes are present alongside *tat* on one packaging plasmid. The addition of the *tat* gene allows for viral transcriptional regulation (Bieniasz *et al.,* 1999). Expression of α9-eYFP and GFP was achieved within the PC12 cells (Figures 3.3 and 3.4) and subsequently the hNPCs (Figure 3.7) using second generation freshly prepared LV supernatant. A second generation transfer plasmid, such as LV-α9-eYFP, can only be packaged using a second generation LV system, however a third generation transfer plasmid, such as LV-fGFP, can be packaged using either a second or a third generation system. This possibly explains why positive GFP expression was observed following use of both second and third generation protocols.

The successful expression of the α9-eYFP protein following a second generation LV protocol, compared to third generation, is likely due to the construct constituents used

within this system, specifically the addition of the *tat* gene within the packaging plasmid; however, we have considered a number of other possibilities. Firstly, it may be due to the size of the LV-α9-eYFP transfer plasmid, which at greater than 10 kilobases, is quite large and may be reaching the upper limit of the capabilities of a third generation system. Research has indicated that viral titre decreases with a larger vector size (Kumar *et al.,* 2001) and protocols have been optimised to combat this (al Yacoub *et al.,* 2007). Lastly, the production of viral supernatant from a third generation system requires successful transfection of four plasmids, whereas second generation only requires transfection of three plasmids, therefore increasing the chance of successful transfection and viral particle production from a second generation system. This however is unlikely as GFP viral supernatant was produced effectively using the third generation system, and it is more probable the lack of α9-eYFP expression using a third generation system is due to one of the previous explanations.

The expression of α9-eYFP and GFP was obtained using second generation LV and 2 µg/mL polybrene. The cationic polymer polybrene is often used to enhance viral transduction efficiency by reducing the charge on the target cell membrane to promote entry of viral plasmids (Davis *et al.,* 2002; Lizée *et al.,* 2004; Zhao *et al.,* 2014). However, polybrene can be toxic to primary cells and it was therefore important to optimise the concentration required to minimise cell death, but without compromising the α9-eYFP protein expression. Varying polybrene concentrations were trialled in PC12 cells using second generation LV, including 2 µg/mL, 4 µg/mL and 6 µg/mL and results showed 2 µg/mL was sufficient to achieve α9-eYFP expression and was therefore used in subsequent experiments. Furthermore, our results for second generation LV indicated one plasmid, noted as '1.1.1' was able to achieve expression in PC12s and not the plasmid noted '2.2.1'. These two plasmids were prepared from glycerol stocks available in the laboratory. Both constructs had previously been prepared from colonies following bacterial transformation of DNA from a ligation reaction (carried out by Dr Melissa Andrews), however it is possible the '2.2.1' plasmid had not been validated for presence of the α9-eYFP coding sequence.

Confirmation of α9-eYFP expression as well as fGFP control expression was detected in PC12 cells using an anti-GFP antibody following WB (Figure 3.4). The results showed a double band for both GFP (one at ~30 kDa and one at ~25 kDa) and α9-

eYFP (one at ~150 kDa and one double band at ~25 kDa). Following WB analysis using an α9 integrin antibody, a double band was also detected at the same positions in lysates from LV-α9-eYFP PC12s (data not shown) which therefore suggests there may be potential cleavage of the eYFP and fGFP proteins. Whether this is the signal peptide that is cleaved (the GFP protein is farnesylated, targeting the protein to the cell membrane) or is caused by a protease specifically expressed within the PC12 cell line or simply degradation is not clear, however this was specific to the PC12 cells as double bands were not present when these experiments were repeated with hNPCs.

To analyse the function of α9 integrin following LV overexpression of α9-eYFP protein, the PC12 cells were grown on TN-C as previously published (Andrews *et al.,* 2009). When the α9β1 integrin heterodimer binds to TN-C, it promotes neurite outgrowth (Andrews *et al.,* 2009). Here, we have confirmed these results and have observed significant neurite outgrowth of the LV-α9-eYFP PC12 cells compared to GFP controls and WT PC12 cells (Figure 3.5). While these results validate the previous findings, they do not align with all findings. As previously reported, PC12 cells do not have an endogenous level of α9 integrin expression, however in our results when both GFP-PC12s and WT PC12s are grown on TN-C, neurite outgrowth was observed. Andrews and colleagues (Andrews *et al.,* 2009) reported no outgrowth from WT PC12 cells under the same culture conditions. Here, the experiment was repeated (n=3) with neurite outgrowth consistently observed (see Table 3.2). This suggests that perhaps the PC12 cells are able to express another receptor that is able to bind to TN-C. Research shows other integrin heterodimers, α7β1 and α8β1, are able to bind to TN-C and promote neurite outgrowth (Mercado *et al.,* 2004) and may therefore have been present within the heterogeneous PC12 cell population. To further investigate this, ICC or WB could be used to assess α7 or α8 integrin subunit expression. In addition, knockdown of these subunits may result in reduced outgrowth from the GFP and WT PC12s, leaving α9 integrin function more apparent. Furthermore, in both the Andrews *et al* paper (2009) and the work carried out here, PC12 cells were cultured in the presence of NGF in the media which acts to stimulate neurite outgrowth. Removing NGF from the media may result in reduced neurite outgrowth from the control groups but also potentially the α9-expressing groups. Whether the α9-PC12s would have been able to put out axonal projections without NGF has yet to be determined.

Compared to the PC12 cell line, the iPSC-derived hNPCs endogenously express both α9 and β1 integrin subunits (Figure 3.6 and 3.7). This expression is low, however α9 integrin expression can be increased following transduction with fresh second generation LV supernatant of LV-α9-eYFP. WB and ICC analysis confirmed overexpression of both the LV-α9-eYFP plasmid and LV-fGFP plasmid within hNPCs (Figure 3.7), although protein expression was only detected by WB after the protein concentration loaded per well was increased from 20 µg to 40 µg per well. Furthermore, as with the PC12 cells, the functionality of the LV-α9-eYFP was analysed using neurite outgrowth assays. Transduced hNPCs were grown on either chicken TN-C as previously reported (Andrews *et al.,* 2009) or varying concentrations of human TN-C (1 µg/mL, 5 µg/mL, 10 µg/mL, 15 µg/mL, 20 µg/mL, 25 µg/mL or 30 µg/mL). As the NPCs are human it was hypothesised there may be a difference in neurite outgrowth from the cells when grown on human TN-C compared to chicken. Specifically, hNPCs may display a higher affinity for human TN-C which may have resulted in the increased neurite outgrowth compared to growth on chicken TN-C. Following transduction of α9-eYFP into hNPCs there was significant neurite outgrowth compared to both GFP and WT controls when grown on 10 µg/mL chicken TN-C and 1 µg/mL, 5 µg/mL, 10 µg/mL of human TN-C (Figure 3.10). Each of these were repeated a minimum of five times. Interestingly, the results from these initial experiments indicated that when cultured specifically on human TN-C, there was a gradual increase in outgrowth from the GFP and WT controls as the TN-C concentration increased. As a follow up, these experiments were repeated (n=1) using higher concentrations of human TN-C: 15 µg/mL, 20 µg/mL, 25 µg/mL or 30 µg/mL (Figure 3.10). These experiments, specifically using the 15 and 20 µg/mL human TN-C, align with the previous results indicating an increase in outgrowth from the GFP and WT hNPC groups as the TN-C concentration increases. At the highest concentrations assessed (25 µg/mL or 30 µg/mL) outgrowth appeared to be more variable between the groups, however as these experiments were carried out only once they would need to be repeated to assess statistical significance.

Together these results suggest that as the concentration of human TN-C increases, the endogenous α9 integrin function is boosted, resulting in a larger impact on neurite outgrowth. Investigation into the expression of α7 and α8 integrin subunits has not

been carried out in the hNPCs which could potentially have influenced the neurite outgrowth in these cases. However, of particular interest is previous research that has shown embryonic DRGs can increase integrin subunit expression at the cell surface in response to an inhibitory, CSPG-rich environment, promoting integrin-induced outgrowth (Condic *et al.,* 1999). It is possible that stem cell-derived NPCs also possess this characteristic and as the concentration of TN-C increased, hNPCs adapted thereby promoting integrin subunit expression resulting in better neurite outgrowth. These results also highlight that hNPC growth fits a sigmoid-shaped curve that can be altered by changing either the expression of a growth promoting protein, α9 integrin, or the concentration of the ECM ligand, TN-C. Increasing α9 integrin expression produced an increase in neurite outgrowth which resulted in a growth plateau at low concentrations of TN-C compared to both GFP-expressing and WT hNPCs. However, as the concentration of TN-C was increased neurite outgrowth from both GFP-expressing and WT hNPCs increased while the outgrowth from the α9-expressing hNPCs remained consistently high. This further suggests the observed results may be specific to the TN-C substrate interacting with the α9 integrin, but could be further analysed by examining the outgrowth from these cells when grown on a different ECM matrix, such as fibronectin. This also raises an interesting question as to whether overexpression of α9 integrin subunit is necessary to increase neurite outgrowth, particularly if these cells were used in an injured environment where TN-C expression is increased (Zhang *et al.,* 1997). Currently the concentration of TN-C at the injury site, or indeed during homeostasis, is not known but further assessment of these cells in an injury model would likely add helpful data to this debate. It may be that as the concentration of TN-C increases, this stimulates further α9 integrin production, transport to the membrane or activation of the integrin. Therefore the adaptation potential of stem cell-derived hNPCs needs to be fully investigated in terms of integrin expression and neuroregeneration.

This work so far has focused on increasing α9 integrin expression, however we also need to consider how this might impact on endogenous proteins, specifically β1 integrin expression. As β1 is the binding partner for α9 integrin, the regulation of endogenous β1 in terms of production, transport and expression may be altered. This has not been assessed in this project but could be monitored using an

immunoprecipitation pull-down assay of β1 bound to α9 integrin before and after viral transduction. This could also be monitored using WB to analyse lysates from WT cells and α9-eYFP-expressing cells and staining the blot for β1 integrin. If a difference in β1 integrin band size is apparent it can be measured. There are a number of potential outcomes from these experiments. It is possible that more β1 integrin would be produced and present within the cell following overexpression of α9-eYFP. It may also be possible that there is no increase in β1 expression and perhaps exogenous α9-eYFP prevents endogenous β1 from binding other α integrin subunits, modifying endogenous integrin function. Whatever the outcome, this is an important question to address in order to ascertain how α9 integrin overexpression could impact on the cell's homeostasis and potential activity *in vivo*.

The hNPCs used in this project were pre-programmed to become hyCCNs (Axol Bioscience). However, during culture the media in which the hNPCs were grown promotes spontaneous differentiation. Neural progenitors that are not pre-programmed have the ability to differentiate into neuronal or glial cells. From the hNPCs cultured during this project, the majority of the cells had a neuronal phenotype and stained positively for βIII-tubulin (Tuj1), a recognised neuronal marker, however, the cultures were also analysed for presence of other cell types including astrocytes and oligodendrocytes (Figure 3.11). Of these further two cell types, only positive staining was observed for GFAP, which suggested developing astrocytes or glial precursor cells were also present within the hNPC culture. When assessing for oligodendrocytes, cells were only in culture for 21 days and it is possible oligodendrocytes had not yet formed. Keeping the cells in culture for a longer time period to assess oligodendrocyte presence would likely answer this question. Alternatively, staining the cells for a marker of immature oligodendrocytes such as NG2 (Polito and Reynolds, 2005), may detect OPCs. The use of GFAP as a marker for immature astrocytes has generated controversy as research suggests GFAP is only expressed within mature, fully differentiated astrocytes (Bignami *et al.,* 1972), but others suggest GFAP is expressed within astrocyte progenitors (Baba *et al.,* 1997). Alternatively, vimentin could have been used to identify developing astrocytes (Gomes *et al.,* 1999). Here, the presence of developing astrocytes was not assessed, however it is likely that glial precursor cells were present within the culture. The proportion of astrocytes in the culture was small

and for the purposes of transplantation, their presence may be beneficial for the survival and differentiation of the NPCs both *in vitro* and *in vivo* (Brown, 1999; Park *et al.,* 2001; Oh *et al.,* 2010). Astrocytes are known to support neuronal function, growth and, via secretion of thrombospondins, can promote synaptogenesis (Ullian *et al.,* 2004, 2001; Christopherson *et al.,* 2005) which is important for both synaptic plasticity and regeneration after injury. Therefore, transplanting a co-culture of hNPCs alongside a small proportion of human astrocytes, may result in a human neuron-glia network that can interact and communicate with one another further promoting the survival of transplanted hNPCs within the rat cortex. Whether rat astrocytes would be able to support the hNPCs in the same way is not fully understood and is out with the scope of this project. Results here from ICC showed positive GFAP staining within the hNPC culture and indicated astrocytes were present *in vitro*. There is potential for these astrocytes to aid in NPC functioning and synaptogenesis *in vitro*, as mentioned above, which also indicates their presence could have been beneficial to hNPCs following transplantation.

The hNPCs were further characterised by assessing expression of deep-layer cortical neuron markers, including Ctip2 and Tbr1, confirming the observations of others (Shi *et al.,* 2012b). Expression of specific markers can determine whether axons will project to the corpus callosum, to other areas of the cortex or to subcortical targets. Both proteins have been identified as markers of layer V/VI cerebral cortex neurons (Bulfone *et al.,* 1995; Hevner *et al.,* 2001; Arlotta *et al.,* 2005; Chen *et al.,* 2005). This cortical area, consisting mainly of pyramidal cells, is associated with neuronal projections to subcortical targets, including the internal capsule, thalamus, brain stem and spinal cord. Ctip2 is a zinc finger transcription factor associated with neuronal nuclei. It is known to be involved in differentiation of NPCs and is involved in regulation and ability of layer V neurons to project to subcortical targets (Arlotta *et al.,* 2005; Chen *et al.,* 2008a). Tbr1 is also a DNA-binding protein involved in neuronal differentiation (Hevner *et al.,* 2001), migration and axonal targeting of neurons to subcortical targets during development (McKenna *et al.,* 2011). Importantly, Ctip2 expression is required for development of CST axons from cortical layer V (Chen *et al.,* 2005) and Tbr1 expression, although mainly associated with layer VI neurons and corticothalamic projections (Hevner *et al.,* 2001), it has also been implicated in

controlling laminar identity and development of the CST (Bedogni *et al.,* 2010; Han *et al.,* 2011). During development, if Tbr1 is not present, this can result in aberant projections from layer VI of the cortex (Han *et al.,* 2011). In culture, expression of both Ctip2 and Tbr1 were observed in hNPCs following ICC analysis showing hNPCs confer deep-layer CCN identity. The results here were significant for progression of the project, specifically for transplant of hNPCs into deep layers of the sensorimotor cortex, as we hypothesised these cells would project subcortically throughout the CST.

The hNPCs were also analysed for progenitor cell and growth-promoting characteristics using DCX as well as certain neurotrophic factors including BDNF and its receptor, TrkB. DCX, a recognised progenitor marker, is highly expressed in developing and immature neurons (Magavi *et al.,* 2000; Brown *et al.,* 2003; Couillard-Despres *et al.,* 2005). The DCX protein is involved in stabilisation of axonal microtubules and migration of developing neurons (Francis *et al.,* 1999; Gleeson *et al.,* 1999). BDNF is a growth factor associated with neuronal development and growth signalling through the transmembrane receptor TrkB. BDNF signalling through TrkB results in neuronal outgrowth and elongation, however research suggests endogenous expression is not sufficient to promote regeneration after injury (Lu *et al.,* 2001). Indeed, overexpression of TrkB within corticospinal neurons can promote regeneration after CNS injury (Hollis *et al.,* 2009). Results from experiments in this chapter showed expression of these proteins. Finally, neuronal phenotype was analysed using antibodies against VGlut1, a recognised marker for excitatory, glutamatergic neurons, which make up approximately 80% of the mammalian cortex. Results show the hNPCs do have a high expression of VGlut1, confirming previous literature (Shi *et al.,* 2012b), suggesting these are glutamatergic cells. Other neurotransmitter receptors, such as GABA transporter 1 (GAT1) or choline acetyltransferase (ChAT) were not assessed so we cannot be sure there are no additional neuronal phenotypes in this culture. Together, the expression of these proteins DCX, BDNF, TrkB and VGlut1 within the hNPCs *in vitro*, heightens the potential of these cells to promote neurite outgrowth, elongation and regeneration *in vivo*.

In summary, here we have successfully generated α9-eYFP-expressing iPSC-derived hNPCs. Furthermore, we have demonstrated that once this exogenous protein is

expressed, it can promote neurite outgrowth when cultured on TN-C. Equally, these cells express endogenous α9 and β1 integrin subunits and are capable of neurite outgrowth on TN-C. Moreover, hNPCs express deep-layer cortical neuron markers, including Ctip2 and Tbr1, important for axonal projections to reach subcortical targets, as well as neurotrophic factors including BDNF and TrkB all of which will be beneficial in transplantation experiments. This is because the expression of these proteins together may contribute to the promotion of axonal elongation, cell survival and targeted subcortical neuronal outgrowth when transplanted *in vivo*.

Chapter 4: *In vivo* analysis of WT iPSC-derived hNPCs

4.1 Introduction and aims

Following *in vitro* characterisation of our population of iPSC-derived hNPCs, the next step of the project involved transplanting iPSC-derived hNPCs into the neonatal rat sensorimotor cortex and characterising them *in vivo*. Transplantation of stem cell-derived cells is a rapidly expanding field, particularly in the area of neuroregeneration. Stem cells have been used for their ability to promote repair and restoration of function in Parkinson's disease (Bjorklund *et al.,* 2002; Brederlau *et al.,* 2006), stroke (Wang *et al.,* 2016), amyotrophic lateral sclerosis (Mazzini *et al.,* 2015), Huntington's disease (McBride *et al.,* 2004) and SCI (Fujimoto *et al.,* 2012; Antonic *et al.,* 2013; Piltti *et al.,* 2015). Research has shown transplanted ESC-derived cells are able to project to and follow fibre tracts within the brain (Denham *et al.,* 2012), including the CST (Ideguchi *et al.,* 2010). The lack of continual, sustainable resources, as well as the ethical debate surrounding use of ESCs, has driven researchers to find alternative methods. This alternative came from the discovery of iPSCs produced by expressing embryonic transcription factors in somatic (including adult-derived) cells resulting in cells reverting to a pluripotent state (Takahashi and Yamanaka, 2006; Takahashi *et al.,* 2007). These pluripotent cells have the same proliferative and expandable properties as ESCs and have the capacity to differentiate into any cell type, including NPCs.

Here we aimed to transplant WT human iPSC-derived hNPCs into the rat sensorimotor cortex, specifically layer V, as neurons in this area project axons within the CST. We aimed to ascertain whether transplanted cells could project axons long distances and follow the CST *in vivo*. After transplantation, tissue was collected at various time points from 2 weeks up to 8 weeks and tissue was analysed using IHC and fluorescent microscopy. Human-specific antibodies were used to identify the transplant sites and projections within the tissue which allowed cell survival and projection trajectory to be mapped over time. In addition, we wanted to build upon the expression profile established in Chapter 3 and to assess the *in vivo* expression of a number of proteins over time including, CCN and maturation markers, as well as to assess to what extent the grafts had an effect on the surrounding host tissue.

4.2 Methods

4.2.1 Neonatal cerebral cortex transplants of WT hNPCs

All procedures were carried out under the UK Home Office Project Licence number 60/4472 and Personal Licence number IC71C2B2B, conformed to the UK Animals (Scientific Procedures) Act (1986) and approved by the Animal Welfare Ethics Committee of the University of St Andrews.

Human NPCs were removed from the dish after 8-9 days in culture (section 2.5.6). Full transplant procedure is detailed in section 2.7.1. Briefly, P0-2 newborn Sprague Dawley rat pups were injected under hypothermic anaesthesia, either unilaterally or bilaterally into two specific sites (1 μL/injection site) for the predicted neonatal sensorimotor cortex (Altman and Bayer, 1995). All pups received 100,000 cells per injection site. Following analysis of the initial tissue batches, the coordinates for subsequent batches were adjusted to improve accuracy of injection (see Table 2.8 for details on injection coordinates). Animals were placed beneath a stereotaxic frame and injected using a Hamilton syringe with an attached custom made 30-gauge stainless steel needle (ESSLAB UK). Cells were injected manually over the course of 1 minute, then the needle was left in place for 2 minutes to prevent backflow from the injection site. Following the transplant, animals were transferred to a pre-warmed cage to recover. Once the entire litter had undergone surgery and woken up, they were returned to the cage with the mother. Pups were monitored closely for 48-72 hours post-surgery to assess any signs of rejection by the mother.

4.2.2 Neural tracing experiments

See section 2.7.2.

4.2.3 Tissue perfusion and sectioning

See section 2.7.4.

4.2.4 IHC analysis of hNPC transplants

Brain tissue was analysed using IHC as described in section 2.8. Briefly, following the blocking step tissue sections were incubated with primary antibody diluted in blocking solution overnight at 4°C (see Table 4.1, full details in Table 2.5). Specifically, to assess graft survival and hNPC projections, human-specific antibodies against HuNu and hNCAM were used. The specificity of these antibodies was assessed on control rat tissue prior to use (Appendix C). Following primary antibody incubation, tissue sections were washed three times for 10 minutes each with 0.02% Tween-20 in PBS. Specifically, for the TN-C antibody, pre-treatment with 0.03% hydrogen peroxidase was required (section 2.8.1). Tissue was subsequently incubated with fluorescently-tagged secondary antibodies (1:750) of the corresponding species (see Table 2.6) and then DAPI (1:10,000). Sections were washed with PBS, mounted onto gelatin-coated slides, dried at RT, and covered with a glass coverslip. Slides were stored at 4°C and covered to protect from the light. Slides were imaged using a Leica D5500 epifluorescent microscope equipped with a DFC550 digital camera (Leica).

Table 4.1 Primary antibodies and dilutions used for IHC analysis

Antibody	Species	IHC dilution
HuNu	Mouse	1:500
hNCAM	Mouse	1:200
TN-C	Rabbit	1:200
GFAP	Rabbit	1:500
MBP	Rabbit	1:50
Tbr1	Rabbit	1:400
Ctip2	Rabbit	1:500
Ctip2	Rat	1:500
DCX	Rabbit	1:500
PKCγ	Rabbit	1:200
Ki67	Mouse	1:100
Iba-1	Rabbit	1:500
WFA	--	1:200

4.3 Results

4.3.1 Identification and survival of WT hNPC transplants *in vivo* over time

Once transplanted into the rat brain, hNPCs were detected in tissue using human-specific antibodies, HuNu and hNCAM. Specifically, the bolus of hNPCs could be detected using the HuNu antibody (Figure 4.1, A-C) and projections from these cells could be detected using the hNCAM antibody (Figure 4.1, D-F, white arrows).

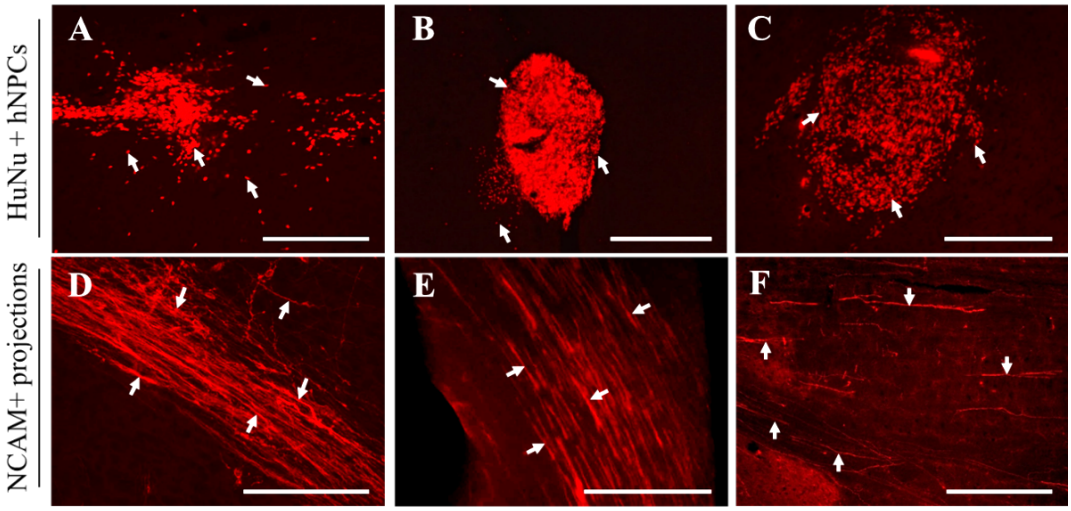

Figure 4.1 Human NPC graft survival was detected *in vivo* using human-specific antibodies. Following transplantation of hNPCs into neonatal rat brain, tissue was harvested at a number of different time points from 2 weeks up until 8 weeks. To detect the transplants, tissue was analysed using IHC and human-specific antibodies including HuNu and hNCAM. The anti-HuNu antibody detected the nuclei (white arrows in **A-C**) of the grafted cells showing the bolus sites whilst the projections from these cells were detected using an anti-hNCAM antibody (white arrows in **D-F**). Scale bars A, C, F = 250 µm, B = 500 µm, D, E = 150 µm.

Transplant survival was observed from 2 weeks up until 8 weeks, however graft survival decreased over time. A breakdown of the graft appearance was divided into three categories including number of animals showing either graft survival, scarring or no graft detected over time from 2 to 8 weeks and is shown in Table 4.2 and Figure 4.2, A. Scarring was defined as non-specific HuNu or hNCAM staining that corresponded with increased GFAP staining (Appendix B).

After 2 weeks *in vivo*, results show there was an 82% (n=14/17) graft survival rate, but after 8 weeks this reduced to 38% (n=5/13). Graft survival was expected to be high at early time points owing to a lack of full immune response in the neonatal rat potentially making graft rejection at this stage very low. Similarly, the number of animals with scarring or no grafts increased over time. For example, at 2 weeks post-transplantation, only 18% (n=3/17) of cases had no surviving cells detected, but at 8 weeks this was increased to just over half the animals 54% (n=7/13). In total, over all time points, no graft or scar could be detected in 28% of animals (n=22/78). However, these cases cannot be termed as graft rejection, as we cannot confirm cells were transplanted because of potential backflow of cells from the injection site or clogging of the needle during transplant.

Table 4.2 Survival of WT hNPC transplants over time

	Number of weeks post-transplantation of WT hNPCs					**Total n (%)**
	2 weeks n (%)	**4 weeks n (%)**	**6 weeks n (%)**	**7 weeks n (%)**	**8 weeks n (%)**	
No. of animals with transplants surviving	14 (82%)	12 (75%)	8 (47%)	8 (53%)	5 (38%)	47 (60%)
No. of animals with scarring	0 (0%)	0 (0%)	2 (12%)	6 (40%)	1 (8%)	9 (12%)
No. of animals with no graft detected	3 (18%)	4 (16%)	7 (41%)	1 (7%)	7 (54%)	22 (28%)
Total	17 (22%)	16 (21%)	17 (22%)	15 (19%)	13 (17%)	78 (100%)

Out of a total of 56 animals with either hNPC grafts surviving or noticeable scarring, 46% (n=26/56) of those had an on-target hNPC injection within the deep layers of the sensorimotor cortex (Figure 4.2, B-C). The remaining 54% (n=30/56) were off target and located in regions adjacent to the target site, including the hippocampus, caudate and/or putamen of the basal ganglia and lateral ventricles. In an attempt to achieve better accuracy with transplant injection and targeting, coordinates were modified over time (Table 2.8). The adjustment of coordinates resulted in improved accuracy of transplants and in batch 12, the last batch of transplants, 64% (n=9/14) of hNPC grafts were on target (Figure 4.2, B). Results also show there was a minimum of 40% of on-target grafts at each time point (Figure 4.2, C).

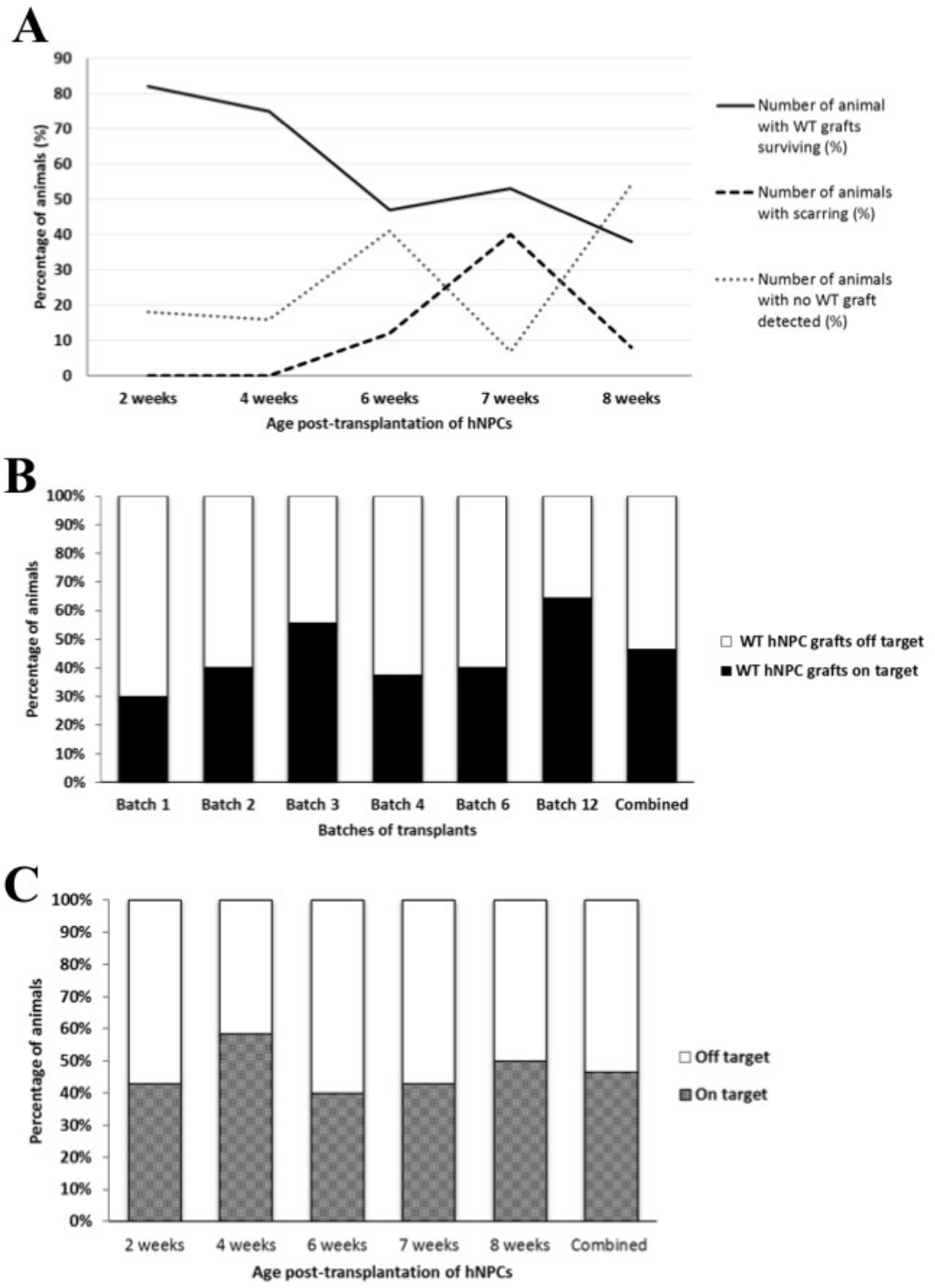

Figure 4.2 Analysis of WT hNPC graft survival and on- and off-target injections. Tissue was analysed for transplant survival over different time points (2, 4, 6, 7 and 8 weeks post-transplantation). Survival was highest at younger time points of 2 and 4 weeks which declined over time (**A**). In contrast, the number of animals that had a clear scar or no transplant survival increased over time (**A**). Transplant coordinates were optimised with each batch of transplants in a bid to improve transplant accuracy, which was relatively low with the first few batches. For example, after the first batch of transplants 30% of grafts were on target within the sensorimotor cortex. However, after coordinate optimisation, this

number increased to 64% of grafts on target in batch 12 (**B**). Combined, 46% of total grafts were on target. Furthermore, each time point contained 40% or more of grafts on target indicating there were on-target injections at each time point (**C**).

4.3.2 Locations of hNPC transplants and their neuronal projections

Variation in coordinates and injection sites throughout the different batches resulted in a number of different hNPC transplant sites. These injection sites were first identified using HuNu and hNCAM antibodies and co-stained using an astrocytic marker, GFAP and DAPI, a nuclear stain. Transplant sites included areas of the cortex, hippocampus, corpus callosum, caudate and/or putamen of the basal ganglia, and striatum (Figures 4.3 and 4.5). These sites varied in size, where the bolus of cells were either together in a ball formation (Figure 4.3, E and G) or had spread out over a larger area (Figure 4.3, D). Analysis of both coronal and sagittal sections revealed projections had started generally within the cortex, corpus callosum, caudate and/or putamen of the basal ganglia and ventricles and projected within mainly these same areas, as well as to the thalamus, internal capsule, cerebral peduncles and pons. The transplant sites and projections for each batch are summarised in brain maps in Figure 4.5.

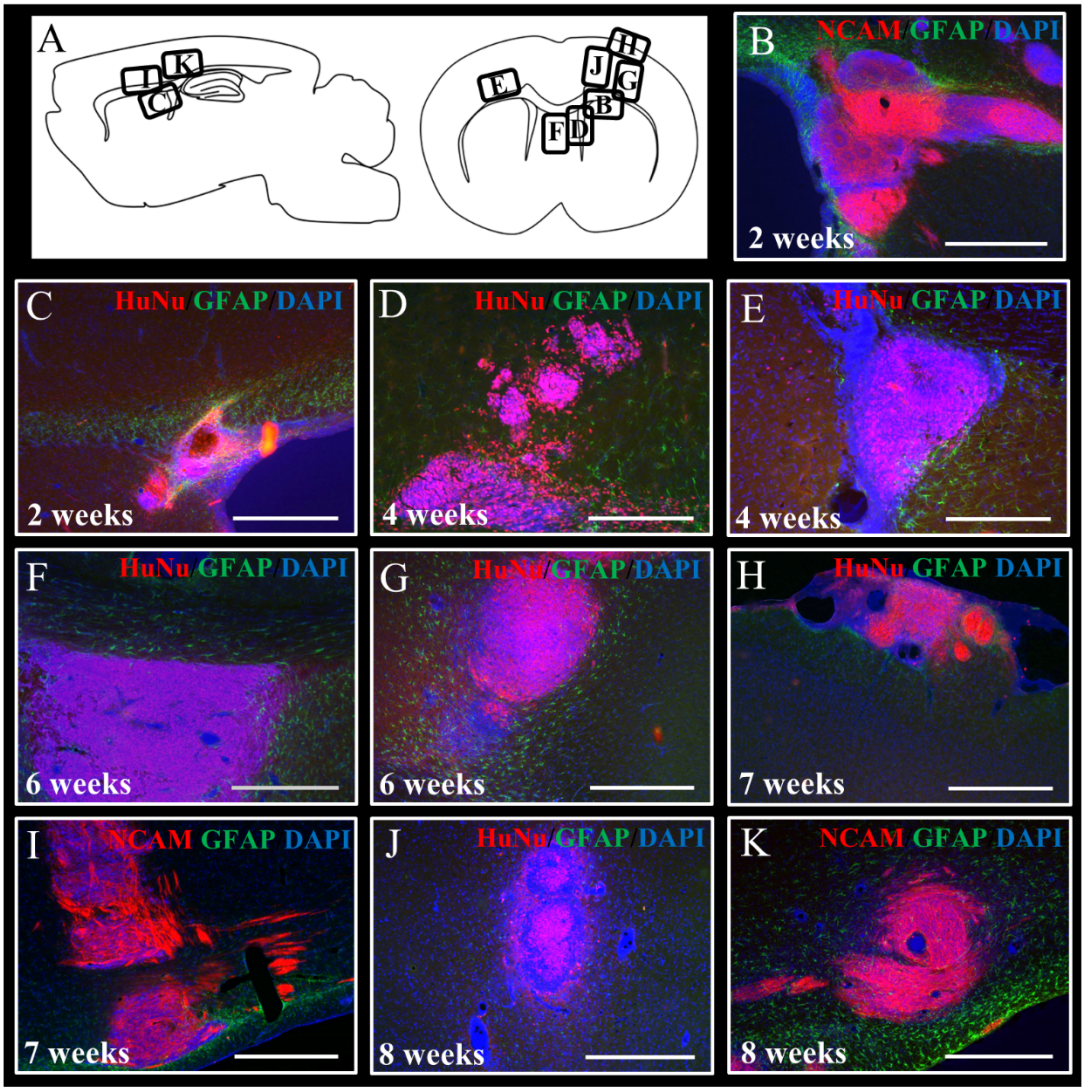

Figure 4.3 Representative images of hNPC transplant locations detected using human-specific antibodies. The tissue was analysed using IHC and injection sites were identified using both HuNu and hNCAM antibodies. IHC results revealed some variation in injection sites. These included the dorsal striatum and corpus callosum (**B** and **C**), areas of the cortex (**D, G, H, I, J** and **K**), the lateral ventricles (**E**), as well as the lateral septum (**F**). Scale bars in B, C, F, G, H, I, J and K = 500 µm; D and E = 250 µm.

As a result of the varied injection sites, the projections from the transplanted hNPCs, identified using an hNCAM antibody, were located in different neuroanatomical regions including the cortex, corpus callosum, lateral septum, dorsal striatum, thalamus, hippocampus, internal capsule, cerebral peduncle and pons (Figures 4.4 and 4.5). These projecting fibres formed bundles and coursed through known axonal pathways in the brain, such as the corpus callosum (Figure 4.4, B) and the internal capsule (Figure 4.4, C and D). Furthermore, IHC analysis also indicated these

projections may be of different thicknesses (indicated by white arrows in Figure 4.4, F, I and J) where the fibre thickness appeared to be noticeably larger compared to others (white arrows in Figure 4.4, G and H) suggesting fibres may have grown in size over time or have bundled together.

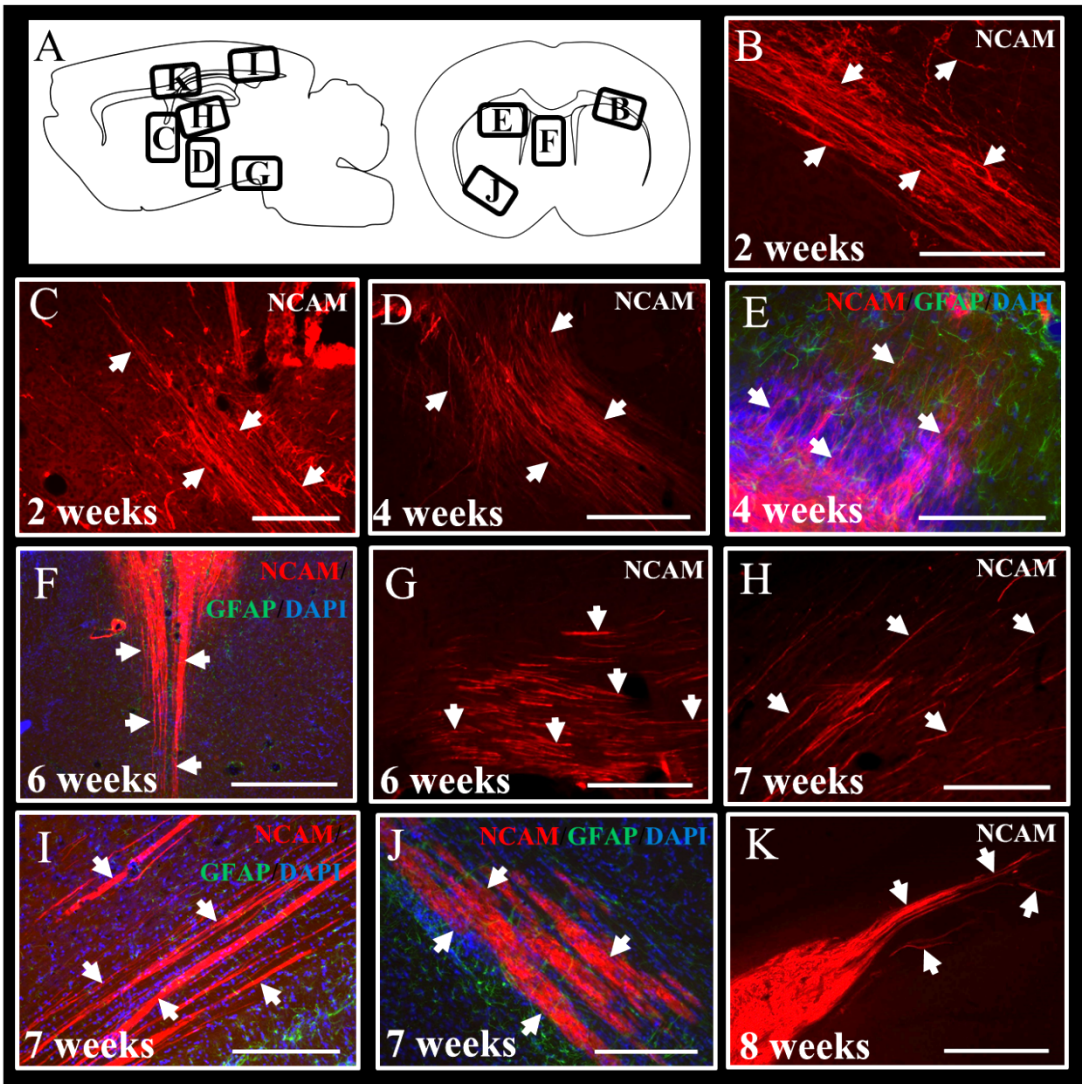

Figure 4.4 Transplanted WT hNPCs extend hNCAM-positive projections throughout the rat brain. The projections from grafted hNPCs could be detected using IHC with an anti-hNCAM antibody and were observed in a number of different neuroanatomical regions. These included the corpus callosum (**B** and **K**), internal capsule (**C** and **D**), dorsal striatum (**E**), lateral septum (**F**), pons (**G**), thalamus (**H**), cortex (**I**) and cerebral peduncles (**J**). Tissue was also stained with an anti-GFAP antibody to identity astrocytes and DAPI to identify all nuclei. Scale bars B, E = 150 µm, C = 200 µm, D, F, K= 500 µm, G, H, I, J= 250 µm.

When transplants were on target, hNCAM-labelled projections were observed within the fibre tracts of the CST, including the internal capsule, cerebral peduncles and pons as well as the pyramids within the brain stem (Figure 4.6). Out of 47 animals showing hNPC survival, 11% (n=5/47) displayed hNCAM-positive projections within the brain stem including the ventral brain stem and the dorsal-caudal brain stem. The exact location of these hNCAM-positive projections was analysed using IHC, as we were interested to ascertain whether these projections were within the CST. Using an anti-protein kinase C γ (PKCγ) antibody, the pyramids of the CST within the brain stem were detected and highlighted this region of interest (Figure 4.6, E). Furthermore, the hNCAM fibres were indeed within this region, suggesting these fibres were projecting within the CST (Figure 4.6). In two out of these five animals, projections were observed beyond the pyramids, projecting up towards the dorsal brain stem in the contralateral cortex, likely beyond the decussation of the pyramids, suggesting fibres had crossed over at the pyramidal decussation. The cervical spinal cords of these five animals were analysed for further projections, however no hNCAM-positive projections were observed within these sections suggesting the hNPCs did not project further than the caudal brain stem. These five animals were isolated from batch 12, where 64% of transplants were on target within the sensorimotor cortex.

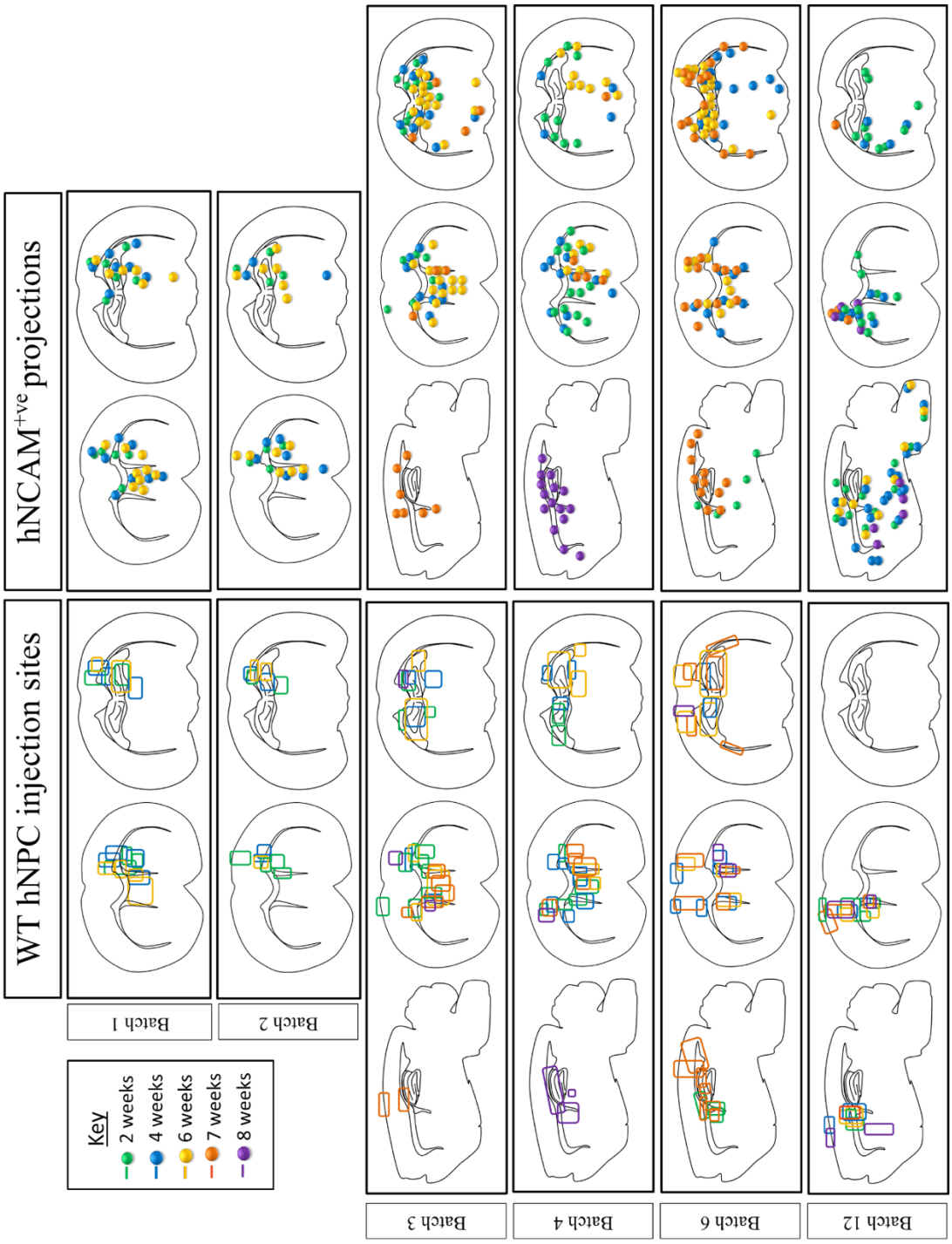

Figure 4.5 Location of injections and fibre projections from WT hNPCs transplants over time. After each batch of transplants, injection sites were analysed for both on- and off-target injections. Coordinates were altered for subsequent transplants based on the results from the previous batches. Injection sites over the different batches can be seen in the first column and the corresponding projection locations are in the second column. The different colours for boxes and dots show the different age groups detailed within the key. In batch 12 transplants, 64% of grafts were on target resulting in projections following areas of the CST, including the internal capsule, cerebral peduncles and pyramids

within the brain stem. Within batch 12 at 4 and at 6 weeks, projections were observed within the dorsal part of the caudal brain stem, likely past the pyramidal decussation.

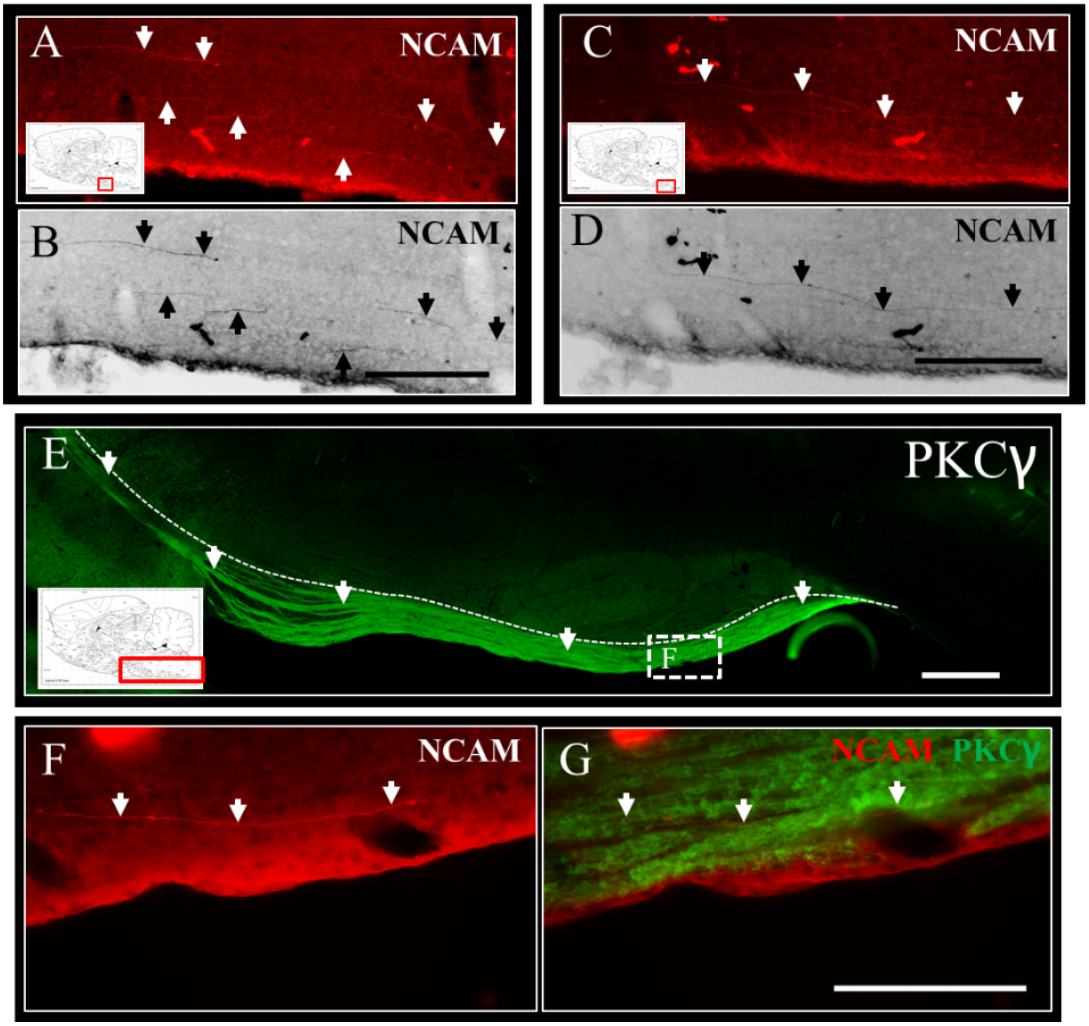

Figure 4.6 Projections from hNPCs were detected within the CST within the pyramids 2 weeks after transplantation. Following IHC analysis, hNCAM-positive projections were detected within the brain stem 2 weeks after transplantation of hNPCs (white and black arrows, **A-D**). Images **B** and **D** have been converted to black and white using ImageJ to allow for clearer detection of hNCAM-positive projections. Using an anti-PKCγ antibody the pyramidal tract within the brain stem was labelled indicated by the white dotted line (as a boundary line) and white arrows in **E**. Furthermore, hNPC projections were located within the pyramidal tract only 2 weeks after hNPC transplantation into the sensorimotor cortex (**F-G**). Scale bars A-D =200 µm; E= 500 µm; F-G = 150 µm.

4.3.3 Tracking of hNCAM projections using BDA tracers

To assess whether the hNPCs could follow projection tracts, such as the CST, or whether they may be pre-programmed to project elsewhere, WT hNPCs were injected with 50 mg/mL BDA tracer. The rationale for injection of BDA with the hNPCs, rather than separate injections at a later time point, was to enable the BDA to be taken up by the endogenous cells at the exact site of the transplant. This would have allowed us to examine whether the transplanted cells were following fibre tracts originating at the injection site, as well as whether the injections were on or off target. Unfortunately, preliminary experiments to inject 50 mg/mL BDA together with the hNPCs did not result in positive axonal tracing. Instead a red haze was detected at the injection site at all time points (data not shown). Unfortunately, time did not allow for optimisation or further testing with BDA tracing.

4.3.4 Did the hNPCs mature *in vivo* over time?

Another main question we aimed to address was whether these cells matured *in vivo* over time. In order to assess maturation, we examined the expression of the progenitor cell marker DCX. As the hNPCs were in a progenitor cell state when transplanted and expressed DCX *in vitro* (section 3.3.6), DCX expression was analysed over the different time points *in vivo*. Firstly, endogenous DCX expression within the cortex was analysed at the different time points. Within the cortex, DCX was detectable within a small proportion of progenitor cells at 2 weeks (Figure 4.7, B and C); however, over time this expression declined and at 8 weeks very little DCX was detected within the cortex (Figure 4.7, J and K). In transplanted animals at 2 weeks, hNCAM-labelled hNPC projections were observed expressing the DCX protein (Figure 4.8, A-C). Furthermore, and contrary to our hypothesis, at 4 weeks and 8 weeks the high expression of DCX remained the same within these cells (Figure 4.8, D-I). In fact, our results show that as long as the transplanted cells survived, DCX was expressed within the hNPC projections suggesting the cells retained their progenitor cell state to some extent.

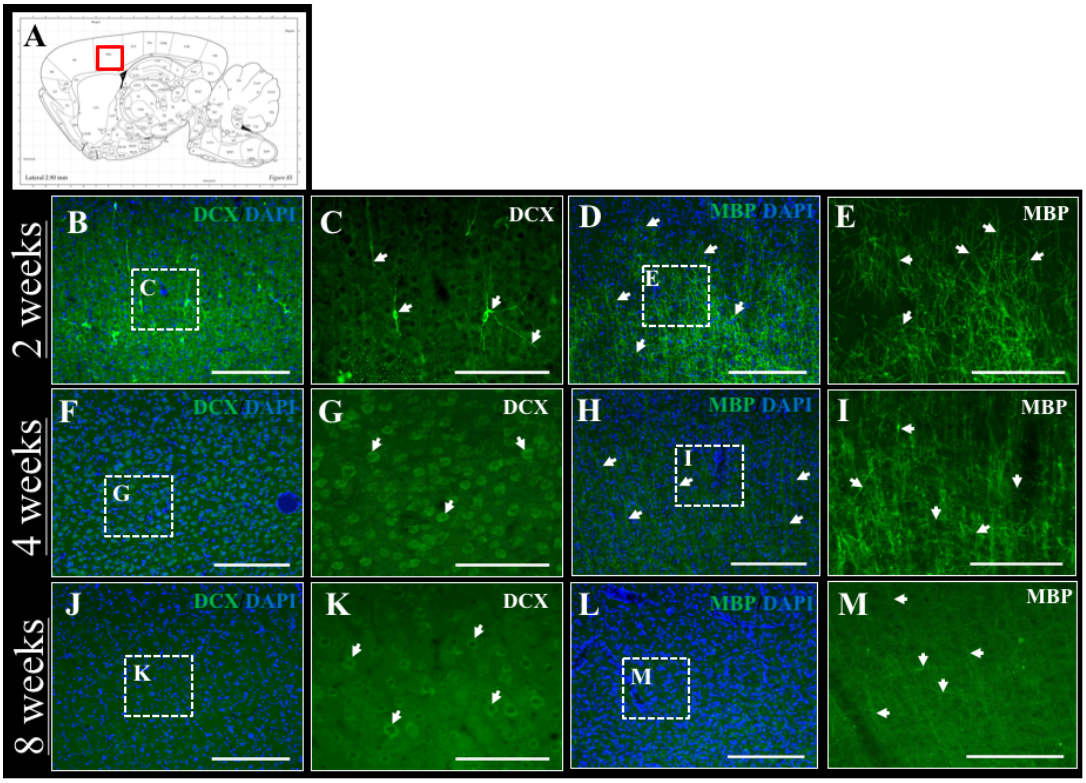

Figure 4.7 Endogenous expression of DCX and MBP in contralateral rat sensorimotor cortex over time. Using IHC, the endogenous expression of the progenitor cell marker DCX and the oligodendrocyte-associated protein MBP, were assessed within the rat sensorimotor cortex over the different developmental time points. At 2 weeks there were only a small proportion of cells expressing DCX (**B-C**) and this declined over time (**F-G**) resulting in very little DCX expression in the cortex at 8 weeks (**J-K**). Similarly, at 2 and at 4 weeks of age MBP expression was high within the cortex (**D, E, H** and **I**). As the brain matured, the number of host myelinated axons increased and resulted in a dense MBP-stain of the cortex at the later time points where it was more difficult to pick out single myelinated fibres (**L-M**). Scale bars in B, D, F, H, J and L= 250 µm and C, E, G, I, K and M =150 µm.

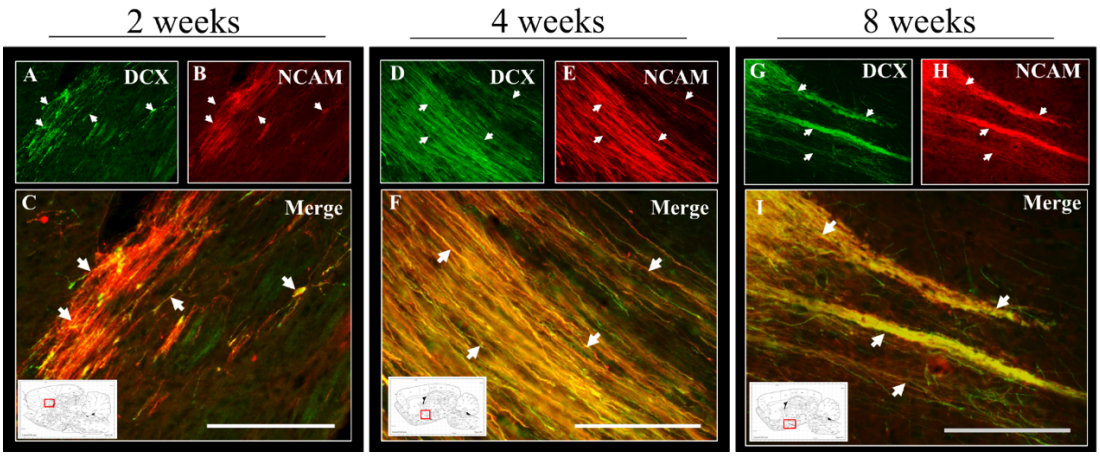

Figure 4.8 hNPCs projections express the progenitor cell marker DCX *in vivo* from 2 weeks up until 8 weeks post-transplantation. IHC analysis of the axonal projections from transplanted hNPCs indicate DCX expression was retained within neuronal projections extending from the transplanted cells from 2 weeks (**A-C**) up until 8 weeks (**G-I**) post-transplantation. Tissue was stained using a DCX and a hNCAM antibody. DCX-positive staining (**A, D** and **G**) co-localised with hNCAM-positive staining across all time points (**C, F** and **I**). Scale bar A-I = 150 µm.

An additional method used to assess hNPC fibre maturation *in vivo* was to examine myelination of projections from the transplanted hNPCs. An antibody against MBP, a protein expressed by myelinating oligodendrocytes, was used to assess this. As with DCX expression, endogenous expression of MBP was examined within the rat cortex over the different time points which followed a similar pattern to DCX. At 2 and 4 weeks of age, endogenous expression of MBP was high within the cortex as myelination is occurring at this stage of development (Figure 4.7, D, E, H and I). At 8 weeks, expression of MBP is not clear, likely due to the dense axonal network present at this time point (Figure 4.7, L and M). When assessing the hNPC transplants, hNCAM-labelled fibres were observed at 2 weeks post-transplant following myelinated axonal tracts within the corona radiata (Figure 4.9, A-C), an area of the CST where projections are gathered from areas of the cortex and guided towards the internal capsule. At 7 weeks, fibre projections were detected within fibre tracts coursing caudally within the corpus callosum and hNCAM-labelled fibres were observed in close proximity to MBP-positive cells (Figure 4.9, E-G). The MBP antibody used in these experiments is able to detect both rat and human variants of the MBP protein and it is therefore unclear whether human oligodendrocytes have differentiated from transplanted progenitor population or if rat oligodendrocytes may

have potentially myelinated the human NCAM-labelled projections. When staining for MBP in the hNPC *in vitro* culture (section 3.3.6), no positive staining was observed suggesting there were no myelinating oligodendrocytes within the hNPC population, however presence of oligodendrocyte precursors was not assessed. Using a human-specific antibody for MBP or an antibody for OPCs, such as anti-NG2 (Polito and Reynolds, 2005), would help answer this question. Nonetheless, our staining of the different age groups indicated that the hNPC projections were able to follow myelinated fibre tracts, such as the CST, and were in close proximity to MBP-positive cells. Moreover, within the bolus/injection site, MBP-positive staining was observed (Figure 4.9, H and I), suggesting either the NCAM-positive fibres from the hNPCs were becoming myelinated or potentially, mature myelinated rat axons penetrated the bolus of cells to interact with the hNPCs.

A further marker for maturation assessed was formation of PNNs, which act to stabilise synapses of mature neurons. Unfortunately however, using the lectin, WFA, no positive WFA staining was observed on or near the transplanted hNPCs (data not shown).

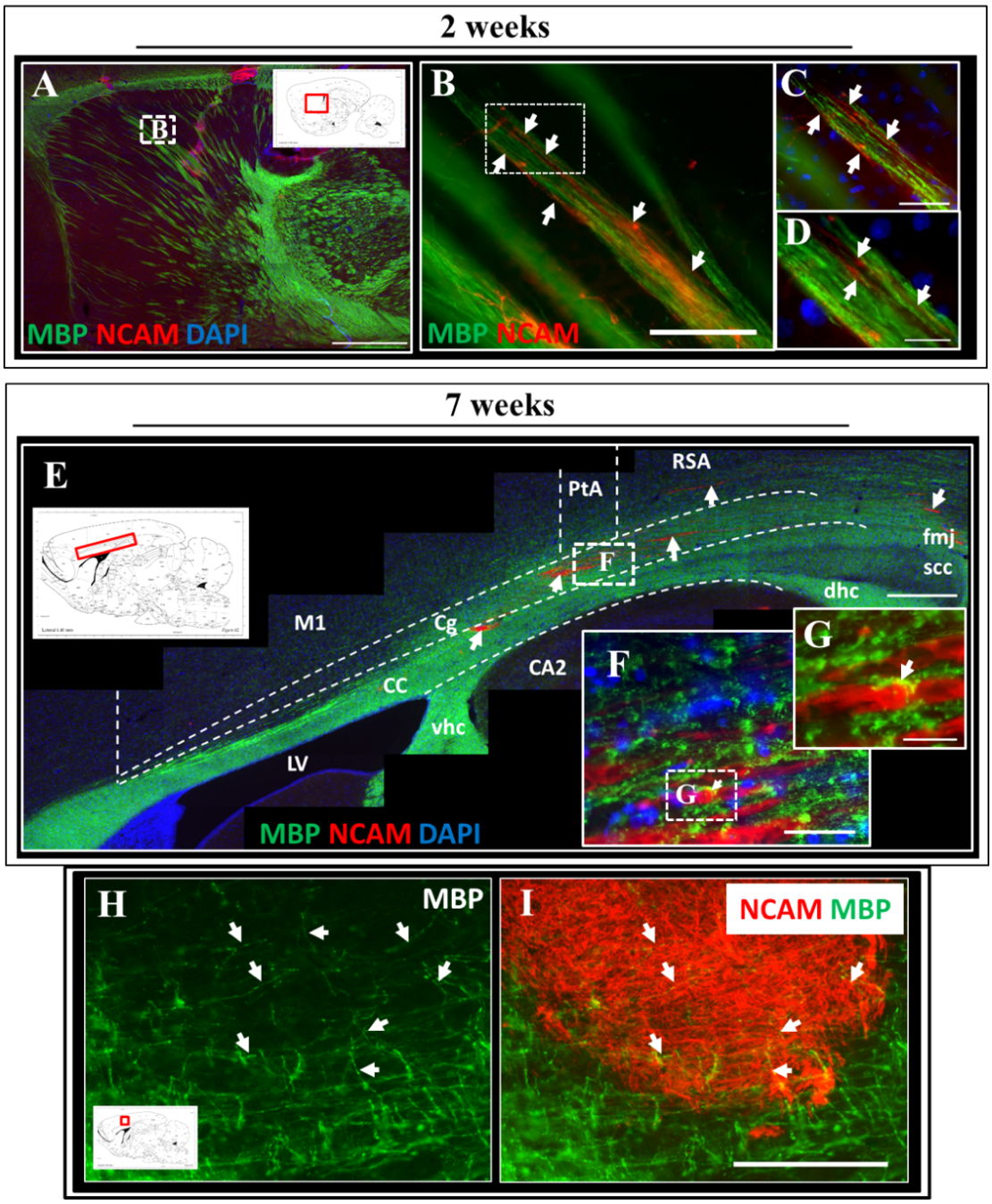

Figure 4.9 Myelination of hNPC projections assessed over time. The hNPC projections were analysed for evidence of myelination using IHC and an anti-MBP antibody, which would suggest the cells matured *in vivo*. At 2 weeks post-transplantation, hNPC projections followed myelinated tracts, such as those in the corona radiata. Human NCAM-labelled fibres were observed within rat myelinated tracts projecting from the top of the corona radiata towards the internal capsule (**A-D**). At 7 weeks, hNPC projections were still detected within myelinated tracts, such as the corpus callosum (**E**) and hNPCs were observed in close proximity to MBP-positive cells (**F-G**, white arrows) and suggested myelination of hNPC projections may have occurred. Furthermore, at 7 weeks, MBP-positive fibres were detected within the bolus sites (**H-I**) suggesting either rat myelinated fibres permeated the human

bolus of cells or myelination of hNPCs had occurred. Scale bars A, E = 1 mm, B = 100 µm; C, F = 50 µm; D, G =20 µm; H, I = 150 µm.

4.3.5 Differences between endogenous rat gene expression and hNPCs gene expression at different time points *in vivo*

In light of results in Chapter 3 where data showed the expression of deep-layer cortical neuron markers, Ctip2 and Tbr1, within the hNPCs *in vitro*, the expression of these two markers was assessed within the hNPCs *in vivo*. Specifically, we wanted to identify whether these cells retained expression of these two markers when transplanted *in vivo*, and also assess if their expression profile would change in response to their local environment, for example if cells were transplanted off target. Furthermore, we wanted to ascertain whether transplanted hNPCs follow the endogenous pattern of expression of these two proteins over time.

Following IHC staining for Ctip2, results were repeatedly inconsistent and therefore not reliable. Two different Ctip2 antibodies were utilised within this project in an attempt to identify Ctip2 expression within firstly, the endogenous tissue and secondly, within the hNPCs *in vivo* over time. One antibody was human-specific (Abcam) and the other was reported to identify both rat and human Ctip2 (Abcam). The human-specific Ctip2 antibody unfortunately also detected endogenous Ctip2 within the rat tissue, however not consistently. Similarly, this antibody detected Ctip2-expressing cells within the HuNu-positive hNPC bolus, but not consistently. The results from this human-specific antibody suggested a proportion of the hNPCs expressed Ctip2 however due to the inconsistency in staining, these results were not reliable. The second Ctip2 antibody used unfortunately was also not reliable and often would not identify endogenous expression or expression within the hNPC graft across a number of trials. These antibodies and analysis of Ctip2 protein expression was therefore not pursued (data not shown).

Results for Tbr1 staining showed that the hNPC population expressed Tbr1 at each time point *in vivo* post-transplantation, from 2 to 8 weeks, regardless of the transplant location (Figure 4.10). For example, transplants within the sensorimotor cortex, hippocampus or striatum all had a population of Tbr1-positive cells. The endogenous

expression of Tbr1 was ascertained using the contralateral cortex, which contained no hNPCs. Results indicated Tbr1 was expressed within deep layers of the cortex across all time points, but there was a slight reduction in the expression over time (Figure 4.10, A, E and I). One observation of note was obtained from grafts that were very densely packed, which showed no Tbr1-expressing cells within the densely-packed centre of the grafts and only cells on the outside of the grafts that were exposed to the endogenous ECM expressed Tbr1 (Figure 4.10, J-L). This suggested cells tightly packed within a bolus may not have interacted with endogenous signalling proteins to further propagate hNPC differentiation. In fact, as our previous results showed, the hNPCs had a high expression of both Ctip2 and Tbr1 before transplantation, but these *in vivo* results for Tbr1 suggest the opposite, where the hNPCs may have reverted to a quiescent progenitor cell fate and require exposure to the endogenous ECM to continue differentiation.

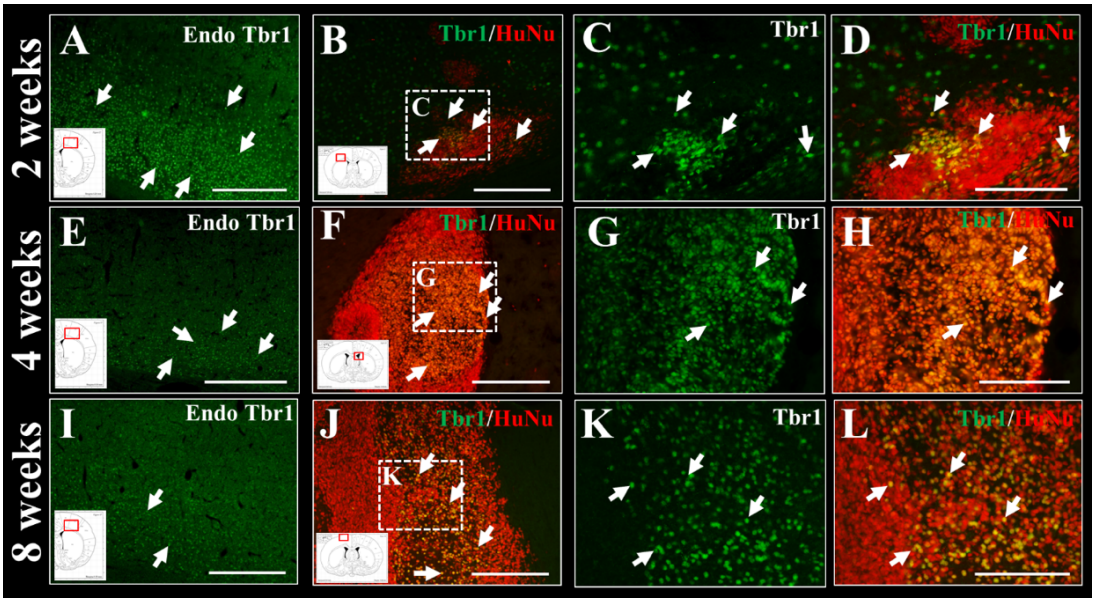

Figure 4.10 The endogenous expression of Tbr1 within the contralateral rat sensorimotor cortex and expression of Tbr1 within the transplanted hNPCs over time. Staining for endogenous (endo) Tbr1 expression in the deep layers of the contralateral rat sensorimotor cortex (that contained no hNPCs) highlighted a reduction in Tbr1 expression over time (**A**, **E** and **I**, white arrows). In contrast and following on from the *in vitro* data, hNPCs had a population of Tbr1-expressing cells after transplantation *in vivo*, observed from 2 weeks up until 8 weeks. Furthermore, this expression did not appear to decrease over time. At 2 and at 4 weeks, hNPCs stained for anti-HuNu co-localised with Tbr1 (**B-D** and **F-H**, respectively). By 8 weeks, a population of Tbr1-expressing cells was still maintained within the hNPCs (**J-L**). In some grafts it was noticed that densely packed areas of hNPCs did not show

expression of Tbr1 (**J-L**) and instead, Tbr1 expression was localised to hNPCs within less dense regions of the graft. Interestingly, the Tbr1 expression in hNPCs was retained in off-target injections, such as those located within the lateral ventricles (**F-H**) suggesting the hNPCs were able to keep their pre-programmed differentiation cell fate *in vivo*. Scale bars in A, E, I = 500 µm; B, F, J = 250 µm and C, D, G, H, K; L = 150 µm.

4.3.6 hNPCs displayed a progenitor cell phenotype *in vivo* over time

The hNPCs were pre-programmed to differentiate into hyCCNs (Axol Bioscience). It was hypothesised that these hNPCs should lose their progenitor cell-like phenotype over time as they mature. However, progenitor cell features were observed within the transplants at all time points, from 2 weeks up to 8 weeks. For example, formation of neural rosettes is a common neural stem cell feature and rosette formation was detected in densely-packed WT hNPC transplants (Figure 4.11). Furthermore, as the hNPCs differentiate over time we would have expected them to lose their proliferative state, instead however large, dense formations were observed within 23% of detectable transplants (n=13/56) (Figure 4.12) and suggested proliferation of cells *in vivo*. When analysed using IHC for expression of Ki67, a general proliferation marker, hNPCs within these large cell formations were Ki67-positive (Figure 4.12, C and D) and expression was retained from 2 weeks up to 8 weeks. Furthermore, in a small number of animals the size of the ventricles had expanded and in some cases severely distorted, suggestive of large tumour formation. However, Ki67 expression was observed across all time points within less dense hNPC grafts, suggesting expression was not solely within the large bolus formations.

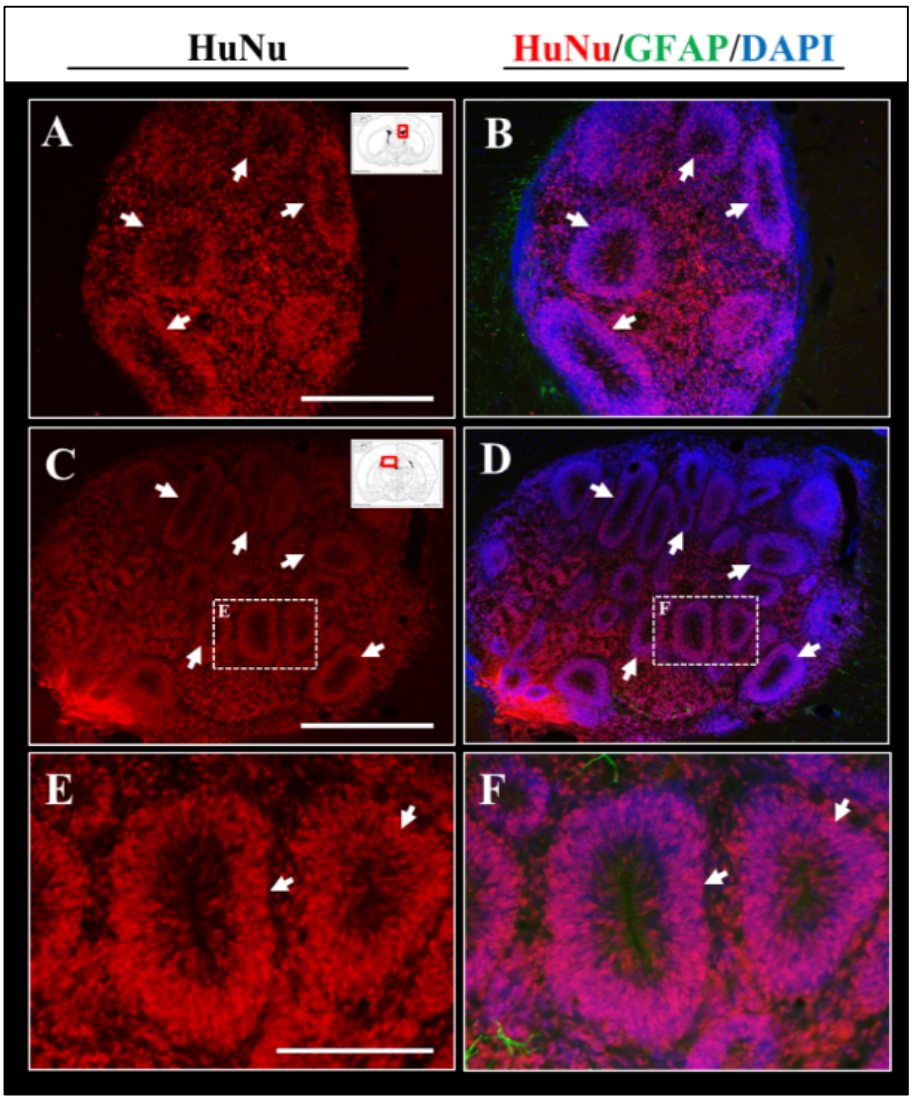

Figure 4.11 WT hNPCs formed neural rosette structures *in vivo*. Representative images taken at 4 weeks post-transplantation of hNPCs showed rosette formation, typical of NSCs (**A-F**, white arrows). Rosettes were observed within hNPC grafts from 2 weeks up to 8 weeks *in vivo*. Tissue was analysed using IHC and antibodies against HuNu, GFAP and DAPI. Scale bars A-B = 250 µm; C-D = 500 µm; E-F = 150 µm.

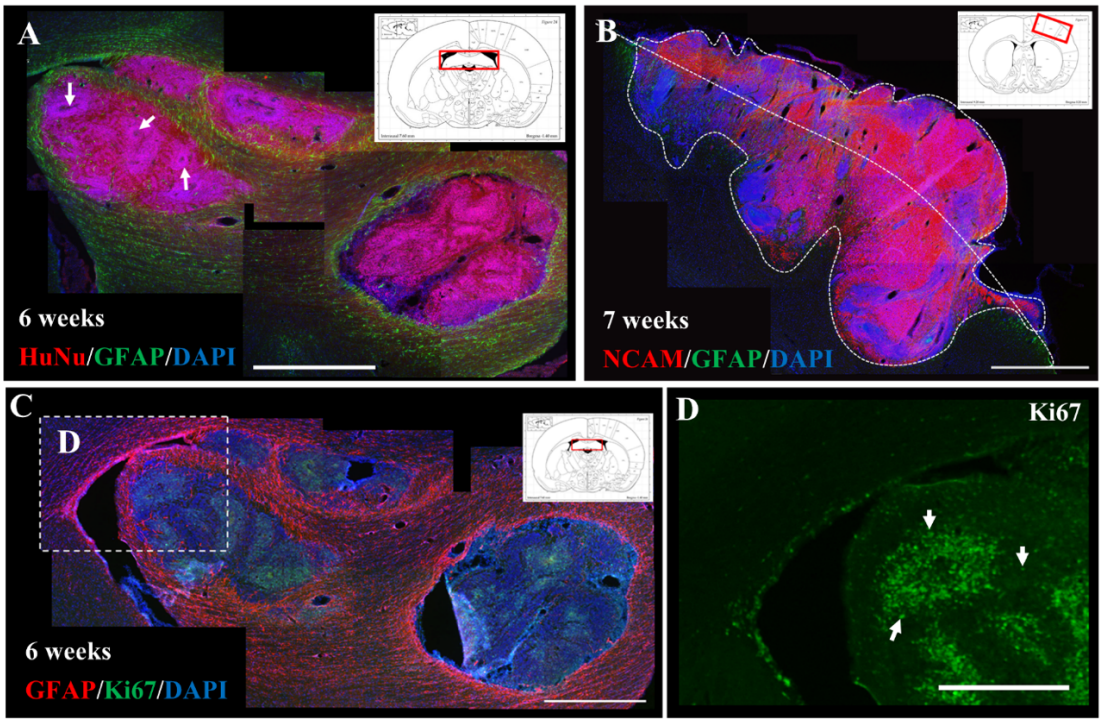

Figure 4.12 hNPCs expressed proliferation markers *in vivo* and displayed large dense cellular formations in some cases. In some of the transplants, large grafts were detected, for example within the fimbria (**A** and **C**) and cortex (**B**). These grafts displayed neural rosette formations (white arrows in **A**). When stained for Ki67, a marker for proliferation, the cells within the core of these dense formations were Ki67-positive (**C** and **D**). Scale bars A-C = 1 mm; D = 500 µm.

4.3.7 The effect of hNPC transplants on the ECM and immune system

From the literature we know transplanting human cells into the rat system will undoubtedly provoke an immune reaction. We hypothesised that the reason the survival of transplanted hNPCs was reduced over time was due to the development and maturation of the rat immune system, as our transplants were performed in neonatal-aged rats. Using IHC, tissue was analysed for both microglia, the main immune cells of the brain using an anti-Iba-1 antibody, and astrocytes, the main glial support cell of the brain using an anti-GFAP antibody. These antibodies were used alongside either hNCAM or HuNu to detect transplanted hNPCs. Our results show at 2 and 4 weeks there was only a very little increase in microglial activation in response to hNPC transplants (Figure 4.13, K, L, N and O) compared to endogenous control Iba-1 IHC (Figure 4.13, J and M) taken from the contralateral cortex that contained no

hNPCs. At the same time points, there was a noticeable increase in GFAP staining (Figure 4.13, B, C, E and F) compared to endogenous control GFAP expression (Figure 4.13, A and D), indicating activation of host astrocytes within the rat brain had occurred. However, at 8 weeks post-transplantation, the response from both cell types, microglia and astrocytes, was greatly increased (Figure 4.13, H, I, Q and R) compared to controls (Figure 4.13, G and P). This result aligned with our hypothesis and showed the immune system produced a larger response over time as it matured, likely resulting in the observed rejection of the transplanted cells. It is therefore possible, with immune-compromised animals, transplant survival could be assessed beyond the 8-week time point.

A further observation was made from the GFAP-immunolabelled transplant sites. The results showed unusual astrocytic formation where the astrocytes had changed from a star-like morphology to an almost neurite-like morphology with elongated processes (Figure 4.13, H, I and Figure 4.14, A-C, white arrows). This morphology was detected at the later time points (6, 7 and 8 weeks) and was commonly, but not solely, detected in grafts where there were large, densely-packed hNPCs. At the earlier time points (2 and 4 weeks) IHC analysis suggested hNPCs projections may have interacted with astrocytes. For example, at 4 weeks hNPC projections were able to reach the caudal brain stem, and following IHC analysis, GFAP-positive astrocytes were observed in close proximity to hNCAM-labelled projections (Figure 4.14, D-F). This suggests that astrocytes may have been interacting with the hNPCs, potentially providing support, a function astrocytes would normally provide to host axonal projections (Walz, 2000; Magistretti, 2011; Suzuki *et al.,* 2011). This potential glial interaction may have enabled elongation of fibres up to a certain peak time point where the axonal hNPC projections were at their longest, but before the host immune response was elicited.

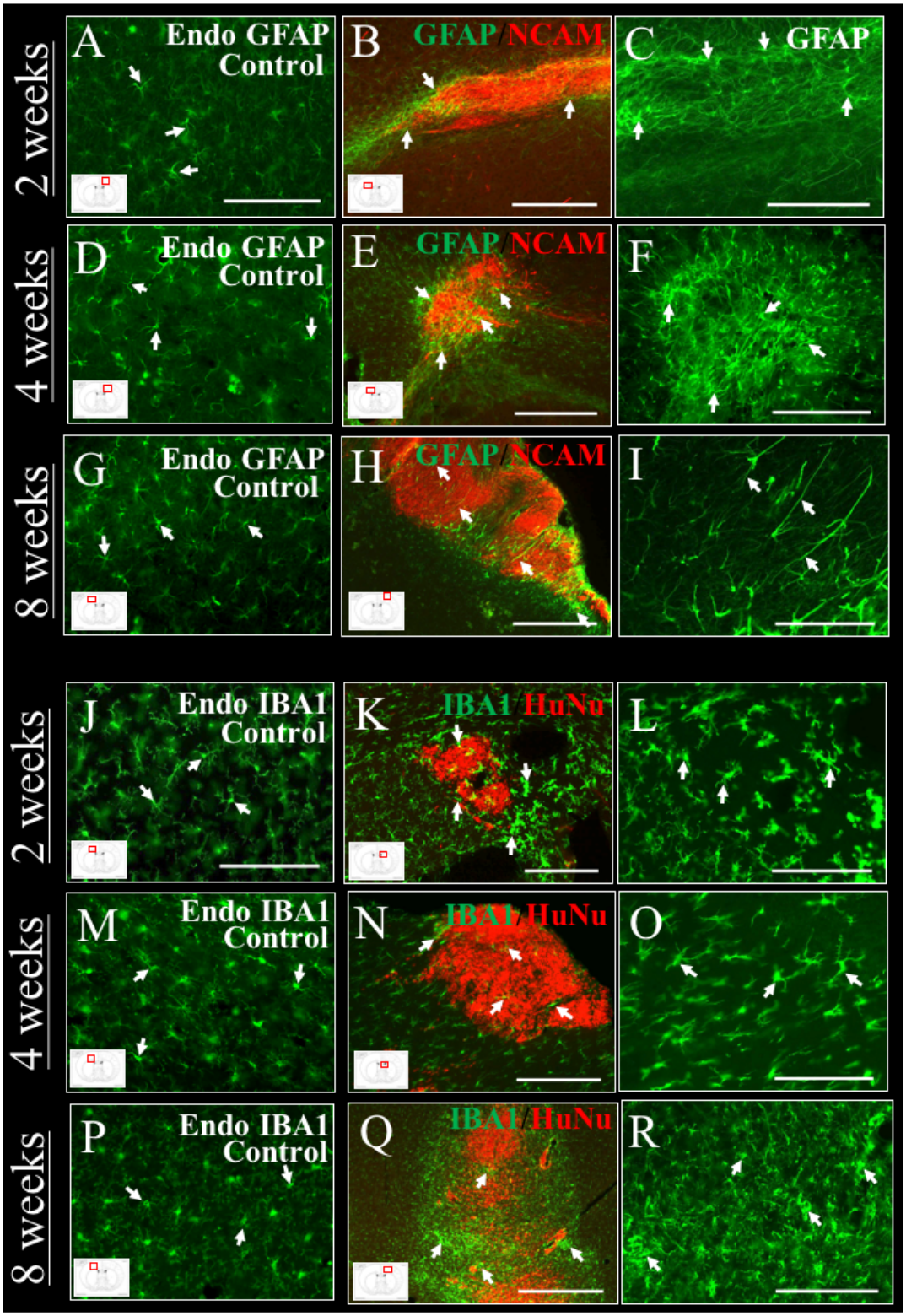

Figure 4.13 Transplant of hNPCs provoked the host immune response over time. The hNPC graft survival rate was high at 2 and at 4 weeks, which declined over time. Following IHC analysis for immune response markers, including microglia (Iba-1) and astrocytes (GFAP), results indicated an increase in the immune reaction to the human grafts over time. At 2 weeks there was a mild increase in GFAP staining at the injection site (**B** and **C**) compared to endogenous control GFAP staining from

contralateral cortex (**A**). This expression increased over time (**E, F**) and by 8 weeks there was a dramatic increase of GFAP staining and a noticeable change in astrocyte morphology (**H, I**) compared to control staining (**G**). When microglial activity was analysed, using an anti-Iba-1 antibody, there was a relatively little immunoreactivity at earlier time points of 2 and 4 weeks (**K, L, N** and **O**) compared to control staining in the contralateral cortex (**J** and **M**), however this response greatly increased by 8 weeks (**Q** and **R**), and may have resulted in the observed graft rejection. Scale bars in A, C, D, F, G, I, J, L, M, O, P, R = 150 μm; B, E, K, and N = 250 μm; H and Q = 500 μm.

Lastly, the expression of the main CNS ECM protein, TN-C was also analysed over time. TN-C although highly expressed during development it is also upregulated after injury (Zhang *et al.,* 1997; Tang *et al.,* 2003). Results from Chapter 3 indicated the hNPCs expressed TN-C in culture and previous research has shown TN-C can be secreted by some cells, including PC12 cells, into the ECM (Andrews *et al.,* 2009). Following IHC, analysis showed increased TN-C expression at the site of transplant from 2 weeks that persisted up to 8 weeks post-hNPC transplantation, with a small increase in expression over time (Figure 4.15). The staining in each case was localised to the injection site and the bolus of hNPCs. The antibody used in these experiments was human-specific and therefore may have only been detecting TN-C either expressed or secreted by the transplanted hNPCs into the ECM.

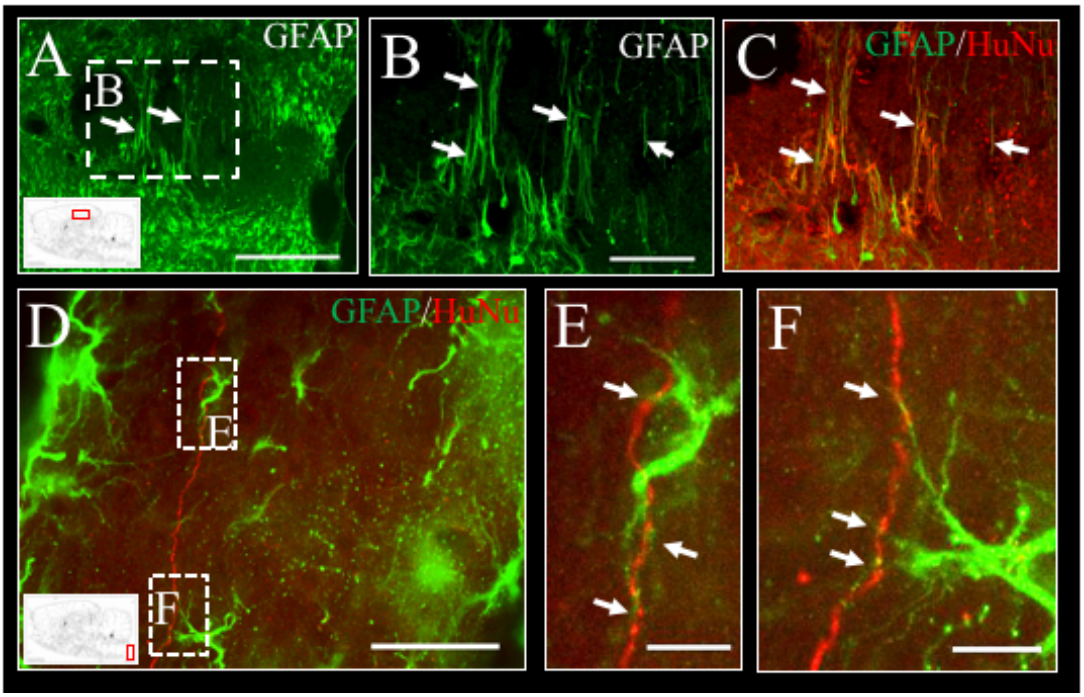

Figure 4.14 Transplantation of hNPCs stimulated an astrocytic response. IHC analysis for host astrocytic reaction to hNPC grafts revealed an unusual astrocytic response (indicated by GFAP staining) showing string-like projections which correlated with a scarred region of HuNu-positive tissue at 7 weeks post-transplantation (**A-C**). However, at earlier time points, such as 4 weeks post-transplantation, in the caudal brain stem hNCAM-positive projections were observed in close proximity to GFAP-positive astrocytes suggesting the hNPCs may have been supported by astrocytes *in vivo* (**D-F**). Scale bar A = 500 µm, B and C = 200 µm, D = 50 µm and E and F = 10 µm.

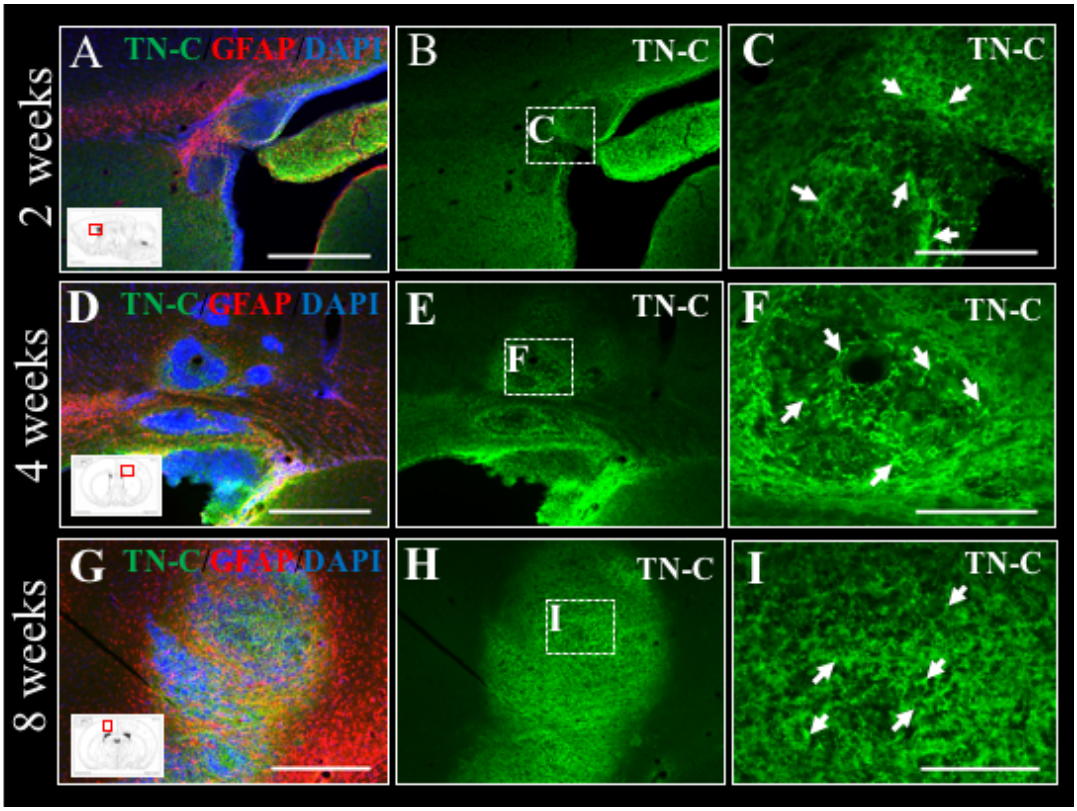

Figure 4.15 Increased expression of TN-C in response to hNPC transplantation. Following transplantation of hNPCs, IHC analysis revealed an upregulation of TN-C, the main ECM protein of the CNS, at the transplant site. This upregulation was apparent at all time points from 2 weeks (**A-C**) up until 8 weeks post-transplantation, however was more apparent at later time points 4 and 8 weeks (**D-I**), suggesting TN-C expression steadily increased over time. Scale bar A-B, D-E, G-H = 500 µm; C, F, I = 150 µm.

4.4 Discussion

Here we aimed to build upon the *in vitro* work discussed in Chapter 3 and transplant WT iPSC-derived hNPCs, pre-programmed to differentiate into cortical neurons, into the neonatal sensorimotor cortex. Specifically, we targeted layer V as this is the area that projects axons within the CST with the aim of assessing graft survival and the ability of hNPCs to extend long-distance axonal projections over time. Following transplantation, tissue was collected at a number of time points, from 2 weeks through to 8 weeks, and analysed for graft survival, axonal projections, graft maturation and expression of cortical neuron markers. Here we present data highlighting hNPC grafts survived up to 8 weeks post-transplant with axonal projections that followed endogenous white matter tracts and reached the caudal brain stem after 4 weeks. Furthermore, we show hNPCs retained expression of both cortical neuron and progenitor cell markers *in vivo*.

Once transplanted, hNPCs were detected using human-specific antibodies to highlight the graft site as well as the projections. The transplants themselves were carried out between P0-2. This age was chosen because the rat immune system is not fully developed immediately after birth and is still in the process of maturing (Reviewed in Marshall-Clarke *et al.,* 2000; Reviewed in Holsapple *et al.,* 2003). Following birth, rodents go through a brief period of immunodeficiency, a window of opportunity, before the animals become immunocompetent. Therefore, to give the hNPCs the best chance of survival and integration into the rat system, the transplants needed to be carried out during this brief window. Transplantation of stem cell-derived cells into rodent neonatal brain within this P0-2 window and without immunosuppression has been carried out before showing promising graft survival and integration (Ideguchi *et al.,* 2010; Denham *et al.,* 2012). Our results show hNPCs can survive in the neonatal rat brain up to 8 weeks, however, survival is highest at earlier time points of 2 and 4 weeks. Beyond this, an immune response is elicited (section 4.3.7) which is likely to be the reason for decreased transplant survival at 6, 7 and 8 weeks. Conversely, research has shown human ESC-derived neurons can survive up to 10 weeks in the Sprague Dawley rat brain following injection at P2 into the striatum without the use of immunosuppression (Denham *et al.,* 2012). This difference suggests there may be

either regional differences within graft survival or embryonic-derived cells may have a better capacity to survive *in vivo*. As the immune system is immature at the early time points, it was expected that there would be 100% survival at 2 and 4 weeks, however transplant survival was 82% and 75%, respectively. During some of the surgeries, the injection needle did clog and therefore there was a chance some of the animals that were designated as not having a detectable transplant, were in fact not injected with hNPCs. Furthermore, the injection site was shallow being between -0.4 and -0.7 mm below the skull and there was a chance the cells could seep back out of the injection site once the needle had been removed. Extra care was taken to remove the injection needle slowly to minimise any backflow from the injection tract, however, it was not always avoidable.

From analysis of the immune response over time, an increase in both Iba-1- and GFAP-positive staining was observed at the transplant site over time (section 4.3.7). The increased GFAP staining could have been, in part, due to a transplanted population of human astrocytes. The antibody used here was able to detect both rat and human variants and in combination with data from Chapter 3, a small population of astrocytes was present in the hNPC *in vitro* culture pre-transplant. In uninjured environments, astrocytes are known to be involved in providing essential support to neurons, including metabolic support (Reviewed in Magistretti, 2011; Suzuki *et al.,* 2011); regulation of the ion homeostasis in the surrounding environment (Reviewed in Walz, 2000); and promotion of synaptogenesis (Ullian *et al.,* 2004, 2001; Christopherson *et al.,* 2005). It is therefore possible that astrocytes within the hNPC culture could have provided this essential support to the hNPCs once transplanted. Indeed, at younger time points, astrocytic cells were observed in close proximity to hNPC projections suggesting astrocytes may have interacted with the hNPC projections (Figure 4.14). However, over time, the increase in GFAP staining was coupled with an increase in microglia activation, highly indicative of an immune reaction (Figure 4.13). This suggested astrocytes may have initially provided support, however, following an increased immune response, such as microglial activation, they switched to pro-inflammatory mediators.

Furthermore, it was observed that in some cases GFAP-expressing cells at the transplant site had taken on an unusual morphology compared to WT tissue. Astrocytes

positive for GFAP have a star-like morphology, however in some cases GFAP-positive cells that had taken on a neuronal-like shape, with a long elongated process, were present at the cortical graft site (Figure 4.14). There are two subtypes of astrocytes, protoplasmic star-like astrocytes and fibrous astrocytes which have longer processes; however, fibrous astrocytes are located within white matter suggesting these cells may not be fibrous astrocytes as the transplant sites are located largely in grey matter. Yet, these cells did have a similar morphology to another cell type, radial glial cells (RGCs), which have an apical elongated process. RGCs develop from neuroepithelial cells during embryogenesis and serve as support for neuronal migration during development. However, research has indicated they can also function as progenitor cells (Reviewed in Hartfuss *et al.,* 2001; Noctor *et al.,* 2002) giving rise to both neurons and glia *in vivo* (Reviewed in Götz *et al.,* 2002; Malatesta *et al.,* 2003). Literature suggests this is actually a distinct astroglial cell type, termed GFAP-expressing radial NSCs, that acts as an intermediate between RGCs and astrocytes (Liu *et al.,* 2006). In addition, *in vivo,* RGCs have been linked to production of adult NSCs located within the subventricular zone in mammals (Merkle *et al.,* 2004). It is therefore possible there is an RGC/GFAP-expressing radial NSC population within the hNPCs, potentially supporting newly forming neurons by aiding migration, but also by differentiating into newly formed neuronal and glial cells. In culture, RGCs can be derived from embryonic NSCs following epidermal growth factor receptor signalling (Gregg and Weiss, 2003), which is known to be a constituent of the hNPC reprogramming protocol (Axol Bioscience). If RGC/GFAP-expressing radial NSCs are within the hNPC culture, further staining would potentially be able to confirm this. Indeed GFAP can detect RGCs (Levitt and Rakic, 1980) and GFAP-expressing radial NSCs (Garcia *et al.,* 2004), however, it can also detect astrocytes and therefore use of a more specific antibody, such anti-radial glial cell marker 2 (RC2) to detect RGCs (Misson *et al.,* 1988), could be used to answer this question. Alternatively, to differentiate between GFAP-expressing radial NSCs and fibrous astrocytes, expression of LeX/CD15 could be analysed as research suggests these two cell types have differential expression of this cell surface protein (Imura *et al.,* 2006). Lastly, use of a human-specific GFAP antibody would allow us to ascertain whether these cells originated from the hNPC graft or if the graft caused a change in morphology of the endogenous cells surrounding the graft site.

From tissue analysis of the injection sites, our results showed significant location variation. Initially, coordinates were based upon the predicted sensorimotor cortex, specifically sensorimotor 1 front limb region (S1FL) layer V, using an atlas of prenatal rat brain development (Altman and Bayer, 1995). Specifically, coordinates were used for embryonic day 22 (E22), which would correspond to P0, as rat embryo gestation is approximately 20-21 days. The first batches of transplants, batch 1 and batch 2, resulted in on average 35% of transplants on target within the sensorimotor cortex. Off-target injections were mainly located below the corpus callosum within the caudate and/or putamen of the basal ganglia. As a result of this and in trying to focus on the area of interest, the injection sites were monitored with each batch of transplants and the coordinates were adjusted as required. It is likely that operator variability affected the transplants. For example, both batch 3 and batch 4 received injections using the same coordinates, however in batch 3, 56% of surviving grafts were on target, compared with 38% in batch 4. These injections were carried out weeks apart and therefore may have introduced operator variability or error. Alternatively, pups in these litters may have been of different sizes owing to the large litter sizes, 12 and 14 respectively, which may have included 'runts' therefore altering the location of the target site and resulting in an increased number of off-target injections. In batch 6, the coordinates were again similar, however, the depth of the transplant was further reduced to -0.45 mm and the accuracy of the injection increased marginally from batch 4, to 40%. The coordinates in batch 12 were altered further to target the sensorimotor area more laterally as a number of injection sites resulted in grafts located below the corpus callosum, centrally in the brain within the striatum, or within the hippocampal region. To correct for this, coordinates were also moved slightly forward and the depth of the injection was reduced further. This optimisation resulted in 64% of detectable graft sites on target. It is very likely that the combination of altered coordinates and user repetition of the technique over time resulted in a large proportion of grafts in batch 12 being on target.

Following IHC analysis, hNCAM-positive fibres were observed emanating from the transplanted hNPCs bolus sites. These fibres were located adjacent to the bolus sites, however, large hNPC fibre bundles were also observed following white matter tracts of the rat brain including the corpus callosum and the internal capsule. Due to the

variation in transplant sites, projections reached a number of neuroanatomical regions, which included the corona radiata, corpus callosum, olfactory bulb, striatum, pallidum, thalamus, internal capsule and areas of the brain stem. In a small proportion of the animals, transplants were detected on top of the cortex, which would suggest either cells were not transplanted into the cortex or, following transplant, cells had flowed out into the subarachnoid space (Figure 4.3, H and Figure 4.12, B). When the injections were delivered on target within the deep layers of the sensorimotor cortex, axonal projections from the transplanted hNPCs could be observed within the corona radiata, internal capsule, cerebral peduncles, pyramids of the brain stem and the dorsal-caudal brain stem likely beyond the pyramidal decussation suggesting hNPCs projections are able to follow the trajectory of the CST. At 2 weeks, the furthest regions where hNCAM positive fibres were observed were the pyramids in the dorsal brain stem (Figure 4.5 and Figure 4.6). The HuNu-postive bolus where these hNCAM fibres originated was on target within the sensorimotor cortex, however, some HuNu positive cells were also observed within the caudate putamen. At 4 and 6 weeks, from on-target injections, hNCAM-positive projections reached the caudal brain stem, however, only a small number of projections achieved this and in two of the pups, projections were observed in the contralateral dorsal-caudal brain stem. A common observation was that the further away the hNCAM projections were from the injection site, the fewer projections there were, suggesting only a small proportion of fibres were able to project these distances. Moreover, these projections appeared very thin, whereas closer to the injection sites large fibre bundles could be detected. It is likely that where there were dense boluses and therefore more cells, more projections formed and bundled and they therefore appeared thicker in diameter. Similarly, as only a few axons projected further away from the bolus sites, there were less fibres to bundle together and therefore appeared smaller in diameter. Further analysis of the tissue using confocal microscopy would provide more information on axon diameter. At later time points where only the nuclei of hNPCs could still be detected due to the immune response, projections were not observed outside of the bolus site. This had been observed previously under different circumstances where projections were not seen outside of boluses within specific regions such as the neocortex (Brundin *et al.,* 1988). This further suggests there are regional differences within the brain determining cell survival and integration.

As TN-C is a ligand for our integrin heterodimer of interest, α9β1, its expression was analysed over time (Figure 4.15). The antibody used was human-specific. Previously our lab has had positive TN-C expression in rat tissue in the absence of human cells with this antibody and therefore there is doubt as to whether this antibody is definitely human-specific. If this is the case, and the antibody is not specific to human antigens, our results here suggest there is an endogenous upregulation of TN-C surrounding the transplant site, which has been shown in response to injury (Zhang *et al.,* 1997). Alternatively, hNPCs may have expressed and secreted TN-C *in vivo* which aligns with the *in vitro* results (section 3.3.4). As TN-C is known to be upregulated at CNS injury sites (Zhang *et al.,* 1997; Andrews *et al.,* 2009), this result was of interest. An upregulation of TN-C at the transplant site, whether from endogenous rat tissue or produced by the grafted cells, may promote further neurite outgrowth from α9-eYFP expressing cells when transplanted *in vivo* (see Chapter 5).

Additionally, one of the main questions we were interested in was whether the transplanted cells show any signs of maturation over time. This was assessed by loss of DCX expression as well as evidence of myelination using an antibody against MBP, a protein expressed by myelinating oligodendrocytes. DCX is a microtubule-associated protein that acts to stabilise immature, developing neurons. In endogenous rat tissue, our data suggested the DCX staining was present in the cortex at 2 weeks of age, although at a very low level. This is in line with published literature suggesting cell proliferation ends at around P15 (Reviewed in Rice and Barone, 2000). Conversely, the hNPCs retained their expression of DCX through until the 8 week time point. This suggests the cells retained their immature neuronal state. It may also suggest that the cells were not fully reacting to any endogenous environmental signals for maturation (such as those from neurotransmitters, growth factors, glial cells and adhesion proteins located within the extracellular environment). This was not expected and is in contrast to previously published literature (Ballout *et al.,* 2016).

The myelination of hNPC projections was assessed over time using an antibody against MBP. This was able to show the hNPCs can follow myelinated tracts, such as those in the corona radiata going into the internal capsule as well as the corpus callosum. At later time points, the IHC results show there were MBP-expressing oligodendrocytes in close proximity to large fibre bundles from hNPC grafts, however, staining alone is

unlikely to confirm myelination, rather electron microscopy and/or confocal microscopy would be required for confirmation. Interestingly, there are regional differences in myelination of the rodent brain, for example the sensorimotor cortex is believed to be fully myelinated by around 2 weeks as research shows no differences in myelination were observed within the mouse sensorimotor cortex between P15 and P45 (Chahboune *et al.,* 2007). Therefore, if axons from the hNPCs are not myelinated at the 2 week time point, this suggests there may be a lag time where the hNPCs take longer to myelinate than the endogenous equivalents. Furthermore, research suggests myelination is beginning at around P2 (Craig *et al.,* 2003) and therefore this transplant window (P0-2) was used to give the hNPCs the best chance of myelination and integration. Moreover, it remains to be seen whether rat oligodendrocytes are able to myelinate human axonal projections. Research has shown following a C5 lateral spinal cord lesion, transplant of human iPSC-derived NSCs can project through the lesion site and are seen to be in direct contact with rat oligodendrocytes but myelination of human axons was not observed (Lu *et al.,* 2014). However, Lu and colleagues also found that projections from the transplanted hNPCs expressed immature neuronal markers and suggested myelination may not occur until the hNSCs matured. Similarly, previous research has shown human ESC-derived OPCs are able to promote remyelination after thoracic contusion injury in adult rats resulting in increased functional recovery (Keirstead *et al.,* 2005). Specifically, part of this remyelination of injured rodent axons corresponded directly to the transplanted human OPCs. Together, this literature suggests myelination of human axons by rat oligodendrocytes may be possible, however the maturation status of the transplanted hNPCs may dictate the myelination outcome. For this project, if future experiments were able to prolong hNPC survival *in vivo*, the maturation of hNPCs could progress and myelination may occur.

To further assess maturation, tissue was analysed for PNN formation, net-like structures composed of extracellular matrix that form around mature neurons, reducing synaptic plasticity. No PNN structures were observed in association with the grafts. However as many of the cells were closely packed together, it is unclear whether this inhibited staining and/or visualisation of PNNs. The retention of an immature cell state may be of interest and beneficial when considering axonal elongation and

regeneration, however, over time this may not be advantageous and it begs the question as to when will neuronal maturation occur within these cells *in vivo*. Recently published *in vitro* research has shown following growth on multi-electrode arrays, hiPSC-derived cortical neurons (Axol Bioscience) require long-term culture of around 20-30 weeks to functionally mature and for synapses to form (Odawara *et al.,* 2016). It is likely therefore that the hNPCs may need to either be in culture for longer before transplantation or survive *in vivo* for longer to offer the best chances for functional integration into the host tissue.

From analysis of the tissue, it was apparent that some batches of cell populations may be more proliferative than others. In 23% of detectable grafts, large dense formations were observed suggestive of cell proliferation. When analysed for Ki67 expression, a proliferation marker, cells within the centre of these dense boluses were positive for Ki67 expression, but those located on the outside of these grafts were not. This suggests the *in vivo* hNPCs transplants may contain two populations of cells: one which is more able to differentiate and mature over time, extending long projections; and another that remains in a progenitor cell state, resulting in continued proliferation. The formation of these two populations may be due to the extent to which the cells are exposed to the extracellular environment. For example, some of the transplants have formed a tight bolus of cells and the cells on the outside of the bolus may be able to interact with host tissue and ECM proteins enabling axonal maturation and growth. On the other hand, cells within the centre of this bolus may not be exposed to this environment and instead have created a niche that reduces interaction with endogenous, and potentially essential, signalling mechanisms to continue the development and maturation of these cells. Support for this hypothesis is shown in Figure 4.12 where Ki67-positive cells were detected within a dense rosette formation within a large bolus of cells. The Ki67-positive cells were retained and localised to the neural rosette, but there were very few cells outside of this rosette formation that were Ki67-positive suggesting that these cells were no longer proliferating and were instead in the process of neuronal maturation. To counter this in future, the number of cells injected at one site could be reduced while the number of injections is increased. This would potentially result in cells spreading out more evenly over the same size area and hopefully reduce the number of tightly packed boluses.

There remains a question however as to whether the extracellular environment can alter or influence the neuronal phenotype of the transplanted hNPCs pre-programmed to differentiate into CCNs. Following collection of *in vitro* data, the expression of deep-layer cortical neuron markers, Ctip2 and Tbr1, were analysed *in vivo*. Unfortunately, the Ctip2 antibody gave inconsistent results over different uses and was therefore discarded. As the hNPCs expressed Ctip2 before transplant (section 3.3.6) it could be suggested they may have retained their expression *in vivo*, however this cannot be confirmed without further analysis using a different Ctip2 antibody. On the other hand, hNPCs retained the expression of Tbr1 *in vivo* (Figure 4.10) and was observed at all time points suggesting the hNPCs have the ability to project to sub-cortical targets *in vivo*. Owing to time constraints, expression of other neuronal markers, such as hippocampal or thalamic neurons, were not assessed. It would have been of particular interest to assess if cells that were transplanted off target into, for example, the hippocampus, were influenced by and were able to respond to environmental signalling to change their expression of certain phenotypic markers associated with different neuroanatomical regions.

Together these results show the hNPC grafts can survive up to 8 weeks *in vivo* although survival was highest at earlier time points. Once transplanted, these cells are able to extend long-distance axonal projections, following white matter tracts, such as the CST. When injections were on target, projections from the hNPC grafts travelled from the sensorimotor cortex through the CST reaching the caudal brain stem after 4 weeks. These results are promising for the progression of the project, providing a viable vehicle for the α9-integrin subunit.

Chapter 5: *In vivo* analysis of α9 integrin-expressing iPSC-derived hNPCs

5.1 Introduction and aims

Previous research has demonstrated that overexpression of the α9 integrin protein can promote neurite outgrowth in the presence of TN-C (Andrews *et al.,* 2009), the ligand for the α9β1 integrin heterodimer. This presents a promising target for neuroregeneration and in particular, axonal regeneration, in conditions such as SCI where long-distance axonal projections may promote repair and restoration of function. Recently, reintroducing α9 integrin along with the integrin activator kindlin-1 into sensory axons of the spinal cord has demonstrated promising results, promoting regeneration and recovery of function after injury (Cheah *et al.,* 2016). In addition, however, data has also shown that the α9 protein is not transported down CST axons following overexpression using viral vectors (Andrews *et al.,* 2016). In light of this, here we have outlined one potential opportunity utilising iPSC-derived hNPCs expressing α9 integrin as a vehicle to increase α9 expression in the CNS.

In this chapter we aimed to transplant α9-eYFP-expressing iPSC-derived hNPCs into the neonatal rat sensorimotor cortex with the goal of analysing cell survival, exogenous integrin expression and long-distance axonal projections over time. This work continues on from the results presented in Chapter 3 highlighting the ability to overexpress α9-eYFP protein within these cells and combines it with the characterisation of WT hNPCs *in vivo* from Chapter 4. We hypothesised that the cell survival and axonal projections from α9-eYFP hNPCs would mirror that observed with WT hNPC transplants.

5.2 Methods

5.2.1 Transplant of α9-eYFP-expressing hNPCs

All procedures were carried out under UK Home Office Project Licence number 60/4472 and Personal Licence number IC71C2B2B, conformed to the UK Animals (Scientific Procedures) Act (1986) and were approved by the Animal Welfare Ethics Committee of the University of St Andrews.

Following transduction of hNPCs with α9-eYFP second generation LV supernatant (section 2.4.12), cells were incubated at 37°C for 4 days before being collected for transplantation (section 2.5.6). The procedure for transplantation of α9-eYFP-expressing hNPCs was the same as for WT hNPCs, detailed in section 2.7. Sprague Dawley pups aged between P0-2 were manually injected either unilaterally or bilaterally into two specific sites (1μL/injection site) for the predicted neonatal sensorimotor cortex (Altman and Bayer, 1995) (see Table 2.8 for injection coordinates).

5.2.2 Neural tracing experiments using BDA

See section 2.7.2

5.2.3 Solutions for perfusion and sectioning

See section 2.7.4

5.2.4 IHC analysis of α9-hNPC transplants

The full IHC protocol is detailed in section 2.8. Primary antibodies used in this analysis are detailed in Table 5.1 (full details in Table 2.5). When staining for TN-C, tissue required pre-treatment with 0.03% hydrogen peroxidase (section 2.8.1). All tissue was mounted onto gelatin-coated slides (section 2.8.2). Tissue was left to air dry before coverslips were mounted using FluorSave (Calbiochem).

Table 5.1 Primary antibodies and dilutions used for IHC analysis of α9-hNPC transplants

Antibody	Species	IHC dilution
HuNu	Mouse	1:500
hNCAM	Mouse	1:200
GFP	Rabbit	1:1,000
TN-C	Rabbit	1:200
GFAP	Rabbit	1:500
Tbr1	Rabbit	1:400
DCX	Rabbit	1:500
Iba-1	Rabbit	1:500

5.3 Results

5.3.1 Analysis of α9-hNPC transplant survival *in vivo* over time

As with analysis of the WT hNPCs transplants, survival of α9-eYFP hNPC transplants was assessed using the human-specific antibodies HuNu and hNCAM. Results indicated α9-eYFP hNPC grafts survived up to 8 weeks *in vivo* (Table 5.2). Out of a total of 59 pups that received an α9-eYFP hNPC transplant 63% (n=37/59) had grafts that survived. Similar to the WT hNPC transplants, survival was highest at the younger time points of 2 and 4 weeks and decreased over time (Table 5.2 and Figure 5.1, A).

Table 5.2 Survival of α9-hNPC transplants over time

	Number of weeks post-transplantation of α9-eYFP hNPCs					**Total n (%)**
	2 weeks n (%)	**4 weeks n (%)**	**6 weeks n (%)**	**7 weeks n (%)**	**8 weeks n (%)**	
No. of animals with transplants surviving	12 (92%)	11 (92%)	5 (42%)	5 (46%)	4 (36%)	37 (63%)
No. of animals with scarring	0 (0%)	0 (0%)	6 (50%)	6 (55%)	7 (64%)	19 (32%)
No. of animals with no graft detected	1 (8%)	1 (8%)	1 (8%)	0 (0%)	0 (0%)	3 (5%)
Total	13 (22%)	12 (20%)	12 (20%)	11 (19%)	11 (19%)	59 (100%)

After 4 weeks *in vivo*, 92% (n=11/12) of α9-hNPCs grafts survived, which was expected in light of results obtained in Chapter 4 from survival of WT transplants. After this, at 6 weeks, survival fell to below 50% and by 8 weeks only 36% (n=4/11) of grafts survived. Furthermore, over time as survival of grafts decreased, the number of pups where scarring was detected increased. Specifically, at 2 and 4 weeks no scars were detected, but at 7 weeks just over half (55%, n=6/11) of the pups had scars and at 8 weeks this increased to 64% (n=7/11). Overall 32% (n=19/59) of pups showed noticeable scarring indicating potential rejection of the cells over time. Out of a total of 59 pups, only 5% (n=3/59) showed no signs of α9-eYFP hNPC survival or scarring. Interestingly, these pups were at the younger time points of 2, 4 and 6 weeks (Table 5.2 and Figure 5.1, A). These three cases cannot be termed as graft rejection, as we

cannot confirm cells were transplanted, because of potential backflow of cells from the injection site or clogging of the needle during transplant.

Of the 56 pups that had detectable graft sites, 34% (n=19/56) were on target within the deep layers of the sensorimotor cortex (Figure 5.1, B-C). The remaining 66% (n=37/56) were off target and located in regions such as the striatum, hippocampus, caudate and/or putamen of the basal ganglia and other areas of the cortex away from the sensorimotor cortex. Batch 11 had the highest percentage of on-target grafts (60%, n=6/10), most likely due to optimisation of transplant coordinates. Following transplantation of WT hNPCs and the injection targeting information gained from those grafts, α9-eYFP transplants were carried out after the WT hNPC grafts and optimisation of transplant coordinates was continued within these grafts. When on- and off-target injections were analysed over the various time points, results show only a small proportion of pups had on-target injections at each time point, with 4 weeks comprising the lowest (18%, n=2/11) and 6 and 8 weeks comprising the highest (46%, n=5/11 in both) (Figure 5.1, C).

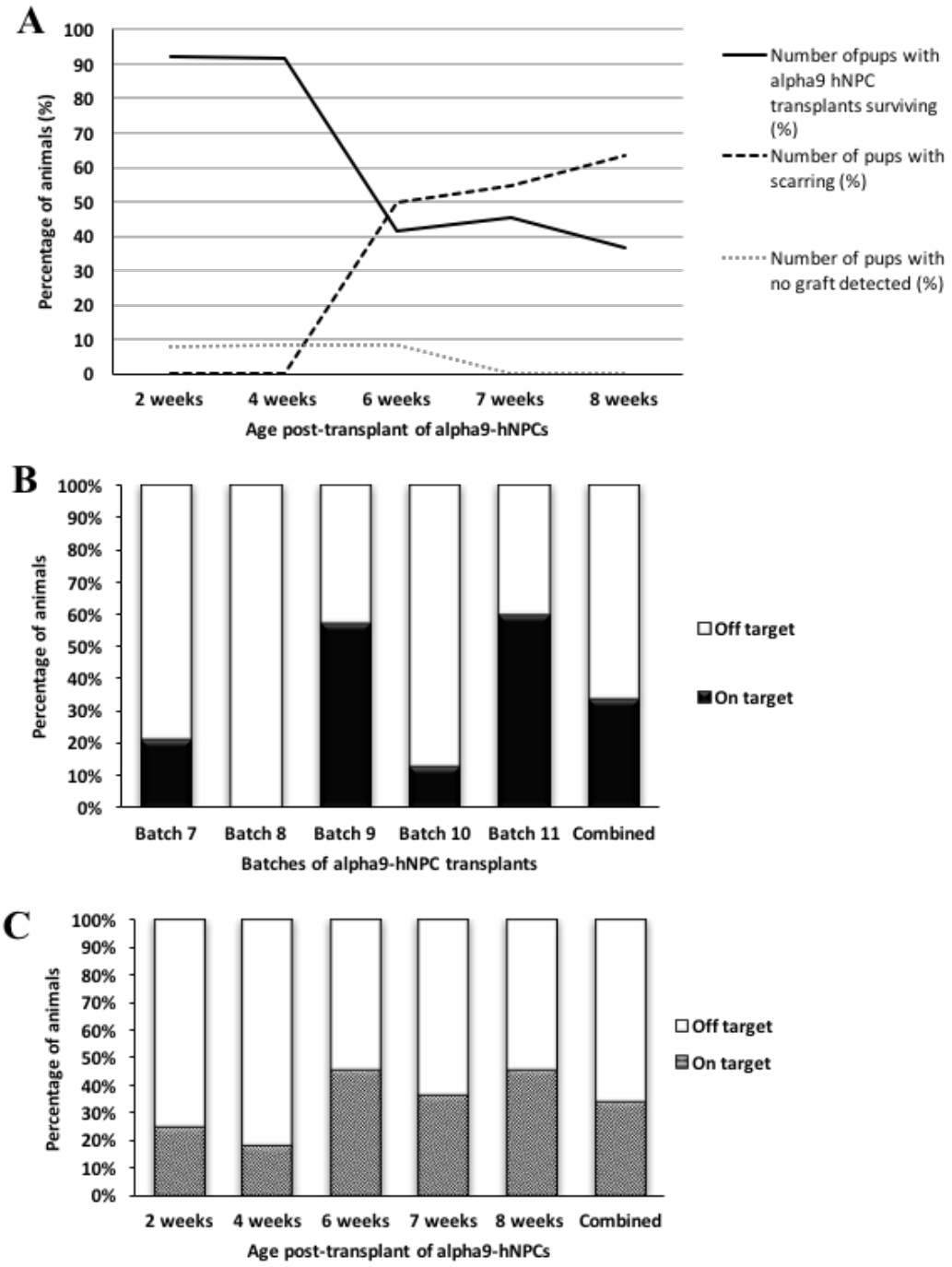

Figure 5.1 Analysis of α9-eYFP hNPC surival and on- and off-target injections. The α9-eYFP hNPC grafts were analysed for survival over the different time points (2, 4, 6, 7 and 8 weeks). Results indicated survival was highest at the younger time points of 2 and 4 weeks, but decreased with age (**A**). Similarly, the number of animals with clear scarring increased over time (**A**). The α9-eYFP hNPC grafts were assessed as to whether they were localised on target within the deep layers of the sensorimotor cortex. The optimisation of coordinates resulted in variation of on-target injections across the different batches (**B**). Transplants within batch 11 resulted in the highest number of on-target injections with 60% of grafts within the sensorimotor cortex (**B**). Over all the α9-eYFP hNPC grafts, 34% of detectable

grafts were on target (**B**) When the on- and off-target analysis was split into the different age groups, there was a small percentage of on-target injections at all time points (**C**). At 4 weeks, specifically there was the lowest amount of on-target injections at 18% (n = 2/11) and 6 and 8 weeks comprised the highest, 46% (n = 5/11) for both (**C**).

5.3.2 Locations of α9-hNPC transplants and their neuronal projections

The target for injections was the sensorimotor cortex, however only 34% of α9-eYFP transplants were localised within this region. Injection sites were identified using IHC and antibodies against HuNu or hNCAM alongside GFP, which identified the exogenous expression of α9-eYFP. Across all time points, GFP-positive staining was observed in the surviving cell bolus and their hNCAM-positive projections shown in Figures 5.2 and 5.3, respectively. Off-target injections were located in a number of regions including the striatum, lateral ventricles, hippocampus and caudate and/or putamen of the basal ganglia (Figures 5.2 and 5.4). Progressing through each batch of transplants, as with WT hNPCs, coordinates were altered in an attempt to further improve the accuracy of injections. The transplant sites and projections for each batch are summarised in brain maps in Figure 5.4.

As a result of the varied injection sites, projections from α9-eYFP transplants were localised in a number of sites including the corpus callosum, internal capsule, thalamus, hippocampus, corona radiata and areas of the cortex (Figure 5.3 and Figure 5.4). Projections were identified with a hNCAM antibody, and the α9-eYFP protein was identified using a GFP antibody. The hNCAM projections co-immunolabelled with GFP expression across all time points (Figure 5.3 and 5.5).

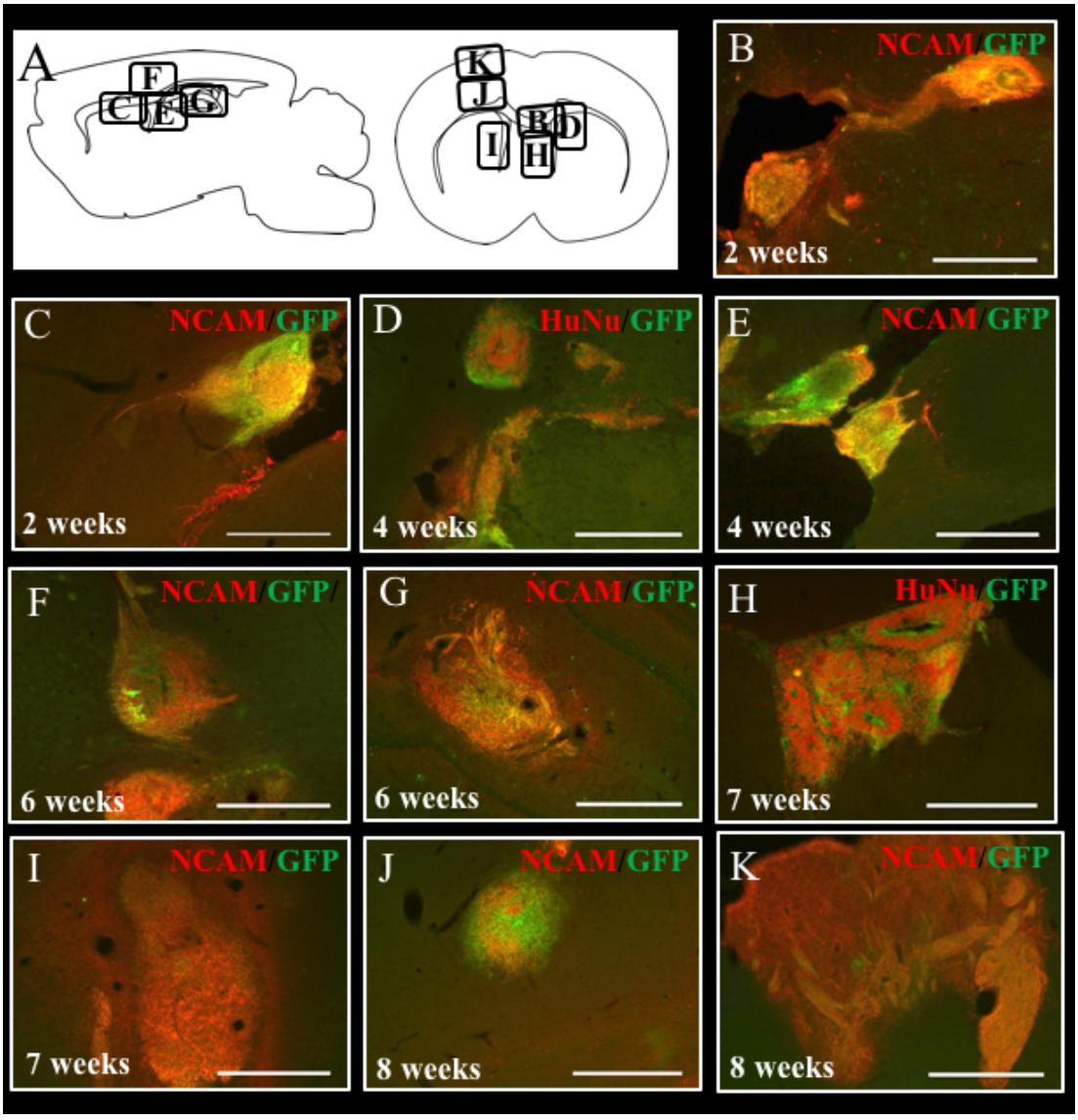

Figure 5.2 Representative images of α9-hNPC transplant locations. As with the WT hNPC grafts, the α9-eYFP injection sites were identified using human-specific antibodies for HuNu and hNCAM. Additionally, the α9-eYFP grafts were stained for GFP to detect α9-eYFP protein expression. Injection sites varied and included sites within the sensorimotor cortex (**F** and **J**), but also off-target sites including the lateral ventricles (**E**), the caudate and/or putamen of the basal ganglia (**B, C, D** and **I**), the hippocampus (**G**), the striatum (**H**) and other areas of the cortex (**K**). Scale bars B-K = 500 µm.

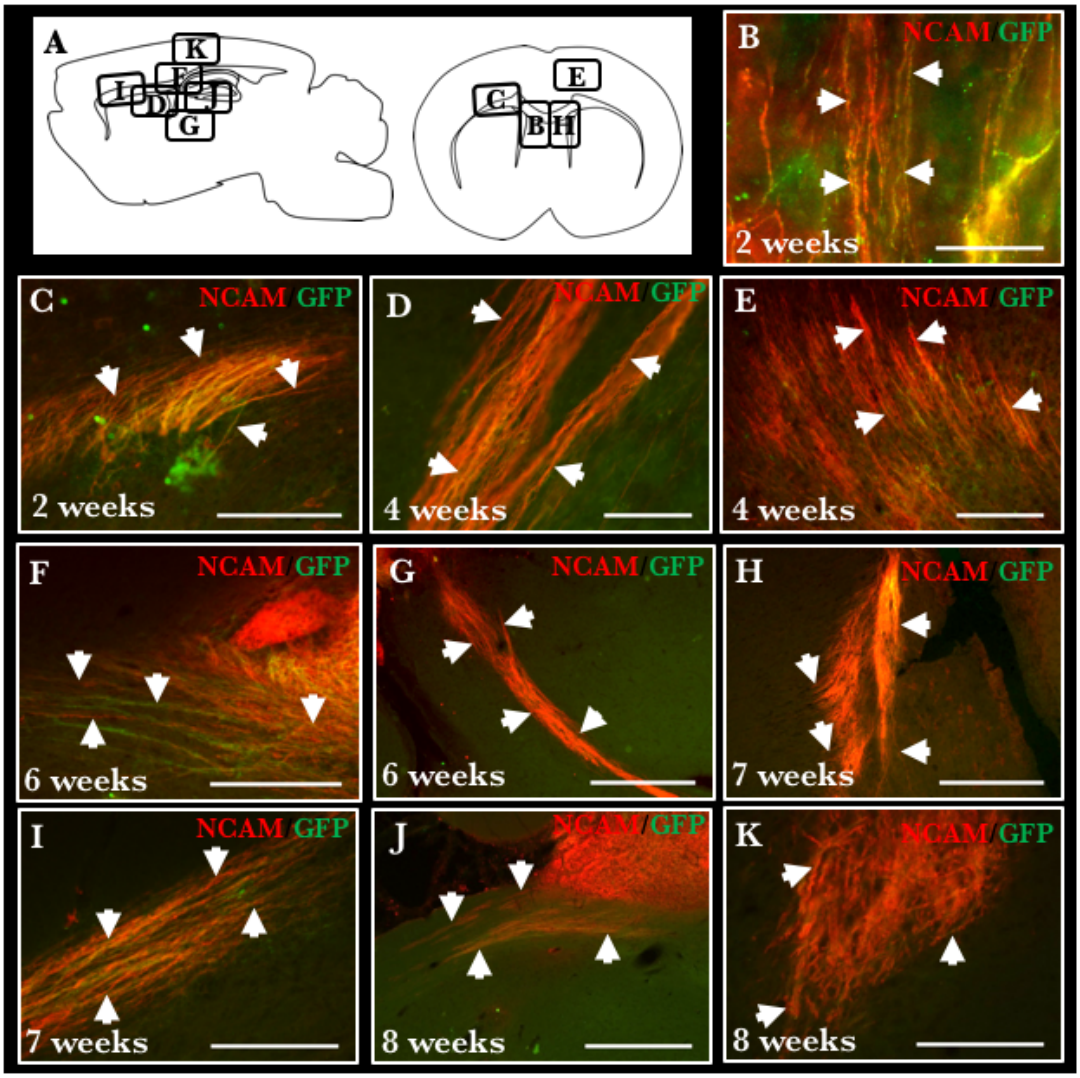

Figure 5.3 Projections from transplanted α9-hNPCs over time. The fibres projecting from the transplanted α9-eYFP hNPCs were detected using antibodies against hNCAM as well as GFP. NCAM-positive projections were observed at all time points, however, at the older time points of 7 and 8 weeks, projections were not observed in many pups and often did not project far from the bolus site. Projections were observed within white matter tracts of the brain including the corpus callosum (**C, I** and **F**), corona radiata (**D**) as well as the internal capsule (**G**). Fibres were also detected in the striatum (**B** and **H**), cortex (**E** and **K**) and thalamus (**J**). Scale bar in B = 25 µm; C, I and K = 150 µm; D = 50 µm; E = 100 µm; F and H = 250 µm; G and J = 500 µm.

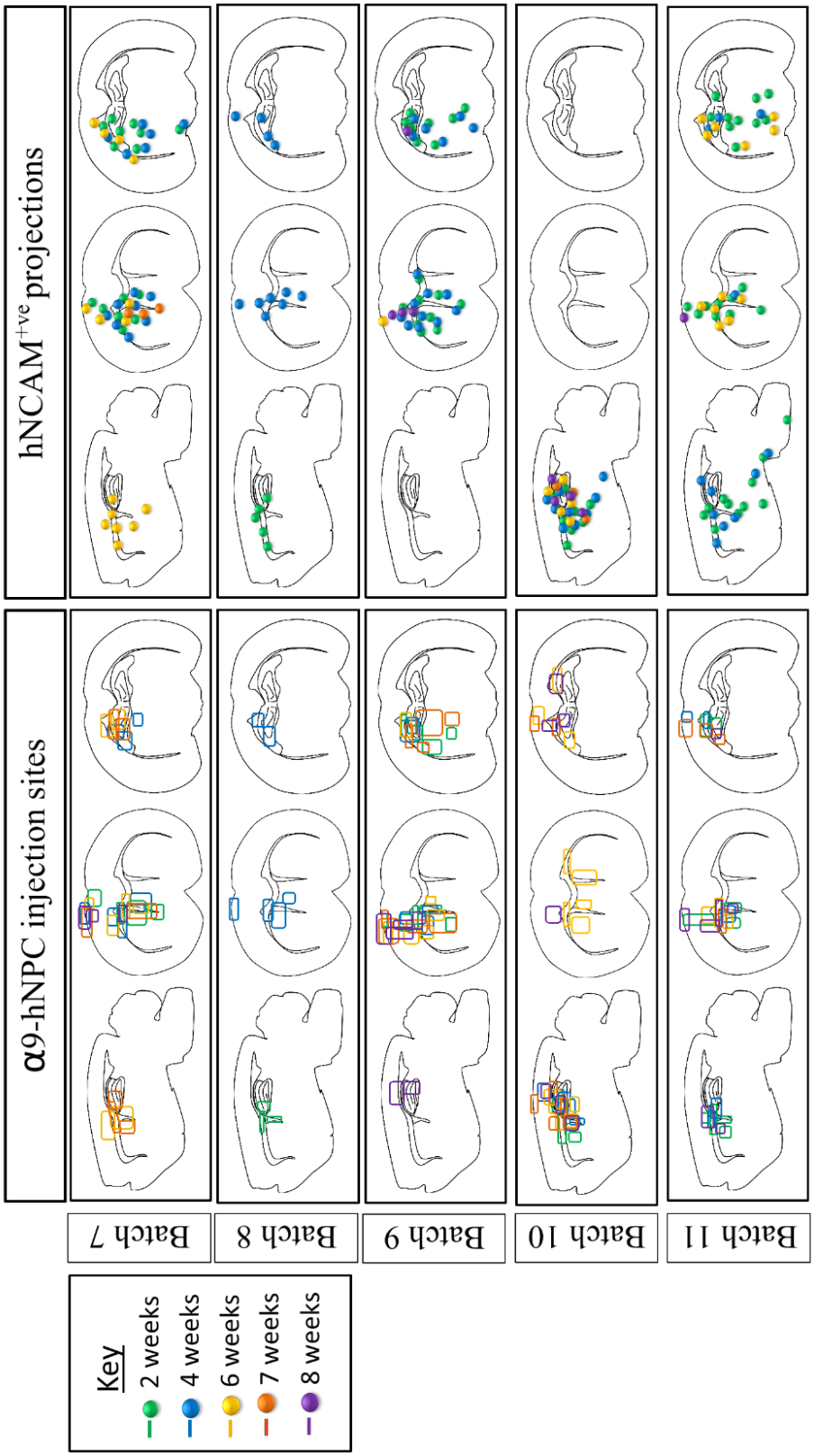

Figure 5.4 α9-hNPC injection sites and their projections over time. Injection sites from α9-eYFP hNPCs were monitored over time and coordinates were altered accordingly. The injection sites from each batch of α9-eYFP hNPC grafts were mapped across the different time points (first column) and

the corresponding projections can be observed in the second column. The different colours, for boxes and dots show the different age groups, detailed within the key. The majority of pups at 7 and 8 weeks displayed few or no hNCAM-positive projections, which is reflected in the brain maps above. Batch 11 resulted in the most on-target injections with 60% of pups (n=6/10) showing grafts within the sensorimotor cortex and projecting to areas of the CST including the internal capsule, cerebral peduncles and brain stem. At 2 weeks, projections were observed within the pyramids of the brain stem in this batch.

5.3.3 α9-eYFP-expressing hNPCs retained their exogenous integrin expression up to 8 weeks post-transplantation

One of the main questions addressed within this chapter was whether transplanted hNPCs retained exogenous α9-eYFP expression *in vivo* over time. Results showed expression of α9-eYFP was retained within hNPC projections as long as the cells survived. At 2 weeks, GFP-positive staining indicated α9-eYFP was localised within the axonal compartment of hNCAM-stained hNPC projections, which appeared vesicular and punctate (Figure 5.5, A-C). At 4 and 6 weeks, positive GFP staining was observed along the entire length of the hNCAM-labelled projections (Figure 5.5, D-I). From results shown in section 5.3.1, at 7 weeks, survival was reduced and a number of pups showed scarring at the injection site. As a result, fewer axonal projections were observed at 7 weeks; however, where hNCAM-positive fibres were present, these fibres consistently co-labelled with GFP expression (Figure 5.3, H-I). In a number of pups, however, even though projections were not observed, a bolus of cells remained with NCAM-positive cells co-labelled with GFP (Figure 5.5, J and K). Similarly, at 8 weeks, a small number of pups had hNCAM-positive fibres which co-labelled with GFP (Figure 5.3, J-K); however, it was more common for there to be a scar at this time point (64%). Where a scar was present, GFP-positive staining was often, but not always, observed in the centre of the scar, most likely labelling the remnants of degenerating α9-eYFP grafts (Figure 5.5, L and M). Where no hNPCs survival or scarring was evident, there was also no detectable GFP expression (data not shown). As a control, tissue containing WT hNPCs was also stained for GFP which showed no positive GFP staining as expected (Appendix D).

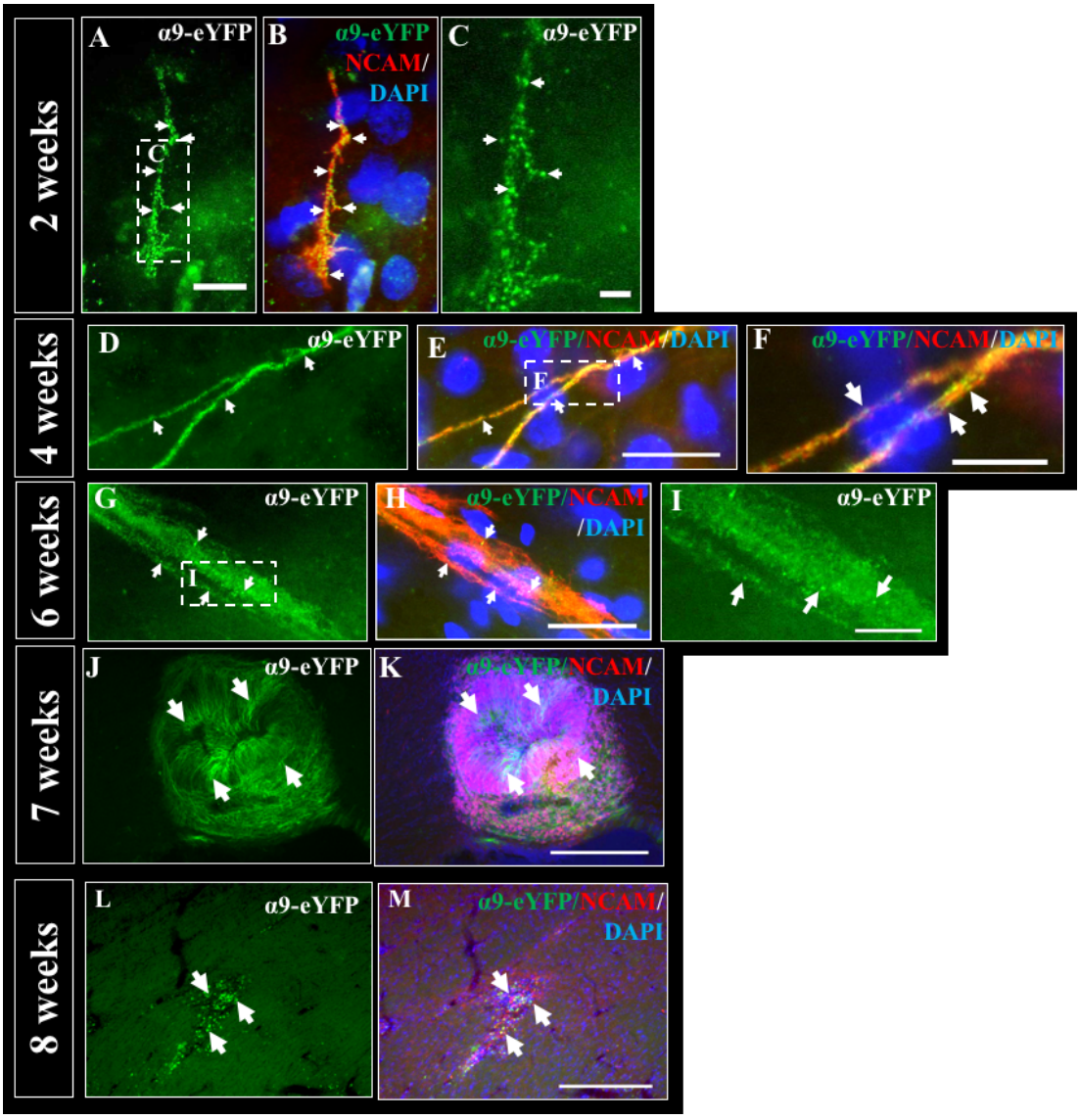

Figure 5.5 Exogenous α9-eYFP expression in transplanted hNPCs over time. Using an anti-GFP antibody, the expression of the exogenous α9-eYFP protein could be detected. Results show that integrin expression was maintained as long as the cells survived. At 2 weeks (**A-C**), α9-eYFP was co-expressed in hNCAM-positive projections with a vesicular, punctate appearance (**A-C**, white arrows). At 4 (**D-F**) and 6 weeks (**G-I**), the α9-eYFP expression was observed along the length of the hNCAM-positive fibres. At 7 weeks, few pups showed hNCAM-positive projections, however, where a bolus was still present, α9-eYFP protein was detected within surviving cells (**J** and **K**, white arrows). Similarly, at 8 weeks, GFP-positive staining was detected within a scarred area suggesting hNPCs can maintain exogenous α9-eYFP expression, but expression diminishes as cells die off (**L** and **M**, white arrows). Scale bar in A-B = 5 µm; C = 2.5 µm; D, E, H and I = 25 µm; F and J = 10 µm and K-N = 250 µm.

5.3.4 α9-eYFP hNPC gene expression over time

Expression of the deep-layer cortical neuron marker, Tbr1, was examined in α9-eYFP expressing hNPC grafts. Results indicated that a small proportion of α9-hNPCs expressed Tbr1 at each time point (Figure 5.6). Tbr1-positive cells were mostly located on the outside of the hNPC-packed boluses with the centre of the bolus remaining largely devoid of Tbr1 expression (Figure 5.6). Expression of Ctip2 in both endogenous rat tissue and transplanted hNPCs was also analysed using two different antibodies, one human-specific and one rat-specific. Results from using these antibodies were unfortunately not consistent across several trials (described in section 4.3.5) and therefore no results could be generated (data not shown).

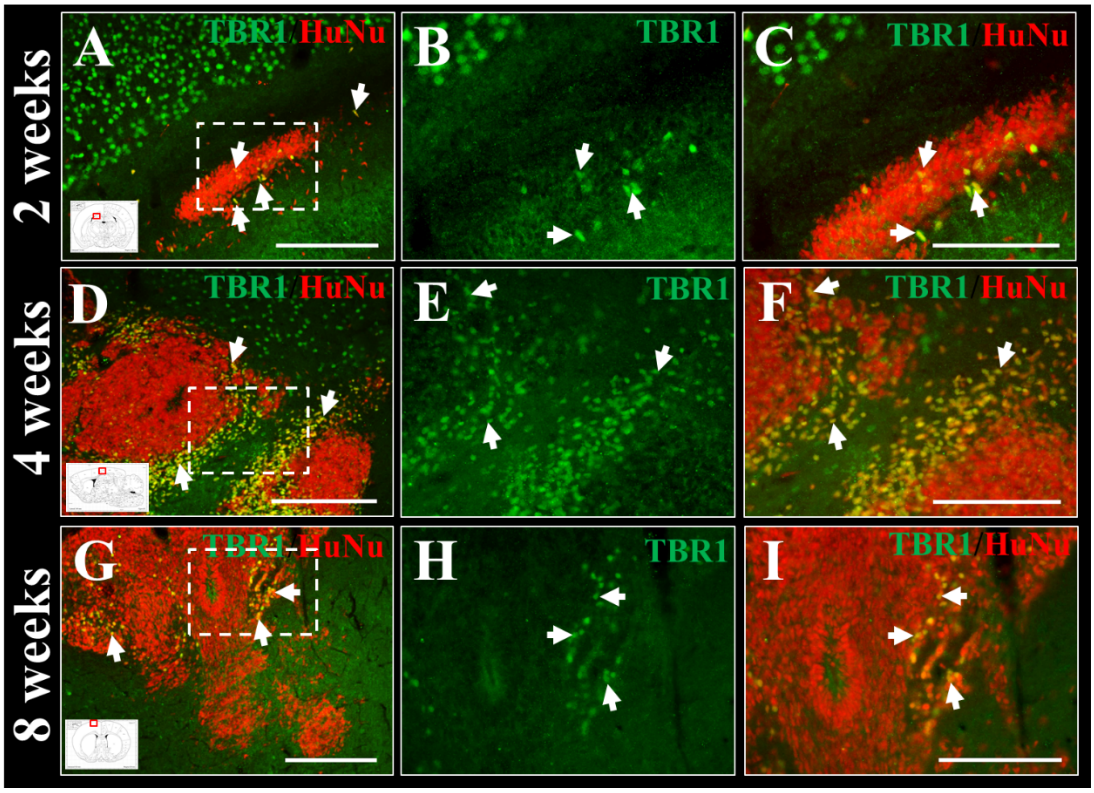

Figure 5.6 Expression of deep-layer cortical neuron maker, Tbr1, in transplanted hNPCs over time. The expression of deep-layer cortical neuron marker, Tbr1, was analysed in the α9-hNPC grafts. Results show at 2 weeks, α9-hNPCs expressed Tbr1, however the expression was not in every cell (white arrows in **A-C**). Similarly, at 4 (**D-F**) and 8 (**G-I**) weeks, a number of cells were expressing Tbr1, but the expression was largely confined to surviving α9-hNPCs located on the outside of the bolus. Scale bar in A, D and G = 250 µm; B, C, E, F, H and I = 150 µm.

5.3.5 The effect of α9-hNPC transplants on the extracellular matrix and the immune system

As observed in data presented in Chapter 4, transplantation of WT hNPCs induced an immune response at the later time points analysed. The immune response was also assessed in α9-eYFP hNPC transplants, examining both the astrocytic response, using an anti-GFAP antibody, and microglia activation, using an anti-Iba-1 antibody. After 2 weeks *in vivo*, there was a small increase in GFAP staining around the α9-eYFP hNPC graft sites suggesting activation of astrocytes (Figure 5.7, A and B). At the same time point, there was no noticeable increase in Iba-1 staining at the injection sites (Figure 5.7, C and D) compared to control tissue (control images are included in Figure 4.13) and this expression is comparable to WT hNPC grafts. At 4 weeks post-transplantation however, a microglial response was detected around the α9-eYFP hNPC graft denoted by a marked increase in Iba-1 immunoreactivity. At 8 weeks, the response from both astrocytes and microglia around the α9-eYFP hNPC injection sites was found to be substantially increased (Figure 5.8, I-L) compared to controls (Figure 4.13). Furthermore, expression of TN-C at the transplant sites of α9-hNPCs was monitored over time. The expression of TN-C was found to be greater at the injection sites soon after transplantation which increased slightly over the different time points (Figure 5.8).

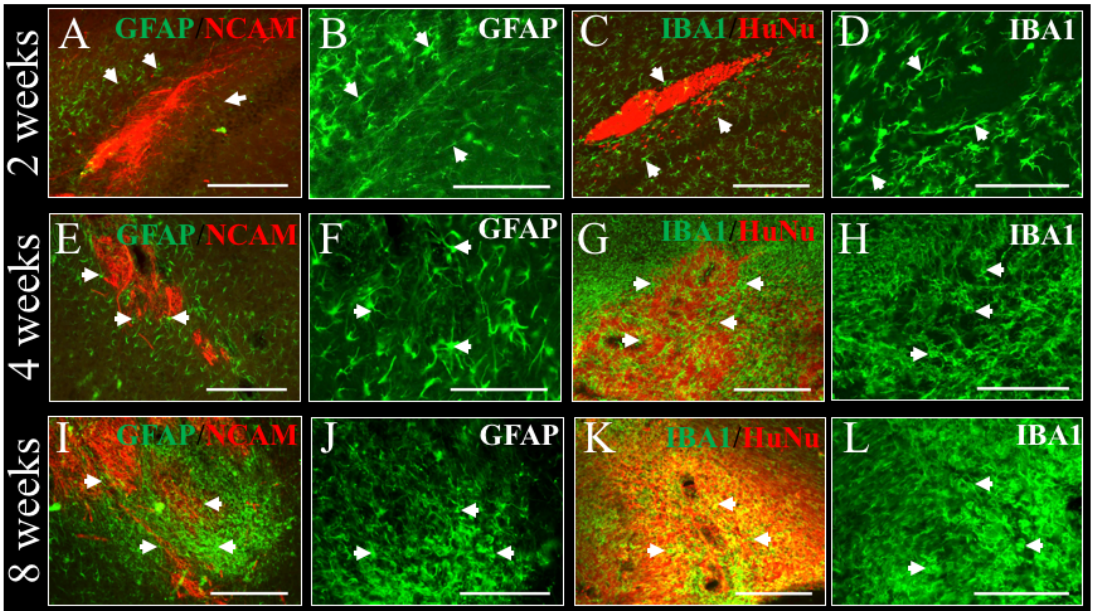

Figure 5.7 The immune response after transplantation of α9-hNPCs. Following analysis of α9-eYFP hNPC grafts over time, transplant survival diminished with time as observed with WT hNPC grafts. Following IHC analysis for immune response markers including activated microglia (Iba-1) and astrocytes (GFAP), results indicate an increase in the immune reaction to the grafts over time. At 2 weeks, the astrocytic reaction (**A** and **B**) and the microglial response (**C** and **D**) was not noticeably increased from control levels (Figure 4.13). At 4 weeks there was a small astrocytic response (**E** and **F**), however there was a large increase in Iba-1 staining (**G** and **H**), suggesting a marked increase in microglial activity, in contrast to the immune response results observed with WT grafts (Figure 4.13). At 8 weeks, both GFAP and Iba-1 staining had greatly increased (**K** and **L**) compared to control tissue, suggesting an immune response had been activated, likely resulting in the observed graft rejection. Scale bar A, C, E and G = 250 µm; I and K = 500 µm; B, D, E, H, J and L = 150 µm.

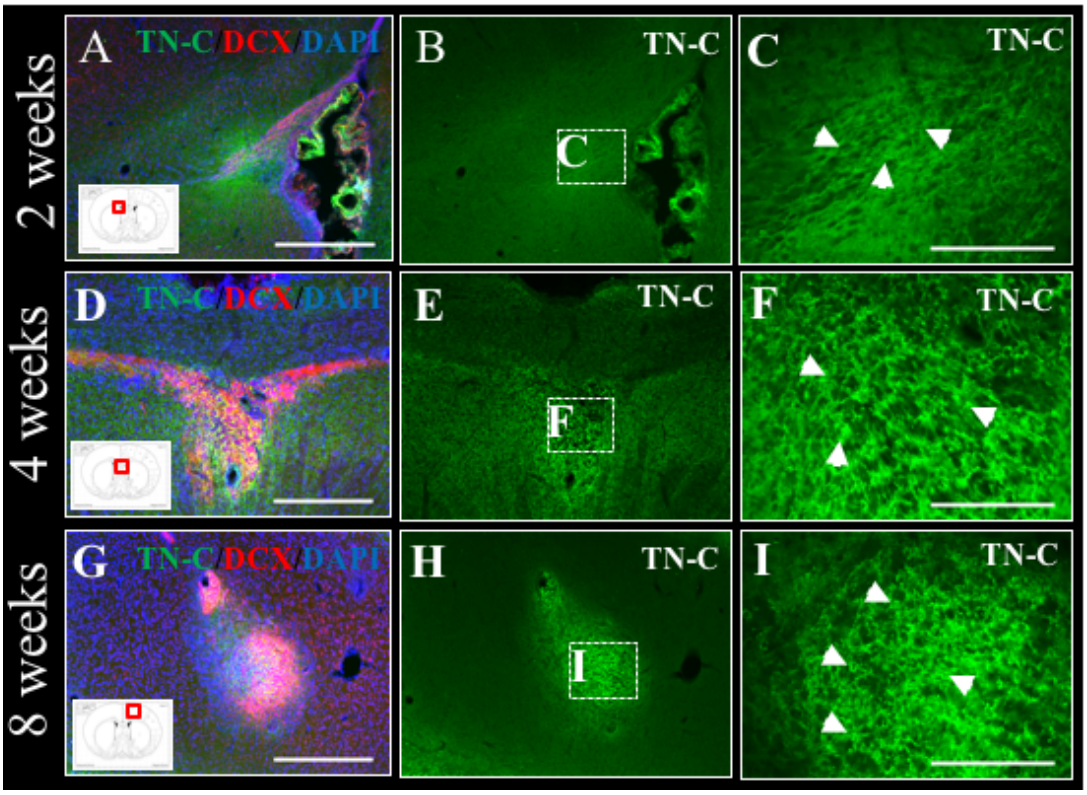

Figure 5.8 Expression of TN-C following transplant of α9-hNPCs. The expression of TN-C was observed following transplant of α9-eYFP-hNPCs and results were comparable to expression levels found with WT hNPC grafts (Figure 4.15). At all time points (**A-I**) (6 and 7 week data not shown) there was an increased expression of TN-C at the injection site (co-labelled with DCX staining in **A**, **D** and **G**). Scale bar A, B, C, E, G and H = 500 µm; C, F and I = 150 µm.

5.3.6 Tracking of α9-eYFP hNPCs projections using BDA tracers

As with WT hNPCs preliminary experiments to inject 50 mg/mL BDA together with the α9-eYFP hNPCs did not result in positive axonal tracing (data not shown). Unfortunately, time did not allow for optimisation or further testing with BDA tracing.

5.4 Discussion

In this chapter, the transplantation of α9-eYFP-expressing hNPCs into the rat sensorimotor cortex has been characterised, taking into account the data collected in Chapters 3 and 4. The main aims of this part of the project were to ascertain whether α9-eYFP-expressing hNPCs could survive *in vivo*, extend long-distance projections from the transplant site and retain the exogenous α9-eYFP expression *in vivo*. It was hypothesised that the overexpression of the α9-eYFP protein may have resulted in longer projections from the hNPCs compared to WT hNPCs due to the growth-promoting properties of α9 integrin. Results showed the α9-eYFP hNPCs followed a similar pattern of graft survival to the WT hNPC transplants where survival was highest at earlier time points. Similarly, surviving grafts produced projections that followed white matter tracts within the brain, including areas of the CST. Furthermore, results showed hNPCs were able to retain expression of α9-eYFP protein *in vivo* over time and this expression was localised to hNCAM-positive projections suggesting it was trafficked within the axonal projections of these cells.

Following IHC using human-specific antibodies, survival of α9-eYFP hNPCs grafts was analysed. Results from α9-eYFP hNPCs emulated the survival findings obtained from transplantation of WT hNPCs. At 2 and 4 weeks, survival was highest with more than 90% of pups showing graft survival (Table 5.2). Beyond these time points, graft survival was observed, but steadily decreased and by 8 weeks only 36% of pups had surviving grafts. Furthermore, at the older age groups, particularly 7 and 8 weeks, although a proportion of transplanted cells survived, only a few pups showed projections outside of the bolus sites. These sites were also surrounded by scar tissue which suggested the cells were in the process of degenerating and the immune response may have inhibited the cells from extending axonal projections through the brain parenchyma.

As for the WT hNPCs, optimisation of coordinates was continued with the α9-eYFP transplants and batch 11 (the last α9-eYFP batch transplanted) coordinates resulted in the most on-target injections with 60% of pups showing grafts located within the sensorimotor cortex. This was probably due to the depth of the grafts being reduced from -0.5 mm to -0.4 mm (Table 2.8). It is also important to note that across the time

points assessed where no graft was detected, it cannot be concluded as transplant death as we cannot determine whether the cells were transplanted.

The furthest projections from α9-eYFP hNPCs were observed in batch 11 at 2 weeks, where hNCAM-positive fibres were present within the pyramids of the brain stem, however, this occurred in only one animal. In general, this was noticeably different from WT hNPC projections, where we observed a number of pups showing hNCAM-positive fibres projecting to the caudal brain stem. From analysis of the α9-eYFP hNPC grafted tissue, it became apparent that projections from α9-eYFP hNPCs were not projecting as far, although projections were not measured and so this cannot be confirmed. This may have been due to a potential reduction in cell numbers after transplant. From the *in vitro* data in Chapter 3, it was noted that following viral transduction approximately 40% of cells detached from the cell culture dish which may have been due to the toxic effects of the polybrene reagent. A number of transduction optimisation experiments were trialled with polybrene to minimise cell death whilst still obtaining α9-eYFP expression (see Chapter 3). Taken together, these two observations lead us to question whether cell death of α9-eYFP hNPCs continued when transplanted *in vivo* and therefore resulted in reduced cell survival and projections compared to WT hNPCs, however individual cell numbers were not counted post-transplantation. It is important to remember, above all, that this was a xenogenic transplant where human cells were transplanted into a rat host.

In accordance with this, the immune reaction occurring in α9-eYFP hNPC transplanted tissue may also shed light on why projections may have been reduced from these cells. IHC data for the immune response indicated there was an increase in activation of microglia at 4 weeks (Figure 5.7). This immune response was observed earlier compared to that of the WT hNPCs (section 4.3.7), suggesting that the immune reaction was greater or accelerated in response to α9-eYFP hNPC grafts. For example, at 6 weeks in WT hNPC grafts, 12% of pups had scarring whereas in α9-eYFP hNPCs 50% of pups showed scarring. This suggested that potentially a lack of immune reaction to the WT hNPCs may have accounted for their increased survival *in vivo* compared to the α9-eYFP hNPCs. By 7 weeks, scarring in both groups was similar whereby 47% of pups showed scarring after WT hNPC transplants and 55% of pups showed scarring after α9-eYFP hNPC transplants. This comparison suggests an

increased immune response to α9-eYFP hNPCs may have occurred earlier indicating a longer time window in which the WT hNPCs survived, allowing for extension of longer axonal projections in a greater number of animals. The main question remains, however, as to why there was a lag time and a difference in immune reaction between the two cell populations. The answer to this may also be linked to the previous discussion point that α9-eYFP hNPCs may have been compromised by the viral transduction using polybrene and this process may have destabilised the grafted cells and their ability to interact or fight off any challenges posed by the host environment. This may have caused the cells to continue to die following transplantation as they did in culture. If a proportion of transplanted cells were undergoing cell death or were in the process of degenerating this may have resulted in secretion of pro-inflammatory and apoptotic factors, which could have stimulated microglial activity, which in turn secrete further cytokines, such as tumour necrosis factor-α (TNF-α) (Reviewed in Hanisch, 2002). Indeed, research has shown that the survival and growth of NSPCs can be hindered by apoptotic factors in the local environment, including interferon-gamma and TNF-α (Ben-Hur *et al.,* 2003; Guadagno *et al.,* 2013). However, this theory contradicts the large body of research suggesting NSPC transplants are anti-inflammatory (Pluchino *et al.,* 2005; Einstein *et al.,* 2007; Lee *et al.,* 2008; Cusimano *et al.,* 2012).

That said it will be important for future work to ascertain whether or not it is the process of viral transduction or the expression of the α9-eYFP protein that is causing this reaction. This was not examined in this project, however as reported in Chapter 3, approximately 40% of cells detached in the days following viral transduction, which was hypothesised to be due to the toxic effects of polybrene. As this result was the same for both viral transduction of α9-eYFP and viral transduction of fGFP, this suggests it was an effect of the viral transduction and not of the α9-eYFP expression. If GFP-expressing hNPCs could be transplanted with survival and projections from these cells assessed, we would expect the results to be similar to the α9-eYFP grafts. Here, 2 μg/mL of polybrene was used as results indicated this to be the most effective concentration to obtain expression whilst maintaining sufficient cell survival. Alternative methods for stable protein overexpression or the use of immunocompromised hosts should be investigated. Stem cells exposed to higher

concentrations of polybrene before transplantation have been studied, for example Song and colleagues transduced MSCs with integrin using LV and 8 μg/mL of polybrene before transplantation into the myocardium of immunosuppressed mice (Song *et al.,* 2009). Importantly, with this study, animals were immunocompromised and transplanted cells were analysed only after one week *in vivo*. This means any immune reaction elicited in response to grafted cells dying off due to exposure to polybrene after one week *in vivo* may possibly not have been detected.

In general, the literature shows that many animal models receiving genetically modified transplants are immunosuppressed and therefore survival of grafts would be prolonged due to the lack of or delay in immune rejection. However, as mentioned earlier, the process of viral transduction may have additionally resulted in cell survival being compromised. If the hNPC grafts were transplanted into immunosuppressed hosts, this would likely prevent cell death as a result of the immune rejection, however the cells may still be compromised. Previous literature would suggest that genetic modification of transplanted cells using LV prior to engraftment does not affect cell viability, providing the immune system is compromised using either immunosuppression or immunocompromised animal models (Behrstock *et al.,* 2008; Fujimoto *et al.,* 2012). Research has also shown some types of stem cells, such as bone marrow-derived MSCs, do not elicit such an increased immune response (Chopp and Li, 2002). Modifying mouse bone marrow-derived MSC grafts to express specific immune-supressing factors such as interleukin-13, can prolong graft survival within the rodent brain, although this is marginal with the difference in survival being only 1 or 2 days (Hoornaert *et al.,* 2016). Modification of the cells in this way would mean the host would not be left vulnerable to infection, but would mean further genetic manipulation of the grafted cells would be required. Following mouse NSC engraftment into the immunocompetent adult mouse brain, research suggests approximately 80% of cells die off and undergo apoptotic cell death within the first 24 hours after transplantation, with only 1% of cells surviving 14 days after transplant. In the days following transplant, the number of cells expressing the hypoxic cell marker, Hypoxyprobe-1, within the graft site increased (Reekmans *et al.,* 2012). This suggests a lack of nutrients, such as oxygen, but also no blood supply, could be contributing factors in transplant cell death.

Transplanted α9-eYFP hNPCs were analysed for the expression of the deep-layer cortical neuron marker, Tbr1, over time. Results showed that some of the α9-eYFP hNPCs retained expression over time *in vivo,* however not every cell expressed Tbr1. In particular, the expression was limited to cells located on the outside of the bolus where they could possibly have interacted with the ECM. Furthermore, it was noted that there may have been a smaller proportion of α9-eYFP hNPCs expressing Tbr1 compared to WT hNPCs. One relevant point to make is the potential of the hostile immune environment to alter the phenotype and differentiation status of the transplanted cells, thus changing their protein expression profile. Research has suggested that following injury, activated astrocytes and microglia can secrete factors, including interleukin-6 and leukaemia inhibitory factor, both of which promote NPC grafts to differentiate into astrocytes (Faijerson *et al.,* 2006; Nakanishi *et al.,* 2007). Furthermore, neonatal astrocytes have been examined for their GFAP expression in relation to adult astrocytes and results indicate that neonatal astrocytes are more reactive than adult astrocytes (Reviewed in Wu and Schwartz, 1998). Whether this would alter the phenotype of the human NPCs used in this project remains to be determined; however, we would hypothesise this was not the case as these cells have been pre-programmed *in vitro* to become CCNs and were therefore already on a specified differentiation path.

As described in Chapter 4, transplants of WT hNPCs results in a localised upregulation of TN-C at the injection site. From analysis of α9-eYFP hNPCs, there was a similar expression over time. As mentioned previously, the TN-C antibody was human-specific but has previously been used in the laboratory in rodent tissue with positive results. As TN-C is present at the injection site of α9-eYFP hNPCs, we would have expected this to potentiate the effect of the overexpressed α9-eYFP protein and potentially to have promoted axonal elongation due to its ligand being present, however this was not clearly observed. It is possible that because there was a high concentration of TN-C at the injection site, this would encourage the α9-eYFP hNPCs to remain localised to the graft site rather than extend long distances beyond the injection site. To confirm this, a rat-specific TN-C antibody could be used to assess whether the observed upregulation of TN-C at the graft site is due to endogenous rat expression or is originating from the hNPCs. Indeed, the *in vitro* results discussed in

section 3.3.4, indicated the hNPCs expressed TN-C in culture. Secondly, the ability of α9-hNPCs to project towards a TN-C rich environment could be assessed, initially *in vitro*, but also *in vivo*, using a cortical stab injury model. In this model, α9-eYFP hNPCs would be transplanted into one region of the cortex with a cortical stab wound in a separate distinct region, which should promote an upregulation of TN-C at the lesion site. The projections from α9-eYFP hNPCs would be analysed for their ability to preferentially project to a TN-C-rich environment.

Furthermore, data from Chapter 3 highlighted that the α9 expression within hNPCs was functional prior to transplantation. Research has shown proteins associated with CNS injury, such as CSPGs and Nogo-A, can inactivate integrins (Hu and Strittmatter, 2008; Tan *et al.,* 2011), but this inactivation can be overcome with the modulation of integrins into their active state using activators, including kindlin-1 (Cheah *et al.,* 2016). As mentioned in Chapter 1, kindlin-1 is not expressed within the CNS (Reviewed in Ussar *et al.,* 2006) and therefore would need to be administered alongside the α9-eYFP hNPCs to induce integrin activation. However, another option is activation of integrins using human-specific antibodies, such as TS2/16 (Hu and Strittmatter, 2008; Tan *et al.,* 2011), which may be the subject of future experimentation. The expression of inhibitory proteins, such as aggrecan, was not assessed within the hNPC-grafted tissue, but there is scope for the expression of such proteins to be upregulated, as an injury-like environment may have been created following injection of the cells.

Together these results show the expression of α9-eYFP protein is maintained within hNPCs following transplantation into the rat brain. Cells are able to maintain this expression throughout the duration of their survival *in vivo*. Furthermore, α9-eYFP expression co-labelled within hNCAM-positive axonal projections, suggesting the exogenous integrin protein was localised and may have been actively transported within the axonal compartment of the hNPCs. Additionally, a proportion of the cells maintained an expression of the deep-layer cortical neuron marker, Tbr1, and as with the WT hNPCs there was a localised upregulation of the main ECM component of the CNS, TN-C, at the transplant site. After obtaining data from transplanted WT hNPCs, where on-target grafts were able to project to the caudal brain stem, likely beyond the pyramidal decussation (see Chapter 4), we hypothesised that α9-eYFP hNPCs may

have the potential to match, if not exceed, the projections observed in WT hNPCs due to the characteristic growth-promoting properties of α9 integrin. However, projections from the α9-eYFP hNPCs only reached the medullary pyramids. There are a number of possibilities that may have led to this outcome, such as a lack of available TN-C ligand outside the transplant site, integrin inactivation at the injection site, lack of cell numbers over time, and/or reduced ability of the cells to extend projections due to viral transduction or increased immune response.

It is possible that any or all of these options occurred following α9-eYFP hNPC transplant. The first line of inquiry in any future study should focus on the viral transduction protocol to examine the mechanisms behind the increased cell death after transplantation and whether their viability had been compromised owing to exposure of the cells to polybrene *in vitro*. To test this, it would be beneficial to transplant GFP-expressing cells to inform further discussion and rule out α9-eYFP expression as a contributing factor to graft rejection. Furthermore, injecting α9-eYFP hNPCs into immune-compromised animals would likely result in further graft survival (of both transplant groups), allowing increased analysis of the α9-eYFP protein capabilities *in vivo*.

Chapter 6: Final discussion and future perspectives

6.1 Summary of key findings

Research surrounding stem cells has expanded since the discovery of iPSCs, transforming the field of neurodegenerative diseases and conditions, such as SCI, where cell replacement may significantly promote CNS repair. With a regenerative approach in mind, this thesis has focused on the use of iPSC-derived human NPCs, assessing their suitability and ability to survive and express growth-promoting integrins after transplantation into the rat neonatal cerebral cortex. This body of work has provided an extensive characterisation of the iPSC-derived hNPCs, both *in vitro* and *in vivo*, showing that these cells endogenously express a number of neuronal and growth-promoting proteins and can survive in the naive neonatal rat brain up to 8 weeks after transplantation. Explicitly, this project addressed whether these cells could be utilised to increase the expression of the growth-promoting integrin subunit, α9, within the CNS. The data presented here has shown exogenous expression of α9-eYFP within hNPCs was achieved following LV transduction. Once expressed within the hNPCs, this protein was functional when grown on TN-C *in vitro* and indeed, once transplanted, α9-eYFP hNPCs retained the expression of α9 integrin for as long as the cells survived *in vivo*.

6.2 Survival of transplanted hNPCs

Survival of WT and α9-eYFP hNPCs *in vivo* was highest at younger time points (Tables 4.2 and 5.2) and gradually declined over time as cells underwent immune-mediated rejection. This was expected as human cells were transplanted into a rat and no immunosuppression was performed. However, previous research has shown transplants of ESC-derived neurons between P0-P2 in the rat striatum can result in substantial survival 10 weeks after grafting without the use of immunosuppression (Denham *et al.,* 2012). These two projects are similar in many ways, including the animal model used, age of animal at time of transplant, the number of cells transplanted and use of stem cell-derived cells. However, there are distinct differences in experimental procedure that may explain the changes in graft survival. These include transplant into the striatum compared to the cortex, the use of ESC-derived cells

compared to iPSC-derived cells, as well as the differentiation status of the cells at the time of transplant, i.e. neurons compared to progenitor cells.

In our study and in Denham *et al* (2012), 100,000 cells were transplanted per site, which may have acted as a protective barrier. For example, cells in the centre of a large bolus of cells may be protected from the immune response due to lack of interaction with the immune system as it is the cells on the outside of the bolus that are compromised first. This theory has previously been investigated with research showing that the greater the number of hNPCs transplanted, the larger the immune response, thus more cells does not necessarily equate to better survival (Ostenfeld *et al.,* 2000). Specifically, results following transplant of 200,000, one million or two million hNPCs into the striatum of a Parkinson's disease rat model showed projections were more common from smaller grafts and an increased immune response was noted in those animals that received a larger cell graft (Ostenfeld *et al.,* 2000). The differences in graft survival discussed here suggest it is therefore either the transplant target site or the animal model that affected graft survival. For example, research has shown regional differences can impact graft survival and maturation following transplantation of hNSCs into the cortex and striatum of uninjured adult immunodeficient mice (Tennstaedt *et al.,* 2015a, 2015b). Importantly this work found the environment of the cortex can promote survival and maturation of hNSCs compared to the striatum and has suggested this could be due to differential neurotrophic protein expression within these regions. Although not directly comparable, one study has suggested the immune response to grafted cells may be different in grey and white matter tissues and has shown the striatum (grey matter) can actually support survival of grafted mouse glial precursors, compared to the forceps minor (white matter) after transplant into immunocompetent mice (Janowski *et al.,* 2014). As both the striatum and cortex are mainly grey matter, this may not explain the differences in graft survival in the cortex compared to the striatum observed by Tennstaedt and colleagues (2015a; 2015b). In our project, differences in cell survival within distinct brain regions were not analysed, however it would be interesting to assess whether on-target injections within the cortex survive longer than off-target injections. To do this, cells would need to be stereologically counted *in vivo* to directly measure cell survival versus cell death.

Research further suggests that the animal model used can greatly influence graft survival. The Denham study (2012) and our study both utilised a neonatal rat model which resulted in survival beyond one month. This is in contrast to recent research by Mattis and colleagues with human NPCs, derived from iPSCs and injected between P0-P4 into the striatum of immune competent mice. In their experiment, cells were rejected within 4 weeks post-transplantation and no grafted cells could be detected beyond this time point (Mattis *et al.,* 2014). Furthermore, 50,000 cells were injected per hemisphere, and they report a dramatic decline in cell survival in the days following transplantation. For example, at 10 days post-transplant, only around 3% of grafted cells survived. They hypothesised iPSC-derived cells could have created a cell-specific immune response, however, when this theory was tested similar rejection was observed after fetal-derived hNPCs were transplanted into the same mouse model (Mattis *et al.,* 2014). Similarly, when P2 immunodeficient mice received hNPC transplants into the cortex, only 1.21% of the graft remained after 8 weeks *in vivo* (Zhou *et al.,* 2015). Therefore, the literature strongly suggests the animal model used in transplantation experiments determines the time scale for immune rejection, with mouse models in general rejecting grafts more quickly compared to rat models (Englund *et al.,* 2002; Reviewed in Roberton *et al.,* 2013; Mattis *et al.,* 2014). The reasons for this are not yet known, but the increased microglial response in mice is one currently recognised theory (Reviewed in Roberton *et al.,* 2013).

It is of utmost importance to consider not only whether the hNPCs are surviving *in vivo*, but also whether they are maturing, extending projections and interacting with host tissue. Moreover, in an injury model, are grafts able to promote any functional outcome? The lack of graft survival after xenotransplantation experiments can often prevent full examination of the graft integration *in vivo,* therefore prolonging cell survival is of high importance. It is possible to extend graft survival using immunodeficient animal models, such as non-obese diabetic/severe combined immunodeficiency (NOD/SCID) mice, however, alternative methods could also be pursued in rats including autologous transplantation, or neonatal desensitisation (Kelly *et al.,* 2009), although there is controversy over whether the latter technique actually prevents immune-mediated rejection (Janowski *et al.,* 2012; Mattis *et al.,* 2014). Alternatively, recent results from a clinical trial in stroke patients revealed the

neuroprotective effects of a bone marrow-derived MSC transplant outlasted the survival of the cells (Steinberg *et al.,* 2016), likely due to secretion of neurotrophic factors, therefore bringing into question the requirement for long-term transplant survival. When considering SCI however, where transplants would be used to replace damaged cells, particularly neurons as in our case, the transplanted cells would likely need to survive in order to maintain reconstructed neuronal connections which have extended through an injury site.

In this project, the low survival of α9-hNPCs specifically has raised some interesting questions regarding use of LV and polybrene to increase expression of proteins in cells destined for transplant. Use of this methodology may compromise the cell survival *in vivo*. However earlier studies have demonstrated that cells which have undergone LV modification without polybrene prior to transplantation are not compromised *in vivo* (Englund *et al.,* 2002; Behrstock *et al.,* 2008). Yet those that have been exposed to polybrene prior to transplant have resulted in poor survival rates (Zhou *et al.,* 2015) including in our study. However, Zhou and colleagues hypothesised that the observed poor survival of GFP-expressing hNPCs grafted within the immunodeficient mouse cortex was due to differentiation status of the cells, the animal model used or neuroanatomical location of transplant. The transduction protocol using LV and 8 μg/mL of polybrene was not reported to be a contributing factor.

6.3 Targeting of hNPC transplants to the sensorimotor cortex

The cells transplanted during this project were targeted to the sensorimotor cortex, specifically layer V, which contains pyramidal cells that project to the spinal cord. Initially, coordinates were chosen using an E22 rat brain atlas as reference (Altman and Bayer, 1995). Following the first round of transplants, grafts were monitored and the subsequent coordinates were altered to better target the region of interest. For each batch of transplants, coordinates were optimised in this way, basing the next set of coordinates on the graft location from the previous batches. In general, the depth of the transplants was reduced over time from -0.7 mm to -0.4 mm. Grafts were also moved more laterally from 1/-1 mm to 1.5/-1.5 mm and finally grafts were moved further forward from -1/-0.5 mm to bregma/1 mm. This optimisation resulted in

improvement of on-target injections for WT hNPCs increasing from 30% in batch 1 to 64% in batch 12. For α9-hNPCs, the coordinates were based on results from WT hNPC grafts in batch 1-6 (excluding batch 5, as this litter was cannibalised by the mother after surgery). Transplants conducted in batches 11 and 12 were based on coordinates from all litters (1-10, excluding 5), and this is likely why these batches resulted in the highest percentage of on-target injections, 60% and 64% respectively.

Batches 3 and 9 had the next most on-target injections with 56% and 57% respectively. Batch 9 coordinates were similar to those used in batch 11 and 12, but the depth of grafts in batch 9 was -0.5 mm compared to -0.4 mm in batch 11 and 12. However, the coordinates in batch 3 were very different compared to batches 9, 11 and 12. After analysis of batch 3 transplants, batch 4 and 6 were transplanted using the same coordinates, however both of these batches resulted in a much lower percentage of on-target injections, 38% and 40%, respectively. This indicated a high degree of variation between the graft location that was not due to coordinates alone. The neonatal skull is very thin and can be pierced easily using a 26-gauge needle, however the injection needle (attached to the Hamilton syringe containing the cells) is not strong enough to go through the skull. Therefore, by hand, a 26-gauge needle was utilised to pierce a hole through the skull to target the injection sites, using a stereotaxic frame to first mark the coordinates with a pen onto the skin, and then to stabilise the needle for injection. Because piercing the skull was done by hand, it was challenging to pierce only the skull and not penetrate into the brain parenchyma. Furthermore, the injection needle containing the hNPCs then had to be lowered (using the stereotaxic frame) so that it was below the skull, but on top of the brain (Figure 6.1, A). From there, the stereotaxic frame was used to lower the syringe and needle containing the hNPCs to the designated coordinates. However, it was not always clear when the tip of the injection needle was on the surface of the brain compared to when it was within the brain tissue (Figure 6.1, B). This therefore resulted in the potential addition of depth to the coordinates and, instead of transplants injected at the desired -0.4 mm, they were injected deeper than this, for example at -0.6 mm. This process of making sure the needle was at the top of the brain rather than within the brain was very delicate and was not obvious and would often have to be gauged using the resistance felt within the needle.

The injection protocol likely added variation to the transplant locations, but may not have been the only source of error resulting in off-target injections. Neonatal rats cannot readily be stabilised during surgery by conventional methods, such as ear bars, because at this age their ears have not fully developed. Therefore, alternative methods need to be used, including potentially cheek bars. Initially, rats were stabilised using Blu Tack (reusable putty-like pressure-sensitive adhesive produced by Bostik), which is easily mouldable to secure the animals in position, however this did not provide consistent stabilisation of the animal for injection. Instead, the head of each animal was measured and a small frame was designed which was kindly 3-D printed by Dr Robert Hammond (School of Medicine, St Andrews University) and used in batches 3-12. This frame was designed to improve stabilisation of the pup's head during the transplantation procedure.

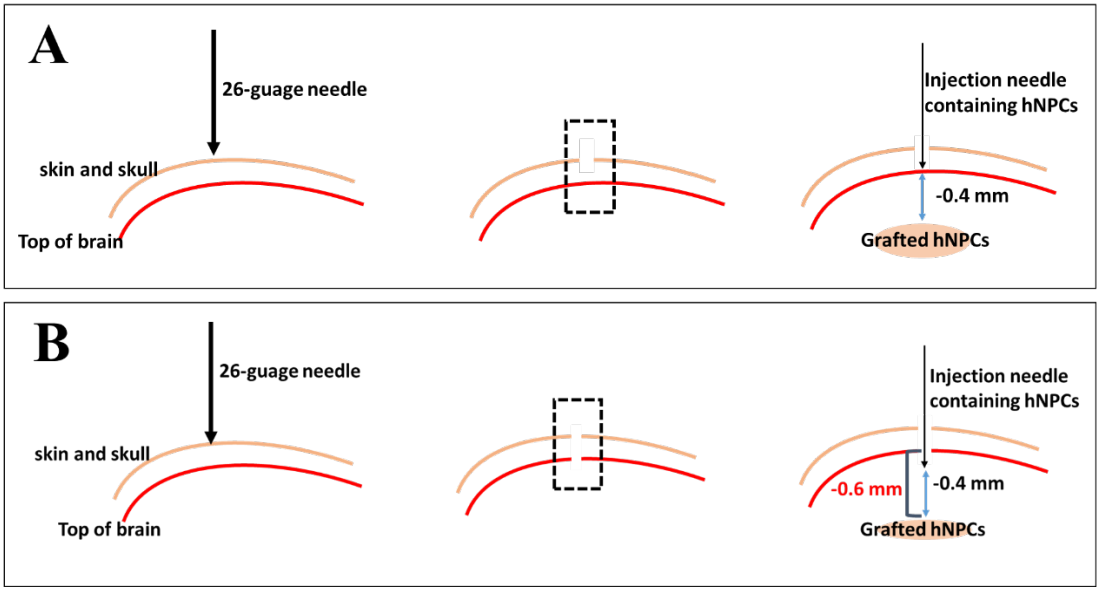

Figure 6.1 Potential variation in injection sites due to transplant protocol. Injection of hNPCs in the layer V of the sensorimotor cortex was carried out using a stereotaxic frame and a Hamilton syringe. However, the needle attached to the Hamilton syringe was not strong enough to pierce through the rat's skull and therefore a 26-guage needle was first used to pierce a hole in the skull by hand (**A**). Using the stereotaxic frame, the injection needle attached to the Hamilton syringe could then be manoeuvred to the designated coordinates (**A**). However, it was not always clear when the tip of the injection needle was on the surface of the brain compared to when it was in the brain tissue resulting in the potential addition of depth to the coordinates (**B**).

Despite the difficulties associated with targeting of injections, results indicate 60% or more of grafts were on target within the last two batches (11 and12) and overall, out of a total of 112 animals with detectable graft sites used across this study 40% (n=45/112) had grafts on target. Future work with these cells should focus on further improving transplant accuracy. For example, some studies in transplant of ESC-derived NPCs into neonatal cerebral cortex of mice have drilled into the skull, to expose the brain surface before injection (Ideguchi *et al.,* 2010), which may increase the accuracy of the depth of the transplant.

6.4 Protein expression and maturation of hNPCs

For transplanted cells to project from the cortex to the spinal cord, it is important to be aware of the expression profile of the cells (Finger *et al.,* 2002; Arlotta *et al.,* 2005; Sano *et al.,* 2017). The hNPCs used within this project expressed the deep-layer cortical neuron marker Tbr1 both *in vitro* and *in vivo* as well as the glutamatergic marker VGlut1 *in vitro*. It would be interesting to further characterise the expression profile *in vivo* examining markers known to be required for projection of neurons within the CST, such as Ctip2 and neuropilin-1 (Arlotta *et al.,* 2005; Sano *et al.,* 2017). Furthermore, as misexpression of these proteins, for example Tbr1, could be preventing CST projections (Han *et al.,* 2011), further research would be beneficial to identify the regulation of these genes within the hNPCs before and after transplant. Our results suggest the hNPC population used here may be more heterogeneous than originally thought, with expression of both astrocytes and GFAP-expressing radial stem cells potentially present within the culture. Further analysis of these and other cells types would need to be carried out before transplantation into an injury model.

One of the recurrent questions throughout this project was whether these cells were mature enough to allow for integration into host tissue. Neural development in a rat is much shorter than development in a human. Recent research has shown maturation of human iPSC-derived NPCs *in vitro* occurs over the course of 20-30 weeks (Odawara *et al.,* 2016) suggesting the hNPCs may need further differentiation *in vitro* before transplantation to promote better tissue integration *in vivo*. However, it may be that a balance is needed between immature and mature features, as these cells still need to

retain the ability to put out long-distance projections through white matter tracts. One of the advantages of using NPCs is their ability to promote secretion of neurotrophins, likely contributing to a growth-promoting environment. It is unclear whether a more differentiated cell type would retain this ability. The hNPCs here were pre-programmed to become CCNs, although this was not confirmed fully within the project. Yet previous research has shown hNPCs can mature over time *in vitro*, including formation of synapses and generation of spontaneous firing (Odawara *et al.,* 2016). This question may be answered by prolonging graft survival *in vivo*. Even though these hNPCs have been derived from iPSCs and are progressing towards differentiation into CCNs, they still retain a number of stem cell traits, raising questions about the developmental stage of these cells. Markers associated with stem cells, such as Oct4, are present within a high proportion of the hNPCs in culture. Furthermore, both *in vitro* and *in vivo* hNPCs express Ki67, a proliferation marker associated with oncogenic cells. It is perhaps more accurate to refer to these transplants as stem cells rather than neuronal progenitor grafts. Future work may address this, including in-depth analysis of stem cell markers, loss of stem cell traits over time *in vitro* and allowing the cells to differentiate further to CCN stage before transplantation.

Furthermore, it would be interesting to investigate whether maturation of these cells affects their ability to integrate into the host brain. Transplanted stem cells and neurons can integrate into the rodent cerebral cortex, indicated by grafts forming synapses and producing functional action potentials *in vivo* (Espuny-Camacho *et al.,* 2013; Tornero *et al.,* 2013). Therefore, there is hope that these iPSC-derived hNPCs could also integrate, providing they have the correct expression profile and are at the correct developmental stage at the time of transplant. As mentioned earlier, these are human cells injected into a rat system, so there is likely to be a lag time. Recent research has indeed demonstrated human NSCs injected into the adult lesioned immunodeficient rat spinal cord only show signs of maturation 3 months post-transplant with oligodendrocytes not detected until 1 year after transplant (Lu *et al.,* 2017). This work highlights the challenges of using human NSPCs within a rat system where maturation of human cells does not match that of the rat host. Longer-term survival of grafted human cells would therefore be required to enable full physiological and functional

characterisation. Yet whether a more differentiated equivalent would result in better integration remains to be seen.

6.5 Is the overexpression of α9 required?

The observed reduction in projections from transplanted α9-eYFP hNPCs compared to WT hNPCs was not expected. As discussed in Chapter 5, this was likely due to the viral transduction and use of polybrene to overexpress the α9-eYFP protein, potentially compromising cell survival following transplantation. Alternative methods of constitutive protein expression could be trialled, however, this body of work has also questioned the requirement for overexpression of α9, as these cells express an endogenous level of the protein which our preliminary results suggest is functional when grown on TN-C. Combining the results from Chapter 3 with the literature, there is evidence to suggest hNPCs could adapt to the environment as shown previously with embryonic DRGs (Condic *et al.,* 1999). When grown on increasing concentrations of human TN-C, WT hNPCs and GFP-hNPCs increasingly put out longer neurites (section 3.3.5), suggesting hNPCs could actively increase expression of TN-C-binding integrins, such as α9β1, α7β1 or α8β1 (Mercado *et al.,* 2004) in response to an inhibitory environment. Previously, embryonic DRGs in culture were able to overcome an inhibitory CSPG-rich environment by endogenously increasing the expression of integrin on the cell surface (Condic *et al.,* 1999; Condic, 2001). This trait is not continued beyond development into adulthood, but increasing exogenous integrin expression in adult DRGs can promote outgrowth (Condic, 2001). If this is the case, and hNPCs are able to adapt in response to glial scar components, it questions whether overexpression of α9 is truly necessary to achieve long-distance axonal outgrowth from hNPCs. As TN-C is upregulated at CNS injury sites, this increase in expression (the concentration of which is currently unknown) may be enough for hNPCs to increase their integrin, including α9, expression. Whether rat TN-C would be able to promote the same adaptation response in hNPCs as human TN-C remains to be seen, and could be tested *in vitro*, however this would likely lead to further experiments for analysing both α9 hNPCs and WT hNPCs in a rat injury model.

6.6 New potential techniques for imaging cell transplants *in vivo*

Graft survival and integration is only part of the challenge when it comes to cell replacement studies. The other aspect that must be considered is monitoring of transplanted grafts over time and their spatial distribution in relation to whole brain tissue and neuronal circuitry. Imaging techniques, such as magnetic resonance imaging (MRI), can provide fundamental information regarding the anatomical location of grafted cells. They cannot however provide information regarding graft-host interaction or cell viability, both of which are important when considering xenotransplantation. The majority of studies, including this one, have utilised 2-dimensional (2-D) IHC protocols to analyse transplanted cells in PFA-fixed, sectioned tissue. Immuno-stained tissue is imaged using light microscopy, such as epifluorescent or confocal, both of which have restricted tissue penetration and therefore tissue must be sectioned thinly. The thickness of tissue sections can present limitations when analysing or tracking cell migration or growth, as numerous serial sections must be analysed to be able to fully map grafts *in vivo*, a process that is very time consuming, for example if an entire rodent brain is to be imaged. Within the last decade, a number of new methods have been developed, such as serial two-photon microscopy (Ragan *et al.,* 2012); optical projection tomography (Gleave *et al.,* 2013); wide-field large-volume tomography (Gong *et al.,* 2016); and light sheet fluorescence microscopy (LSFM) (Ahrens *et al.,* 2013). All of these are recognised for their ability to analyse thicker tissue sections which enable the creation of 3-dimensional (3-D) views of neural circuitry. Follow-on work from this project has taken tissue from WT hNPC grafts and imaged this using LSFM in preliminary collaborative experiments with Professor Kishan Dholakia's group (School of Physics and Astronomy, St Andrews University). This work has set out to image transplanted hNCAM-positive projections from hNPCs alongside host astrocytes with the aim of analysing 3-D human grafts within the rat brain (Figure 6.2). It would be interesting to examine deeper sections of grafted cells within the host rat brain using additional methods of analysis in conjunction with LSFM, such as optical tissue clearance to further characterise our cell transplants.

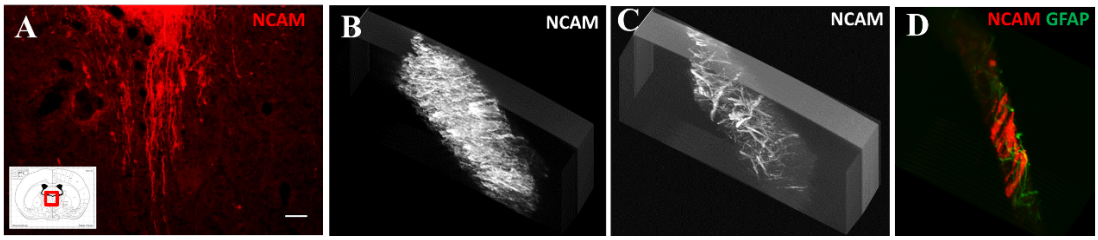

Figure 6.2 Projections from WT hNPCs detected using LSFM. Analysis was carried out on the hNPC grafts *in vivo* using LSFM where a 3-D image of the transplanted cells and axonal projection can be observed. Tissue was stained using the standard IHC protocol (section 2.8.1) to detect hNCAM-positive NPC projections 6 weeks post-transplantation (**A**). Following LSFM analysis, a dense region of projections was identified where it is difficult to single out lone projection fibres (**B**). However, in a less dense region, single fibres can clearly be identified in 3-D view (**C**). Furthermore, two cell types, such as hNPCs (indicated by hNCAM staining) and astrocytes (indicated by GFAP staining), can be imaged together (**D**) with the aim of acquiring larger scale images to analyse the graft in 3-D view *in vivo* interacting with surrounding tissue. Scale bar in A = 50 µm. Tissue was stained using anti-hNCAM and anti-GFAP primary antibodies and AlexaFluors goat-anti mouse 568 and goat-anti rabbit 488 (see Tables 2.5 and 2.6 for full antibody details). LSFM was carried out by Dr Kaley McCluskey and Dr Jonathan Nylk in Professor Kishan Dholakia's group within the School of Physics and Astronomy at the University of St Andrews.

To analyse thicker sections of tissue using optical brain imaging, such as LSFM, light scattering and refraction can be reduced using tissue clearing. Optical tissue clearing involves infiltrating the brain tissue with clearing agents and methods, such as CLARITY and iDISCO, to remove lipids from the brain effectively making the tissue transparent, letting light travel through it and thus allowing analysis of brain tissue, including the intact rodent brain (Ertürk *et al.,* 2011; Hama *et al.,* 2011; Chung *et al.,* 2013; Ke *et al.,* 2013; Tomer *et al.,* 2014; Costantini *et al.,* 2015; Renier *et al.,* 2016). With respect to cell transplantation, it is of high importance that an imaging technique can primarily decipher grafted cells from host cells, but also provide information on transplanted cell engraftment, tracking cell migration and identifying graft-host interactions. Recent work has shown human eGFP-expressing ESC-derived neuroepithelial stem cell transplants can be imaged *in vivo* following transplant into the mouse striatum or hippocampus, using a combination of tissue clearing, LSFM, 3D MRI and rabies virus-based retrograde tracing which enabled projections of grafted cells to be tracked throughout the host brain. Furthermore, this work has highlighted

the ability of this combination of techniques to identify innervation of human grafted boluses by host rat cells, suggesting potential graft-host interaction (Doerr *et al.,* 2017).

Some methods of optical clearing can result in loss of tissue structure and reduction of fluorescent fluorophores, but newer protocols are being developed to prolong fluorescent signals (Schwarz *et al.,* 2015). Furthermore some imaging techniques, such as block-face serial tomography (FAST), do not require any clearing (Seiriki *et al.,* 2017). Although this new technique requires histological sectioning, it allows imaging of large sections of tissue with high resolution, including an entire mouse brain, large sections of primate tissue, including a nuclear-stained adult marmoset hemisphere, and a nuclear-stained, 1,000 mm^3 region of the primary visual cortex in human post-mortem tissue. Furthermore, FAST can image tissue at the same speed as current LSFM techniques, yet it does not require tissue clearing thereby preventing any interference with the fluorescence signal (Seiriki *et al.,* 2017). Thus, new optical brain imaging techniques are providing exciting opportunities for imaging whole brain tissue at the cellular and subcellular level in both animal and human post-mortem tissue.

One further optical imaging technique that has proven useful for analysis of cell grafts *in vivo* is bioluminescence imaging (BLI) (Sher *et al.,* 2009; Takahashi *et al.,* 2011; Bernau *et al.,* 2014; Hwang *et al.,* 2014; Tennstaedt *et al.,* 2015a). This technique relies on transplanted cells exogenously expressing luciferase, which can emit light when in contact with its substrate luciferin, which is injected into the animal after cell transplantation and before imaging. The advantages of using BLI are that it is a non-invasive approach that allows analysis of grafted cells without compromising the host. Furthermore, and contrary to previous opinions within the field, recent research has confirmed that grafted cells deep within the tissue, for example the striatum, can be detected long term using this technique (Bernau *et al.,* 2014). Following transplant of luciferase-expressing hNPCs into the adult rat cortex and striatum, BLI was used to track the survival and migration of cells up to 12 weeks after transplant (Bernau *et al.,* 2014). Furthermore, luciferase expression can be designed to be under the control of cell-specific promoters, for example DCX or synapsin-I, allowing the differentiation and maturation of transplanted cells to be monitored *in vivo* (Tennstaedt *et al.,* 2015a). Although BLI may not provide as much information, such as graft integration, as the

previous imaging techniques discussed, it allows the survival of grafted cells to be analysed over time without the need to compromise the animal and the experiment. This technique may prove useful for the progression of this project when thinking about SCI injury models and assessing cell migration and projections towards an injury site. Indeed, luciferase-expressing NSPCs have been injected into the mouse spinal cord following laminectomy at L3 and tracked using BLI (Takahashi *et al.,* 2011). Therefore, it is possible to detect these cells within the rodent spinal cord, however there is a limit on detection of grafts less than 1,000 cells without opening up the animal. This method may therefore allow analysis of migration of hNPCs *in vivo*, but it also presents challenges, such as tracking of long-distance projections, especially single fibres, from luciferase-expressing hNPCs which would likely not be detected.

6.7 Concluding remarks

In terms of stem cell transplantation, and specifically iPSC-derived hNPC grafts, this work has confirmed previous research showing grafts can survive in immune competent neonatal rats, including longer than what has been documented in mice (Denham *et al.,* 2012; Mattis *et al.,* 2014). After a month *in vivo*, these cells can project to the caudal brain stem from the cerebral cortex. Unfortunately, these cells have not projected as far as in other comparable studies and this is likely due to targeting of the injections and gene expression, both of which would need further optimisation and analysis. In terms of integrin expression *in vivo*, this project has sparked a number of interesting questions around α9 integrin expression in hNPCs. Firstly, does overexpression of α9 using LV and polybrene hinder cell survival *in vivo*? Secondly, can hNPCs adapt to an inhibitory environment and upregulate expression of growth-promoting integrins, a trait shown previously in embryonic DRGs (Condic *et al.,* 1999)?

Although these cells were not characterised within a SCI model, there is substantial evidence from both the literature and data derived within this project that these cells, both WT and α9-expressing, should be transplanted into a rat injury model to assess their regenerative capacity, whether that be through cell replacement to reconstruct

damaged axonal connections or to provide trophic support by secretion of growth-promoting factors. Further support for transplantation of both α9-hNPCs and WT hNPCs into a rat injury model stems from research showing a lesioned environment can actually enhance both hNPC survival and migration compared to intact control animals (Behrstock *et al.,* 2008). This work specifically focused on hNPC grafts into the lesioned striatum of a Huntington's disease rat model under immunosuppression. In this case, before transplantation, the hNPCs were modified using LV (with no reported use of polybrene) to secrete GDNF. Furthermore, even though this project has focused largely on potential repair of SCI, there is scope for the transplantation of these genetically manipulated cells to be applied to a number of other neurological diseases and conditions where cells are lost, such as Parkinson's disease and Alzheimer's disease.

Here, this body of work has positively presented one potential avenue to target neuronal replacement in SCI and beyond, using genetically manipulated cells to overcome components of the inhibitory milieu created after CNS injury. However, due to the multitude of inhibitory proteins associated with CNS axonal injury, it is anticipated that cell transplantation alone would not be able to promote long-term functional recovery. Rather further interventions to influence the SCI pathophysiology, perhaps relating to the environment, alongside cell grafts would be required to reinstate neurological function after SCI.

References

Abrams, M.B., Dominguez, C., Pernold, K., Reger, R., Wiesenfeld-Hallin, Z., Olson, L., Prockop, D., 2009. Multipotent mesenchymal stromal cells attenuate chronic inflammation and injury-induced sensitivity to mechanical stimuli in experimental spinal cord injury. *Restor. Neurol. Neurosci.* 27, 307–321.

Ahrens, M.B., Orger, M.B., Robson, D.N., Li, J.M., Keller, P.J., 2013. Whole-brain functional imaging at cellular resolution using light-sheet microscopy. *Nat. Methods* 10, 413–420.

Akesson, E., Holmberg, L., Jönhagen, M.E., Kjaeldgaard, A., Falci, S., Sundström, E., Seiger, A., 2001. Solid human embryonic spinal cord xenografts in acute and chronic spinal cord cavities: a morphological and functional study. *Exp. Neurol.* 170, 305–316.

al Yacoub, N., Romanowska, M., Haritonova, N., Foerster, J., 2007. Optimized production and concentration of lentiviral vectors containing large inserts. *J. Gene Med.* 9, 579–584.

Aloy, E.M., Weinmann, O., Pot, C., Kasper, H., Dodd, D.A., Rülicke, T., Rossi, F., Schwab, M.E., 2007. Synaptic destabilization by neuronal Nogo-A. *Brain Cell Biol.* 35, 137–157.

Altman J, Bayer SA. 1995. Atlas of prenatal rat brain development. Boca Raton, CRC Press.

Alves, J.N., Muir, E.M., Andrews, M.R., Ward, A., Michelmore, N., Dasgupta, D., Verhaagen, J., Moloney, E.B., Keynes, R.J., Fawcett, J.W., Rogers, J.H., 2014. AAV vector-mediated secretion of chondroitinase provides a sensitive tracer for axonal arborisations. *J. Neurosci. Methods* 227, 107–120.

Anderson, M.A., Burda, J.E., Ren, Y., Ao, Y., O'Shea, T.M., Kawaguchi, R., Coppola, G., Khakh, B.S., Deming, T.J., Sofroniew, M.V., 2016. Astrocyte scar formation aids CNS axon regeneration. *Nature* 532, 195–200.

Andrews, M.R., Czvitkovich, S., Dassie, E., Vogelaar, C.F., Faissner, A., Blits, B., Gage, F.H., ffrench-Constant, C., Fawcett, J.W., 2009. α9 integrin promotes neurite outgrowth on tenascin-C and enhances sensory axon regeneration. *J. Neurosci.* 29, 5546–5557.

Andrews, M.R., Soleman, S., Cheah, M., Tumbarello, D.A., Mason, M.R.J., Moloney, E., Verhaagen, J., Bensadoun, J.-C., Schneider, B., Aebischer, P., Fawcett, J.W., 2016. Axonal localisation of integrins in the CNS is neuronal type and age dependent. *eNeuro.* 3:0029-16

Andrews, M.R., Stelzner, D.J., 2007. Evaluation of olfactory ensheathing and schwann cells after implantation into a dorsal injury of adult rat spinal cord. *J. Neurotrauma* 24, 1773–1792.

Antonic, A., Sena, E.S., Lees, J.S., Wills, T.E., Skeers, P., Batchelor, P.E., Macleod, M.R., Howells, D.W., 2013. Stem cell transplantation in traumatic spinal cord injury: A systematic review and meta-analysis of animal studies. *PLoS Biol* 11, e1001738.

Arjonen, A., Alanko, J., Veltel, S., Ivaska, J., 2012. Distinct recycling of active and inactive β1 integrins. *Traffic* Cph. Den. 13, 610–625.

Arlotta, P., Molyneaux, B.J., Chen, J., Inoue, J., Kominami, R., Macklis, J.D., 2005. Neuronal subtype-specific genes that control corticospinal motor neuron development *In Vivo*. *Neuron* 45, 207–221.

Asea, A., 2008. Heat shock proteins and toll-like receptors. *Handb. Exp. Pharmacol.* 111–127.

Asher, R.A., Morgenstern, D.A., Fidler, P.S., Adcock, K.H., Oohira, A., Braistead, J.E., Levine, J.M., Margolis, R.U., Rogers, J.H., Fawcett, J.W., 2000. Neurocan is upregulated in injured brain and in cytokine-treated astrocytes. *J. Neurosci.* 20, 2427–2438.

Asher, R.A., Morgenstern, D.A., Shearer, M.C., Adcock, K.H., Pesheva, P., Fawcett, J.W., 2002. Versican is upregulated in CNS injury and is a product of oligodendrocyte lineage cells. *J. Neurosci.* 22, 2225–2236.

Atwal, J.K., Pinkston-Gosse, J., Syken, J., Stawicki, S., Wu, Y., Shatz, C., Tessier-Lavigne, M., 2008. PirB is a functional receptor for myelin inhibitors of axonal regeneration. *Science* 322, 967–970.

Baba, H., Nakahira, K., Morita, N., Tanaka, F., Akita, H., Ikenaka, K., 1997. GFAP gene expression during development of astrocyte. *Dev. Neurosci.* 19, 49–57.

Babcock, A.A., Wirenfeldt, M., Holm, T., Nielsen, H.H., Dissing-Olesen, L., Toft-Hansen, H., Millward, J.M., Landmann, R., Rivest, S., Finsen, B., Owens, T., 2006. Toll-like receptor 2 signaling in response to brain injury: An innate bridge to neuroinflammation. *J. Neurosci.* 26, 12826–12837.

Bae, K.S., Park, J.B., Kim, H.S., Kim, D.S., Park, D.J., Kang, S.J., 2011. Neuron-like differentiation of bone marrow-derived mesenchymal stem cells. *Yonsei Med. J.* 52, 401–412.

Baghbaderani, B.A., Tian, X., Neo, B.H., Burkall, A., Dimezzo, T., Sierra, G., Zeng, X., Warren, K., Kovarcik, D.P., Fellner, T., Rao, M.S., 2015. cGMP-manufactured human induced pluripotent stem cells are available for pre-clinical and clinical applications. *Stem Cell Rep.* 5, 647–659.

Baker, D.E.C., Harrison, N.J., Maltby, E., Smith, K., Moore, H.D., Shaw, P.J., Heath, P.R., Holden, H., Andrews, P.W., 2007. Adaptation to culture of human embryonic stem cells and oncogenesis *in vivo*. *Nat. Biotechnol.* 25, 207–215.

Ballout, N., Frappé, I., Péron, S., Jaber, M., ZIbara, K., Gaillard, A., 2016. Development and maturation of embryonic cortical neurons grafted into the damaged adult motor cortex. *Front. Neural Circuits* 10.

Bambakidis, N.C., Miller, R.H., 2004. Transplantation of oligodendrocyte precursors and sonic hedgehog results in improved function and white matter sparing in the spinal cords of adult rats after contusion. *Spine J.* 4, 16–26.

Bareyre, F.M., Garzorz, N., Lang, C., Misgeld, T., Büning, H., Kerschensteiner, M., 2011. *In vivo* imaging reveals a phase-specific role of STAT3 during central and peripheral nervous system axon regeneration. *Proc. Natl. Acad. Sci. U. S. A.* 108, 6282–6287.

Bareyre, F.M., Kerschensteiner, M., Raineteau, O., Mettenleiter, T.C., Weinmann, O., Schwab, M.E., 2004. The injured spinal cord spontaneously forms a new intraspinal circuit in adult rats. *Nat. Neurosci.* 7, 269–277. doi:10.1038/nn1195

Barres, B.A., Burne, J.F., Holtmann, B., Thoenen, H., Sendtner, M., Raff, M.C., 1996. Ciliary neurotrophic factor enhances the rate of oligodendrocyte generation. *Mol. Cell. Neurosci.* 8, 146–156.

Barres, B.A., Schmid, R., Sendnter, M., Raff, M.C., 1993. Multiple extracellular signals are required for long-term oligodendrocyte survival. *Dev. Camb. Engl.* 118, 283–295.

Bartsch, S., Bartsch, U., Dorries, U., Faissner, A., Weller, A., Ekblom, P., Schachner, M., 1992a. Expression of tenascin in the developing and adult cerebellar cortex. *J. Neurosci.* 12, 736–749.

Bartsch, U., Bartsch, S., Dörries, U., Schachner, M., 1992b. Immunohistological localisation of tenascin in the developing and lesioned adult mouse optic nerve. *Eur. J. Neurosci.* 4, 338–352.

Bartsch, U., Faissner, A., Trotter, J., Dorries, U., Bartsch, S., Mohajeri, H., Schachner, M., 1994. Tenascin demarcates the boundary between the myelinated and nonmyelinated part of retinal ganglion cell axons in the developing and adult mouse. *J. Neurosci.* 14, 4756–4768.

Bartus, K., James, N.D., Didangelos, A., Bosch, K.D., Verhaagen, J., Yáñez-Muñoz, R.J., Rogers, J.H., Schneider, B.L., Muir, E.M., Bradbury, E.J., 2014. Large-scale chondroitin sulfate proteoglycan digestion with chondroitinase gene therapy leads to reduced pathology and modulates macrophage phenotype following spinal cord contusion injury. *J. Neurosci.* 34, 4822–4836.

Bedogni, F., Hodge, R.D., Elsen, G.E., Nelson, B.R., Daza, R.A.M., Beyer, R.P., Bammler, T.K., Rubenstein, J.L.R., Hevner, R.F., 2010. Tbr1 regulates regional and laminar identity of postmitotic neurons in developing neocortex. *Proc. Natl. Acad. Sci. U. S. A.* 107, 13129–13134.

Behrstock, S., Ebert, A.D., Klein, S., Schmitt, M., Moore, J.M., Svendsen, C.N., 2008. Lesion-induced increase in survival and migration of human neural progenitor cells releasing GDNF. *Cell Transplant.* 17, 753–762.

Ben-Hur, T., Ben-Menachem, O., Furer, V., Einstein, O., Mizrachi-Kol, R., Grigoriadis, N., 2003. Effects of proinflammatory cytokines on the growth, fate, and motility of multipotential neural precursor cells. *Mol. Cell. Neurosci.* 24, 623–631.

Bernau, K., Lewis, C.M., Petelinsek, A.M., Benink, H.A., Zimprich, C.A., Meyerand, M.E., Suzuki, M., Svendsen, C.N., 2014. *In vivo* tracking of human neural progenitor cells in the rat brain using bioluminescence imaging. *J. Neurosci. Methods* 228, 67–78.

Bickenbach, J, Officer, A, Shakespeare, T, von Groote, P.(Eds), 2013. *International perspectives on SCI*. World Health Organisation/International Spinal Cord Society, Geneva.

Bieniasz, P.D., Grdina, T.A., Bogerd, H.P., Cullen, B.R., 1999. Highly divergent lentiviral tat proteins activate viral gene expression by a common mechanism. *Mol. Cell. Biol.* 19, 4592–4599.

Bignami, A., Asher, R., Perides, G., 1992. Co-localisation of hyaluronic acid and chondroitin sulfate proteoglycan in rat cerebral cortex. *Brain Res.* 579, 173–177.

Bignami, A., Eng, L.F., Dahl, D., Uyeda, C.T., 1972. Localisation of the glial fibrillary acidic protein in astrocytes by immunofluorescence. *Brain Res.* 43, 429–435.

Binder, D.K., Scharfman, H.E., 2004. Brain-derived neurotrophic factor. *Growth Factors Chur Switz.* 22, 123–131.

Bjorklund, L.M., Sánchez-Pernaute, R., Chung, S., Andersson, T., Chen, I.Y.C., McNaught, K.S.P., Brownell, A.-L., Jenkins, B.G., Wahlestedt, C., Kim, K.-S., Isacson, O., 2002. Embryonic stem cells develop into functional dopaminergic neurons after transplantation in a Parkinson rat model. *Proc. Natl. Acad. Sci. U. S. A.* 99, 2344–2349.

Black, J.A., Waxman, S.G., Sims, T.J., Gilmore, S.A., 1986. Effects of delayed myelination by oligodendrocytes and Schwann cells on the macromolecular structure of axonal membrane in rat spinal cord. *J. Neurocytol.* 15, 745–761.

Blackmore, M., Letourneau, P.C., 2006. L1, β1 integrin, and cadherins mediate axonal regeneration in the embryonic spinal cord. *J. Neurobiol.* 66, 1564–1583.

Boivin, A., Pineau, I., Barrette, B., Filali, M., Vallières, N., Rivest, S., Lacroix, S., 2007. Toll-like receptor signaling is critical for Wallerian degeneration and functional recovery after peripheral nerve injury. *J. Neurosci.* 27, 12565–12576.

Bonner, J.F., Connors, T.M., Silverman, W.F., Kowalski, D.P., Lemay, M.A., Fischer, I., 2011. Grafted neural progenitors integrate and restore synaptic connectivity across the injured spinal cord. *J. Neurosci.* 31, 4675–4686.

Bozoyan, L., Khlghatyan, J., Saghatelyan, A., 2012. Astrocytes control the development of the migration-promoting vasculature scaffold in the postnatal brain via VEGF signaling. *J. Neurosci.* 32, 1687–1704.

Bracken, M.B., Shepard, M.J., Collins, W.F., Holford, T.R., Baskin, D.S., Eisenberg, H.M., Flamm, E., Leo-Summers, L., Maroon, J.C., Marshall, L.F., Perot, P.L., Piepmeier, J., Sonntag, V.K.H., Wagner, F.C., Wilberger, J.L., Winn, H.R., Young, W., 1992. Methylprednisolone or naloxone treatment after acute spinal cord injury: 1-year follow-up data. *J. Neurosurg.* 76, 23–31.

Bracken, M.B., Shepard, M.J., Holford, T.R., Leo-Summers, L., Aldrich, E.F., Fazl, M., Fehlings, M.G., Herr, D.L., Hitchon, P.W., Marshall, L.F., Nockels, R.P., Pascale, V., Perot, P.L., Piepmeier, J., Sonntag, V.K., Wagner, F., Wilberger, J.E., Winn, H.R., Young, W., 1998. Methylprednisolone or tirilazad mesylate administration after acute spinal cord injury: 1-year follow up. Results of the third national acute spinal cord injury randomized controlled trial. *J. Neurosurg.* 89, 699–706.

Bradbury, E.J., Moon, L.D.F., Popat, R.J., King, V.R., Bennett, G.S., Patel, P.N., Fawcett, J.W., McMahon, S.B., 2002. Chondroitinase ABC promotes functional recovery after spinal cord injury. *Nature* 416, 636–640.

Brederlau, A., Correia, A.S., Anisimov, S.V., Elmi, M., Paul, G., Roybon, L., Morizane, A., Bergquist, F., Riebe, I., Nannmark, U., Carta, M., Hanse, E., Takahashi, J., Sasai, Y., Funa, K., Brundin, P., Eriksson, P.S., Li, J.-Y., 2006. Transplantation of human embryonic stem cell-derived cells to a rat model of Parkinson's disease: Effect of *in vitro* differentiation on graft survival and teratoma formation. *Stem Cells* 24, 1433–1440.

Bridgewater, R.E., Norman, J.C., Caswell, P.T., 2012. Integrin trafficking at a glance. *J Cell Sci* 125, 3695–3701.

Brösamle, C., Huber, A.B., Fiedler, M., Skerra, A., Schwab, M.E., 2000. Regeneration of lesioned corticospinal tract fibers in the adult rat induced by a recombinant, humanized IN-1 antibody fragment. *J. Neurosci.* 20, 8061–8068.

Brown, D.R., 1999. Neurons depend on astrocytes in a coculture system for protection from glutamate toxicity. *Mol. Cell. Neurosci.* 13, 379–389.

Brown, J.P., Couillard-Després, S., Cooper-Kuhn, C.M., Winkler, J., Aigner, L., Kuhn, H.G., 2003. Transient expression of doublecortin during adult neurogenesis. *J. Comp. Neurol.* 467, 1–10.

Brown, M.D., Cornejo, B.J., Kuhn, T.B., Bamburg, J.R., 2000. Cdc42 stimulates neurite outgrowth and formation of growth cone filopodia and lamellipodia. *J. Neurobiol.* 43, 352–364.

Brundin, P., Strecker, R.E., Widner, H., Clarke, D.J., Nilsson, O.G., Astedt, B., Lindvall, O., Björklund, A., 1988. Human fetal dopamine neurons grafted in a

rat model of Parkinson's disease: immunological aspects, spontaneous and drug-induced behaviour, and dopamine release. *Exp. Brain Res.* 70, 192–208.

Bulfone, A., Smiga, S.M., Shimamura, K., Peterson, A., Puelles, L., Rubenstein, J.L.R., 1995. T-Brain-1: A homolog of Brachyury whose expression defines molecularly distinct domains within the cerebral cortex. *Neuron* 15, 63–78.

Burnstock, G., Knight, G.E., 2004. Cellular distribution and functions of P2 receptor subtypes in different systems. *Int. Rev. Cytol.* 240, 31–304.

Buss, A., Pech, K., Merkler, D., Kakulas, B.A., Martin, D., Schoenen, J., Noth, J., Schwab, M.E., Brook, G.A., 2005. Sequential loss of myelin proteins during Wallerian degeneration in the human spinal cord. *Brain J. Neurol.* 128, 356–364.

Butenschön, J., Zimmermann, T., Schmarowski, N., Nitsch, R., Fackelmeier, B., Friedemann, K., Radyushkin, K., Baumgart, J., Lutz, B., Leschik, J., 2016. PSA-NCAM positive neural progenitors stably expressing BDNF promote functional recovery in a mouse model of spinal cord injury. *Stem Cell Res. Ther.* 7, 11.

Cafferty, W.B.J., Duffy, P., Huebner, E., Strittmatter, S.M., 2010. MAG and OMgp synergize with Nogo-A to restrict axonal growth and neurological recovery after spinal cord trauma. *J. Neurosci.* 30, 6825–6837.

Cai, D., Qiu, J., Cao, Z., McAtee, M., Bregman, B.S., Filbin, M.T., 2001. Neuronal cyclic AMP controls the developmental loss in ability of axons to regenerate. *J. Neurosci.* 21, 4731–4739.

Calderwood, D.A., 2004. Integrin activation. *J. Cell Sci.* 117, 657–666.

Calderwood, D.A., Campbell, I.D., Critchley, D.R., 2013. Talins and kindlins: partners in integrin-mediated adhesion. *Nat. Rev. Mol. Cell Biol.* 14, 503–517.

Calderwood, D.A., Yan, B., Pereda, J.M. de, Alvarez, B.G., Fujioka, Y., Liddington, R.C., Ginsberg, M.H., 2002. The phosphotyrosine binding-like domain of talin activates integrins. *J. Biol. Chem.* 277, 21749–21758.

Calderwood, D.A., Zent, R., Grant, R., Rees, D.J.G., Hynes, R.O., Ginsberg, M.H., 1999. The talin head domain binds to integrin β subunit cytoplasmic tails and regulates integrin activation. *J. Biol. Chem.* 274, 28071–28074.

Callera, F., do Nascimento, R.X., 2006. Delivery of autologous bone marrow precursor cells into the spinal cord via lumbar puncture technique in patients with spinal cord injury: A preliminary safety study. *Exp. Hematol.* 34, 130–131.

Cantinieaux, D., Quertainmont, R., Blacher, S., Rossi, L., Wanet, T., Noël, A., Brook, G., Schoenen, J., Franzen, R., 2013. Conditioned medium from bone marrow-derived mesenchymal stem cells improves recovery after spinal cord injury in rats: an original strategy to avoid cell transplantation. *PloS One* 8, e69515.

Cao, Q., He, Q., Wang, Y., Cheng, X., Howard, R.M., Zhang, Y., DeVries, W.H., Shields, C.B., Magnuson, D.S.K., Xu, X.-M., Kim, D.H., Whittemore, S.R., 2010. Transplantation of ciliary neurotrophic factor-expressing adult oligodendrocyte precursor cells promotes remyelination and functional recovery after spinal cord injury. *J. Neurosci.* 30, 2989–3001.

Cao, Q.-L., Howard, R.M., Dennison, J.B., Whittemore, S.R., 2002. Differentiation of engrafted neuronal-restricted precursor cells is inhibited in the traumatically injured spinal cord. *Exp. Neurol.* 177, 349–359.

Caroni, P., Schwab, M.E., 1988. Antibody against myelin-associated inhibitor of neurite growth neutralizes nonpermissive substrate properties of CNS white matter. Neuron 1, 85–96.

Carulli, D., Pizzorusso, T., Kwok, J.C.F., Putignano, E., Poli, A., Forostyak, S., Andrews, M.R., Deepa, S.S., Glant, T.T., Fawcett, J.W., 2010. Animals lacking link protein have attenuated perineuronal nets and persistent plasticity. *Brain J. Neurol.* 133, 2331–2347.

Carulli, D., Rhodes, K.E., Brown, D.J., Bonnert, T.P., Pollack, S.J., Oliver, K., Strata, P., Fawcett, J.W., 2006. Composition of perineuronal nets in the adult rat cerebellum and the cellular origin of their components. *J. Comp. Neurol.* 494, 559–577.

Carulli, D., Rhodes, K.E., Fawcett, J.W., 2007. Upregulation of aggrecan, link protein 1, and hyaluronan synthases during formation of perineuronal nets in the rat cerebellum. *J. Comp. Neurol.* 501, 83–94.

Caswell, P.T., Norman, J.C., 2006. Integrin trafficking and the control of cell migration. *Traffic* 7, 14–21.

Chahboune, H., Ment, L.R., Stewart, W.B., Ma, X., Rothman, D.L., Hyder, F., 2007. Neurodevelopment of C57B/L6 mouse brain assessed by *in vivo* diffusion tensor imaging. *NMR Biomed.* 20, 375–382.

Cheah, M., Andrews, M.R., Chew, D.J., Moloney, E.B., Verhaagen, J., Fässler, R., Fawcett, J.W., 2016. Expression of an activated integrin promotes long-distance sensory axon regeneration in the spinal cord. *J. Neurosci.* 36, 7283–7297.

Chen, B., Schaevitz, L.R., McConnell, S.K., 2005. Fezl regulates the differentiation and axon targeting of layer 5 subcortical projection neurons in cerebral cortex. *Proc. Natl. Acad. Sci. U. S. A.* 102, 17184–17189.

Chen, B., Wang, S.S., Hattox, A.M., Rayburn, H., Nelson, S.B., McConnell, S.K., 2008a. The Fezf2–Ctip2 genetic pathway regulates the fate choice of subcortical projection neurons in the developing cerebral cortex. *Proc. Natl. Acad. Sci. U.S.A.* 105, 11382–11387.

Chen, C., Huang, X., Atakilit, A., Zhu, Q.-S., Corey, S.J., Sheppard, D., 2006. The Integrin alpha9beta1 contributes to granulopoiesis by enhancing granulocyte colony-stimulating factor receptor signaling. *Immunity* 25, 895–906.

Chen, L., Liao, G., Waclaw, R.R., Burns, K.A., Linquist, D., Campbell, K., Zheng, Y., Kuan, C.-Y., 2007. Rac1 controls the formation of midline commissures and the competency of tangential migration in ventral telencephalic neurons. *J. Neurosci.* 27, 3884–3893.

Chen, L.-X., Ma, S.-M., Zhang, P., Fan, Z.-C., Xiong, M., Cheng, G.-Q., Yang, Y., Qiu, Z.-L., Zhou, W.-H., Li, J., 2015. Neuroprotective effects of oligodendrocyte progenitor cell transplantation in premature rat brain following hypoxic-ischemic injury. *PLoS ONE* 10, e0115997.

Chen, M.S., Huber, A.B., van der Haar, M.E., Frank, M., Schnell, L., Spillmann, A.A., Christ, F., Schwab, M.E., 2000. Nogo-A is a myelin-associated neurite outgrowth inhibitor and an antigen for monoclonal antibody IN-1. *Nature* 403, 434–439.

Chen, P.-W., Luo, R., Jian, X., Randazzo, P.A., 2014. The Arf6 GTPase-activating proteins ARAP2 and ACAP1 define distinct endosomal compartments that regulate integrin α5β1 traffic. *J. Biol. Chem.* 289, 30237–30248.

Chen, Q., Smith, G.M., Shine, H.D., 2008b. Immune activation is required for NT-3-induced axonal plasticity in chronic spinal cord injury. *Exp. Neurol.* 209, 497–509.

Chen, X., Li, Y., Wang, L., Katakowski, M., Zhang, L., Chen, J., Xu, Y., Gautam, S.C., Chopp, M., 2002. Ischemic rat brain extracts induce human marrow stromal cell growth factor production. *Neuropathology* 22, 275–279.

Cheng, L., Sapieha, P., Kittlerova, P., Hauswirth, W.W., Di Polo, A., 2002. TrkB gene transfer protects retinal ganglion cells from axotomy-induced death *in vivo*. *J. Neurosci.* 22, 3977–3986.

Chesler, M., Young, W., Hassan, A.Z., Sakatani, K., Moriya, T., 1994. Elevation and clearance of extracellular K^+ following graded contusion of the rat spinal cord. *Exp. Neurol.* 125, 93–98.

Chew, D.J., Fawcett, J.W., Andrews, M.R., 2012. Chapter 14 - The challenges of long-distance axon regeneration in the injured CNS, in: Stephen B. Dunnett and Anders Björklund (Ed.), *Progress in brain research, functional neural transplantation III primary and stem cell therapies for brain repair, Part II*. Elsevier, pp. 253–294.

Chin, M.H., Mason, M.J., Xie, W., Volinia, S., Singer, M., Peterson, C., Ambartsumyan, G., Aimiuwu, O., Richter, L., Zhang, J., Khvorostov, I., Ott, V., Grunstein, M., Lavon, N., Benvenisty, N., Croce, C.M., Clark, A.T., Baxter, T., Pyle, A.D., Teitell, M.A., Pelegrini, M., Plath, K., Lowry, W.E., 2009. Induced pluripotent stem cells and embryonic stem cells are distinguished by gene expression signatures. *Cell Stem Cell* 5, 111–123.

Choi, C.K., Zareno, J., Digman, M.A., Gratton, E., Horwitz, A.R., 2011. Cross-correlated fluctuation analysis reveals phosphorylation-regulated paxillin-FAK complexes in nascent adhesions. *Biophys. J.* 100, 583–592.

Chopp, M., Li, Y., 2002. Treatment of neural injury with marrow stromal cells. *Lancet Neurol.* 1, 92–100.

Christopherson, K.S., Ullian, E.M., Stokes, C.C.A., Mullowney, C.E., Hell, J.W., Agah, A., Lawler, J., Mosher, D.F., Bornstein, P., Barres, B.A., 2005. Thrombospondins are astrocyte-secreted proteins that promote CNS synaptogenesis. *Cell* 120, 421–433.

Chung, K., Wallace, J., Kim, S.-Y., Kalyanasundaram, S., Andalman, A.S., Davidson, T.J., Mirzabekov, J.J., Zalocusky, K.A., Mattis, J., Denisin, A.K., Pak, S., Bernstein, H., Ramakrishnan, C., Grosenick, L., Gradinaru, V., Deisseroth, K., 2013. Structural and molecular interrogation of intact biological systems. *Nature* 497, 332–337.

Cízková, D., Rosocha, J., Vanický, I., Jergová, S., Cízek, M., 2006. Transplants of human mesenchymal stem cells improve functional recovery after spinal cord injury in the rat. *Cell. Mol. Neurobiol.* 26, 1167–1180.

Clegg, D.O., Wingerd, K.L., Hikita, S.T., Tolhurst, E.C., 2003. Integrins in the development, function and dysfunction of the nervous system. *Front. Biosci. J. Virtual Libr.* 8, d723-750.

Cohen, J., Burne, J.F., Winter, J., Bartlett, P., 1986. Retinal ganglion cells lose response to laminin with maturation. *Nature* 322, 465–467.

Condic, M.L., 2001. Adult neuronal regeneration induced by transgenic integrin expression. *J. Neurosci.* 21, 4782–4788.

Condic, M.L., Snow, D.M., Letourneau, P.C., 1999. Embryonic neurons adapt to the inhibitory proteoglycan aggrecan by increasing integrin expression. *J. Neurosci.* 19, 10036–10043.

Costantini, I., Ghobril, J.-P., Di Giovanna, A.P., Allegra Mascaro, A.L., Silvestri, L., Müllenbroich, M.C., Onofri, L., Conti, V., Vanzi, F., Sacconi, L., Guerrini, R.,

Markram, H., Iannello, G., Pavone, F.S., 2015. A versatile clearing agent for multi-modal brain imaging. *Sci. Rep.* 5, 9808.

Couillard-Despres, S., Winner, B., Schaubeck, S., Aigner, R., Vroemen, M., Weidner, N., Bogdahn, U., Winkler, J., Kuhn, H.-G., Aigner, L., 2005. Doublecortin expression levels in adult brain reflect neurogenesis. *Eur. J. Neurosci.* 21, 1–14.

Craig, A., Ling Luo, N., Beardsley, D.J., Wingate-Pearse, N., Walker, D.W., Hohimer, A.R., Back, S.A., 2003. Quantitative analysis of perinatal rodent oligodendrocyte lineage progression and its correlation with human. *Exp. Neurol.* 181, 231–240.

Cummings, B.J., Uchida, N., Tamaki, S.J., Salazar, D.L., Hooshmand, M., Summers, R., Gage, F.H., Anderson, A.J., 2005. Human neural stem cells differentiate and promote locomotor recovery in spinal cord-injured mice. *Proc. Natl. Acad. Sci. U. S. A.* 102, 14069–14074.

Cusimano, M., Biziato, D., Brambilla, E., Donegà, M., Alfaro-Cervello, C., Snider, S., Salani, G., Pucci, F., Comi, G., Garcia-Verdugo, J.M., Palma, M.D., Martino, G., Pluchino, S., 2012. Transplanted neural stem/precursor cells instruct phagocytes and reduce secondary tissue damage in the injured spinal cord. *Brain J. Neurol.* 135, 447–460.

Cyranoski, D., 2012. Stem-cell pioneer banks on future therapies. *Nat. News* 488, 139.

Danen, E.H.J., 2013. Integrins: An overview of structural and functional aspects. *Landes Bioscience.*

Danilov, C.A., Steward, O., 2015. Conditional genetic deletion of PTEN after a spinal cord injury enhances regenerative growth of CST axons and motor function recovery in mice. *Exp. Neurol.* 266, 147–160.

David, S., Aguayo, A.J., 1981. Axonal elongation into peripheral nervous system "bridges" after central nervous system injury in adult rats. *Science* 214, 931–933.

Davies, J.E., Huang, C., Proschel, C., Noble, M., Mayer-Proschel, M., Davies, S.J.A., 2006. Astrocytes derived from glial-restricted precursors promote spinal cord repair. *J. Biol.* 5, 7.

Davies, J.E., Pröschel, C., Zhang, N., Noble, M., Mayer-Pröschel, M., Davies, S.J.A., 2008. Transplanted astrocytes derived from BMP- or CNTF-treated glial-restricted precursors have opposite effects on recovery and allodynia after spinal cord injury. *J. Biol.* 7, 24.

Davies, S.J.A., Shih, C.-H., Noble, M., Mayer-Proschel, M., Davies, J.E., Proschel, C., 2011. Transplantation of specific human astrocytes promotes functional recovery after spinal cord injury. *PloS One* 6, e17328.

Davis, H.E., Morgan, J.R., Yarmush, M.L., 2002. Polybrene increases retrovirus gene transfer efficiency by enhancing receptor-independent virus adsorption on target cell membranes. *Biophys. Chem.* 97, 159–172.

de Vivo, L., Landi, S., Panniello, M., Baroncelli, L., Chierzi, S., Mariotti, L., Spolidoro, M., Pizzorusso, T., Maffei, L., Ratto, G.M., 2013. Extracellular matrix inhibits structural and functional plasticity of dendritic spines in the adult visual cortex. *Nat. Commun.* 4, 1484.

De Winter, F., Oudega, M., Lankhorst, A.J., Hamers, F.P., Blits, B., Ruitenberg, M.J., Pasterkamp, R.J., Gispen, W.H., Verhaagen, J., 2002. Injury-induced class 3 semaphorin expression in the rat spinal cord. *Exp. Neurol.* 175, 61–75.

Deepa, S.S., Carulli, D., Galtrey, C., Rhodes, K., Fukuda, J., Mikami, T., Sugahara, K., Fawcett, J.W., 2006. Composition of perineuronal net extracellular matrix in rat brain a different disaccharide composition for the net-associated proteoglycans. *J. Biol. Chem.* 281, 17789–17800.

DeMali, K.A., Wennerberg, K., Burridge, K., 2003. Integrin signaling to the actin cytoskeleton. *Curr. Opin. Cell Biol*. 15, 572–582.

Denda, S., Reichardt, L.F., 2007. Studies on Integrins in the Nervous System. *Methods Enzymol.* 426, 203–221.

Denham, M., Parish, C.L., Leaw, B., Wright, J., Reid, C.A., Petrou, S., Dottori, M., Thompson, L.H., 2012. Neurons derived from human embryonic stem cells extend long-distance axonal projections through growth along host white matter tracts after intra-cerebral transplantation. *Front. Cell. Neurosci.* 6.

Dergham, P., Ellezam, B., Essagian, C., Avedissian, H., Lubell, W.D., McKerracher, L., 2002. Rho signaling pathway targeted to promote spinal cord repair. *J. Neurosci.* 22, 6570–6577.

Di Paolo, G., Pellegrini, L., Letinic, K., Cestra, G., Zoncu, R., Voronov, S., Chang, S., Guo, J., Wenk, M.R., De Camilli, P., 2002. Recruitment and regulation of phosphatidylinositol phosphate kinase type 1γ by the FERM domain of talin. *Nature* 420, 85–89.

Dietz, V., Curt, A., 2006. Neurological aspects of spinal-cord repair: Promises and challenges. *Lancet Neurol.* 5, 688–694.

Doerr, J., Schwarz, M.K., Wiedermann, D., Leinhaas, A., Jakobs, A., Schloen, F., Schwarz, I., Diedenhofen, M., Braun, N.C., Koch, P., Peterson, D.A., Kubitscheck, U., Hoehn, M., Brüstle, O., 2017. Whole-brain 3D mapping of human neural transplant innervation. *Nat. Commun.* 8, ncomms14162.

Domeniconi, M., Cao, Z., Spencer, T., Sivasankaran, R., Wang, K., Nikulina, E., Kimura, N., Cai, H., Deng, K., Gao, Y., He, Z., Filbin, M., 2002. Myelin-associated glycoprotein interacts with the Nogo66 receptor to inhibit neurite outgrowth. *Neuron* 35, 283–290.

Doucette, R., 1991. PNS-CNS transitional zone of the first cranial nerve. *J. Comp. Neurol.* 312, 451–466.

Draper, J.S., Smith, K., Gokhale, P., Moore, H.D., Maltby, E., Johnson, J., Meisner, L., Zwaka, T.P., Thomson, J.A., Andrews, P.W., 2004. Recurrent gain of chromosomes 17q and 12 in cultured human embryonic stem cells. *Nat. Biotechnol.* 22, 53–54.

Du, K., Zheng, S., Zhang, Q., Li, S., Gao, X., Wang, J., Jiang, L., Liu, K., 2015. PTEN deletion promotes regrowth of corticospinal tract axons 1 year after spinal cord injury. *J. Neurosci.* 35, 9754–9763.

Dull, T., Zufferey, R., Kelly, M., Mandel, R.J., Nguyen, M., Trono, D., Naldini, L., 1998. A third-generation lentivirus vector with a conditional packaging system. *J. Virol.* 72, 8463–8471.

Duncan, I.D., Aguayo, A.J., Bunge, R.P., Wood, P.M., 1981. Transplantation of rat Schwann cells grown in tissue culture into the mouse spinal cord. *J. Neurol. Sci.* 49, 241–252.

Dunphy, J.L., Moravec, R., Ly, K., Lasell, T.K., Melancon, P., Casanova, J.E., 2006. The Arf6 GEF GEP100/BRAG2 regulates cell adhesion by controlling endocytosis of β1 integrins. *Curr. Biol.* 16, 315–320.

Edgerton, V.R., Harkema, S., 2011. Epidural stimulation of the spinal cord in spinal cord injury: current status and future challenges. *Expert Rev. Neurother.* 11, 1351–1353.

Einstein, O., Fainstein, N., Vaknin, I., Mizrachi-Kol, R., Reihartz, E., Grigoriadis, N., Lavon, I., Baniyash, M., Lassmann, H., Ben-Hur, T., 2007. Neural precursors attenuate autoimmune encephalomyelitis by peripheral immunosuppression. *Ann. Neurol.* 61, 209–218.

Ekström, P.A.R., Mayer, U., Panjwani, A., Pountney, D., Pizzey, J., Tonge, D.A., 2003. Involvement of alpha7beta1 integrin in the conditioning-lesion effect on sensory axon regeneration. *Mol. Cell. Neurosci.* 22, 383–395.

Elkabes, S., DiCicco-Bloom, E.M., Black, I.B., 1996. Brain microglia/macrophages express neurotrophins that selectively regulate microglial proliferation and function. *J. Neurosci.* 16, 2508–2521.

Englund, U., Bjorklund, A., Wictorin, K., Lindvall, O., Kokaia, M., 2002. Grafted neural stem cells develop into functional pyramidal neurons and integrate into host cortical circuitry. *Proc. Natl. Acad. Sci. U. S. A.* 99, 17089–17094.

Ertürk, A., Mauch, C.P., Hellal, F., Förstner, F., Keck, T., Becker, K., Jährling, N., Steffens, H., Richter, M., Hübener, M., Kramer, E., Kirchhoff, F., Dodt, H.U., Bradke, F., 2011. Three-dimensional imaging of the unsectioned adult spinal cord to assess axon regeneration and glial responses after injury. *Nat. Med.* 18, 166–171.

Espuny-Camacho, I., Michelsen, K.A., Gall, D., Linaro, D., Hasche, A., Bonnefont, J., Bali, C., Orduz, D., Bilheu, A., Herpoel, A., Lambert, N., Gaspard, N., Péron, S., Schiffmann, S.N., Giugliano, M., Gaillard, A., Vanderhaeghen, P., 2013. Pyramidal neurons derived from human pluripotent stem cells integrate efficiently into mouse brain circuits *in vivo*. *Neuron* 77, 440–456.

Eva, R., Andrews, M.R., Franssen, E.H.P., Fawcett, J.W., 2012. Chapter three – intrinsic mechanisms regulating axon regeneration: An integrin perspective, in: Jeffrey L. Goldberg and Ephraim F. Trakhtenberg (Ed.), *International review of neurobiology, axon growth and regeneration: Part 2*. Academic Press, pp. 75–104.

Eva, R., Dassie, E., Caswell, P.T., Dick, G., ffrench-Constant, C., Norman, J.C., Fawcett, J.W., 2010. Rab11 and its effector Rab coupling protein contribute to the trafficking of β1 integrins during axon growth in adult dorsal root ganglion neurons and PC12 cells. *J. Neurosci.* 30, 11654–11669.

Eva, R., Fawcett, J., 2014. Integrin signalling and traffic during axon growth and regeneration. *Curr. Opin. Neurobiol.* 27, 179–185.

Evaniew, N., Noonan, V.K., Fallah, N., Kwon, B.K., Rivers, C.S., Ahn, H., Bailey, C.S., Christie, S.D., Fourney, D.R., Hurlbert, R.J., Linassi, A.G., Fehlings, M.G., Dvorak, M.F., 2015. Methylprednisolone for the treatment of patients with acute spinal cord injuries: A propensity score-matched cohort study from a Canadian multi-center spinal cord injury Registry. *J. Neurotrauma* 32, 1674–1683.

Evans, M.J., Kaufman, M.H., 1981. Establishment in culture of pluripotential cells from mouse embryos. *Nature* 292, 154–156.

Evers, M.R., Salmen, B., Bukalo, O., Rollenhagen, A., Bösl, M.R., Morellini, F., Bartsch, U., Dityatev, A., Schachner, M., 2002. Impairment of L-type Ca2+ channel-dependent forms of hippocampal synaptic plasticity in mice deficient

in the extracellular matrix glycoprotein tenascin-C. *J. Neurosci.* 22, 7177–7194.

Fabes, J., Anderson, P., Brennan, C., Bolsover, S., 2007. Regeneration-enhancing effects of EphA4 blocking peptide following corticospinal tract injury in adult rat spinal cord. *Eur. J. Neurosci.* 26, 2496–2505.

Fabes, J., Anderson, P., Yáñez-Muñoz, R.J., Thrasher, A., Brennan, C., Bolsover, S., 2006. Accumulation of the inhibitory receptor EphA4 may prevent regeneration of corticospinal tract axons following lesion. *Eur. J. Neurosci.* 23, 1721–1730.

Faijerson, J., Tinsley, R.B., Apricó, K., Thorsell, A., Nodin, C., Nilsson, M., Blomstrand, F., Eriksson, P.S., 2006. Reactive astrogliosis induces astrocytic differentiation of adult neural stem/progenitor cells *in vitro*. *J. Neurosci. Res.* 84, 1415–1424.

Fan, C., Zheng, Y., Cheng, X., Qi, X., Bu, P., Luo, X., Kim, D.H., Cao, Q., 2012. Transplantation of D15A-expressing glial-restricted-precursor-derived astrocytes improves anatomical and locomotor recovery after spinal cord injury. *Int. J. Biol. Sci.* 9, 78–93.

Fang, H., Liu, C., Yang, M., Li, H., Zhang, F., Zhang, W., Zhang, J., 2017. Neurotrophic factor and Trk signaling mechanisms underlying the promotion of motor recovery after acute spinal cord injury in rats. *Exp. Ther. Med.* 14, 652–656.

Faulkner, J.R., Herrmann, J.E., Woo, M.J., Tansey, K.E., Doan, N.B., Sofroniew, M.V., 2004. Reactive astrocytes protect tissue and preserve function after spinal cord injury. *J. Neurosci.* 24, 2143–2155.

Fawcett, J.W., 2015. Chapter 10 - The extracellular matrix in plasticity and regeneration after CNS injury and neurodegenerative disease, in: Numa Dancause, S.N. and S.R. (Ed.), *Progress in Brain Research, Sensorimotor RehabilitationAt the Crossroads of Basic and Clinical Sciences*. Elsevier, pp. 213–226.

Fehlings, M.G., Theodore, N., Harrop, J., Maurais, G., Kuntz, C., Shaffrey, C.I., Kwon, B.K., Chapman, J., Yee, A., Tighe, A., McKerracher, L., 2011. A phase I/IIa clinical trial of a recombinant Rho protein antagonist in acute spinal cord injury. *J. Neurotrauma* 28, 787–796.

Féron, F., Perry, C., Cochrane, J., Licina, P., Nowitzke, A., Urquhart, S., Geraghty, T., Mackay-Sim, A., 2005. Autologous olfactory ensheathing cell transplantation in human spinal cord injury. *Brain J. Neurol.* 128, 2951–2960.

Filous, A.R., Miller, J.H., Coulson-Thomas, Y.M., Horn, K.P., Alilain, W.J., Silver, J., 2010. Immature astrocytes promote CNS axonal regeneration when combined with chondroitinase ABC. *Dev. Neurobiol.* 70, 826–841.

Finger, J.H., Bronson, R.T., Harris, B., Johnson, K., Przyborski, S.A., Ackerman, S.L., 2002. The netrin 1 receptors Unc5h3 and Dcc are necessary at multiple choice points for the guidance of corticospinal tract axons. *J. Neurosci.* 22, 10346–10356.

Fouad, K., Schnell, L., Bunge, M.B., Schwab, M.E., Liebscher, T., Pearse, D.D., 2005. Combining schwann cell bridges and olfactory-ensheathing glia grafts with chondroitinase promotes locomotor recovery after complete transection of the spinal cord. *J. Neurosci.* 25, 1169–1178.

Fournier, A.E., GrandPre, T., Strittmatter, S.M., 2001. Identification of a receptor mediating Nogo-66 inhibition of axonal regeneration. *Nature* 409, 341–346.

Francis, F., Koulakoff, A., Boucher, D., Chafey, P., Schaar, B., Vinet, M.C., Friocourt, G., McDonnell, N., Reiner, O., Kahn, A., McConnell, S.K., Berwald-Netter, Y., Denoulet, P., Chelly, J., 1999. Doublecortin is a developmentally regulated, microtubule-associated protein expressed in migrating and differentiating neurons. *Neuron* 23, 247–256.

Franssen, E.H.P., Zhao, R.-R., Koseki, H., Kanamarlapudi, V., Hoogenraad, C.C., Eva, R., Fawcett, J.W., 2015. Exclusion of integrins from CNS axons is regulated by Arf6 activation and the AIS. *J. Neurosci.* 35, 8359–8375.

Fry, E.J., Chagnon, M.J., López-Vales, R., Tremblay, M.L., David, S., 2010. Corticospinal tract regeneration after spinal cord injury in receptor protein tyrosine phosphatase sigma deficient mice. *Glia* 58, 423–433.

Fujimoto, Y., Abematsu, M., Falk, A., Tsujimura, K., Sanosaka, T., Juliandi, B., Semi, K., Namihira, M., Komiya, S., Smith, A., Nakashima, K., 2012. Treatment of a mouse model of spinal cord injury by transplantation of human induced pluripotent stem cell-derived long-term self-renewing neuroepithelial-like stem cells. *Stem Cells* Dayt. Ohio 30, 1163–1173.

Gall, C.M., Pinkstaff, J.K., Lauterborn, J.C., Xie, Y., Lynch, G., 2003. Integrins regulate neuronal neurotrophin gene expression through effects on voltage-sensitive calcium channels. *Neuroscience* 118, 925–940.

Galtrey, C.M., Fawcett, J.W., 2007. The role of chondroitin sulfate proteoglycans in regeneration and plasticity in the central nervous system. *Brain Res. Rev.* 54, 1–18.

Galtrey, C.M., Kwok, J.C.F., Carulli, D., Rhodes, K.E., Fawcett, J.W., 2008. Distribution and synthesis of extracellular matrix proteoglycans, hyaluronan, link proteins and tenascin-R in the rat spinal cord. *Eur. J. Neurosci.* 27, 1373–1390.

Garcia, A.D.R., Doan, N.B., Imura, T., Bush, T.G., Sofroniew, M.V., 2004. GFAP-expressing progenitors are the principal source of constitutive neurogenesis in adult mouse forebrain. *Nat. Neurosci.* 7, 1233–1241.

García-Alías, G., Barkhuysen, S., Buckle, M., Fawcett, J.W., 2009. Chondroitinase ABC treatment opens a window of opportunity for task-specific rehabilitation. *Nat. Neurosci.* 12, 1145–1151.

Gardiner, N.J., Fernyhough, P., Tomlinson, D.R., Mayer, U., von der Mark, H., Streuli, C.H., 2005. α7 integrin mediates neurite outgrowth of distinct populations of adult sensory neurons. *Mol. Cell. Neurosci.* 28, 229–240.

Gaspard, N., Bouschet, T., Hourez, R., Dimidschstein, J., Naeije, G., van den Ameele, J., Espuny-Camacho, I., Herpoel, A., Passante, L., Schiffmann, S.N., Gaillard, A., Vanderhaeghen, P., 2008. An intrinsic mechanism of corticogenesis from embryonic stem cells. *Nature* 455, 351–357.

Gensel, J.C., Nakamura, S., Guan, Z., van Rooijen, N., Ankeny, D.P., Popovich, P.G., 2009. Macrophages promote axon regeneration with concurrent neurotoxicity. *J. Neurosci.* 29, 3956–3968.

George, R., Griffin, J.W., 1994. Delayed macrophage responses and myelin clearance during Wallerian degeneration in the central nervous system: The dorsal radiculotomy model. *Exp. Neurol.* 129, 225–236.

Gleave, J.A., Lerch, J.P., Henkelman, R.M., Nieman, B.J., 2013. A method for 3D immunostaining and optical imaging of the mouse brain demonstrated in neural progenitor cells. *PLoS ONE* 8.

Gledhill, R.F., Harrison, B.M., McDonald, W.I., 1973. Demyelination and remyelination after acute spinal cord compression. *Exp. Neurol.* 38, 472–487.

Gleeson, J.G., Lin, P.T., Flanagan, L.A., Walsh, C.A., 1999. Doublecortin is a microtubule-associated protein and is expressed widely by migrating neurons. *Neuron* 23, 257–271.

Goldshmit, Y., Galea, M.P., Wise, G., Bartlett, P.F., Turnley, A.M., 2004. Axonal regeneration and lack of astrocytic gliosis in EphA4-deficient mice. *J. Neurosci.* 24, 10064–10073.

Goldshmit, Y., McLenachan, S., Turnley, A., 2006. Roles of Eph receptors and ephrins in the normal and damaged adult CNS. *Brain Res. Rev.* 52, 327–345.

Goldshmit, Y., Spanevello, M.D., Tajouri, S., Li, L., Rogers, F., Pearse, M., Galea, M., Bartlett, P.F., Boyd, A.W., Turnley, A.M., 2011. EphA4 blockers promote axonal regeneration and functional recovery following spinal cord injury in mice. *PLoS ONE* 6.

Gomes, F.C.A., Paulin, D., Moura Neto, V., 1999. Glial fibrillary acidic protein (GFAP): modulation by growth factors and its implication in astrocyte differentiation. *Braz. J. Med. Biol. Res.* 32, 619–631.

Gong, H., Xu, D., Yuan, J., Li, X., Guo, C., Peng, J., Li, Y., Schwarz, L.A., Li, A., Hu, B., Xiong, B., Sun, Q., Zhang, Y., Liu, J., Zhong, Q., Xu, T., Zeng, S., Luo, Q., 2016. High-throughput dual-colour precision imaging for brain-wide connectome with cytoarchitectonic landmarks at the cellular level. *Nat. Commun.* 7, ncomms12142.

Gonzenbach, R.R., Zoerner, B., Schnell, L., Weinmann, O., Mir, A.K., Schwab, M.E., 2012. Delayed anti-nogo-a antibody application after spinal cord injury shows progressive loss of responsiveness. *J. Neurotrauma* 29, 567–578.

Götz, M., Bolz, J., Joester, A., Faissner, A., 1997. Tenascin-C synthesis and influence on axonal growth during rat cortical development. *Eur. J. Neurosci.* 9, 496–506.

Götz, M., Hartfuss, E., Malatesta, P., 2002. Radial glial cells as neuronal precursors: a new perspective on the correlation of morphology and lineage restriction in the developing cerebral cortex of mice. *Brain Res. Bull.* 57, 777–788.

Graziadei, P.P., Graziadei, G.A., 1979. Neurogenesis and neuron regeneration in the olfactory system of mammals. I. Morphological aspects of differentiation and structural organization of the olfactory sensory neurons. *J. Neurocytol.* 8, 1–18.

Gregg, C., Weiss, S., 2003. Generation of functional radial glial cells by embryonic and adult forebrain neural stem cells. *J. Neurosci.* 23, 11587–11601.

Griffiths, I.R., McCulloch, M.C., 1983. Nerve fibres in spinal cord impact injuries. Part 1. Changes in the myelin sheath during the initial 5 weeks. *J. Neurol. Sci.* 58, 335–349.

Guadagno, J., Xu, X., Karajgikar, M., Brown, A., Cregan, S.P., 2013. Microglia-derived TNFα induces apoptosis in neural precursor cells via transcriptional activation of the Bcl-2 family member Puma. *Cell Death Dis.* 4, e538.

Guest, J.D., Hiester, E.D., Bunge, R.P., 2005. Demyelination and Schwann cell responses adjacent to injury epicenter cavities following chronic human spinal cord injury. *Exp. Neurol.* 192, 384–393.

Gupta, S.K., Vlahakis, N.E., 2009. Integrin α9β1 mediates enhanced cell migration through nitric oxide synthase activity regulated by Src tyrosine kinase. *J. Cell Sci.* 122, 2043–2054.

Gupton, S.L., Gertler, F.B., 2010. Integrin signaling switches the cytoskeletal and exocytic machinery that drives neuritogenesis. *Dev. Cell* 18, 725–736.

Haas, C., Fischer, I., 2013. Human astrocytes derived from glial restricted progenitors support regeneration of the injured spinal cord. *J. Neurotrauma* 30, 1035–1052.

Hains, B.C., Waxman, S.G., 2006. Activated microglia contribute to the maintenance of chronic pain after spinal cord injury. *J. Neurosci.* 26, 4308–4317.

Hama, H., Kurokawa, H., Kawano, H., Ando, R., Shimogori, T., Noda, H., Fukami, K., Sakaue-Sawano, A., Miyawaki, A., 2011. Scale: a chemical approach for fluorescence imaging and reconstruction of transparent mouse brain. *Nat. Neurosci.* 14, 1481–1488.

Han, W., Kwan, K.Y., Shim, S., Lam, M.M.S., Shin, Y., Xu, X., Zhu, Y., Li, M., Šestan, N., 2011. TBR1 directly represses Fezf2 to control the laminar origin and development of the corticospinal tract. *Proc. Natl. Acad. Sci. U. S. A.* 108, 3041–3046.

Hanisch, U.-K., 2002. Microglia as a source and target of cytokines. *Glia* 40, 140–155.

Harper, M.M., Ye, E.-A., Blong, C.C., Jacobson, M.L., Sakaguchi, D.S., 2010. Integrins contribute to initial morphological development and process outgrowth in rat adult hippocampal progenitor cells. *J. Mol. Neurosci.* MN 40, 269–283.

Hartfuss, E., Galli, R., Heins, N., Götz, M., 2001. Characterization of CNS precursor subtypes and radial glia. *Dev. Biol.* 229, 15–30.

Hawryluk, G.W.J., Mothe, A., Wang, J., Wang, S., Tator, C., Fehlings, M.G., 2012. An *in vivo* characterization of trophic factor production following neural precursor cell or bone marrow stromal cell transplantation for spinal cord injury. *Stem Cells Dev.* 21, 2222–2238.

Haynes, S.E., Hollopeter, G., Yang, G., Kurpius, D., Dailey, M.E., Gan, W.-B., Julius, D., 2006. The P2Y12 receptor regulates microglial activation by extracellular nucleotides. *Nat. Neurosci.* 9, 1512–1519.

Herrmann, J.E., Imura, T., Song, B., Qi, J., Ao, Y., Nguyen, T.K., Korsak, R.A., Takeda, K., Akira, S., Sofroniew, M.V., 2008. STAT3 is a critical regulator of astrogliosis and scar formation after spinal cord injury. *J. Neurosci.* 28, 7231–7243.

Hevner, R.F., Shi, L., Justice, N., Hsueh, Y., Sheng, M., Smiga, S., Bulfone, A., Goffinet, A.M., Campagnoni, A.T., Rubenstein, J.L., 2001. Tbr1 regulates differentiation of the preplate and layer 6. *Neuron* 29, 353–366.

Hiraga, A., Kuwabara, S., Doya, H., Kanai, K., Fujitani, M., Taniguchi, J., Arai, K., Mori, M., Hattori, T., Yamashita, T., 2006. Rho-kinase inhibition enhances axonal regeneration after peripheral nerve injury. *J. Peripher. Nerv. Syst*. JPNS 11, 217–224.

Hollis, E.R., Jamshidi, P., Löw, K., Blesch, A., Tuszynski, M.H., 2009. Induction of corticospinal regeneration by lentiviral trkB-induced Erk activation. *Proc. Natl. Acad. Sci. U.S.A.* 106, 7215–7220.

Holmqvist, S., Lehtonen, Š., Chumarina, M., Puttonen, K.A., Azevedo, C., Lebedeva, O., Ruponen, M., Oksanen, M., Djelloul, M., Collin, A., Goldwurm, S., Meyer, M., Lagarkova, M., Kiselev, S., Koistinaho, J., Roybon, L., 2016. Creation of a library of induced pluripotent stem cells from Parkinsonian patients. *NPJ Park. Dis.* 2, 16009.

Holsapple, M.P., West, L.J., Landreth, K.S., 2003. Species comparison of anatomical and functional immune system development. *Birth Defects Res. B. Dev. Reprod. Toxicol.* 68, 321–334.

Hong, J.Y., Lee, S.H., Lee, S.C., Kim, J.-W., Kim, K.-P., Kim, S.M., Tapia, N., Lim, K.T., Kim, J., Ahn, H.-S., Ko, K., Shin, C.Y., Lee, H.T., Schöler, H.R., Hyun, J.K., Han, D.W., 2014. Therapeutic potential of induced neural stem cells for spinal cord injury. *J. Biol. Chem.* 289, 32512–32525.

Honmou, O., Felts, P.A., Waxman, S.G., Kocsis, J.D., 1996. Restoration of normal conduction properties in demyelinated spinal cord axons in the adult rat by transplantation of exogenous Schwann cells. *J. Neurosci.* 16, 3199–3208.

Hoornaert, C.J., Le Blon, D., Quarta, A., Daans, J., Goossens, H., Berneman, Z., Ponsaerts, P., 2017. Concise review: Innate and adaptive immune recognition of allogeneic and xenogeneic cell transplants in the central nervous system. *Stem Cells Transl. Med.* 6, 1434–1441.

Hoornaert, C.J., Luyckx, E., Reekmans, K., Dhainaut, M., Guglielmetti, C., Le Blon, D., Dooley, D., Fransen, E., Daans, J., Verbeeck, L., Quarta, A., De Vocht, N., Lemmens, E., Goossens, H., Van der Linden, A., Roobrouck, V.D., Verfaillie, C., Hendrix, S., Moser, M., Berneman, Z.N., Ponsaerts, P., 2016. *In vivo* interleukin-13-primed macrophages contribute to reduced alloantigen-specific T cell activation and prolong immunological survival of allogeneic mesenchymal stem cell implants. *Stem Cells* Dayt. Ohio 34, 1971–1984.

Horner, P.J., Power, A.E., Kempermann, G., Kuhn, H.G., Palmer, T.D., Winkler, J., Thal, L.J., Gage, F.H., 2000. Proliferation and differentiation of progenitor cells throughout the intact adult rat spinal cord. *J. Neurosci.* 20, 2218–2228.

Hsu, J.-Y.C., Stein, S.A., Xu, X.-M., 2005. Temporal and spatial distribution of growth-associated molecules and astroglial cells in the rat corticospinal tract during development. *J. Neurosci. Res.* 80, 330–340.

Hu, F., Strittmatter, S.M., 2008. The N-terminal domain of Nogo-A inhibits cell adhesion and axonal outgrowth by an integrin-specific mechanism. *J. Neurosci.* 28, 1262–1269.

Huang, E.J., Reichardt, L.F., 2003. Trk receptors: roles in neuronal signal transduction. *Annu. Rev. Biochem.* 72, 609–642.

Huang, X.Z., Wu, J.F., Ferrando, R., Lee, J.H., Wang, Y.L., Farese, R.V., Sheppard, D., 2000. Fatal bilateral chylothorax in mice lacking the integrin alpha9beta1. *Mol. Cell. Biol.* 20, 5208–5215.

Huang, Z., Shimazu, K., Woo, N.H., Zang, K., Müller, U., Lu, B., Reichardt, L.F., 2006. Distinct roles of the beta 1-class integrins at the developing and the mature hippocampal excitatory synapse. *J. Neurosci.* 26, 11208–11219.

Humphries, J.D., Wang, P., Streuli, C., Geiger, B., Humphries, M.J., Ballestrem, C., 2007. Vinculin controls focal adhesion formation by direct interactions with talin and actin. *J. Cell Biol.* 179, 1043–1057.

Hunt, M., Lu, P., Tuszynski, M.H., 2017. Myelination of axons emerging from neural progenitor grafts after spinal cord injury. *Exp. Neurol.* 296, 69–73.

Hurlbert, R.J., 2014. Methylprednisolone for the Treatment of Acute Spinal Cord Injury: *Point. Neurosurgery* 61, 32–35.

Hurtado, A., Moon, L.D.F., Maquet, V., Blits, B., Jérôme, R., Oudega, M., 2006. Poly (D,L-lactic acid) macroporous guidance scaffolds seeded with Schwann cells genetically modified to secrete a bi-functional neurotrophin implanted in the completely transected adult rat thoracic spinal cord. *Biomaterials* 27, 430–442.

Hwang, D.W., Jin, Y., Lee, D.H., Kim, H.Y., Cho, H.N., Chung, H.J., Park, Y., Youn, H., Lee, S.J., Lee, H.J., Kim, S.U., Wang, K.-C., Lee, D.S., 2014. *In vivo* bioluminescence imaging for prolonged survival of transplanted human neural stem cells Using 3D biocompatible scaffold in corticectomized rat model. *PLOS ONE* 9, e105129.

Hynes, R.O., 2002. Integrins: Bidirectional, allosteric signaling machines. Cell 110, 673–687.

Hynes, R.O., 1987. Integrins: a family of cell surface receptors. *Cell* 48, 549–554.

Ideguchi, M., Palmer, T.D., Recht, L.D., Weimann, J.M., 2010. Murine embryonic stem cell-derived pyramidal neurons integrate into the cerebral cortex and appropriately project axons to subcortical targets. *J. Neurosci.* 30, 894–904.

Imura, T., Nakano, I., Kornblum, H.I., Sofroniew, M.V., 2006. Phenotypic and functional heterogeneity of GFAP-expressing cells *in vitro*: Differential expression of LeX/CD15 by GFAP-expressing multipotent neural stem cells and non-neurogenic astrocytes. *Glia* 53, 277–293.

Irintchev, A., Rollenhagen, A., Troncoso, E., Kiss, J.Z., Schachner, M., 2005. Structural and functional aberrations in the cerebral cortex of tenascin-C deficient mice. *Cereb. Cortex* 15, 950–962.

Jain, A., McKeon, R.J., Brady-Kalnay, S.M., Bellamkonda, R.V., 2011. Sustained delivery of activated Rho GTPases and BDNF promotes axon growth in CSPG-rich regions following spinal cord injury. *PloS One* 6, e16135.

Jakeman, L.B., Wei, P., Guan, Z., Stokes, B.T., 1998. Brain-derived neurotrophic factor stimulates hindlimb stepping and sprouting of cholinergic fibers after spinal cord injury. *Exp. Neurol.* 154, 170–184.

Janowski, M., Engels, C., Gorelik, M., Lyczek, A., Bernard, S., Bulte, J.W.M., Walczak, P., 2014. Survival of neural progenitors allografted into the CNS of immunocompetent recipients is highly dependent on transplantation site. *Cell Transplant.* 23, 253–262.

Janowski, M., Jablonska, A., Kozlowska, H., Orukari, I., Bernard, S., Bulte, J.W., Lukomska, B., Walczak, P., 2012. Neonatal desensitization does not universally prevent xenograft rejection. *Nat. Methods* 9, 856–858.

Jessen, K.R., Mirsky, R., 2016. The repair Schwann cell and its function in regenerating nerves. *J. Physiol.* 594, 3521–3531.

Jin, D., Liu, Y., Sun, F., Wang, X., Liu, X., He, Z., 2015. Restoration of skilled locomotion by sprouting corticospinal axons induced by co-deletion of PTEN and SOCS3. *Nat. Commun.* 6, ncomms9074.

Joester, A., Faissner, A., 2001. The structure and function of tenascins in the nervous system. *Matrix Biol.* 20, 13–22.

Johansson, C.B., Momma, S., Clarke, D.L., Risling, M., Lendahl, U., Frisén, J., 1999. Identification of a neural stem cell in the adult mammalian central nervous system. *Cell* 96, 25–34.

Jones, J.L., Walker, R.A., 1999. Integrins: a role as cell signalling molecules. *Mol. Pathol.* 52, 208–213.

Jones, L.L., Margolis, R.U., Tuszynski, M.H., 2003. The chondroitin sulfate proteoglycans neurocan, brevican, phosphacan, and versican are differentially regulated following spinal cord injury. *Exp. Neurol.* 182, 399–411.

Jones, P.L., Jones, F.S., 2000. Tenascin-C in development and disease: gene regulation and cell function. *Matrix Biol.* 19, 581–596.

Jongbloets, B.C., Pasterkamp, R.J., 2014. Semaphorin signalling during development. *Development* 141, 3292–3297.

Joset, A., Dodd, D.A., Halegoua, S., Schwab, M.E., 2010. Pincher-generated Nogo-A endosomes mediate growth cone collapse and retrograde signaling. *J. Cell Biol.* 188, 271–285.

Jung, D.-I., Ha, J., Kang, B.-T., Kim, J.-W., Quan, F.-S., Lee, J.-H., Woo, E.-J., Park, H.-M., 2009. A comparison of autologous and allogenic bone marrow-derived mesenchymal stem cell transplantation in canine spinal cord injury. *J. Neurol. Sci.* 285, 67–77.

Kadoya, K., Lu, P., Nguyen, K., Lee-Kubli, C., Kumamaru, H., Yao, L., Knackert, J., Poplawski, G., Dulin, J., Strobl, H., Takashima, Y., Biane, J., Conner, J., Zhang, S.-C., Tuszynski, M.H., 2016. Spinal cord reconstitution with homologous neural grafts enables robust corticospinal regeneration. *Nat. Med.* 22, 479–487.

Kaneko, S., Iwanami, A., Nakamura, M., Kishino, A., Kikuchi, K., ShIbata, S., Okano, H.J., Ikegami, T., Moriya, A., Konishi, O., Nakayama, C., Kumagai, K., Kimura, T., Sato, Y., Goshima, Y., Taniguchi, M., Ito, M., He, Z., Toyama, Y., Okano, H., 2006. A selective Sema3A inhibitor enhances regenerative responses and functional recovery of the injured spinal cord. *Nat. Med.* 12, 1380–1389.

Kanno, H., Pearse, D.D., Ozawa, H., Itoi, E., Bunge, M.B., 2015. Schwann cell transplantation for spinal cord injury repair: its significant therapeutic potential and prospectus. *Rev. Neurosci.* 26, 121–128.

Karaoz, E., Kabatas, S., Duruksu, G., Okcu, A., Subasi, C., Ay, B., Musluman, M., Civelek, E., 2012. Reduction of lesion in injured rat spinal cord and partial functional recovery of motility after bone marrow derived mesenchymal stem cell transplantation. *Turk. Neurosurg.* 22, 207–217.

Karimi-Abdolrezaee, S., Eftekharpour, E., Wang, J., Morshead, C.M., Fehlings, M.G., 2006. Delayed transplantation of adult neural precursor cells promotes remyelination and functional neurological recovery after spinal cord injury. *J. Neurosci.* 26, 3377–3389.

Karimi-Abdolrezaee, S., Eftekharpour, E., Wang, J., Schut, D., Fehlings, M.G., 2010. Synergistic effects of transplanted adult neural stem/progenitor cells, chondroitinase, and growth factors promote functional repair and plasticity of the chronically injured spinal cord. *J. Neurosci.* 30, 1657–1676.

Kaushal, V., Koeberle, P.D., Wang, Y., Schlichter, L.C., 2007. The Ca2+-activated K+ channel KCNN4/KCa3.1 contributes to microglia activation and nitric oxide-dependent neurodegeneration. *J. Neurosci.* 27, 234–244.

Ke, M.-T., Fujimoto, S., Imai, T., 2013. SeeDB: a simple and morphology-preserving optical clearing agent for neuronal circuit reconstruction. *Nat. Neurosci.* 16, 1154–1161.

Keirstead, H.S., Nistor, G., Bernal, G., Totoiu, M., Cloutier, F., Sharp, K., Steward, O., 2005. Human embryonic stem cell-derived oligodendrocyte progenitor cell transplants remyelinate and restore locomotion after spinal cord injury. *J. Neurosci.* 25, 4694–4705.

Kelly, C.M., Precious, S.V., Scherf, C., Penketh, R., Amso, N.N., Battersby, A., Allen, N.D., Dunnett, S.B., Rosser, A.E., 2009. Neonatal desensitization allows long-term survival of neural xenotransplants without immunosuppression. *Nat. Methods* 6, 271–273.

Khatiwala, R., Cai, C., 2016. Strategies to enhance the effectiveness of adult stem cell therapy for ischemic heart diseases affecting the elderly patients. *Stem Cell Rev.* 12, 214–223.

Khazaei, M., Siddiqui, A.M., Fehlings, M.G., 2014. The potential for iPS-derived stem cells as a therapeutic strategy for spinal cord injury: opportunities and challenges. *J. Clin. Med.* 4, 37–65. doi:10.3390/jcm4010037

Kigerl, K.A., Gensel, J.C., Ankeny, D.P., Alexander, J.K., Donnelly, D.J., Popovich, P.G., 2009. Identification of two distinct macrophage subsets with divergent effects causing either neurotoxicity or regeneration in the injured mouse spinal cord. *J. Neurosci.* 29, 13435–13444.

Kigerl, K.A., Lai, W., Rivest, S., Hart, R.P., Satoskar, A.R., Popovich, P.G., 2007. Toll-like receptor (TLR)-2 and TLR-4 regulate inflammation, gliosis, and myelin sparing after spinal cord injury. *J. Neurochem.* 102, 37–50.

Kim, D., Kim, C.-H., Moon, J.-I., Chung, Y.-G., Chang, M.-Y., Han, B.-S., Ko, S., Yang, E., Cha, K.Y., Lanza, R., Kim, K.-S., 2009. Generation of human induced pluripotent stem cells by direct delivery of reprogramming proteins. *Cell Stem Cell* 4, 472–476.

Kim, S., Honmou, O., Kato, K., Nonaka, T., Houkin, K., Hamada, H., Kocsis, J.D., 2006. Neural differentiation potential of peripheral blood- and bone-marrow-derived precursor cells. *Brain Res.* 1123, 27–33.

Kim, S.-H., Turnbull, J., Guimond, S., 2011. Extracellular matrix and cell signalling: the dynamic cooperation of integrin, proteoglycan and growth factor receptor. *J. Endocrinol.* 209, 139–151.

Kobayashi, Y., Okada, Y., Itakura, G., Iwai, H., Nishimura, S., Yasuda, A., Nori, S., Hikishima, K., Konomi, T., Fujiyoshi, K., Tsuji, O., Toyama, Y., Yamanaka, S., Nakamura, M., Okano, H., 2012. Pre-evaluated safe human iPSC-derived neural stem cells promote functional recovery after spinal cord injury in common marmoset without tumorigenicity. *PLOS ONE* 7, e52787.

Kohama, I., Lankford, K.L., Preiningerova, J., White, F.A., Vollmer, T.L., Kocsis, J.D., 2001. Transplantation of cryopreserved adult human Schwann cells enhances axonal conduction in demyelinated spinal cord. *J. Neurosci.* 21, 944–950.

Koizumi, S., Shigemoto-Mogami, Y., Nasu-Tada, K., Shinozaki, Y., Ohsawa, K., Tsuda, M., Joshi, B.V., Jacobson, K.A., Kohsaka, S., Inoue, K., 2007. UDP acting at P2Y6 receptors is a mediator of microglial phagocytosis. *Nature* 446, 1091–1095.

Krebs, D.L., Hilton, D.J., 2001. SOCS proteins: negative regulators of cytokine signaling. *Stem Cells* Dayt. Ohio 19, 378–387.

Kubasak, M.D., Jindrich, D.L., Zhong, H., Takeoka, A., McFarland, K.C., Muñoz-Quiles, C., Roy, R.R., Edgerton, V.R., Ramón-Cueto, A., Phelps, P.E., 2008. OEG implantation and step training enhance hindlimb-stepping ability in adult spinal transected rats. *Brain J. Neurol.* 131, 264–276.

Kumar, M., Keller, B., Makalou, N., Sutton, R.E., 2001. Systematic Determination of the Packaging Limit of Lentiviral Vectors. *Hum. Gene Ther.* 12, 1893–1905.

Kwon, B.K., Liu, J., Oschipok, L., Teh, J., Liu, Z.W., Tetzlaff, W., 2004. Rubrospinal neurons fail to respond to brain-derived neurotrophic factor applied to the spinal cord injury site 2 months after cervical axotomy. *Exp. Neurol.* 189, 45–57.

Lang, C., Bradley, P.M., Jacobi, A., Kerschensteiner, M., Bareyre, F.M., 2013. STAT3 promotes corticospinal remodelling and functional recovery after spinal cord injury. *EMBO Rep.* 14, 931–937.

Łastowska, M., Cotterill, S., Bown, N., Cullinane, C., Variend, S., Lunec, J., Strachan, T., Pearson, A.D.J., Jackson, M.S., 2002. Breakpoint position on 17q identifies the most aggressive neuroblastoma tumors. *Genes. Chromosomes Cancer* 34, 428–436.

Lee, D.-H., Lee, J.Y., Oh, B.-M., Phi, J.H., Kim, S.-K., Bang, M.S., Kim, S.U., Wang, K.-C., 2013. Functional recovery after injury of motor cortex in rats: effects of rehabilitation and stem cell transplantation in a traumatic brain injury model of cortical resection. *Childs Nerv. Syst.* 29, 403–411.

Lee, J.O., Bankston, L.A., Arnaout, M.A., Liddington, R.C., 1995. Two conformations of the integrin A-domain (I-domain): a pathway for activation? *Struct. Lond. Engl.* 1993 3, 1333–1340.

Lee, S.-T., Chu, K., Park, H.-K., Jung, K.-H., Kim, M., Lee, S.K., Roh, J.-K., 2008. New Concept of Neural Stem Cell Transplantation: Anti-inflammatory Role. *Int. J. Stem Cells* 1, 36–42.

Lefcort, F., Venstrom, K., McDonald, J.A., Reichardt, L.F., 1992. Regulation of expression of fibronectin and its receptor, alpha 5 beta 1, during development and regeneration of peripheral nerve. *Dev. Camb. Engl.* 116, 767–782.

Lehmann, M., Fournier, A., Selles-Navarro, I., Dergham, P., Sebok, A., Leclerc, N., Tigyi, G., McKerracher, L., 1999. Inactivation of Rho Signaling Pathway Promotes CNS Axon Regeneration. *J. Neurosci.* 19, 7537–7547.

Lehnardt, S., Lehmann, S., Kaul, D., Tschimmel, K., Hoffmann, O., Cho, S., Krueger, C., Nitsch, R., Meisel, A., Weber, J.R., 2007. Toll-like receptor 2 mediates CNS injury in focal cerebral ischemia. *J. Neuroimmunol.* 190, 28–33.

Lemons, M.L., Condic, M.L., 2006. Combined integrin activation and intracellular cAMP cause Rho GTPase dependent growth cone collapse on laminin-1. *Exp. Neurol.* 202, 324–335.

Letourneau, P.C., Shattuck, T.A., 1989. Distribution and possible interactions of actin-associated proteins and cell adhesion molecules of nerve growth cones. *Development* 105, 505–519.

Levitt, P., Rakic, P., 1980. Immunoperoxidase localisation of glial fibrillary acidic protein in radial glial cells and astrocytes of the developing rhesus monkey brain. *J. Comp. Neurol.* 193, 815–840.

Lewandowski, G., Steward, O., 2014. AAVshRNA-mediated suppression of PTEN in adult rats in combination with salmon fibrin administration enables regenerative growth of corticospinal axons and enhances recovery of voluntary motor function after cervical spinal cord injury. *J. Neurosci.* 34, 9951–9962.

Li, Y., Field, P.M., Raisman, G., 1997. Repair of Adult Rat Corticospinal Tract by Transplants of Olfactory Ensheathing Cells. *Science* 277, 2000–2002.

Liebscher, T., Schnell, L., Schnell, D., Scholl, J., Schneider, R., Gullo, M., Fouad, K., Mir, A., Rausch, M., Kindler, D., Hamers, F.P.T., Schwab, M.E., 2005. Nogo-A antibody improves regeneration and locomotion of spinal cord-injured rats. *Ann. Neurol.* 58, 706–719.

Lin, R., Kwok, J.C.F., Crespo, D., Fawcett, J.W., 2008. Chondroitinase ABC has a long-lasting effect on chondroitin sulphate glycosaminoglycan content in the injured rat brain. *J. Neurochem.* 104, 400–408.

Lipson, A.C., Widenfalk, J., Lindqvist, E., Ebendal, T., Olson, L., 2003. Neurotrophic properties of olfactory ensheathing glia. *Exp. Neurol.* 180, 167–171.

Liu, K., Lu, Y., Lee, J.K., Samara, R., Willenberg, R., Sears-Kraxberger, I., Tedeschi, A., Park, K.K., Jin, D., Cai, B., Xu, B., Connolly, L., Steward, O., Zheng, B., He, Z., 2010. PTEN deletion enhances the regenerative ability of adult corticospinal neurons. *Nat. Neurosci.* 13, 1075–1081.

Liu, X., Bolteus, A.J., Balkin, D.M., Henschel, O., Bordey, A., 2006. GFAP-expressing cells in the postnatal subventricular zone display a unique glial phenotype intermediate between radial glia and astrocytes. *Glia* 54, 394–410.

Lizée, G., Gonzales, M.I., Topalian, S.L., 2004. Lentivirus vector-mediated expression of tumor-associated epitopes by human antigen presenting cells. *Hum. Gene Ther.* 15, 393–404.

Looijenga, L.H.J., Hersmus, R., Gillis, A.J.M., Pfundt, R., Stoop, H.J., van Gurp, R.J.H.L.M., Veltman, J., Beverloo, H.B., van Drunen, E., van Kessel, A.G., Pera, R.R., Schneider, D.T., Summersgill, B., Shipley, J., McIntyre, A., van der Spek, P., Schoenmakers, E., Oosterhuis, J.W., 2006. Genomic and expression profiling of human spermatocytic seminomas: primary spermatocyte as tumorigenic precursor and DMRT1 as candidate chromosome 9 gene. *Cancer Res.* 66, 290–302.

Lopez-Verrilli, M.A., Picou, F., Court, F.A., 2013. Schwann cell-derived exosomes enhance axonal regeneration in the peripheral nervous system. *Glia* 61, 1795–1806.

Lu, P., Blesch, A., Graham, L., Wang, Y., Samara, R., Banos, K., Haringer, V., Havton, L., Weishaupt, N., Bennett, D., Fouad, K., Tuszynski, M.H., 2012a. Motor axonal regeneration after partial and complete spinal cord transection. *J. Neurosci.* 32, 8208–8218.

Lu, P., Blesch, A., Tuszynski, M.H., 2001. Neurotrophism without neurotropism: BDNF promotes survival but not growth of lesioned corticospinal neurons. *J. Comp. Neurol.* 436, 456–470.

Lu, P., Ceto, S., Wang, Y., Graham, L., Wu, D., Kumamaru, H., Staufenberg, E., Tuszynski, M.H., 2017. Prolonged human neural stem cell maturation supports recovery in injured rodent CNS. *J. Clin. Invest.* 127, 3287–3299.

Lu, P., Wang, Y., Graham, L., McHale, K., Gao, M., Wu, D., Brock, J., Blesch, A., Rosenzweig, E.S., Havton, L.A., Zheng, B., Conner, J.M., Marsala, M., Tuszynski, M.H., 2012b. Long-distance growth and connectivity of neural stem cells after severe spinal cord injury. *Cell* 150, 1264–1273.

Lu, P., Woodruff, G., Wang, Y., Graham, L., Hunt, M., Wu, D., Boehle, E., Ahmad, R., Poplawski, G., Brock, J., Goldstein, L.S.B., Tuszynski, M.H., 2014. Long-distance axonal growth from human induced pluripotent stem cells after spinal cord injury. *Neuron* 83, 789–796.

Lu, X., Lu, D., Scully, M., Kakkar, V., 2008. The role of integrins in cancer and the development of anti-integrin therapeutic agents for cancer therapy. *Perspect. Med. Chem.* 2, 57–73.

Ma, D.K., Bonaguidi, M.A., Ming, G., Song, H., 2009. Adult neural stem cells in the mammalian central nervous system. *Cell Res.* 19, 672–682.

Ma, K., Fox, L., Shi, G., Shen, J., Liu, Q., Pappas, J.D., Cheng, J., Qu, T., 2011. Generation of neural stem cell-like cells from bone marrow-derived human mesenchymal stem cells. *Neurol. Res.* 33, 1083–1093.

Macaya, D., Spector, M., 2012. Injectable hydrogel materials for spinal cord regeneration: a review. *Biomed. Mater.* 7, 12001.

Mackay-Sim, A., Féron, F., Cochrane, J., Bassingthwaighte, L., Bayliss, C., Davies, W., Fronek, P., Gray, C., Kerr, G., Licina, P., Nowitzke, A., Perry, C., Silburn, P. a. S., Urquhart, S., Geraghty, T., 2008. Autologous olfactory ensheathing cell transplantation in human paraplegia: A 3-year clinical trial. *Brain J. Neurol.* 131, 2376–2386.

Mackay-Sim, A., St John, J.A., 2011. Olfactory ensheathing cells from the nose: Clinical application in human spinal cord injuries. *Exp. Neurol.* 229, 174–180.

Magavi, S.S., Leavitt, B.R., Macklis, J.D., 2000. Induction of neurogenesis in the neocortex of adult mice. *Nature* 405, 951–955.

Magistretti, P.J., 2011a. Neuron-glia metabolic coupling and plasticity. *Exp. Physiol.* 96, 407–410.

Malatesta, P., Hack, M.A., Hartfuss, E., Kettenmann, H., Klinkert, W., Kirchhoff, F., Götz, M., 2003. Neuronal or glial progeny: regional differences in radial glia fate. *Neuron* 37, 751–764.

Mao, L., Jia, J., Zhou, X., Xiao, Y., Wang, Y., Mao, X., Zhen, X., Guan, Y., Alkayed, N.J., Cheng, J., 2013. Delayed administration of a PTEN inhibitor BPV improves functional recovery after experimental stroke. *Neuroscience* 231, 272–281.

Marshall-Clarke, S., Reen, D., Tasker, L., Hassan, J., 2000. Neonatal immunity: how well has it grown up? *Immunol. Today* 21, 35–41.

Mattis, V.B., Wakeman, D.R., Tom, C., Dodiya, H.B., Yeung, S.Y., Tran, A.H., Bernau, K., Ornelas, L., Sahabian, A., Reidling, J., Sareen, D., Thompson, L.M., Kordower, J.H., Svendsen, C.N., 2014. Neonatal immune-tolerance in mice does not prevent xenograft rejection. *Exp. Neurol.* 254, 90–98.

Mayfield Brain and Spine, 2016. *Anatomy of the human spine* [ONLINE] Available at www.mayfieldclinic.com/PE-AnatSpine.htm. [Accessed 3 October 2017].

Mayshar, Y., Ben-David, U., Lavon, N., Biancotti, J.-C., Yakir, B., Clark, A.T., Plath, K., Lowry, W.E., Benvenisty, N., 2010. Identification and classification of chromosomal aberrations in human induced pluripotent stem cells. *Cell Stem Cell* 7, 521–531.

Mazzini, L., Gelati, M., Profico, D.C., Sgaravizzi, G., Projetti Pensi, M., Muzi, G., Ricciolini, C., Rota Nodari, L., Carletti, S., Giorgi, C., Spera, C., Domenico, F., Bersano, E., Petruzzelli, F., Cisari, C., Maglione, A., Sarnelli, M.F., Stecco, A., Querin, G., Masiero, S., Cantello, R., Ferrari, D., Zalfa, C., Binda, E., Visioli, A., Trombetta, D., Novelli, A., Torres, B., Bernardini, L., Carriero, A., Prandi, P., Servo, S., Cerino, A., Cima, V., Gaiani, A., Nasuelli, N., Massara, M., Glass, J., Sorarù, G., Boulis, N.M., Vescovi, A.L., 2015. Human neural stem cell transplantation in ALS: initial results from a phase I trial. *J. Transl. Med.* 13, 17.

McBride, J.L., Behrstock, S.P., Chen, E.-Y., Jakel, R.J., Siegel, I., Svendsen, C.N., Kordower, J.H., 2004. Human neural stem cell transplants improve motor function in a rat model of Huntington's disease. *J. Comp. Neurol.* 475, 211–219.

McKenna, W.L., Betancourt, J., Larkin, K.A., Abrams, B., Guo, C., Rubenstein, J.L.R., Chen, B., 2011. Tbr1 and Fezf2 regulate alternate corticofugal neuronal identities during neocortical development. *J. Neurosci.* 31, 549–564.

McKerracher, L., David, S., Jackson, D.L., Kottis, V., Dunn, R.J., Braun, P.E., 1994. Identification of myelin-associated glycoprotein as a major myelin-derived inhibitor of neurite growth. *Neuron* 13, 805–811.

McTigue, D.M., Wei, P., Stokes, B.T., 2001. Proliferation of NG2-positive cells and altered oligodendrocyte numbers in the contused rat spinal cord. *J. Neurosci.* 21, 3392–3400.

Mehta, S.T., Luo, X., Park, K.K., Bixby, J.L., Lemmon, V.P., 2016. Hyperactivated Stat3 boosts axon regeneration in the CNS. *Exp. Neurol.* 280, 115–120.

Meijering, E., Jacob, M., Sarria, J.-C.F., Steiner, P., Hirling, H., Unser, M., 2004. Design and validation of a tool for neurite tracing and analysis in fluorescence microscopy images. *Cytom. Part J. Int. Soc. Anal. Cytol.* 58, 167–176.

Mendoza, P., Ortiz, R., Díaz, J., Quest, A.F.G., Leyton, L., Stupack, D., Torres, V.A., 2013. Rab5 activation promotes focal adhesion disassembly, migration and invasiveness in tumor cells. *J Cell Sci* 126, 3835–3847.

Mercado, M.L.T., Nur-e-Kamal, A., Liu, H.-Y., Gross, S.R., Movahed, R., Meiners, S., 2004. Neurite outgrowth by the alternatively spliced region of human tenascin-C is mediated by neuronal α7β1 integrin. *J. Neurosci.* 24, 238–247.

Merkle, F.T., Tramontin, A.D., García-Verdugo, J.M., Alvarez-Buylla, A., 2004. Radial glia give rise to adult neural stem cells in the subventricular zone. *Proc. Natl. Acad. Sci. U. S. A.* 101, 17528–17532.

Miao, T., Wu, D., Zhang, Y., Bo, X., Subang, M.C., Wang, P., Richardson, P.M., 2006. Suppressor of cytokine signaling-3 suppresses the ability of activated signal transducer and activator of transcription-3 to stimulate neurite growth in rat primary sensory neurons. *J. Neurosci.* 26, 9512–9519.

Michele, M., Faissner, A., 2009. Tenascin-C stimulates contactin-dependent neurite outgrowth via activation of phospholipase C. *Mol. Cell. Neurosci.* 41, 397–408.

Mikol, D.D., Gulcher, J.R., Stefansson, K., 1990. The oligodendrocyte-myelin glycoprotein belongs to a distinct family of proteins and contains the HNK-1 carbohydrate. *J. Cell Biol.* 110, 471–479.

Milligan, E.D., Watkins, L.R., 2009. Pathological and protective roles of glia in chronic pain. *Nat. Rev. Neurosci.* 10, 23–36.

Miragall, F., Dermietzel, R., 1992. Immunocytochemical localisation of cell adhesion molecules in the developing and mature olfactory system. *Microsc. Res. Tech.* 23, 157–172.

Miragall, F., Kadmon, G., Husmann, M., Schachner, M., 1988. Expression of cell adhesion molecules in the olfactory system of the adult mouse: presence of the embryonic form of N-CAM. *Dev. Biol.* 129, 516–531.

Misson, J.P., Edwards, M.A., Yamamoto, M., Caviness, V.S., 1988. Identification of radial glial cells within the developing murine central nervous system: studies based upon a new immunohistochemical marker. *Brain Res. Dev. Brain Res.* 44, 95–108.

Mitalipova, M.M., Rao, R.R., Hoyer, D.M., Johnson, J.A., Meisner, L.F., Jones, K.L., Dalton, S., Stice, S.L., 2005. Preserving the genetic integrity of human embryonic stem cells. *Nat. Biotechnol.* 23, 19–20.

Mitrovic, N., Dörries, U., Schachner, M., 1994. Expression of the extracellular matrix glycoprotein tenascin in the somatosensory cortex of the mouse during

postnatal development: an immunocytochemical and *in situ* hybridization analysis. *J. Neurocytol.* 23, 364–378.

Miyamoto, S., Teramoto, H., Coso, O.A., Gutkind, J.S., Burbelo, P.D., Akiyama, S.K., Yamada, K.M., 1995. Integrin function: molecular hierarchies of cytoskeletal and signaling molecules. *J. Cell Biol.* 131, 791–805.

Monnier, P.P., Sierra, A., Schwab, J.M., Henke-Fahle, S., Mueller, B.K., 2003. The Rho/ROCK pathway mediates neurite growth-inhibitory activity associated with the chondroitin sulfate proteoglycans of the CNS glial scar. *Mol. Cell. Neurosci.* 22, 319–330.

Montgomery, C.T., Tenaglia, E.A., Robson, J.A., 1996. Axonal growth into tubes implanted within lesions in the spinal cords of adult rats. *Exp. Neurol.* 137, 277–290.

Moreau-Fauvarque, C., Kumanogoh, A., Camand, E., Jaillard, C., Barbin, G., Boquet, I., Love, C., Jones, E.Y., Kikutani, H., Lubetzki, C., Dusart, I., Chédotal, A., 2003. The transmembrane semaphorin Sema4D/CD100, an inhibitor of axonal growth, is expressed on oligodendrocytes and upregulated after CNS lesion. *J. Neurosci.* 23, 9229–9239.

Moreno-Layseca, P., Streuli, C.H., 2014. Signalling pathways linking integrins with cell cycle progression. *Matrix Biol.* 34, 144–153.

Moser, M., Legate, K.R., Zent, R., Fässler, R., 2009. The tail of integrins, talin, and kindlins. *Science* 324, 895–899.

Mukhopadhyay, G., Doherty, P., Walsh, F.S., Crocker, P.R., Filbin, M.T., 1994. A novel role for myelin-associated glycoprotein as an inhibitor of axonal regeneration. *Neuron* 13, 757–767.

Munz, M., Rasminsky, M., Aguayo, A.J., Vidal-Sanz, M., Devor, M.G., 1985. Functional activity of rat brainstem neurons regenerating axons along peripheral nerve grafts. *Brain Res.* 340, 115–125.

Muramatsu, R., Ueno, M., Yamashita, T., 2009. Intrinsic regenerative mechanisms of central nervous system neurons. *Biosci. Trends* 3, 179–183.

Myer, D.J., Gurkoff, G.G., Lee, S.M., Hovda, D.A., Sofroniew, M.V., 2006. Essential protective roles of reactive astrocytes in traumatic brain injury. *Brain* 129, 2761–2772.

Myers, J.P., Santiago-Medina, M., Gomez, T.M., 2011. Regulation of axonal outgrowth and pathfinding by integrin-ECM interactions. *Dev. Neurobiol.* 71, 901–923.

Nakanishi, M., Niidome, T., Matsuda, S., Akaike, A., Kihara, T., Sugimoto, H., 2007. Microglia-derived interleukin-6 and leukaemia inhibitory factor promote astrocytic differentiation of neural stem/progenitor cells. *Eur. J. Neurosci.* 25, 649–658.

Naldini, L., Blömer, U., Gallay, P., Ory, D., Mulligan, R., Gage, F.H., Verma, I.M., Trono, D., 1996. *In vivo* gene delivery and stable transduction of nondividing cells by a lentiviral vector. *Science* 272, 263–267.

National Institute for Clinical Excellence. 2016. Neuroprotective pharmacological interventions. spinal injury: Assessment and initial management. NICE Guideline.No.41.

National Spinal Cord Injury Statistical Center 2017. Facts and figures at a glance. Birmingham, AL: University of Alabama at Birmingham.

Neuhuber, B., Timothy Himes, B., Shumsky, J.S., Gallo, G., Fischer, I., 2005. Axon growth and recovery of function supported by human bone marrow stromal

cells in the injured spinal cord exhibit donor variations. *Brain Res.* 1035, 73–85.

Niederöst, B., Oertle, T., Fritsche, J., McKinney, R.A., Bandtlow, C.E., 2002. Nogo-A and myelin-associated glycoprotein mediate neurite growth inhibition by antagonistic regulation of RhoA and Rac1. *J. Neurosci.* 22, 10368–10376.

Ning, K., Drepper, C., Valori, C.F., Ahsan, M., Wyles, M., Higginbottom, A., Herrmann, T., Shaw, P., Azzouz, M., Sendtner, M., 2010. PTEN depletion rescues axonal growth defect and improves survival in SMN-deficient motor neurons. *Hum. Mol. Genet.* 19, 3159–3168.

Niwa, H., Miyazaki, J., Smith, A.G., 2000. Quantitative expression of Oct-3/4 defines differentiation, dedifferentiation or self-renewal of ES cells. *Nat. Genet.* 24, 372–376.

Noctor, S.C., Flint, A.C., Weissman, T.A., Wong, W.S., Clinton, B.K., Kriegstein, A.R., 2002. Dividing precursor cells of the embryonic cortical ventricular zone have morphological and molecular characteristics of radial glia. *J. Neurosci.* 22, 3161–3173.

Nori, S., Okada, Y., Yasuda, A., Tsuji, O., Takahashi, Y., Kobayashi, Y., Fujiyoshi, K., Koike, M., Uchiyama, Y., Ikeda, E., Toyama, Y., Yamanaka, S., Nakamura, M., Okano, H., 2011. Grafted human-induced pluripotent stem-cell–derived neurospheres promote motor functional recovery after spinal cord injury in mice. *Proc. Natl. Acad. Sci. U.S.A.* 201108077.

Odawara, A., Katoh, H., Matsuda, N., Suzuki, I., 2016. Physiological maturation and drug responses of human induced pluripotent stem cell-derived cortical neuronal networks in long-term culture. *Sci. Rep.* 6, srep26181.

Ogawa, Y., Sawamoto, K., Miyata, T., Miyao, S., Watanabe, M., Nakamura, M., Bregman, B.S., Koike, M., Uchiyama, Y., Toyama, Y., Okano, H., 2002. Transplantation of *in vitro*-expanded fetal neural progenitor cells results in neurogenesis and functional recovery after spinal cord contusion injury in adult rats. *J. Neurosci. Res.* 69, 925–933.

Oh, J., McCloskey, M.A., Blong, C.C., Bendickson, L., Nilsen-Hamilton, M., Sakaguchi, D.S., 2010. Astrocyte-derived interleukin-6 promotes specific neuronal differentiation of neural progenitor cells from adult hippocampus. *J. Neurosci. Res.* 88, 2798–2809.

Ohsawa, K., Irino, Y., Nakamura, Y., Akazawa, C., Inoue, K., Kohsaka, S., 2007. Involvement of P2X4 and P2Y12 receptors in ATP-induced microglial chemotaxis. *Glia* 55, 604–616.

Ohtake, Y., Park, D., Abdul-Muneer, P.M., Li, H., Xu, B., Sharma, K., Smith, G.M., Selzer, M.E., Li, S., 2014. The effect of systemic PTEN antagonist peptides on axon growth and functional recovery after spinal cord injury. *Biomaterials* 35, 4610–4626.

Ohtaki, H., Ylostalo, J.H., Foraker, J.E., Robinson, A.P., Reger, R.L., Shioda, S., Prockop, D.J., 2008. Stem/progenitor cells from bone marrow decrease neuronal death in global ischemia by modulation of inflammatory/immune responses. *Proc. Natl. Acad. Sci. U. S. A.* 105, 14638–14643.

Olby, N.J., Blakemore, W.F., 1996. Primary demyelination and regeneration of ascending axons in the dorsal funiculus of the rat spinal cord following photochemically induced injury. *J. Neurocytol.* 25, 465–480.

Olson, J.K., Miller, S.D., 2004. Microglia initiate central nervous system innate and adaptive immune responses through multiple TLRs. *J. Immunol.* Baltim. Md 1950 173, 3916–3924.

Osaka, M., Honmou, O., Murakami, T., Nonaka, T., Houkin, K., Hamada, H., Kocsis, J.D., 2010. Intravenous administration of mesenchymal stem cells derived from bone marrow after contusive spinal cord injury improves functional outcome. *Brain Res.* 1343, 226–235.

Ostenfeld, T., Caldwell, M.A., Prowse, K.R., Linskens, M.H., Jauniaux, E., Svendsen, C.N., 2000. Human neural precursor cells express low levels of telomerase *in vitro* and show diminishing cell proliferation with extensive axonal outgrowth following transplantation. *Exp. Neurol.* 164, 215–226.

Pal, R., Venkataramana, N.K., Bansal, A., Balaraju, S., Jan, M., Chandra, R., Dixit, A., Rauthan, A., Murgod, U., Totey, S., 2009. *Ex vivo*-expanded autologous bone marrow-derived mesenchymal stromal cells in human spinal cord injury/paraplegia: A pilot clinical study. *Cytotherapy* 11, 897–911.

Palmer, E.L., Rüegg, C., Ferrando, R., Pytela, R., Sheppard, D., 1993. Sequence and tissue distribution of the integrin alpha 9 subunit, a novel partner of beta 1 that is widely distributed in epithelia and muscle. *J. Cell Biol.* 123, 1289–1297.

Park, C.-H., Minn, Y.-K., Lee, J.-Y., Choi, D.H., Chang, M.-Y., Shim, J.-W., Ko, J.-Y., Koh, H.-C., Kang, M.J., Kang, J.S., Rhie, D.-J., Lee, Y.-S., Son, H., Moon, S.Y., Kim, K.-S., Lee, S.-H., 2005. *In vitro* and *in vivo* analyses of human embryonic stem cell-derived dopamine neurons. *J. Neurochem.* 92, 1265–1276.

Park, K.K., Liu, K., Hu, Y., Smith, P.D., Wang, C., Cai, B., Xu, B., Connolly, L., Kramvis, I., Sahin, M., He, Z., 2008. Promoting axon regeneration in the adult CNS by modulation of the PTEN/mTOR pathway. *Science* 322, 963–966.

Park, K.W., Lin, C.-Y., Lee, Y.-S., 2014. Expression of Suppressor of Cytokine Signaling-3 (SOCS3) and its role in neuronal death after complete spinal cord injury. *Exp. Neurol.* 261, 65–75.

Park, K.W., Lin, C.-Y., Li, K., Lee, Y.-S., 2015. Effects of reducing suppressors of cytokine signaling-3 (SOCS3) expression on dendritic outgrowth and demyelination after spinal cord injury. *PLOS ONE* 10, e0138301.

Park, L.C.H., Zhang, H., Gibson, G.E., 2001. Co-culture with astrocytes or microglia protects metabolically impaired neurons. *Mech. Ageing Dev.* 123, 21–27.

Pasterkamp, R.J., Giger, R.J., Ruitenberg, M.J., Holtmaat, A.J., De Wit, J., De Winter, F., Verhaagen, J., 1999. Expression of the gene encoding the chemorepellent semaphorin III is induced in the fibroblast component of neural scar tissue formed following injuries of adult but not neonatal CNS. *Mol. Cell. Neurosci.* 13, 143–166.

Pasterkamp, R.J., Verhaagen, J., 2001. Emerging roles for semaphorins in neural regeneration. *Brain Res. Brain Res. Rev.* 35, 36–54.

Paul, N.R., Jacquemet, G., Caswell, P.T., 2015. Endocytic trafficking of integrins in cell migration. *Curr. Biol.* CB 25, R1092-1105.

Pearse, D.D., Pereira, F.C., Marcillo, A.E., Bates, M.L., Berrocal, Y.A., Filbin, M.T., Bunge, M.B., 2004. cAMP and Schwann cells promote axonal growth and functional recovery after spinal cord injury. *Nat. Med.* 10, 610–616.

Pearse, D.D., Sanchez, A.R., Pereira, F.C., Andrade, C.M., Puzis, R., Pressman, Y., Golden, K., Kitay, B.M., Blits, B., Wood, P.M., Bunge, M.B., 2007. Transplantation of Schwann cells and/or olfactory ensheathing glia into the

contused spinal cord: Survival, migration, axon association, and functional recovery. *Glia* 55, 976–1000. d

Perrin, F.E., Lacroix, S., Avilés-Trigueros, M., David, S., 2005. Involvement of monocyte chemoattractant protein-1, macrophage inflammatory protein-1alpha and interleukin-1beta in Wallerian degeneration. *Brain J. Neurol.* 128, 854–866.

Petit, A., Sellers, D.L., Liebl, D.J., Tessier-Lavigne, M., Kennedy, T.E., Horner, P.J., 2007. Adult spinal cord progenitor cells are repelled by netrin-1 in the embryonic and injured adult spinal cord. *Proc. Natl. Acad. Sci. U.S.A.* 104, 17837–17842.

Piltti, K.M., Avakian, S.N., Funes, G.M., Hu, A., Uchida, N., Anderson, A.J., Cummings, B.J., 2015. Transplantation dose alters the dynamics of human neural stem cell engraftment, proliferation and migration after spinal cord injury. *Stem Cell Res.* 15, 341–353.

Pluchino, S., Zanotti, L., Rossi, B., Brambilla, E., Ottoboni, L., Salani, G., Martinello, M., Cattalini, A., Bergami, A., Furlan, R., Comi, G., Constantin, G., Martino, G., 2005. Neurosphere-derived multipotent precursors promote neuroprotection by an immunomodulatory mechanism. *Nature* 436, 266–271.

Polito, A., Reynolds, R., 2005. NG2-expressing cells as oligodendrocyte progenitors in the normal and demyelinated adult central nervous system. *J. Anat.* 207, 707–716.

Previtali, S.C., Feltri, M.L., Archelos, J.J., Quattrini, A., Wrabetz, L., Hartung, H., 2001. Role of integrins in the peripheral nervous system. *Prog. Neurobiol.* 64, 35–49.

Qiu, J., Cai, D., Dai, H., McAtee, M., Hoffman, P.N., Bregman, B.S., Filbin, M.T., 2002. Spinal axon regeneration induced by elevation of cyclic AMP. *Neuron* 34, 895–903.

Radtke, C., Schmitz, B., Spies, M., Kocsis, J.D., Vogt, P.M., 2009. Peripheral glial cell differentiation from neurospheres derived from adipose mesenchymal stem cells. *Int. J. Dev. Neurosci.* 27, 817–823.

Ragan, T., Kadiri, L.R., Venkataraju, K.U., Bahlmann, K., Sutin, J., Taranda, J., Arganda-Carreras, I., Kim, Y., Seung, H.S., Osten, P., 2012. Serial two-photon tomography for automated *ex vivo* mouse brain imaging. *Nat. Methods* 9, 255–258.

Ramer, L.M., Au, E., Richter, M.W., Liu, J., Tetzlaff, W., Roskams, A.J., 2004. Peripheral olfactory ensheathing cells reduce scar and cavity formation and promote regeneration after spinal cord injury. *J. Comp. Neurol.* 473, 1–15.

Ramón-Cueto, A., Nieto-Sampedro, M., 1994. Regeneration into the spinal cord of transected dorsal root axons is promoted by ensheathing glia transplants. *Exp. Neurol.* 127, 232–244.

Ramón-Cueto, A., Nieto-Sampedro, M., 1992. Glial cells from adult rat olfactory bulb: immunocytochemical properties of pure cultures of ensheathing cells. *Neuroscience* 47, 213–220.

Ramón-Cueto, A., Plant, G.W., Avila, J., Bunge, M.B., 1998. Long-distance axonal regeneration in the transected adult rat spinal cord is promoted by olfactory ensheathing glia transplants. *J. Neurosci.* 18, 3803–3815.

Reekmans, K., De Vocht, N., Praet, J., Fransen, E., Le Blon, D., Hoornaert, C., Daans, J., Goossens, H., Van der Linden, A., Berneman, Z., Ponsaerts, P., 2012.

Spatiotemporal evolution of early innate immune responses triggered by neural stem cell grafting. *Stem Cell Res. Ther.* 3, 56.

Reichardt, L.F., Tomaselli, K.J., 1991. Extracellular matrix molecules and their receptors: Functions in neural development. *Annu. Rev. Neurosci.* 14, 531–570.

Rejc, E., Angeli, C., Harkema, S., 2015. Effects of lumbosacral spinal cord epidural stimulation for standing after chronic complete paralysis in humans. *PLOS ONE* 10, e0133998.

Renier, N., Adams, E.L., Kirst, C., Wu, Z., Azevedo, R., Kohl, J., Autry, A.E., Kadiri, L., Umadevi Venkataraju, K., Zhou, Y., Wang, V.X., Tang, C.Y., Olsen, O., Dulac, C., Osten, P., Tessier-Lavigne, M., 2016. Mapping of brain activity by automated volume analysis of immediate early genes. *Cell* 165, 1789–1802.

Reuter, V.E., 2005. Origins and molecular biology of testicular germ cell tumors. *Mod. Pathol. Off. J. U. S. Can. Acad. Pathol.* Inc 18 Suppl 2, S51-60.

Rice, D., Barone, S., 2000. Critical periods of vulnerability for the developing nervous system: evidence from humans and animal models. *Environ. Health Perspect.* 108, 511–533.

Richardson, P.M., McGuinness, U.M., Aguayo, A.J., 1980. Axons from CNS neurons regenerate into PNS grafts. *Nature* 284, 264–265.

Rigato, F., Garwood, J., Calco, V., Heck, N., Faivre-Sarrailh, C., Faissner, A., 2002. Tenascin-C promotes neurite outgrowth of embryonic hippocampal neurons through the alternatively spliced fibronectin type III BD domains via activation of the cell adhesion molecule F3/contactin. *J. Neurosci.* 22, 6596–6609.

Roberton, V.H., Evans, A.E., Harrison, D.J., Precious, S.V., Dunnett, S.B., Kelly, C.M., Rosser, A.E., 2013. Is the adult mouse striatum a hostile host for neural transplant survival? *Neuroreport* 24, 1010–1015.

Roberts, M., Barry, S., Woods, A., van der Sluijs, P., Norman, J., 2001. PDGF-regulated Rab4-dependent recycling of alphavbeta3 integrin from early endosomes is necessary for cell adhesion and spreading. *Curr. Biol.* CB 11, 1392–1402.

Rose, D.M., Liu, S., Woodside, D.G., Han, J., Schlaepfer, D.D., Ginsberg, M.H., 2003. Paxillin binding to the alpha 4 integrin subunit stimulates LFA-1 (integrin alpha L beta 2)-dependent T cell migration by augmenting the activation of focal adhesion kinase/proline-rich tyrosine kinase-2. *J. Immunol.* Baltim. Md 1950 170, 5912–5918.

Saberi, H., Firouzi, M., Habibi, Z., Moshayedi, P., Aghayan, H.R., Arjmand, B., Hosseini, K., Razavi, H.E., Yekaninejad, M.S., 2011. Safety of intramedullary Schwann cell transplantation for postrehabilitation spinal cord injuries: 2-year follow-up of 33 cases. *J. Neurosurg. Spine* 15, 515–525.

Saito, F., Nakatani, T., Iwase, M., Maeda, Y., Hirakawa, A., Murao, Y., Suzuki, Y., Onodera, R., Fukushima, M., Ide, C., 2008. Spinal cord injury treatment with intrathecal autologous bone marrow stromal cell transplantation: the first clinical trial case report. *J. Trauma* 64, 53–59.

Sanchez-Ramos, J., Song, S., Cardozo-Pelaez, F., Hazzi, C., Stedeford, T., Willing, A., Freeman, T.B., Saporta, S., Janssen, W., Patel, N., Cooper, D.R., Sanberg, P.R., 2000. Adult bone marrow stromal cells differentiate into neural cells *in vitro*. *Exp. Neurol.* 164, 247–256.

Sano, N., Shimogawa, T., Sakaguchi, H., Ioroi, Y., Miyawaki, Y., Morizane, A., Miyamoto, S., Takahashi, J., 2017. Enhanced axonal extension of subcortical

projection neurons isolated from murine embryonic cortex using neuropilin-1. *Front. Cell. Neurosci.* 11, 123.

Sasaki, M., Radtke, C., Tan, A.M., Zhao, P., Hamada, H., Houkin, K., Honmou, O., Kocsis, J.D., 2009. BDNF-hypersecreting human mesenchymal stem cells promote functional recovery, axonal sprouting, and protection of corticospinal neurons after spinal cord injury. *J. Neurosci.* 29, 14932–14941.

Sayyad, W.A., Fabris, P., Torre, V., 2016. The role of Rac1 in the growth cone dynamics and force generation of DRG neurons. PLoS ONE 11.

Schaefer, L., Babelova, A., Kiss, E., Hausser, H.-J., Baliova, M., Krzyzankova, M., Marsche, G., Young, M.F., Mihalik, D., Götte, M., Malle, E., Schaefer, R.M., Gröne, H.-J., 2005. The matrix component biglycan is proinflammatory and signals through Toll-like receptors 4 and 2 in macrophages. *J. Clin. Invest.* 115, 2223–2233.

Schaller, M.D., Hildebrand, J.D., Shannon, J.D., Fox, J.W., Vines, R.R., Parsons, J.T., 1994. Autophosphorylation of the focal adhesion kinase, pp125FAK, directs SH2-dependent binding of pp60src. *Mol. Cell. Biol.* 14, 1680–1688.

Schwaiger, F.W., Hager, G., Schmitt, A.B., Horvat, A., Hager, G., Streif, R., Spitzer, C., Gamal, S., Breuer, S., Brook, G.A., Nacimiento, W., Kreutzberg, G.W., 2000. Peripheral but not central axotomy induces changes in Janus kinases (JAK) and signal transducers and activators of transcription (STAT). *Eur. J. Neurosci.* 12, 1165–1176.

Schwartz, M.A., Assoian, R.K., 2001. Integrins and cell proliferation: regulation of cyclin-dependent kinases via cytoplasmic signaling pathways. *J. Cell Sci.* 114, 2553–2560.

Schwartz, M.A., Shattil, S.J., 2000. Signaling networks linking integrins and Rho family GTPases. *Trends Biochem. Sci.* 25, 388–391.

Schwarz, M.K., Scherbarth, A., Sprengel, R., Engelhardt, J., Theer, P., Giese, G., 2015. Fluorescent-protein stabilization and high-resolution imaging of cleared, intact mouse brains. *PloS One* 10, e0124650.

Schweigreiter, R., Bandtlow, C.E., 2006. Nogo in the injured spinal cord. *J. Neurotrauma* 23, 384–396.

Schweitzer, J., Becker, T., Lefebvre, J., Granato, M., Schachner, M., Becker, C.G., 2005. Tenascin-C is involved in motor axon outgrowth in the trunk of developing zebrafish. *Dev. Dyn. Off. Publ. Am. Assoc. Anat.* 234, 550–566.

See, J., Bonner, J., Neuhuber, B., Fischer, I., 2010. Neurite outgrowth of neural progenitors in presence of inhibitory proteoglycans. *J. Neurotrauma* 27, 951–957.

Seiriki, K., Kasai, A., Hashimoto, T., Schulze, W., Niu, M., Yamaguchi, S., Nakazawa, T., Inoue, K., Uezono, S., Takada, M., Naka, Y., Igarashi, H., Tanuma, M., Waschek, J.A., Ago, Y., Tanaka, K.F., Hayata-Takano, A., Nagayasu, K., Shintani, N., Hashimoto, R., Kunii, Y., Hino, M., Matsumoto, J., Yabe, H., Nagai, T., Fujita, K., Matsuda, T., Takuma, K., Baba, A., Hashimoto, H., 2017. High-speed and scalable whole-brain imaging in rodents and primates. *Neuron* 94, 1085–1100.e6.

Sharp, J., Frame, J., Siegenthaler, M., Nistor, G., Keirstead, H.S., 2010. Human embryonic stem cell-derived oligodendrocyte progenitor cell transplants improve recovery after cervical spinal cord injury. *Stem Cells* Dayt. Ohio 28, 152–163.

Shen, L.H., Li, Y., Chen, J., Zhang, J., Vanguri, P., Borneman, J., Chopp, M., 2006. Intracarotid transplantation of bone marrow stromal cells increases axon-myelin remodeling after stroke. *Neuroscience* 137, 393–399.

Shen, Y., Tenney, A.P., Busch, S.A., Horn, K.P., Cuascut, F.X., Liu, K., He, Z., Silver, J., Flanagan, J.G., 2009. PTPσ is a receptor for chondroitin sulfate proteoglycan, an inhibitor of neural regeneration. *Science* 326, 592–596.

Sheppard, A.M., Hamilton, S.K., Pearlman, A.L., 1991. Changes in the distribution of extracellular matrix components accompany early morphogenetic events of mammalian cortical development. *J. Neurosci.* 11, 3928–3942.

Sher, F., van Dam, G., Boddeke, E., Copray, S., 2009. Bioluminescence imaging of Olig2-neural stem cells reveals improved engraftment in a demyelination mouse model. *Stem Cells* Dayt. Ohio 27, 1582–1591.

Shi, Y., Kirwan, P., Livesey, F.J., 2012a. Directed differentiation of human pluripotent stem cells to cerebral cortex neurons and neural networks. *Nat. Protoc.* 7, 1836–1846.

Shi, Y., Kirwan, P., Smith, J., Robinson, H.P.C., Livesey, F.J., 2012b. Human cerebral cortex development from pluripotent stem cells to functional excitatory synapses. *Nat. Neurosci.* 15, 477–486.

Shields, S.A., Blakemore, W.F., Franklin, R.J., 2000. Schwann cell remyelination is restricted to astrocyte-deficient areas after transplantation into demyelinated adult rat brain. *J. Neurosci. Res.* 60, 571–578.

Silver, J., Miller, J.H., 2004. Regeneration beyond the glial scar. *Nat. Rev. Neurosci.* 5, 146–156.

Smith, L.L., Cheung, H.K., Ling, L.E., Chen, J., Sheppard, D., Pytela, R., Giachelli, C.M., 1996. Osteopontin N-terminal domain contains a cryptic adhesive sequence recognized by alpha9beta1 integrin. *J. Biol. Chem*. 271, 28485–28491.

Smith, P.D., Sun, F., Park, K.K., Cai, B., Wang, C., Kuwako, K., Martinez-Carrasco, I., Connolly, L., He, Z., 2009. SOCS3 deletion promotes optic nerve regeneration *in vivo*. *Neuron* 64, 617–623.

Solomon, S., Pitossi, F., Rao, M.S., 2015. Banking on iPSC--is it doable and is it worthwhile. *Stem Cell Rev.* 11, 1–10.

Song, S.-W., Chang, W., Song, B.-W., Song, H., Lim, S., Kim, H.-J., Cha, M.-J., Choi, E., Im, S.-H., Chang, B.-C., Chung, N., Jang, Y., Hwang, K.-C., 2009. Integrin-linked kinase is required in hypoxic mesenchymal stem cells for strengthening cell adhesion to ischemic myocardium. *Stem Cells* Dayt. Ohio 27, 1358–1365.

Song, X.-Y., Li, F., Zhang, F.-H., Zhong, J.-H., Zhou, X.-F., 2008. Peripherally-derived BDNF promotes regeneration of ascending sensory neurons after spinal cord injury. *PloS One* 3, e1707.

Sontag, C.J., Uchida, N., Cummings, B.J., Anderson, A.J., 2014. Injury to the spinal cord niche alters the engraftment dynamics of human neural stem cells. *Stem Cell Rep.* 2, 620–632.

Sparling, J.S., Bretzner, F., Biernaskie, J., Assinck, P., Jiang, Y., Arisato, H., Plunet, W.T., Borisoff, J., Liu, J., Miller, F.D., Tetzlaff, W., 2015. Schwann cells generated from neonatal skin-derived precursors or neonatal peripheral nerve improve functional recovery after acute transplantation into the partially injured cervical spinal cord of the rat. *J. Neurosci.* 35, 6714–6730.

Spinal Research UK. 2016. *Spinal Research* [ONLINE] Available at: https://www.spinal-research.org. [Accessed 27 September 2017].

Stacpoole, S.R.L., Bilican, B., Webber, D.J., Luzhynskaya, A., He, X.L., Compston, A., Karadottir, R., Franklin, R.J.M., Chandran, S., 2011. Derivation of neural precursor cells from human ES cells at 3% O(2) is efficient, enhances survival and presents no barrier to regional specification and functional differentiation. *Cell Death Differ.* 18, 1016–1023.

Staniszewska, I., Sariyer, I.K., Lecht, S., Brown, M.C., Walsh, E.M., Tuszynski, G.P., Safak, M., Lazarovici, P., Marcinkiewicz, C., 2008. Integrin α9β1 is a receptor for nerve growth factor and other neurotrophins. *J. Cell Sci.* 121, 504–513.

Staniszewska, I., Zaveri, S., Del Valle, L., Oliva, I., Rothman, V.L., Croul, S.E., Roberts, D.D., Mosher, D.F., Tuszynski, G.P., Marcinkiewicz, C., 2007. Interaction of alpha9beta1 integrin with thrombospondin-1 promotes angiogenesis. *Circ. Res.* 100, 1308–1316.

Steinberg, G.K., Kondziolka, D., Wechsler, L.R., Lunsford, L.D., Coburn, M.L., Billigen, J.B., Kim, A.S., Johnson, J.N., Bates, D., King, B., Case, C., McGrogan, M., Yankee, E.W., Schwartz, N.E., 2016. Clinical outcomes of transplanted modified bone marrow–derived mesenchymal stem cells in stroke: A phase 1/2a study. *Stroke* 116, 012995.

Steward, O., Sharp, K.G., Yee, K.M., Hatch, M.N., Bonner, J.F., 2014. Characterization of ectopic colonies that form in widespread areas of the nervous system with neural stem cell transplants into the site of a severe spinal cord injury. *J. Neurosci.* 34, 14013–14021.

Stout, R.D., Jiang, C., Matta, B., Tietzel, I., Watkins, S.K., Suttles, J., 2005. Macrophages sequentially change their functional phenotype in response to changes in microenvironmental influences. *J. Immunol.* Baltim. Md 1950 175, 342–349.

Strekalova, T., Sun, M., Sibbe, M., Evers, M., Dityatev, A., Gass, P., Schachner, M., 2002. Fibronectin domains of extracellular matrix molecule tenascin-C modulate hippocampal learning and synaptic plasticity. *Mol. Cell. Neurosci.* 21, 173–187.

Sun, F., Park, K.K., Belin, S., Wang, D., Lu, T., Chen, G., Zhang, K., Yeung, C., Feng, G., Yankner, B.A., He, Z., 2011. Sustained axon regeneration induced by co-deletion of PTEN and SOCS3. *Nature* 480, 372–375.

Sun, Y., Xu, C.-C., Li, J., Guan, X.-Y., Gao, L., Ma, L.-X., Li, R.-X., Peng, Y.-W., Zhu, G.-P., 2013. Transplantation of oligodendrocyte precursor cells improves locomotion deficits in rats with spinal cord irradiation injury. *PloS One* 8, e57534.

Suzuki, A., Stern, S.A., Bozdagi, O., Huntley, G.W., Walker, R.H., Magistretti, P.J., Alberini, C.M., 2011. Astrocyte-neuron lactate transport is required for long-term memory formation. *Cell* 144, 810–823.

Tabakow, P., Jarmundowicz, W., Czapiga, B., Fortuna, W., Miedzybrodzki, R., Czyz, M., Huber, J., Szarek, D., Okurowski, S., Szewczyk, P., Gorski, A., Raisman, G., 2013. Transplantation of autologous olfactory ensheathing cells in complete human spinal cord injury. *Cell Transplant.* 22, 1591–1612.

Tabakow, P., Raisman, G., Fortuna, W., Czyz, M., Huber, J., Li, D., Szewczyk, P., Okurowski, S., Miedzybrodzki, R., Czapiga, B., Salomon, B., Halon, A., Li, Y., Lipiec, J., Kulczyk, A., Jarmundowicz, W., 2014. Functional regeneration of supraspinal connections in a patient with transected spinal cord following transplantation of bulbar olfactory ensheathing cells with peripheral nerve bridging. *Cell Transplant.* 23, 1631–1655.

Takagi, J., Petre, B.M., Walz, T., Springer, T.A., 2002. Global conformational rearrangements in integrin extracellular domains in outside-in and inside-out signaling. *Cell* 110, 599–511.

Takahashi, K., Tanabe, K., Ohnuki, M., Narita, M., Ichisaka, T., Tomoda, K., Yamanaka, S., 2007. Induction of pluripotent stem cells from adult human fibroblasts by defined factors. *Cell* 131, 861–872.

Takahashi, K., Yamanaka, S., 2006. Induction of pluripotent stem cells from mouse embryonic and adult fibroblast cultures by defined factors. *Cell* 126, 663–676.

Takahashi, Y., Tsuji, O., Kumagai, G., Hara, C.M., Okano, H.J., Miyawaki, A., Toyama, Y., Okano, H., Nakamura, M., 2011. Comparative study of methods for administering neural stem/progenitor cells to treat spinal cord injury in mice. *Cell Transplant.* 20, 727–739.

Takami, T., Oudega, M., Bates, M.L., Wood, P.M., Kleitman, N., Bunge, M.B., 2002. Schwann cell but not olfactory ensheathing glia transplants improve hindlimb locomotor performance in the moderately contused adult rat thoracic spinal cord. *J. Neurosci.* 22, 6670–6681.

Tan, C.L., Andrews, M.R., Kwok, J.C.F., Heintz, T.G.P., Gumy, L.F., Fässler, R., Fawcett, J.W., 2012. Kindlin-1 enhances axon growth on inhibitory chondroitin sulfate proteoglycans and promotes sensory axon regeneration. *J. Neurosci.* 32, 7325–7335.

Tan, C.L., Kwok, J.C.F., Patani, R., Chandran, S., Fawcett, J.W., 2011. Integrin activation promotes axon growth on inhibitory CSPGs by enhancing integrin signaling. *J. Neurosci.* 31, 6289–6295.

Tang, X., Davies, J.E., Davies, S.J.A., 2003. Changes in distribution, cell associations, and protein expression levels of NG2, neurocan, phosphacan, brevican, versican V2, and tenascin-C during acute to chronic maturation of spinal cord scar tissue. *J. Neurosci. Res.* 71, 427–444.

Taooka, Y., Chen, J., Yednock, T., Sheppard, D., 1999. The integrin alpha9beta1 mediates adhesion to activated endothelial cells and transendothelial neutrophil migration through interaction with vascular cell adhesion molecule-1. *J. Cell Biol.* 145, 413–420.

Tarui, T., Miles, L.A., Takada, Y., 2001. Specific interaction of angiostatin with integrin alpha(v)beta(3) in endothelial cells. *J. Biol. Chem.* 276, 39562–39568.

Tennstaedt, A., Aswendt, M., Adamczak, J., Collienne, U., Selt, M., Schneider, G., Henn, N., Schaefer, C., Lagouge, M., Wiedermann, D., Kloppenburg, P., Hoehn, M., 2015a. Human neural stem cell intracerebral grafts show spontaneous early neuronal differentiation after several weeks. *Biomaterials* 44, 143–154.

Tennstaedt, A., Mastropietro, A., Nelles, M., Beyrau, A., Hoehn, M., 2015b. *In Vivo* fate imaging of intracerebral stem cell grafts in mouse brain. *PloS One* 10, e0144262.

Termeer, C., Benedix, F., Sleeman, J., Fieber, C., Voith, U., Ahrens, T., Miyake, K., Freudenberg, M., Galanos, C., Simon, J.C., 2002. Oligosaccharides of hyaluronan activate dendritic cells via toll-like receptor 4. *J. Exp. Med.* 195, 99–111.

Tetzlaff, W., Okon, E.B., Karimi-Abdolrezaee, S., Hill, C.E., Sparling, J.S., Plemel, J.R., Plunet, W.T., Tsai, E.C., Baptiste, D., Smithson, L.J., Kawaja, M.D., Fehlings, M.G., Kwon, B.K., 2011. A systematic review of cellular

transplantation therapies for spinal cord injury. *J. Neurotrauma* 28, 1611–1682.

Thomson, J.A., Itskovitz-Eldor, J., Shapiro, S.S., Waknitz, M.A., Swiergiel, J.J., Marshall, V.S., Jones, J.M., 1998. Embryonic stem cell lines derived from human blastocysts. *Science* 282, 1145–1147.

Tirkkonen, M., Tanner, M., Karhu, R., Kallioniemi, A., Isola, J., Kallioniemi, O.P., 1998. Molecular cytogenetics of primary breast cancer by CGH. *Genes. Chromosomes Cancer* 21, 177–184.

Tomer, R., Ye, L., Hsueh, B., Deisseroth, K., 2014. Advanced CLARITY for rapid and high-resolution imaging of intact tissues. *Nat. Protoc.* 9, 1682–1697.

Tonge, D.A., de Burgh, H.T., Docherty, R., Humphries, M.J., Craig, S.E., Pizzey, J., 2012. Fibronectin supports neurite outgrowth and axonal regeneration of adult brain neurons *in vitro*. *Brain Res.* 1453, 8–16.

Tornero, D., Wattananit, S., Grønning Madsen, M., Koch, P., Wood, J., Tatarishvili, J., Mine, Y., Ge, R., Monni, E., Devaraju, K., Hevner, R.F., Brüstle, O., Lindvall, O., Kokaia, Z., 2013. Human induced pluripotent stem cell-derived cortical neurons integrate in stroke-injured cortex and improve functional recovery. Brain J. Neurol. 136, 3561–3577.

Totoiu, M.O., Keirstead, H.S., 2005. Spinal cord injury is accompanied by chronic progressive demyelination. *J. Comp. Neurol.* 486, 373–383.

Toyama, K., Honmou, O., Harada, K., Suzuki, J., Houkin, K., Hamada, H., Kocsis, J.D., 2009. Therapeutic benefits of angiogenetic gene-modified human mesenchymal stem cells after cerebral ischemia. *Exp. Neurol.* 216, 47–55.

Trahanas, D.M., Cuda, C.M., Perlman, H., Schwulst, S.J., 2015. Differential activation of infiltrating monocyte-derived cells after mild and severe traumatic brain injury. *Shock Augusta Ga* 43, 255–260.

Trivedi, A., Olivas, A.D., Noble-Haeusslein, L.J., 2006. Inflammation and spinal cord injury: Infiltrating leukocytes as determinants of injury and repair processes. *Clin. Neurosci. Res.* 6, 283–292.

Uhlin-Hansen, L., Wik, T., Kjellen, L., Berg, E., Forsdahl, F., Kolset, S.O., 1993. Proteoglycan metabolism in normal and inflammatory human macrophages. *Blood* 82, 2880–2889.

Ullian, E.M., Harris, B.T., Wu, A., Chan, J.R., Barres, B.A., 2004. Schwann cells and astrocytes induce synapse formation by spinal motor neurons in culture. *Mol. Cell. Neurosci.* 25, 241–251.

Ullian, E.M., Sapperstein, S.K., Christopherson, K.S., Barres, B.A., 2001. Control of synapse number by glia. *Science* 291, 657–661.

Ussar, S., Wang, H.-V., Linder, S., Fässler, R., Moser, M., 2006. The Kindlins: Subcellular localisation and expression during murine development. *Exp. Cell Res*. 312, 3142–3151.

Vachon, P.H., 2011. Integrin signaling, cell survival, and anoikis: Distinctions, differences, and differentiation. *J. Signal Transduct.* Vol. 2011, 738137

Vallières, N., Berard, J.L., David, S., Lacroix, S., 2006. Systemic injections of lipopolysaccharide accelerates myelin phagocytosis during Wallerian degeneration in the injured mouse spinal cord. *Glia* 53, 103–113.

Vavrek, R., Pearse, D.D., Fouad, K., 2007. Neuronal populations capable of regeneration following a combined treatment in rats with spinal cord transection. *J. Neurotrauma* 24, 1667–1673.

Venkataramana, N.K., Kumar, S.K.V., Balaraju, S., Radhakrishnan, R.C., Bansal, A., Dixit, A., Rao, D.K., Das, M., Jan, M., Gupta, P.K., Totey, S.M., 2010. Open-labeled study of unilateral autologous bone-marrow-derived mesenchymal stem cell transplantation in Parkinson's disease. *Transl. Res. J. Lab. Clin. Med*. 155, 62–70.

Vlahakis, N.E., Young, B.A., Atakilit, A., Hawkridge, A.E., Issaka, R.B., Boudreau, N., Sheppard, D., 2007. Integrin alpha9beta1 directly binds to vascular endothelial growth factor (VEGF)-A and contributes to VEGF-A-induced angiogenesis. *J. Biol. Chem.* 282, 15187–15196.

Vlahakis, N.E., Young, B.A., Atakilit, A., Sheppard, D., 2005. The lymphangiogenic vascular endothelial growth factors VEGF-C and -D are ligands for the integrin alpha9beta1. *J. Biol. Chem.* 280, 4544–4552.

Vogelezang, M.G., Liu, Z., Relvas, J.B., Raivich, G., Scherer, S.S., ffrench-Constant, C., 2001. α4 Integrin Is Expressed during peripheral nerve regeneration and enhances neurite outgrowth. *J. Neurosci.* 21, 6732–6744.

von Zglinicki, T., Pilger, R., Sitte, N., 2000. Accumulation of single-strand breaks is the major cause of telomere shortening in human fibroblasts. *Free Radic. Biol. Med.* 28, 64–74.

Walz, W., 2000. Role of astrocytes in the clearance of excess extracellular potassium. *Neurochem. Int.* 36, 291–300.

Wang, H., Katagiri, Y., McCann, T.E., Unsworth, E., Goldsmith, P., Yu, Z.-X., Tan, F., Santiago, L., Mills, E.M., Wang, Y., Symes, A.J., Geller, H.M., 2008. Chondroitin-4-sulfation negatively regulates axonal guidance and growth. *J Cell Sci* 121, 3083–3091.

Wang, K.C., Koprivica, V., Kim, J.A., Sivasankaran, R., Guo, Y., Neve, R.L., He, Z., 2002. Oligodendrocyte-myelin glycoprotein is a Nogo receptor ligand that inhibits neurite outgrowth. *Nature* 417, 941–944.

Wang, Y., Bai, Y., Li, X., Hu, Q., Lin, C., Xiao, Z., Liu, Y., Xu, J., Shen, L., Li, L., 2004. Fetal human neural progenitors can be the target for tumor transformation. *Neuroreport* 15, 1907–1912.

Wang, Y., Zhao, Z., Rege, S.V., Wang, M., Si, G., Zhou, Y., Wang, S., Griffin, J.H., Goldman, S.A., Zlokovic, B.V., 2016. 3K3A-activated protein C stimulates postischemic neuronal repair by human neural stem cells in mice. *Nat. Med.* 22(9):1050-5

Wanigasekara, Y., Keast, J.R., 2006. Nerve growth factor, glial cell line–derived neurotrophic factor and neurturin prevent semaphorin 3A–mediated growth cone collapse in adult sensory neurons. *Neuroscience* 142, 369–379.

Wanner, I.B., Anderson, M.A., Song, B., Levine, J., Fernandez, A., Gray-Thompson, Z., Ao, Y., Sofroniew, M.V., 2013. Glial scar borders are formed by newly proliferated, elongated astrocytes that interact to corral inflammatory and fibrotic cells via STAT3-dependent mechanisms after spinal cord injury. *J. Neurosci.* 33, 12870–12886.

Waxman, S.G., 2010. Chapter 13. Control of Movement, in: *Clinical Neuroanatomy.* The McGraw-Hill Companies, New York, NY.

Wegener, K.L., Partridge, A.W., Han, J., Pickford, A.R., Liddington, R.C., Ginsberg, M.H., Campbell, I.D., 2007. Structural basis of integrin activation by talin. *Cell* 128, 171–182.

Weidner, N., Ner, A., Salimi, N., Tuszynski, M.H., 2001. Spontaneous corticospinal axonal plasticity and functional recovery after adult central nervous system injury. *Proc. Natl. Acad. Sci. U. S. A.* 98, 3513–3518.

Welniarz, Q., Dusart, I., Gallea, C., Roze, E., 2015. One hand clapping: lateralization of motor control. *Front. Neuroanat.* 9:75.

Werner, A., Willem, M., Jones, L.L., Kreutzberg, G.W., Mayer, U., Raivich, G., 2000. Impaired axonal regeneration in α7 integrin-deficient mice. *J. Neurosci.* 20, 1822–1830.

Wictorin, K., Björklund, A., 1992. Axon outgrowth from grafts of human embryonic spinal cord in the lesioned adult rat spinal cord. *Neuroreport* 3, 1045–1048.

Willis, D., Li, K.W., Zheng, J.-Q., Chang, J.H., Smit, A.B., Smit, A., Kelly, T., Merianda, T.T., Sylvester, J., van Minnen, J., Twiss, J.L., 2005. Differential transport and local translation of cytoskeletal, injury-response, and neurodegeneration protein mRNAs in axons. *J. Neurosci.* 25, 778–791.

Willson, C.A., Irizarry-Ramírez, M., Gaskins, H.E., Cruz-Orengo, L., Figueroa, J.D., Whittemore, S.R., Miranda, J.D., 2002. Upregulation of EphA receptor expression in the injured adult rat spinal cord. *Cell Transplant.* 11, 229–239.

Willson, C.A., Miranda, J.D., Foster, R.D., Onifer, S.M., Whittemore, S.R., 2003. Transection of the adult rat spinal cord upregulates EphB3 receptor and ligand expression. *Cell Transplant.* 12, 279–290.

Winton, M.J., Dubreuil, C.I., Lasko, D., Leclerc, N., McKerracher, L., 2002. Characterization of new cell permeable C3-like proteins that inactivate Rho and stimulate neurite outgrowth on inhibitory substrates. *J. Biol. Chem.* 277, 32820–32829.

Woodbury, D., Schwarz, E.J., Prockop, D.J., Black, I.B., 2000. Adult rat and human bone marrow stromal cells differentiate into neurons. *J. Neurosci. Res.* 61, 364–370.

Woodhall, E., West, A.K., Chuah, M.I., 2001. Cultured olfactory ensheathing cells express nerve growth factor, brain-derived neurotrophic factor, glia cell line-derived neurotrophic factor and their receptors. *Brain Res. Mol. Brain Res.* 88, 203–213.

Woods, A.J., White, D.P., Caswell, P.T., Norman, J.C., 2004. PKD1/PKCmu promotes alphavbeta3 integrin recycling and delivery to nascent focal adhesions. *EMBO J.* 23, 2531–2543.

Wu, V.W., Schwartz, J.P., 1998. Cell culture models for reactive gliosis: New perspectives. *J. Neurosci. Res.* 51, 675–681.

Xiong, J.-P., Stehle, T., Goodman, S.L., Arnaout, M.A., 2003. New insights into the structural basis of integrin activation. *Blood* 102, 1155–1159.

Xiong, L.-L., Liu, F., Lu, B.-T., Zhao, W.-L., Dong, X.-J., Liu, J., Zhang, R.-P., Zhang, P., Wang, T.-H., 2017. Bone marrow mesenchymal stem-cell transplantation promotes functional improvement associated with CNTF-STAT3 activation after hemi-sectioned spinal cord injury in tree shrews. *Front. Cell. Neurosci.* 11, 172.

Xu, X.M., Chen, A., Guénard, V., Kleitman, N., Bunge, M.B., 1997. Bridging Schwann cell transplants promote axonal regeneration from both the rostral and caudal stumps of transected adult rat spinal cord. *J. Neurocytol.* 26, 1–16.

Xu, X.M., Guénard, V., Kleitman, N., Aebischer, P., Bunge, M.B., 1995. A combination of BDNF and NT-3 promotes supraspinal axonal regeneration

into Schwann cell grafts in adult rat thoracic spinal cord. *Exp. Neurol.* 134, 261–272.

Yamout, B., Hourani, R., Salti, H., Barada, W., El-Hajj, T., Al-Kutoubi, A., Herlopian, A., Baz, E.K., Mahfouz, R., Khalil-Hamdan, R., Kreidieh, N.M.A., El-Sabban, M., Bazarbachi, A., 2010. Bone marrow mesenchymal stem cell transplantation in patients with multiple sclerosis: a pilot study. *J. Neuroimmunol.* 227, 185–189.

Yang, L., Blumbergs, P.C., Jones, N.R., Manavis, J., Sarvestani, G.T., Ghabriel, M.N., 2004. Early expression and cellular localisation of proinflammatory cytokines interleukin-1beta, interleukin-6, and tumor necrosis factor-alpha in human traumatic spinal cord injury. *Spine* 29, 966–971.

Yi, J.-H., Katagiri, Y., Susarla, B., Figge, D., Symes, A.J., Geller, H.M., 2012. Alterations in sulfated chondroitin glycosaminoglycans following controlled cortical impact injury in mice. *J. Comp. Neurol.* 520, 3295–3313.

Yin, Y., Cui, Q., Li, Y., Irwin, N., Fischer, D., Harvey, A.R., Benowitz, L.I., 2003. Macrophage-derived factors stimulate optic nerve regeneration. *J. Neurosci.* 23, 2284–2293.

Yokosaki, Y., Matsuura, N., Higashiyama, S., Murakami, I., Obara, M., Yamakido, M., Shigeto, N., Chen, J., Sheppard, D., 1998. Identification of the ligand binding site for the integrin α9β1 in the third fibronectin type iii repeat of tenascin-C. *J. Biol. Chem.* 273, 11423–11428.

Yokosaki, Y., Palmer, E.L., Prieto, A.L., Crossin, K.L., Bourdon, M.A., Pytela, R., Sheppard, D., 1994. The integrin alpha 9 beta 1 mediates cell attachment to a non-RGD site in the third fibronectin type III repeat of tenascin. *J. Biol. Chem*. 269, 26691–26696.

Yoon, S.H., Shim, Y.S., Park, Y.H., Chung, J.K., Nam, J.H., Kim, M.O., Park, H.C., Park, S.R., Min, B.-H., Kim, E.Y., Choi, B.H., Park, H., Ha, Y., 2007. Complete spinal cord injury treatment using autologous bone marrow cell transplantation and bone marrow stimulation with granulocyte macrophage-colony stimulating factor: Phase I/II clinical trial. *Stem Cells* Dayt. Ohio 25, 2066–2073.

Young, B.A., Taooka, Y., Liu, S., Askins, K.J., Yokosaki, Y., Thomas, S.M., Sheppard, D., 2001. The cytoplasmic domain of the integrin alpha9 subunit requires the adaptor protein paxillin to inhibit cell spreading but promotes cell migration in a paxillin-independent manner. *Mol. Biol. Cell* 12, 3214–3225.

Young, W., Koreh, I., 1986. Potassium and calcium changes in injured spinal cords. Brain Res. 365, 42–53.

Zhang, K., Chen, J., 2012. The regulation of integrin function by divalent cations. *Cell Adhes. Migr.* 6, 20–29.

Zhang, S., Huang, F., Gates, M., Holmberg, E.G., 2013. Role of endogenous Schwann cells in tissue repair after spinal cord injury. *Neural Regen. Res.* 8, 177–185.

Zhang, X., Jiang, G., Cai, Y., Monkley, S.J., Critchley, D.R., Sheetz, M.P., 2008. Talin depletion reveals independence of initial cell spreading from integrin activation and traction. *Nat. Cell Biol.* 10, 1062–1068.

Zhang, Y., Wang, H., 2012. Integrin signalling and function in immune cells. *Immunology* 135, 268–275.

Zhang, Y., Winterbottom, J.K., Schachner, M., Lieberman, A.R., Anderson, P.N., 1997. Tenascin-C expression and axonal sprouting following injury to the spinal dorsal columns in the adult rat. *J. Neurosci. Res.* 49, 433–450.

Zhao, C., Wu, N., Deng, F., Zhang, H., Wang, N., Zhang, W., Chen, X., Wen, S., Zhang, J., Yin, L., Liao, Z., Zhang, Z., Zhang, Q., Yan, Z., Liu, W., Wu, D., Ye, J., Deng, Y., Zhou, G., Luu, H.H., Haydon, R.C., Si, W., He, T.-C., 2014. Adenovirus-mediated gene transfer in mesenchymal stem cells can be significantly enhanced by the cationic polymer polybrene. *PLoS ONE* 9.

Zhao, R.-R., Andrews, M.R., Wang, D., Warren, P., Gullo, M., Schnell, L., Schwab, M.E., Fawcett, J.W., 2013. Combination treatment with anti-Nogo-A and chondroitinase ABC is more effective than single treatments at enhancing functional recovery after spinal cord injury. *Eur. J. Neurosci.* 38, 2946–2961.

Zhao, R.-R., Muir, E.M., Alves, J.N., Rickman, H., Allan, A.Y., Kwok, J.C., Roet, K.C.D., Verhaagen, J., Schneider, B.L., Bensadoun, J.-C., Ahmed, S.G., Yáñez-Muñoz, R.J., Keynes, R.J., Fawcett, J.W., Rogers, J.H., 2011. Lentiviral vectors express chondroitinase ABC in cortical projections and promote sprouting of injured corticospinal axons. *J. Neurosci. Methods* 201, 228–238.

Zhao, X., Guan, J.-L., 2011. Focal adhesion kinase and its signaling pathways in cell migration and angiogenesis. *Adv. Drug Deliv. Rev.* 63, 610–615.

Zhou, F.-W., Fortin, J.M., Chen, H.-X., Martinez-Diaz, H., Chang, L.-J., Reynolds, B.A., Roper, S.N., 2015. Functional integration of human neural precursor cells in mouse cortex. *PLOS ONE* 10, e0120281.

Zhu, H., Lensch, M.W., Cahan, P., Daley, G.Q., 2011. Investigating monogenic and complex diseases with pluripotent stem cells. *Nat. Rev. Genet.* 12, 266–275.

Appendix

Appendix A: Neurite outgrowth assays from hNPCs

Table 1: hNPC neurite outgrowth: chicken 10 µg/mL TN-C

n=1			n=2			n=3		
alpha9	GFP	WT	alpha9	GFP	WT	alpha9	GFP	WT
284.20	47.10	40.14	481.84	57.86	90.21	443.26	54.71	34.96
130.73	65.19	22.74	354.35	35.80	69.17	165.12	22.34	65.40
178.94	39.73	21.69	295.62	121.29	52.94	176.11	41.05	26.78
149.12	62.04	24.32	155.29	36.63	60.32	336.06	28.79	48.36
170.85	67.51	21.66	331.85	75.91	53.59	161.72	56.66	44.73
114.36	56.89	18.47	230.95	52.90	81.20	207.52	48.18	38.45
137.68	76.16	25.62	134.90	40.14	35.86	168.64	38.04	39.59
163.63	56.41	30.59	111.88	37.10	46.23	179.06	29.66	32.04
186.79	58.76	21.52	212.46	55.94	26.95	267.47	54.01	63.03
144.90	41.28	18.84	92.30	46.46	45.99	308.53	45.95	50.15
174.22	45.81	38.87	253.60	33.70	29.52	248.24	39.17	25.01
251.63	42.09	59.71	149.55	39.47	74.73	149.02	39.26	26.00
234.57	72.09	13.17	145.85	41.60	48.13	275.75	56.14	60.35
156.00	63.11	28.49	1017.26	37.93	50.21	198.78	32.62	47.78
137.89	68.78	36.37	427.24	35.30	50.44	226.49	36.54	27.47
135.16	59.91	103.44	414.07	53.38	46.71	158.99	34.53	19.88
139.53	51.66	49.24	405.14	38.90	47.61	167.08	28.52	31.21
202.34	28.11	105.54	554.94	43.64	33.13	172.84	42.86	53.58
156.79	100.22	56.70	202.37	41.72	32.18	179.60	47.67	22.39
96.10	71.96	23.72	238.62	45.60	63.13	128.46	69.32	39.42
257.57	65.64	44.86	183.33	40.84	53.90	208.71	29.83	77.92
117.84	42.53	44.20	175.41	47.38	39.34	623.62	34.59	42.59
118.18	59.79	48.30	178.86	27.59	33.39	273.90	32.38	34.29
228.65	32.40	56.87	234.94	40.61	44.60	203.75	28.32	20.53
89.85	37.61	25.21	306.72	46.70	44.32	137.00	54.84	30.86
128.06	97.36	47.60	222.53	55.61	41.78	184.80	39.66	57.84
150.00	55.55	15.78	145.19	48.48	44.74	176.10	24.40	19.93
79.20	33.89	58.39	108.83	24.98	67.22	228.09	93.96	27.35
182.83	29.53	35.61	258.41	72.51	37.13	281.75	41.53	31.42
108.79	42.06	27.68	357.30	52.97	34.66	142.10	84.07	52.34

n=4			n=5			n=6		
alpha9	GFP	WT	alpha9	GFP	WT	alpha9	GFP	WT
195.66	48.28	42.97	103.81	59.03	106.93	274.13	135.02	41.27
261.55	71.74	61.57	239.04	104.62	79.71	455.68	59.28	65.37
229.64	76.63	79.63	106.29	88.29	40.42	202.97	55.36	75.11
132.55	38.60	58.28	194.01	37.61	84.43	151.32	35.85	39.43
94.04	46.77	88.53	111.68	39.35	47.92	120.43	64.15	27.84
113.41	79.94	97.83	169.42	112.10	82.51	115.09	59.88	62.62
260.24	48.68	37.05	107.54	86.13	72.70	128.96	61.01	66.28
227.77	75.30	55.02	109.11	48.97	62.32	154.57	37.71	54.18
177.16	79.43	53.24	118.89	54.80	34.03	384.47	89.31	51.25
148.00	49.50	54.93	70.81	112.77	89.50	376.18	50.56	47.79
158.06	43.66	78.37	151.52	28.16	81.53	147.15	42.07	72.59
123.46	46.48	54.56	161.79	44.01	84.64	115.20	53.51	44.37
103.59	42.10	26.76	149.84	51.80	72.89	331.31	53.10	47.17
138.94	55.67	42.78	175.56	47.78	51.86	147.33	65.02	59.58
182.48	75.01	44.69	183.34	40.35	65.61	159.06	64.26	47.88
116.01	23.58	76.64	203.82	54.81	54.13	163.04	77.50	83.77
160.91	37.57	41.50	120.71	100.68	61.71	244.73	87.49	49.66
80.53	69.88	57.79	140.09	49.15	53.45	201.20	104.04	33.60
182.82	38.93	106.42	172.61	37.16	54.22	170.89	75.94	77.57
174.66	30.69	66.33	138.72	44.95	38.58	136.66	53.85	77.00
99.65	97.22	63.34	208.90	143.97	65.74	142.80	44.45	38.92
195.40	48.25	94.42	162.44	95.38	57.89	113.67	76.23	56.70
125.71	73.88	54.15	183.10	57.95	75.50	149.93	72.42	55.71
138.27	57.26	71.27	140.46	33.18	40.19	166.88	49.78	63.36
137.03	89.64	59.92	152.65	39.81	60.84	262.30	68.97	39.72
169.71	38.58	70.48	184.04	32.24	73.16	337.47	45.42	59.02
193.77	27.86	55.33	134.73	33.31	47.00	240.14	66.31	71.20
149.72	37.97	99.99	132.69	83.15	96.93	184.59	57.07	62.30
121.27	80.84	75.83	140.33	88.10	64.24	478.72	58.94	58.53
215.04	55.88	66.31	125.43	44.97	80.28	121.12	88.65	31.06

Table 2: hNPC neurite outgrowth: Human 1 µg/mL TN-C

n=1		
alpha9	GFP	WT
227.69	104.10	39.02
115.73	41.67	61.19
351.66	26.59	55.58
230.61	60.73	81.18
223.84	34.50	32.68
197.12	37.48	36.48
295.26	39.93	49.31
234.03	33.66	41.16
535.38	59.65	31.34
565.81	38.83	67.77
223.06	45.92	50.63
215.09	46.04	34.80
277.07	36.37	46.21
290.11	90.72	47.59
138.90	52.42	59.08
165.03	30.56	37.73
128.57	29.78	41.22
177.14	26.64	65.74
205.28	33.05	41.68
235.76	32.35	57.36
109.27	64.77	55.53
105.52	71.04	36.98
123.11	81.73	85.81
128.81	40.64	100.40
425.17	44.92	37.54
279.89	58.87	36.45
174.41	39.29	52.62
202.46	51.35	89.36
218.37	89.33	58.93
242.42	40.15	37.76

n=2		
alpha9	GFP	WT
513.86	37.02	31.68
230.76	43.47	52.38
232.64	33.82	59.38
197.65	37.19	55.77
432.86	21.40	39.00
368.90	24.18	31.93
441.04	43.03	31.16
220.42	43.32	54.35
337.01	56.78	39.00
151.28	226.98	46.62
168.19	30.20	45.26
153.40	28.21	33.93
175.51	28.29	52.67
220.10	25.66	34.56
250.26	47.60	22.41
223.26	23.41	27.32
165.85	27.05	27.79
289.65	27.32	22.06
155.35	58.86	16.56
293.04	62.25	25.83
167.26	47.91	42.72
148.03	66.88	29.25
286.89	47.91	44.05
300.30	78.93	40.85
200.81	39.65	36.07
216.51	52.88	67.55
190.17	52.39	43.12
353.11	31.16	47.04
243.37	26.39	50.55
181.78	31.34	74.79

n=3		
alpha9	GFP	WT
124.62	71.68	122.89
121.80	88.78	84.39
164.55	108.87	83.57
88.00	110.15	64.13
114.07	42.28	77.58
110.68	53.22	66.87
100.98	61.43	94.98
218.33	107.69	103.80
161.06	70.82	86.88
91.65	52.94	73.63
118.90	64.33	69.92
88.43	90.93	60.76
84.70	82.36	97.75
119.02	80.88	58.20
128.22	85.14	49.62
119.21	84.47	49.43
162.66	104.95	73.41
76.56	61.34	70.94
167.62	101.89	53.12
152.28	82.05	89.35
161.03	91.18	120.79
125.92	77.29	76.98
133.98	57.55	53.18
179.88	58.97	45.64
147.61	67.87	96.94
96.69	50.66	48.17
92.87	31.76	85.99
185.90	67.58	68.17
125.17	86.37	91.84
161.19	56.10	57.13

n=4		
alpha9	GFP	WT
83.41	103.46	98.95
81.83	107.76	69.61
119.42	79.00	136.42
172.14	59.35	131.30
94.15	115.21	98.15
125.76	136.54	83.75
191.50	138.47	70.43
138.34	107.08	126.18
123.43	132.06	74.32
101.67	117.84	45.84
132.52	109.08	76.27
98.63	164.29	119.86
103.41	104.37	70.36
86.13	54.48	98.43
159.24	88.38	63.75
135.68	83.62	89.51
86.35	104.41	113.88
90.13	46.37	83.71
50.30	73.40	126.59
74.61	134.58	70.83
141.40	83.28	85.04
67.26	94.18	57.01
130.01	79.38	98.80
139.61	77.02	209.44
164.38	148.49	60.90
151.15	32.68	86.17
140.84	68.23	63.81
200.17	73.92	141.15
86.51	87.52	69.49
159.28	70.44	146.08

n=5		
alpha9	GFP	WT
244.50	78.63	91.63
262.24	33.24	36.59
166.56	109.80	32.23
158.10	39.52	30.07
138.38	29.68	80.53
181.24	39.02	80.33
206.56	47.69	25.91
250.28	47.75	71.08
155.13	43.47	124.12
158.19	33.80	69.18
186.11	41.50	45.45
322.12	38.33	61.94
165.22	42.73	55.14
231.25	37.18	51.69
177.82	28.10	28.22
186.91	44.16	48.75
249.98	54.18	49.69
201.11	38.95	36.16
266.41	48.29	34.00
207.12	33.46	56.81
150.05	32.52	34.05
130.20	42.35	68.64
144.53	66.89	60.62
141.34	49.31	34.26
159.32	59.10	65.70
174.61	122.54	31.49
173.06	69.38	53.39
239.05	41.53	65.33
176.25	56.10	59.38
181.11	61.22	38.47

Table 3: hNPCs neurite outgrowth: Human 5 µg/mL TN-C

n=1		
alpha9	GFP	WT
181.34	72.85	46.44
176.00	70.93	72.81
377.43	86.17	53.67
180.14	42.56	30.68
189.80	78.61	63.62
134.35	56.93	79.80
431.92	55.18	77.06
228.23	40.21	159.86
137.62	44.40	49.15
117.83	51.94	68.64
156.75	84.18	106.85
163.63	31.16	108.18
116.95	37.97	81.05
113.26	41.51	46.16
99.17	49.14	58.77
143.61	20.87	50.50
133.47	26.88	86.53
237.88	32.54	90.53
210.98	72.60	54.02
388.91	90.98	48.70
196.07	78.41	42.24
195.57	99.63	54.61
287.75	85.43	73.30
257.38	49.63	65.59
172.51	121.33	103.19
255.83	40.11	80.97
249.70	42.11	86.89
211.66	46.24	97.77
158.38	79.67	74.56
194.54	46.09	77.67

n=2		
alpha9	GFP	WT
232.01	88.19	52.27
268.70	97.70	87.43
180.24	50.81	55.19
319.83	49.96	53.07
406.75	31.24	44.29
250.79	28.38	39.92
188.93	43.79	53.12
134.72	46.00	31.44
255.48	48.43	44.09
165.48	36.41	38.86
172.59	61.73	66.47
171.55	64.92	49.49
151.65	144.05	80.46
159.46	87.68	77.63
241.76	50.97	70.13
98.00	38.21	109.60
148.13	39.90	48.37
151.76	71.68	72.33
163.31	36.79	19.49
185.61	25.74	70.80
467.63	42.90	41.82
220.44	46.85	33.51
194.83	28.02	45.36
271.70	45.46	49.22
326.41	34.66	30.64
186.28	46.56	48.28
172.67	55.81	54.01
337.64	44.89	56.90
944.33	44.45	41.09
536.50	58.17	47.33

n=3		
alpha9	GFP	WT
129.38	113.28	144.20
137.77	83.06	63.71
194.67	227.25	121.85
151.60	88.52	68.91
119.40	163.31	74.49
78.48	104.89	75.93
178.75	49.18	134.04
102.82	50.63	66.35
74.71	50.30	121.76
116.46	149.29	62.93
79.43	114.96	81.49
151.76	48.29	60.44
240.16	72.29	75.97
125.24	81.70	87.90
75.78	119.29	31.49
122.40	41.62	96.12
74.48	60.88	54.11
178.80	65.83	24.23
132.96	75.05	43.56
137.87	127.05	41.12
177.75	69.30	56.37
82.79	93.17	56.59
91.05	35.28	86.03
82.65	57.67	78.77
91.89	42.64	90.75
120.54	126.73	54.23
176.74	129.21	78.78
176.17	84.79	86.25
82.25	88.00	61.84
96.74	95.23	62.52

n=4		
alpha9	GFP	WT
84.30	59.14	118.19
138.42	56.20	138.77
109.30	76.69	91.66
85.35	73.67	115.48
96.96	70.03	26.32
230.15	52.20	64.29
138.17	59.00	107.35
141.08	83.72	96.87
91.85	34.49	76.39
172.66	67.03	66.51
133.44	54.58	36.44
107.21	98.18	98.83
149.29	76.96	84.25
91.99	103.09	48.41
118.81	132.13	91.99
77.67	96.25	110.44
87.15	97.87	136.86
194.16	154.80	49.66
120.68	110.83	129.81
92.03	130.69	116.12
108.41	97.20	94.04
140.34	100.97	62.57
87.26	62.97	62.59
138.28	77.26	28.59
145.37	110.05	44.26
101.65	85.99	42.30
97.30	85.50	61.56
150.85	135.91	134.33
207.39	142.75	123.16
96.07	100.56	51.49

n=5		
alpha9	GFP	WT
143.80	62.46	92.23
127.00	46.14	121.30
157.40	80.78	164.65
141.19	55.16	175.35
134.81	79.52	98.91
267.66	199.48	70.27
145.99	93.46	101.03
290.70	78.61	159.60
215.23	178.42	119.43
165.34	83.37	155.23
179.38	146.26	123.11
158.37	91.99	139.31
314.42	85.95	125.53
275.20	80.68	123.46
87.09	227.79	132.56
265.30	95.16	139.31
164.00	60.35	165.76
371.13	56.32	111.59
287.97	169.11	126.16
126.52	154.41	124.72
192.00	81.62	155.75
132.38	147.93	90.82
130.02	196.89	132.34
88.65	188.90	123.25
78.68	218.95	69.61
64.30	218.95	128.74
258.15	208.71	123.21
352.53	191.44	119.62
128.64	195.96	118.38
370.10	214.59	112.35

Table 4: hNPCs neurite outgrowth: Human 10 µg/mL TN-C

n=1		
alpha9	GFP	WT
242.84	123.10	75.34
126.19	82.77	71.44
116.88	63.67	67.91
330.71	58.05	89.85
117.63	67.81	73.58
189.27	71.13	108.94
116.57	139.23	98.58
175.92	84.56	58.35
109.25	95.03	44.61
207.54	45.02	66.60
93.80	55.93	82.13
123.75	43.08	89.96
254.62	57.72	67.98
181.96	182.11	64.32
120.95	153.35	64.72
135.53	143.33	144.83
136.02	189.75	149.15
204.96	104.16	67.58
270.91	82.70	74.61
123.84	55.07	87.86
167.36	132.92	63.94
300.80	86.12	78.58
154.60	43.58	79.25
71.13	48.07	61.88
382.37	34.43	54.95
458.04	44.21	54.44
242.56	111.31	61.67
102.11	91.53	55.63
150.87	119.76	84.21
147.15	93.55	113.75

n=2		
alpha9	GFP	WT
257.27	85.71	46.95
471.54	68.55	79.56
413.44	65.37	67.04
541.13	104.59	103.60
308.18	43.50	90.89
139.90	51.97	52.18
138.15	103.80	36.75
314.08	54.48	40.55
268.26	44.95	38.02
322.32	36.39	115.32
213.34	45.77	158.02
280.76	38.27	45.76
228.94	138.61	40.32
226.76	59.17	53.55
159.92	140.95	74.47
214.25	76.55	93.29
321.65	69.72	66.54
507.09	55.74	57.36
264.04	159.78	120.33
302.75	85.51	86.67
247.03	95.31	59.88
238.47	85.25	49.65
149.25	92.25	30.72
366.84	54.41	47.40
298.07	63.57	38.68
383.91	56.34	71.66
309.34	109.21	191.45
192.70	44.69	99.50
218.74	193.52	106.87
206.21	120.62	110.35

n=3		
alpha9	GFP	WT
123.98	89.14	241.35
100.21	149.18	112.79
107.76	61.34	141.07
98.91	93.76	126.41
183.87	144.87	77.43
92.25	145.14	87.05
114.08	77.91	131.00
76.99	175.90	57.02
184.01	76.66	97.73
235.58	122.81	48.46
200.69	76.00	53.70
132.45	142.26	80.45
102.69	118.66	156.92
62.38	72.12	81.24
109.62	93.35	66.19
142.30	75.55	34.97
90.69	126.74	152.24
166.94	93.07	199.99
138.54	106.87	111.95
130.22	84.20	117.93
190.65	141.09	104.67
243.83	182.71	136.73
98.94	120.20	47.84
129.17	94.89	94.64
250.86	72.05	94.51
170.02	60.85	119.28
97.88	128.35	89.04
141.28	74.70	63.62
99.25	49.64	68.09
159.97	107.32	129.45

n=4		
alpha9	GFP	WT
282.46	125.05	108.67
183.50	98.55	181.58
185.24	141.12	68.55
195.31	106.61	137.55
151.18	141.61	153.24
366.53	75.33	86.16
220.10	79.31	190.92
137.87	230.37	186.84
168.90	176.18	141.94
179.82	115.66	89.25
79.19	86.05	127.04
113.88	130.40	79.53
116.67	134.09	93.05
107.43	114.91	146.15
154.91	126.47	199.93
157.56	97.81	197.46
166.05	193.51	222.52
125.91	125.97	68.83
157.91	67.38	115.41
114.71	63.67	65.49
201.91	172.91	85.08
96.38	110.78	53.91
175.94	142.82	106.83
121.40	113.67	175.62
135.37	115.06	85.62
238.95	100.73	198.74
20.61	202.49	87.04
97.90	146.52	72.62
173.04	70.82	151.09
141.84	116.54	196.35

n=5		
alpha9	GFP	WT
296.01	394.88	135.21
260.54	125.88	155.55
302.16	104.64	82.10
230.24	116.90	112.95
221.60	283.59	94.22
248.59	247.86	148.31
117.39	110.34	54.80
131.68	84.50	104.12
131.63	188.63	206.17
102.96	125.46	84.63
150.20	118.39	155.04
98.59	117.21	117.26
203.62	82.99	96.64
334.53	114.41	110.34
142.76	154.37	96.28
213.69	185.11	217.85
183.39	220.76	44.25
160.93	76.81	108.19
205.99	145.24	124.11
132.46	166.79	165.15
135.90	184.50	124.60
192.01	77.91	178.20
233.92	134.81	171.31
148.29	251.10	151.00
146.62	225.59	113.95
225.48	140.88	194.86
169.72	265.02	96.45
175.50	139.53	77.06
120.97	158.18	102.03
115.15	231.84	115.60

n=6		
alpha9	GFP	WT
266.59	277.11	209.86
189.69	225.63	179.14
298.45	128.83	321.75
225.21	136.78	241.54
112.54	209.29	242.30
120.29	139.97	179.10
259.08	203.01	196.24
122.29	82.22	301.27
201.98	178.97	115.38
156.78	131.61	100.68
310.99	68.16	98.36
250.00	209.65	121.30
156.04	175.40	123.85
208.20	109.92	131.00
278.70	158.08	120.83
223.67	126.99	143.08
129.13	160.73	108.65
126.32	145.95	73.47
147.70	120.12	181.09
132.27	113.58	165.08
139.12	135.99	130.36
220.64	96.92	104.45
123.01	92.77	64.25
224.51	92.38	101.73
214.78	157.05	89.86
215.33	198.43	256.38
203.32	172.86	100.07
196.60	146.36	173.23
133.38	207.37	143.50
188.69	182.40	123.21

Table 5: hNPCs neurite outgrowth: Human 15, 20, 25 and 30 µg/mL TN-C

Human 15µg/mL TN-C		
n=1		
alpha9	GFP	WT
216.52	173.26	186.92
296.05	185.17	141.70
122.75	316.90	146.09
226.97	206.95	172.91
118.85	135.21	147.06
145.34	225.06	185.59
303.38	208.20	135.26
231.25	118.08	220.03
116.97	149.77	104.79
122.48	202.76	201.57
97.34	147.20	143.95
87.74	217.12	105.95
99.36	174.45	145.19
96.99	124.25	137.85
100.55	103.50	144.24
384.27	101.60	128.85
182.97	95.77	159.84
228.92	151.69	90.82
104.60	113.70	120.47
127.11	138.25	144.05
119.97	113.11	93.39
289.97	154.29	141.07
161.24	103.58	120.18
182.05	192.09	127.91
185.79	95.53	160.42
142.49	104.80	132.26
234.18	91.52	121.05
272.53	226.38	115.57
196.24	301.08	163.77
125.52	211.65	187.02

Human 20 µg/mL TN-C		
n=1		
alpha9	GFP	WT
236.26	206.23	188.45
164.99	362.92	132.41
132.56	326.60	199.60
374.94	239.33	220.49
184.59	223.83	242.21
312.17	161.01	198.81
105.96	196.97	131.60
80.98	125.74	198.62
98.95	143.49	193.15
750.08	194.05	128.88
323.08	92.96	119.82
157.95	175.54	183.47
119.40	143.10	136.81
134.89	93.25	171.89
187.82	150.69	179.81
107.09	151.05	199.68
282.29	121.90	128.31
149.21	142.42	166.25
106.58	141.63	96.53
120.72	222.51	203.35
91.96	240.88	157.29
110.13	239.40	254.46
194.63	134.71	126.67
228.97	164.33	200.90
124.52	153.65	137.59
124.91	167.61	135.57
121.39	236.14	199.71
171.70	183.61	164.86
173.40	166.10	209.39
166.29	191.57	293.91

Human 25 µg/mL TN-C		
n=1		
alpha9	GFP	WT
310.81	237.15	179.74
264.29	210.07	232.67
225.47	278.35	282.10
134.77	156.38	202.75
118.02	414.30	279.57
136.00	182.70	146.55
168.91	133.49	166.44
237.83	231.87	187.04
162.04	75.95	234.27
433.29	99.90	191.04
134.68	107.12	274.20
170.90	110.16	239.65
103.01	155.91	166.23
124.95	152.31	268.63
162.56	164.12	253.17
299.19	88.70	245.43
184.30	222.73	164.92
324.33	149.25	320.78
140.58	85.96	213.94
232.66	87.31	205.87
391.02	85.13	130.28
159.17	86.11	368.95
123.67	98.46	369.75
122.92	93.23	242.97
177.84	132.70	237.45
145.61	179.14	192.61
146.48	81.43	296.36
146.08	155.16	213.89
145.45	188.99	423.77
118.02	225.36	295.63

Human 30 µg/mL TN-C		
n=1		
alpha9	GFP	WT
132.26	258.04	179.22
227.30	304.32	262.23
169.43	251.07	197.11
149.74	284.02	159.36
176.53	215.92	147.14
179.67	193.50	216.81
238.86	200.02	184.59
118.82	176.88	176.93
125.27	181.10	166.16
165.13	190.38	201.74
157.64	332.27	187.46
177.96	128.78	241.36
122.19	358.42	153.87
172.58	232.99	146.66
183.13	240.17	169.23
172.65	224.16	92.83
261.49	198.46	124.37
126.98	210.62	207.52
251.95	194.24	213.31
169.55	286.28	141.56
144.78	249.58	149.79
181.37	192.97	395.84
633.00	174.63	127.34
331.90	150.35	201.05
190.53	228.77	195.19
138.13	175.48	129.36
155.42	171.22	126.73
127.61	225.13	143.82
160.56	303.88	244.02
166.65	347.60	225.30

Appendix B: Presence of scar after hNPC transplantation

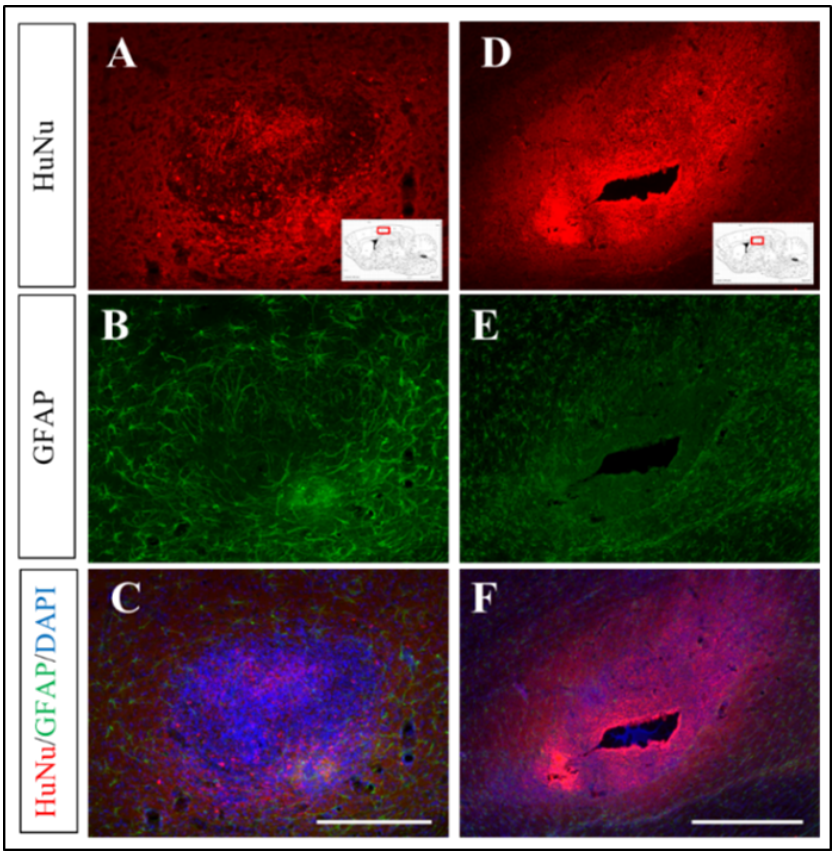

Figure 1 Representative images showing scarring at 7 weeks post-transplantation of WT hNPCs. Scarring was defined as non-specific HuNu (**A-D**) or hNCAM staining that corresponded with increased GFAP staining (**B-E**). Scale bar A-C = 250 µm; D-F = 500 µm.

Appendix C: HuNu and hNCAM antibodies are human-specific

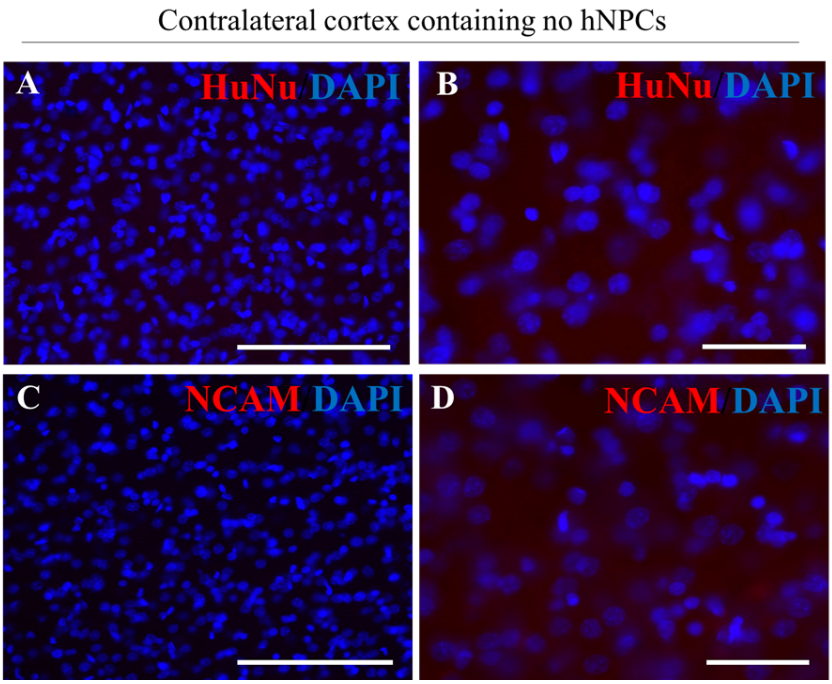

Figure 2 Both HuNu and hNCAM antibodies are human-specific. The HuNu and hNCAM antibodies were assessed for their human-specificity using the contralateral cortex which contained no hNPCs. Both HuNu (**A-B**) and hNCAM (**C-D**) did not stain the endogenous rat tissue indicating both antibodies were indeed specific to only the human cells. Scale bar in A and C = 150 µm; B and D = 50 µm.

Appendix D: WT hNPC grafts and projections are not positive for GFP

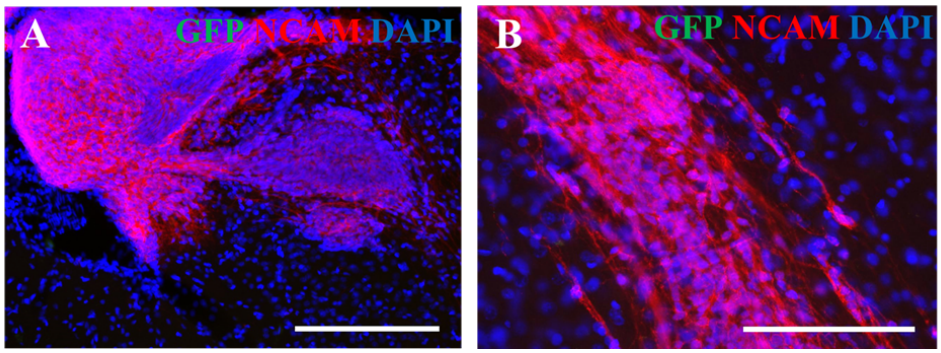

Figure 3 WT hNPC grafts and projections are not GFP-positive. The WT hNPC grafts were assessed using IHC and an anti-GFP antibody so assess whether they stain positive for GFP. Results show no GFP-positive staining was observed within the grafts (**A**) or the projections (**B**) from WT hNPCs suggesting the GFP expression within the α9-eYFP hNPCs and fGFP-hNPCs is indeed due to the exogenous protein expression. Scale bar in A = 250 μm and B = 150 μm.

Appendix E: Publications

Forbes LH, Andrews MR. Restoring axonal localisation and transport of transmembrane receptors to promote repair within the injured CNS: a critical step in CNS regeneration. *Neural Regen Res* 2017;12:27-30

Piksarv P, Marti D, Le T, Unterhuber A, **Forbes LH**, Andrews MR, Stingle A, Drexler W, Andersen PE and Dholakia K. Integrated single- and two-photon light sheet microscopy using accelerating beams. *Sci Rep*. 2017; 7: 1435

Chen M, Mas, J, **Forbes LH**, Andrews MR and Dholakia K. Depth-resolved multimodal imaging: Wavelength Modulated Spatially Offset Raman Spectroscopy with Optical Coherence Tomography. *J Biophotonics*. Accepted July 2017.

Quraishe S*, **Forbes LH*** and Andrews MR. The extracellular environment of the CNS: Influence on Plasticity, Sprouting and Regeneration after spinal cord injury. *Invited review to Neural Plasticity, submitted Oct 2017* (*These authors contributed equally).